Antimicrobial Peptide Daptomycin and its Inhibition by Pulmonary Surfactant: Biophysical Studies using Model Membrane Systems

by

Brenda Yasie Lee

A thesis
presented to the University of Waterloo
in fulfillment of the
thesis requirement for the degree of
Doctor of Philosophy
in
Biology (Nanotechnology)

Waterloo, Ontario, Canada, 2017

EXAMINING COMMITTEE MEMBERSHIP

The following served on the Examining Committee for this thesis. The decision of the Examining Committee is by majority vote.

EXTERNAL EXAMINER:

DR. ELMAR JOSEF PRENNER
Associate Professor
Department of Biological Sciences
University of Calgary

SUPERVISOR:

DR. ZOYA LEONENKO
Professor
Department of Biology
Department of Physics & Astronomy
University of Waterloo

INTERNAL MEMBER:

DR. BARBARA A. MOFFATT
Professor
Department of Biology
University of Waterloo

INTERNAL-EXTERNAL MEMBER:

DR. MAUD GORBET
Associate Professor
Department of Systems Design Engineering
University of Waterloo

MEMBER:

DR. MICHAEL PALMER
Associate Professor
Department of Chemistry
University of Waterloo

AUTHOR'S DECLARATION

This thesis consists of material all of which I authored or co-authored: see Statement of Contributions included in the thesis. This is a true copy of the thesis, including any required final revisions, as accepted by my examiners.

I understand that my thesis may be made electronically available to the public.

STATEMENT OF CONTRIBUTIONS

All of the experiments presented in this thesis were conducted by myself and designed by myself with advice and guidance from my committee members: Dr. Zoya Leonenko, Dr. Michael Palmer, and Dr. Barbara Moffatt.

All of the figures presented in this thesis were drawn by myself with occasional advice and guidance from Craig Christoff at CryoDragon Inc., unless otherwise noted in the figure caption.

Specific exceptions to the above statements are noted as follows:

Chapter 5: A portion of the preliminary data for this study was obtained by undergraduate student Victoria Higgins, whom I trained and co-supervised. However, all of the experiments were redone using new stock solutions and updated experimental protocols. For these new experiments, undergraduate students Jeff Lam and Maureen Li (whom I trained and co-supervised) helped with a portion of sample preparation and the acquisition of preliminary fluorescence emission spectra.

Chapter 6: The monolayer compression isotherms and insertion assays obtained for this study were primarily performed and repeated by myself, with support from Jeff Lam and Maureen Li for data collection of a subset of experiments pertaining to lung surfactant and bacterial membrane lipid model systems.

The antibiotics daptomycin and CB-182,462 used for this work were generously donated by Dr. Jared Silverman of Cubist Pharmaceuticals (now a subsidiary of Merck & Co.).

ABSTRACT

Daptomycin is a lipopeptide antibiotic that is clinically used to treat severe infections caused by Gram-positive bacteria. It is highly potent against resistant strains of bacteria such as methicillin-resistant *Staphylococcus aureus*. However, in cases of community-acquired pneumonia (a leading cause of death worldwide), daptomycin is somehow inhibited by lung surfactant and therefore unable to exert its bactericidal activity against *Streptococcus pneumoniae*, the primary cause of this disease. This thesis presents the successful development of lipid model systems to mimic the lipid composition of *S. pneumoniae* bacterial membranes, human cell membranes, and both synthetic and natural lung surfactant. Experiments were performed that help to elucidate the basis for daptomycin's inhibition by lung surfactant, culminating in a new, detailed model of daptomycin sequestration that summarizes the findings from these studies.

Daptomycin is believed to be sequestered by lung surfactant and has been shown to insert into this surfactant. Fluorescence spectroscopy experiments were used to test the interaction of daptomycin with different lipid model membranes in the presence of calcium. It was discovered that at physiologically relevant calcium concentrations, daptomycin induced larger changes in fluorescence intensity with lung surfactant than in the bacterial membrane and human membrane models. This suggests that daptomycin has a greater affinity for lung surfactant at lower calcium concentrations, which may account for its inhibition in these conditions.

Using Langmuir-Blodgett monolayer techniques, studies were performed on how daptomycin affects monolayer properties. Compression isotherms provided data on monolayer compressibility, and it was found that daptomycin and calcium reduce the compressibility of lung surfactant monolayers, possibly improving its function. Constant-area insertion assays provided additional data that verified daptomycin's avid binding to lung surfactant at low calcium concentrations.

Scanning probe microscopy techniques were employed to obtain atomic force microscopy and Kelvin probe force microscopy images for monolayers in air. In the presence of daptomycin and calcium, the lung surfactant monolayers exhibited multilayer formation and increased electrical surface potential. Atomic force microscopy images taken of model lipid bilayers in liquid show multi-bilayer formation for the lung surfactant bilayers in the presence of daptomycin and calcium. This provides further evidence that daptomycin and calcium induce multilayer formation in lung surfactant.

These findings allowed for the development of a novel model of daptomycin inhibition by lung surfactant. In the presence of physiological levels of calcium, daptomycin binds to lung surfactant and is sequestered. This binding causes a decrease in lung surfactant compressibility, allowing it to easily form multilayers that effectively reinforce the sequestration of daptomycin. The lipid models, methods, and experimental protocols developed in this thesis will help foster future studies in the field of membrane biophysics.

ACKNOWLEDGEMENTS

This doctoral dissertation represents a culmination of over six years' worth of experiences and milestones at the University of Waterloo. First and foremost, I would like to thank my supervisor, Dr. Zoya Leonenko, for taking me under her wing. Without her constant support and guidance, this thesis would not have been possible. I would also like to thank Dr. Leonenko for her commitment to her lab members and providing each and every one of them, including myself, with as many opportunities as possible to help them progress further in their future careers by encouraging scientific investigation and making sure we had all the necessary skills and knowledge to do so. The freedom she has provided us with has allowed me to pursue multiple passions of mine: teaching and scientific graphic design, all of which has helped me grow as a researcher and educator. As a recipient of her continuous mentorship and leadership, I want to express my sincerest gratitude to Dr. Leonenko for playing such a large role in shaping my future. I can never thank her enough for all that she has done for me.

Thank you to Dr. Michael Palmer for opening the doors to his lab so that I could benefit from the expertise of his team in fluorescence spectroscopy, daptomycin, and its derivatives. I am also grateful to Dr. Palmer for his collaborative support and the many helpful discussions we have had regarding experimental procedures and results. I am thankful for the opportunity to have worked in his lab and to have experienced his mentorship and sense of humour firsthand.

I would also like to thank Dr. Barbara Moffatt for her ongoing support and mentorship throughout my journey as both a graduate student and community helper. Dr. Moffatt provided me with invaluable support and critique related to experimental design and data analysis, all of which helped me fine-tune my experiments and ensure the implementation of strict protocols and data collection procedures for my project.

In our lab, I would first like to thank Dr. Ravi Gaikwad, who introduced me to the JPK atomic force microscope when I first joined Dr. Zoya Loenenko's lab. Ravi spent months training me on the JPK and helped a nervous undergraduate student gain her ground by providing constant moral support and friendship along the way. I am grateful for all of his mentorship in helping me gain expertise in atomic force microscopy and appreciating scientific investigation. I would also like to than Drs. Elizabeth Drolle and Robert D.E. Henderson for helping to train me not only on the AIST-NT atomic force microscope, but also the Langmuir-Blodgett trough. I appreciate all of the helpful discussions and friendly comradery we had along the way. Next, I would like to offer my deepest gratitude to Jeff Lam, Maureen Li, and Victoria Higgins for their collaborative support and assistance with my project. Your friendship and support have been invaluable throughout these years. Thank you to all of my labmates (Morgan, Stephen, Francis, Jennifer, Jingsi, Nancy Mei, Kelsey, Vince, Ravi, Simon, Nancy Elewa, and Tavo, just to name a few) for making my lab experience one that I will cherish forever.

I have also worked with numerous researchers outside of our lab. Thank you to Dr. Jared Silverman for not only supplying daptomycin and CB-182,462 for my project, but for the helpful discussions we had regarding these peptides. I have greatly benefited from Dr. Silverman's expertise. Thank you to Dr. Sid Ragona and Dr. Marc Richter for providing additional training and support for the JPK atomic force microscope, specifically with regards to imaging in liquid environments; as well as Dr. Andrey Krayev from AIST-NT for his support and guidance with the SmartSPM's AFM and KPFM capabilities. In Dr. Palmer's lab, I would like to thank Dr. Oscar TianHua Zhang and Robert Taylor for their training, support and helpful discussions in all things fluorescence spectroscopy and daptomycin.

On a final note, I would like to thank Craig Christoff for spending countless days, nights, and weekends in the lab with me while I was running experiments and for providing me with guidance and support for graphic design and being able to calm my nerves during times of high stress and looming deadlines. I could not have done this without your moral support.

DEDICATION

To my amazing father, Richard Lee, for his unwavering support, love and encouragement to continually strive for academic excellence and to be the best that I can be. Also for his dedicated effort and selflessness in helping me with Tutoring Beyond Borders while I was immersed in my studies. You have always been my greatest role model.

To my hardworking mother, Jenny Chiou, for her years of sacrifice and perseverance in making this family the most unique and loving environment a child could ever wish for. It has been a tough and formidable journey, we made it through, and it is time to enjoy the fruits of your labour. You have been an inspiration to all of us.

To my loving mama, Mina Chan, for being my closest friend and confidant since the day I entered this world. No matter what, no matter where, I could always depend on you because you were always there for me. It is now time for me to master all of your delicious recipes!

To my sister, Jessie Lee, for showing me that life is precious and that you have to make the most of it while you still can. I am proud of your bravery in facing the greatest odds, and I can't wait to see Ashley and Rosabel grow and reach for the stars.

To my best friend, Craig Christoff, for his constant encouragement and support. You have shown me the true meaning of how good things come to those who wait. Your dedication to never giving up and fighting for what you want has encouraged me to do the same, and I look forward to seeing our business flourish in years to come.

Last but not least, to Dr. Zoya Leonenko, without whom none of this would have been possible. I am the person I am today because of you and the opportunities you have given me. I am forever indebted to you for your kindness and support, and I am grateful to call you my lifelong mentor and friend. *We miss you, Marsik.*

TABLE OF CONTENTS

LIST OF FIGURES

LIST OF TABLES

LIST OF ABBREVIATIONS

Abbreviation	Full Meaning
462	CB-182,462
AFM	atomic force microscopy
AM-KPFM	amplitude modulation Kelvin probe force microscopy
AMP	antimicrobial peptide
ARDS	acute respiratory distress syndrome
BLES®	bovine lipid extract surfactant
BM	bacterial membrane
CAP	community-acquired pneumonia
Chol	cholesterol
CL	cardiolipin
cSSSI	complicated skin and skin structure infections
DAG	diacylglycerol
DAP	daptomycin
DGDG	galactosylglucosyldiacylglycerol
DOPG	1,2-dioleoyl-*sn*-glycero-3-[phospho-*rac*-(1-glycerol)] (sodium salt)
DOPS	1,2-dioleoyl-*sn*-glycero-3-[phospho-L-serine] (sodium salt)
DPPC	1,2-dipalmitoyl-*sn*-glycero-3-phosphocholine
DRSP	drug-resistant *Streptococcus pneumoniae*
DSC	differential scanning calorimetry
E. coli	*Escherichia coli*
EMEA	European Medicines Agency
FDA	Food and Drug Administration
FRET	fluorescence resonance energy transfer

HEPES	4-(2-hydroxyethyl)-1-piperazineethanesulfonic acid
HM	human membrane
KPFM	Kelvin probe force microscopy
LB	Langmuir-Blodgett (Trough)
LPS	lipopolysaccharide
LS	lung surfactant
LTA	Lipoteichoic acid
LUV	large unilamellar vesicles
MBC	minimal bactericidal concentration
MGDG	monoglucosyldiacylglycerol
MIC	minimum inhibitory concentration
MOA	mechanism of action
MRSA	methicillin-resistant *Staphylococcus aureus*
NBD	7-nitro-2,1,3-benzoxadiazol
NMR	nuclear magnetic resonance
NOESY	Nuclear Overhauser effect spectroscopy
PBFI	potassium-sensitive fluorescent probe
PBP	penicillin-binding protein
PC	phosphatidylcholine
PE	phosphatidylethanolamine
PG	phosphatidylglycerol
POPE	1-palmitoyl-2-oleoyl-*sn*-glycero-3-phosphoethanolamine
PRP	penicillinase-resistant penicillin
PRSP	penicillin-resistant *Streptococcus pneumoniae*
PS	phosphatidylserine
PTFE	polytetrafluoroethylene
S. aureus	*Staphylococcus aureus*
S. fradiae	*Streptomyces fradiae*

S. pneumoniae	*Streptococcus pneumoniae* or *pneumococcus*
S. roseosporus	*Streptomyces roseosporus*
SM	sphingomyelin (egg, chicken)
SP	surfactant protein
SUV	small unilamellar vesicles
TMS	tetramethylsilane
TOCL	1,1'2,2'-tetraoleoyl cardiolipin (sodium salt)
VRE	vancomycin-resistant *Enterococcus*

LIST OF SYMBOLS

Symbol	Full Meaning
A	absolute area
N_A	Avogadro's number
c	concentration
ΔV	difference in electrical surface potential
Δh	difference in height
$\Delta \varphi$	difference in phase signal
C_s^{-1}	elastic compressibility modulus
M	molar mass
a_m	molecular area
M_w	molecular weight
n	number of moles
Π	surface pressure
V	volume
λ	wavelength

CHAPTER 1

1 INTRODUCTION

We live in a world of innovation and adaptation on every scale imaginable, from nanoscopic to macroscopic. As we increase our knowledge in the scientific community, we continuously fuel our desire for advancement and innovation. When new discoveries come to light, a period of adaptation occurs where everything is encouraged to adjust and conform to those changes placed upon them. The relationship between pathogens and drugs is no different. As we discover new antibiotics, their associated target bacteria can adapt, mutate, and evolve to thrive in new conditions. Unfortunately for us, we have to go back to the drawing board and come up with alternative ways to tackle these resistant strains of pathogenic microorganisms.

There has always been a never-ending struggle for humans to overcome the illnesses they contract from pathogenic strains of bacteria. Before the invention of drugs and antibiotics, a failure to improve one's condition would have almost certainly meant death. Although herbal medicine goes back thousands of years, pharmaceutical drug research has only been in existence for just over a century [1]. During this century of research, technological advances have allowed

for better and stronger drugs to be made to overcome both the symptoms and the root of the illness itself. But as time progressed, pathogenic bacteria caught up with our progress and eventually self-adapted to resist the drugs we created to target them specifically.

Antibiotics such as tetracycline, streptomycin, and penicillin are not as effective as they once were. An example is methicillin-resistant *Staphylococcus aureus* (MRSA), a superbug that is resistant not only to methicillin, but also penicillin, tetracycline, erythromycin and more [2]. For a while, the only antibiotic that could still exert antimicrobial activity against MRSA was vancomycin, but by 2002, strains of vancomycin-resistant *Staphylococcus aureus* (VRSA) had already appeared across the globe [3]. This gave us no choice but to adapt and continue researching new ways to treat MRSA and many other illnesses that have become resistant to popular antibiotics.

Daptomycin is an antimicrobial peptide that was in development for approximately two decades before receiving FDA approval in 2003 to treat infections caused by Gram-positive microorganisms [4-8]. It has a distinct mechanism of action that allows it to target bacteria that are resistant to numerous antibiotics, but the details of this mechanism are still unclear [4, 8, 9]. Even more peculiar is its inhibition by pulmonary surfactant when used to treat community-acquired pneumonia (CAP) caused by *Streptococcus pneumoniae* [10]. Due to its broad spectrum of bactericidal activity and unique, organ-specific inhibition, it is therefore imperative that we pursue further research into elucidating daptomycin's mechanism of action to benefit future antibiotic discovery, development and optimization.

This chapter will provide a thorough introduction to the different antibiotic compounds presented in this thesis as well as the necessary background information on antimicrobial peptides, cell membranes and lung surfactant. This chapter will also help give a brief overview of what the scientific community has discovered so far to elucidate daptomycin's mechanism of action and inhibition by lung surfactant. Subsequent chapters will detail the development of lipid membrane models, the methods and techniques used for the experiments in this thesis, and

present my experimental work on elucidating daptomycin's organ-specific inhibition and mechanism of action.

1.1 Antimicrobial Peptides

Antimicrobial peptides (AMPs) are small proteins made up of approximately 15-50 amino acids and are naturally derived from living organisms to confer host defense [11]. These molecules have evolved throughout the years in the so-called "arms race for survival" between living organisms, but they share similar features such as size and electrostatic properties [12]. There are many classes of AMPs, but their antimicrobial activity and specificity can be defined by their individual characteristics such as size, peptide sequence, charge and hydrophobicity [12-14].

Although each antimicrobial peptide may have its own specific mechanism of action, certain steps need to occur in order to induce bacterial cell death [13]. First, the AMP must be attracted to the bacterial surface. One of the most obvious mechanisms for such an attraction is the electrostatic bonding between peptides and bacterial surface structures [13, 15]. Since the majority of AMPs are cationic peptides with amphiphilic properties, they have a tendency to attack and permeabilize the negatively-charged bacterial cell membranes, where the net negative charge is brought upon by the lipopolysaccharides (LPS) in Gram-negative bacteria and teichoic acids in Gram-positive bacteria [13, 15, 16].

Once these AMPs have approached bacterial cell surfaces, they must be able to attach to and traverse the capsular polysaccharides found in both Gram-negative and Gram-positive bacteria [13, 17]. Afterwards, the AMPs must get through a layer of LPS in order to reach the outer membrane of Gram-negative bacteria and a layer of teichoic and lipoteichoic acids before they can interact with the cytoplasmic membrane of Gram-positive bacteria [13, 17].

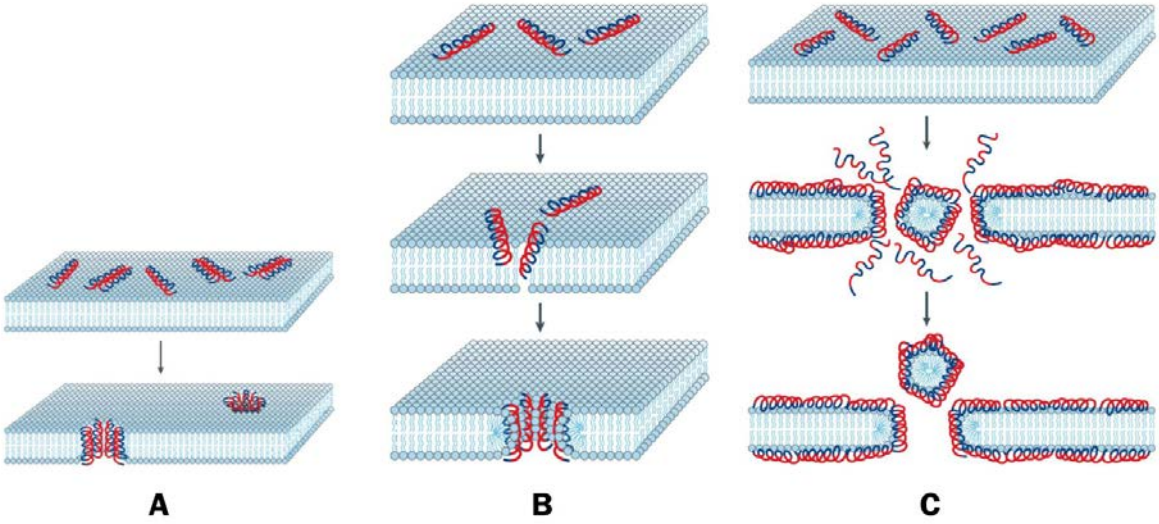

Figure 1.1 AMPs can kill bacteria via transmembrane pores. There are various proposed models in which antimicrobial peptides can target and subsequently kill bacteria through the formation of transmembrane pores in the bacterial cell membrane. (A) In the barrel-stave model, the attached peptides aggregate and insert into the bacterial cell membrane to form a pore. (B) In the toroidal-pore model, the attached peptides aggregate and cause each bilayer leaflet to bend around the pore. (C) In the carpet model, AMPs are oriented parallel to the surface of the membrane to disrupt its integrity, causing localized areas of the membrane to form micelles (Adapted from [13]).

As soon as the antimicrobial peptide has worked its way to the bacterial membrane, it starts to interact with the membrane. Although the mechanisms by which some AMPs inhibit pathogen infections are not yet fully known, studies have shown that AMPs can use various methods to mediate cell killing, three of which pertain to the formation of transmembrane pores as seen in *Figure 1.1* [13, 15]. In the barrel-stave model, barrels made of peptide helices aggregate and insert into the membrane, parallel to the direction of phospholipid chains, to form pores with diameters between 2 to 4 nm [18-22]. This configuration has been found with the AMP alamethicin through studies in oriented circular dichroism, neutron scattering, and synchrotron-based X-ray scattering [20, 21, 23]. In the toroidal-pore model, the AMP helices insert perpendicularly into the bilayer and induce a local membrane curvature so that the inner and outer leaflets are connected together [22, 24, 25]. Studies have shown that magainins, protegrins

and melittin use the toroidal-pore method of forming pores [21, 24, 26]. Meanwhile, the carpet model explains how AMPs such as ovispirin orientate themselves parallel to the bacterial membrane surface and cover it in a carpet-like manner until such a high AMP concentration is reached that the bilayer is disrupted and forced to form micelles [27-32]. However, these are not the only ways of destroying bacterial cells.

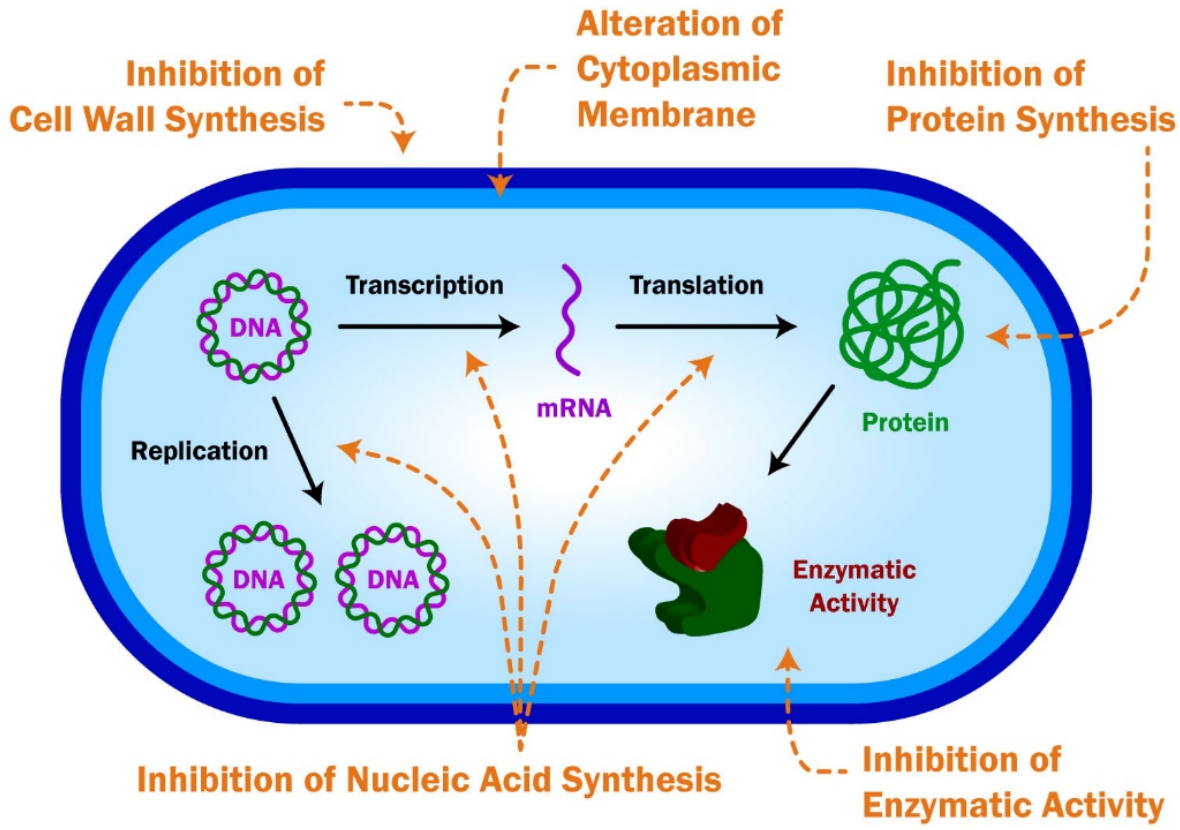

Figure 1.2 AMPs can kill bacteria via intracellular targets. Antimicrobial peptides can also induce cell death through intracellular modes of action. In this figure, an example bacterial target is presented with a cell wall and cytoplasmic membrane. Depending on the AMP, different methods can be used to disrupt crucial cell processes within the bacterial cell. Some of these processes are highlighted in the image: inhibition of cell wall synthesis, inhibition of nucleic acid and protein synthesis (affecting DNA replication and transcription as well as mRNA translation), inhibition of enzymatic activity, and alteration of the cytoplasmic membrane [13].

Over the past few years, there has been increasing evidence which indicates that AMPs can not only form pores, but can also target intracellular molecules to disrupt crucial cell processes such as DNA and protein synthesis (***Figure 1.2***) [13]. For example, an autolysin in the bacterial cell wall can be activated by the introduction of an AMP Pep5, which causes the cell to lyse [33].

With over 2000 AMPs known [11, 15, 34], there are many opportunities to gain further insight into the mechanisms of actions that pertain to the AMPs we are interested in studying. Technological advances in methodology can help us learn more about these AMPs and their mechanisms, but no single technique can provide us with all the information we need. Current research has focused on microscopy, X-ray crystallography, NMR spectroscopy, fluorescence spectroscopy, black lipid membranes, circular dichroism and neutron diffraction, but a combination of these techniques along with other methodologies will be required to fully understand each antibiotic's mechanism of action [13].

1.2 Bacterial Resistance

Unfortunately, when a new and highly effective antimicrobial peptide is discovered, experience tells us that the bacteria it was meant to target will eventually grow resistant to its attacks. Over the past few years, an increasing number of Gram-positive pathogens such as staphylococci, streptococci and enterococci have become resistant to common antibiotics [5]. Specifically, serious infections caused by multi-drug resistant strains of methicillin-resistant *Staphyloccocus aureus* (MRSA), vancomyin-resistant enterococci (VRE) and penicillin-resistant or drug-resistant *Streptococcus pneumoniae* (PRSP or DRSP) are on the rise and the need to develop new and effective agents to treat these diseases is an ongoing mission [35-39].

Although vancomycin, which inhibits cell wall synthesis, has been widely used for treatment against serious Gram-positive infections [40], its increasing ineffectiveness against infections with Gram-positive pathogens has sparked concern in the healthcare system [37, 39, 41]. As the

future of this antibiotic is questionable, novel antimicrobial agents have been developed to somewhat replace vancomycin by carrying out its bactericidal actions against the same bacteria, but in different ways.

Table 1.1 Various antibiotics used to treat MRSA and their mechanisms of action. The name, mechanisms of actions, and known issues are presented for select antibiotics that are commonly used to treat methicillin-resistant *Staphylococcus aureus* (Adapted from [42-44]).

Antibiotic	Mechanism of Action	Comments
Clindamycin	Inhibits protein synthesis by binding to 50S ribosome	Treatment failures reported
Daptomycin[a]	Membrane depolarization	Cannot be used for MRSA-based pneumonia; treatment failures reported for patients previously treated with vancomycin
Doxycycline	Inhibits protein synthesis by binding to 30S ribosome	Clinical experience in treating MRSA is limited
Linezolid	Prevents formation of 70S initiation complex by binding to 23S rRNA of 50S ribosomal subunit	Prolonged therapy may cause myelosuppression
Minocycline	Inhibits protein synthesis by binding to 30S ribosome	Clinical experience in treating MRSA is limited
Quinupristin-dalfopristin	Inhibits protein synthesis	Poor tolerability has restricted its use
Telavancin[a]	Inhibits cell wall synthesis	May cause potential fetal risk
Tigecycline	Inhibits protein synthesis by binding to 30S ribosome	Should not be routinely used for bacteremia
Trimethoprim-sulfamethoxazole	Inhibits biosynthesis of folic acids	Caution for sulfa allergies
Vancomycin[a]	Inhibits cell wall synthesis	Treatment failures reported; may cause infusion-related reactions

[a] Dose should be adjusted for renal function

Recently introduced agents (see *Table 1.1*) that are bactericidal against Gram-positive organisms include linezolid, telavancin, tigecycline, and daptomycin [5, 36, 37, 45, 46]. Of these four,

daptomycin is the only drug from the cyclic lipopeptide class of antimicrobial peptides. It has strong bactericidal activity against MRSA and other resistant strains of bacteria, and it only requires one dose per day [38, 46]. Its unique proposed mechanism of action, which involves the calcium-dependent depolarization of the bacterial cell membrane (causing cell death), means that there is a low chance of cross-resistance between daptomycin and other antimicrobial agents [39, 47]. Simply put, daptomycin is a young player in the field of antibiotics, and further research will need to be done to elucidate its mechanism of action.

1.3 Daptomycin

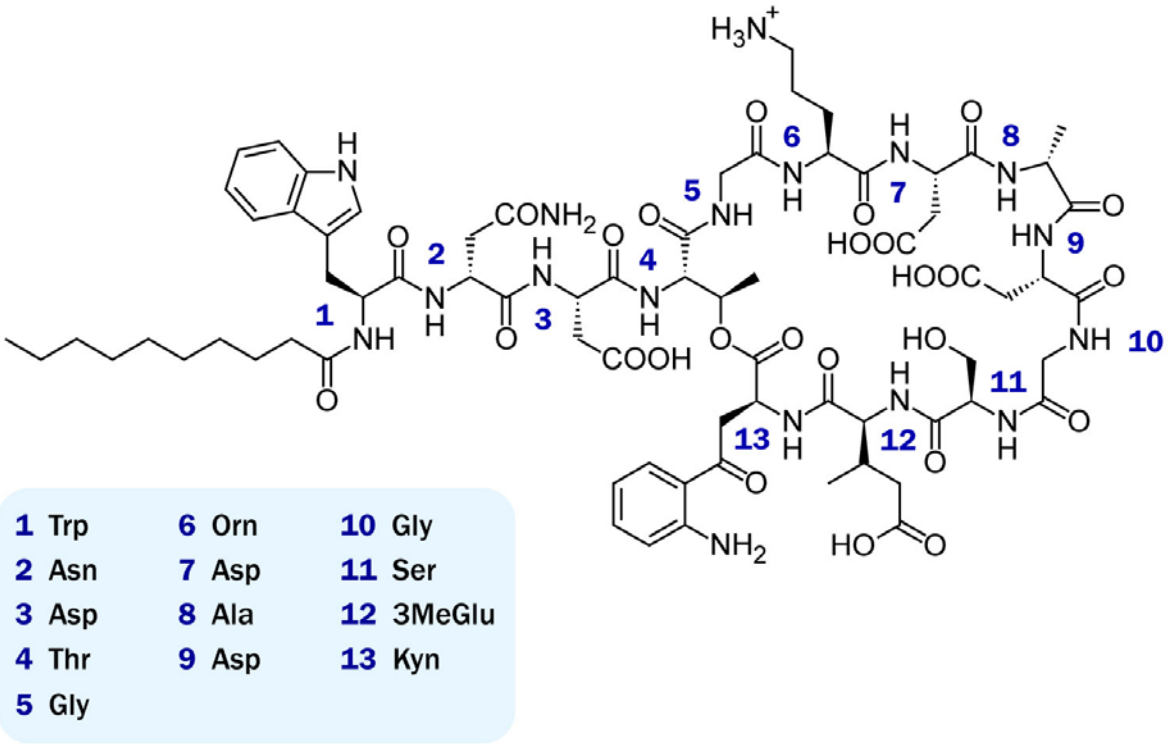

Figure 1.3 Chemical structure of daptomycin. Daptomycin is a cyclic lipopeptide antibiotic with 13 amino acids and a decanoyl side chain. It has two nonproteinogenic amino acids: L-3-methylglutamic acid (3MeGlu) in the 12th position as well as the unusual and unique L-kynurenine (Kyn) residue in the 13th position.

Daptomycin (***Figure 1.3***) is a 13-member cyclic antimicrobial lipopeptide that is produced by the actinobacterium *Streptomyces roseosporus* through fermentation, and supplementing decanoic acid to its growth medium allows for increased daptomycin yield [5, 8]. This process gives it its decanoyl side chain linked to the N-terminal tryptophan of the cyclic amino acid peptide. However, its large molecular weight of around 1620 g/mol restricts it from being absorbed from the gastrointestinal tract and hence its distribution into tissues [5, 35, 48, 49].

Daptomycin has proven to exert bactericidal activity against every clinically important Gram-positive pathogen *in vitro*, including those which are highly resistant and leave us with limited therapeutic options such as MRSA, VRE and DRSP [49-53]. Currently, daptomycin is only available as an intravenous injection to target Gram-positive organisms [5].

1.3.1 History and Development

Daptomycin (developed under the name LY 146032) was discovered by Eli Lilly and Company (Indianapolis, Indiana, USA) in the early 1980s through the screening of bacterial fermentation extracts for antimicrobial activity [6, 7, 49]. Specifically, Eli Lilly isolated *Streptomyces roseosporus* from a soil sample that came from Mount Ararat in Turkey [54]. Throughout the 1980s and 1990s, almost twenty Phase I and Phase II clinical studies with around 400 subjects were conducted with daptomycin, presenting highly encouraging results against bacteremia and skin and soft tissue infections [49]. The results for the treatment of endocarditis suggested a higher dosage of daptomycin would be required, but upon testing this increased dosage (at 4 mg/kg every 12 hours), Eli Lilly observed cases of reversible skeletal muscle toxicity and ceased its development of daptomycin in 1991 [5, 49, 55, 56]. Unfortunately, at this point in time, the rise of bacterial resistance to common drugs continued, which prompted Cubist Pharmaceuticals Inc. (Lexington, Massachusetts, USA) to step in.

In 1997, Cubist took over daptomycin research and development by licensing worldwide rights from Eli Lilly [6, 7, 57]. Cubist believed that the first step was to find the optimal dosing regimen of daptomycin, which is exactly what they did. In order to determine what kind of dosing regimen would have the least effect on skeletal muscle, two separate studies were conducted with dogs to compare repeated intravenous daptomycin administration once-daily (intervals of 24 hours) versus twice-daily (intervals of 8 hours) for a total period of 20 days [58]. Parameters such as dosing interval, drug concentration in the plasma and concentration-time curve areas were examined, but the results showed that the strongest correlation was between skeletal muscle toxicity and dosing intervals [58]. From their data, Cubist determined that a once-daily dosing regimen appeared to minimize skeletal muscle toxicity, and further licensing studies and clinical usage confirmed their findings, since skeletal muscle toxicity only arose in rare cases [6, 58].

Figure 1.4 Vials of Cubicin® and Cubicin® RF. Daptomycin is available under the trademarked name Cubicin®, once-a-day daptomycin for injection. Although these two different formulations have different methods of reconstitution and storage requirements, both have the same indications, limitations of use, and general performance.

Moving on to Phase III clinical trials, Cubist decided to test the safety and efficacy of daptomycin in the treatment of complicated skin and skin structure infections (cSSSIs) caused by Gram-

positive pathogens [49, 57, 59]. The drug would be tested against those of current standards of widely used drugs, such as vancomycin, that targeted the same types of cSSSIs. Two randomized, international trials were performed with 1092 patients who had contracted cSSSIs. Before randomization, the investigator assigned one of two comparator drugs (either a penicillinase-resistant penicillin (PRP) or vancomycin) to each treatment group to be compared with daptomycin [59]. Once randomized, patients in each group would receive daptomycin (through a 30-minute intravenous infusion at 4 mg/kg) or, depending on which group, either PRP (4-12 g daily in equally-divided intravenous doses) or vancomycin (1 g twice-daily 60-minute intravenous infusions) [59]. At the end of the clinical trials, it was determined that among the 902 clinically evaluable patients, the success rate for daptomycin was 83.4% compared to the comparator-treated groups of 84.2% [6, 59, 60]. However, 63% of those patients successfully treated by daptomycin only required less than a week of therapy, whereas only 33% of those who took the comparator drugs had recovered within that time frame [6, 59]. This meant that daptomycin was just as good as the other drugs already in use, being safe and efficient for treatment with cSSSIs [59].

Around the time that these Phase III clinical trials were performed, daptomycin (marketed as Cubicin® by Cubist, see ***Figure 1.4***) gained Food and Drug Administration (FDA) approval from the United States of America in September 2003 [5, 10, 47]. Additional approval by the European Medicines Agency (EMEA) was granted in January 2006 for the use of daptomycin in treating cSSSIs caused by Gram-positive pathogens with a once-daily dosage of 4 mg/kg [5, 6]. In March 2006, further FDA approval was granted for the use of daptomycin at a once-daily dosage of 6 mg/kg to treat bacteremia and right-sided endocarditis caused by *Staphylococcus aureus* [5, 6]. Currently, studies are still underway to further elucidate daptomycin's mechanism of action.

1.3.2 Mechanism of Action

Daptomycin is the a clinically-approved drug from a class of antimicrobial peptides called the cyclic lipopeptides [47]. Its distinctive structure (13-member amino acid cyclic head and decanoyl side-chain lipophilic tail) allows daptomycin to have a novel mechanism of action [6, 61]. Its acidic nature and negative charge at neutral pH allow it to be highly soluble in aqueous solutions, while its lipid tail and hydrophobic amino acids give it its amphipathic properties [4]. Although its precise mechanism of action is still unclear, it is distinct from other antimicrobial peptides as it does not kill bacteria by penetrating the cytoplasm, but rather by disrupting multiple aspects of the bacterial plasma membrane [5, 36, 49].

For the past couple of decades, there have been various studies that have tried to determine daptomycin's precise mechanism of action. One of the first studies reported that daptomycin caused bacterial cell death by inhibiting the formation of precursor molecules required in peptidoglycan biosynthesis [62]. Later, studies suggested that daptomycin targeted the lipoteichoic acids on the surface of Gram-positive organisms [63-65]. These latter models were refuted when further studies showed that bactericidal activity against various bacterial isolates was still present in the absence of peptidoglycan and lipoteichoic acid synthesis [61, 66].

In the late 1980s, a new proposed mechanism of action for daptomycin was suggested (see *Figure 1.5*), one that was more complex than its predecessors and is now a primary focus of much research in determining the specifics of daptomycin's mechanism of action [62]. This proposed multi-step mechanism of action involves the calcium-dependent binding of its tail and subsequent insertion into the cell membrane of Gram-positive bacteria [61]. An oligomerization event occurs where daptomycin oligomerizes to form ion channels, pores or aggregated structures that trigger a depolarization event [4, 61]. This disrupts the membrane's functional integrity, which in turn causes an arrest of DNA, RNA and protein synthesis and ultimately bacterial cell death [56, 61, 65, 67]. This oligomerization event was recently demonstrated, where

membrane lesions were shown to be caused by daptomycin oligomers on model membrane vesicles [68].

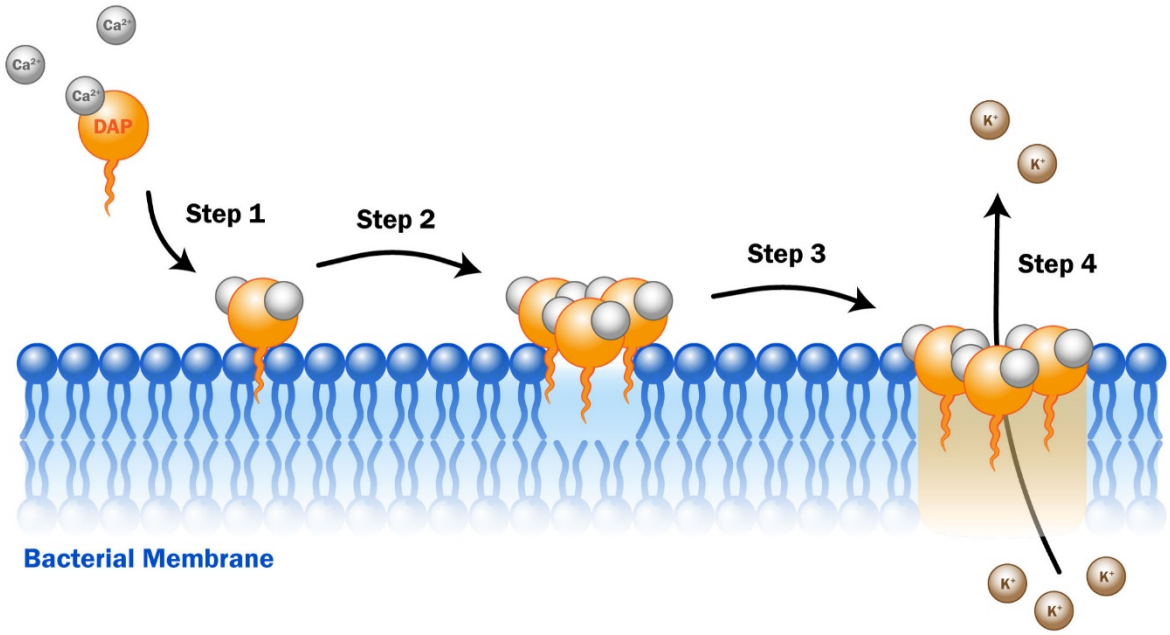

Figure 1.5 Proposed model of daptomycin's mechanism of action. Daptomycin has a proposed distinct mechanism of action which physically changes the bacterial membrane and causes rapid depolarization. The steps shown in the figure represent a general overview of the different stages of this mechanism: (1) daptomycin inserts into the bacterial membrane upon binding to calcium, (2) daptomycin oligomerizes on the surface to (3) form an ion channel that disrupts the functional integrity of the cytoplasmic membrane by (4) triggering a release of intracellular potassium (K^+), which causes rapid cell death (Adapted from [61]).

It is clear that daptomycin's mechanism of action is calcium-dependent, since its bactericidal activity is at its highest at a calcium concentration of around 50 mg/L, a level comparable to the free Ca^{2+} concentration in human serum [50, 69-71]. It is also clear that daptomycin has rapid bactericidal effects as it is capable of killing over 99.9% of MRSA bacteria within the span of an hour [61, 67, 72, 73]. But several questions still need to be answered to help elucidate daptomycin's mechanism of action, such as its possible interference with cell activity and its

structure-activity relationships. Of particular interest is the unique inhibition of daptomycin when it is used treat community-acquired pneumonia caused by *Streptococcus pneumoniae*.

1.3.3 Organ-Specific Inhibition of Daptomycin within the Lungs

As an FDA-approved member of the lipopeptide antibiotic family, daptomycin has a unique mechanism of action that is powerful against Gram-positive bacteria, even those that are resistant to common therapeutic drugs such as vancomycin and methicillin [10]. *Streptococcus pneumoniae*, or *Pneumococcus*, is one of these Gram-positive bacteria that is susceptible to daptomycin. In fact, the minimum inhibitory concentration to kill 90% of the *S. pneumoniae* isolates tested *in vitro* was 0.06 μg/mL [74]. Accordingly, one would expect daptomycin to be very potent in treating community-acquired pneumonia, whose main causative agent is *S. pneumoniae* [75]. However, this is not the case.

During Phase III clinical trials, studies were conducted for patients with community-acquired pneumonia, but daptomycin failed to meet the noninferiority criteria against its comparator ceftriaxone [10]. But how could daptomycin be efficient against *S. pneumoniae in vitro* but not *in vivo*? Daptomycin's low efficacy against this disease has been attributed to its inhibition by pulmonary (lung) surfactant, a crucial component of the lung's alveolar air-liquid interface [10].

This lung surfactant (see ***Figure 1.6***) is a phospholipoprotein complex, whose primary constituent is dipalmitoylphosphatidylcholine (DPPC), along with other surfactant proteins and neutral lipids [76-78]. It is synthesized by type II alveolar cells and forms a monolayer lipid film that coats the air-liquid interface of the lung's alveoli [79]. Apart from increasing pulmonary compliance by reducing alveolar surface tension to facilitate lung inflation and deflation during respiration, lung surfactant also plays a role in pulmonary innate immunity, which is an important function since the lung is constantly exposed to air that is contaminated with microbes [80]. But how exactly does daptomycin get inhibited by the thin film surfactant inside our lungs?

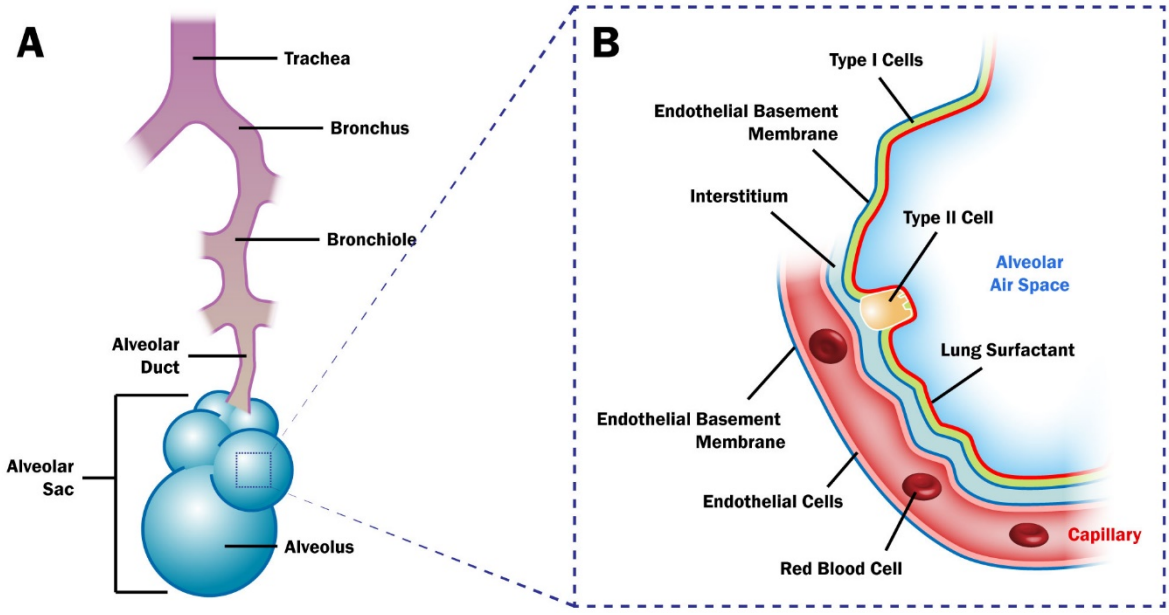

Figure 1.6 Lung surfactant lines the alveolar air-liquid interface. (A) When we breath, the air we inhale and exhale travels through a respiratory tree of different structures: trachea, bronchus, bronchiole, alveolar duct, to the alveoli within the alveolar sac. Each alveolus is hollow and is a basic unit of respiration, since it is located at the end of the respiratory tree. (B) At each alveolus gas exchange occurs at the alveolar membrane, which has direct access to capillary beds. This allows for the rapid diffusion of carbon dioxide and oxygen molecules. While alveolar Type I cells form the structure of the alveoli, Type II cells secrete lung surfactant, which covers the surface of the alveolus to reduce surface tension and enhance lung compliance.

The answer lies in the composition and vast amount of lung surfactant lining our alveolar surfaces. Lung surfactant is made up of primarily phosphatidylcholine (PC) and approximately 10% phosphatidylglycerol (PG), amongst low levels of other lipids and molecules [76-78]. Not only is PG found in Gram-positive bacterial cell membranes, but daptomycin is known to interact with lipid vesicles of pure PC at high levels of calcium, with the presence of PG enhancing daptomycin insertion into the membrane [10, 81]. With there being hundreds of millions of alveoli inside the human lung, the vast amount of pulmonary surfactant covering the alveolar surface area greatly exceeds the surface area of any bacterial cells [10]. If daptomycin cannot differentiate between lung surfactant and the bacterial cell surface, then the huge amount

of lung surfactant with some PG content will certainly sequester the daptomycin, preventing it from attaching to the bacteria and effectively inhibiting its bactericidal activity [9, 10, 82]. This is now presumed to be the first case of organ-specific inhibition of an antibiotic [10], which means that further research will need to be performed to better understand daptomycin's precise mechanism of action and prevent its sequestering by lung surfactant.

1.3.4 Brief Overview of Recent Studies

Many studies have been done on daptomycin in recent years to shed light on daptomycin's structure, mechanism of action, and bactericidal activity. The following subsections will review different categories of recent advances in daptomycin research.

1.3.4.1 Structural Studies

Daptomycin was discovered in the early 1980s as a fermentation product of *Streptomyces roseosporus* [7]. Since then, there has been an ongoing quest to elucidate its three-dimensional structure and its mechanism of action [83].

Daptomycin is a cyclic lipopeptide that is the only one of its class to be approved for clinical use. It has 13 amino acid residues (see ***Figure 1.3***): tryptophan (Trp-1), D-asparagine-2 (Asn-2), aspartic acid-3 (Asp-3), threonine-4 (Thr-4), glycine-5 (Gly-5), ornithine-6 (Orn-6), aspartic acid-7 (Asp-7), D-alanine-8 (Ala-8), aspartic acid-9 (Asp-9), glycine-10 (Gly-10), D-serine-11 (Ser-11), (2S,3R)-3-methylglutamic acid-12 (mGlu-12), and kynurenine-13 (Kyn-13) [81, 84-86]. Daptomycin's 10-membered ring is formed by amino acids Thr-4 to Kyn-13, where an ester bond between the hydroxyl group of Thr-4 and the *C*-terminal carboxyl group of Kyn-13 links the amino acids into the shape of a ring [81, 84, 86]. Meanwhile, the decanoyl side chain branches off at the *N*-terminal residue, Trp-1 [84, 86]. It is also important to note that with one basic

amino acid residue (Orn-6) and four acidic residues (Asp-3, Asp-7, Asp-9, mGlu-12), daptomycin possesses an overall molecular charge of -3 at neutral pH level [81, 86].

Numerous studies have been performed that focus on the structure of daptomycin, whether it be the properties of its amino acids or its three-dimensional structure and orientation through aggregation. In its native state without calcium, daptomycin is known as apo-daptomycin and detailed nuclear magnetic resonance (NMR) spectroscopic studies have been performed to elucidate its three-dimensional structure. NMR spectroscopy is especially useful in determining the composition of organic compounds, since it is capable of determining the entire structure of one molecule using just one set of analytical tests [87-89]. Using an isotope with a nuclear spin of $I = ½$, such as hydrogen-1 (^{1}H) or carbon-13 (^{13}C), we can see whether it is at a lower or higher energy state depending on whether it aligns itself with or against the magnetic field it has been placed in, respectively [88]. Should a nucleus in a lower energy state be present, electromagnetic radiation can be applied whose energy is absorbed, allowing that particular nucleus to jump to a higher energy state. This means that we can either observe the absorption of energy that the nucleus receives, or the subsequent release of energy when the electromagnetic radiation has been emitted (the relaxation stage where the nucleus returns from a higher energy state to a lower energy state) [88].

In real molecules, the magnetic field experienced by each nucleus includes not only the applied magnetic field, but also the magnetic effect of nearby nuclei and electrons [88]. Therefore, it is common practice to reference the resonant frequencies against a zero standard, usually tetramethylsilane (TMS) for ^{1}H NMR spectra [90]. In NMR spectroscopy, a series of peaks (the NMR spectrum) is obtained and plotted as absorbance versus frequency. The difference between the TMS zero standard point and each peak frequency is known as the chemical shift in parts per million (ppm), and these can be compared to characteristic chemical shifts of known atoms and functional groups [87, 88, 90]. As a result, the structure of a particular molecule can be easily determined.

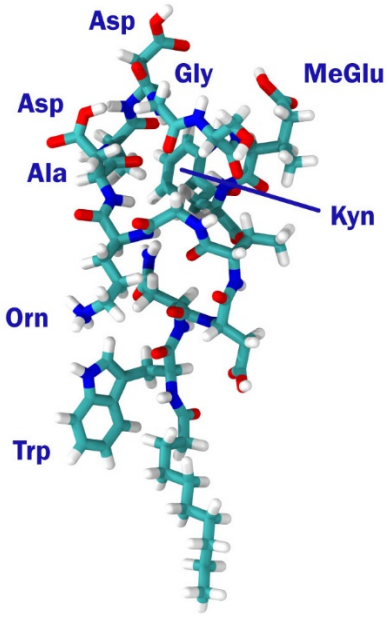

Figure 1.7 3D structure of apo-daptomycin. This three-dimensional structure of apo-daptomycin (in its native state without calcium bound to it) was obtained using the lowest energy results from NOESY spectra in 2D NMR spectroscopy (Adapted from [84]).

In a study from 2004, apo-daptomycin was shown not to have a well-defined conformational structure in aqueous solution [81]. In a later study, this structure was determined through 2D NMR spectroscopy, in which two frequency axes were used as opposed to the one in 1D NMR [84]. For 1D experiments, NMR spectra were measured with a 0.8 mM concentration of daptomycin and both ^{1}H and ^{13}C chemical shifts (ppm) were reported for each amino acid residue of the molecule [84]. Subsequently, 2D NOESY (Nuclear Overhauser effect spectroscopy) spectra were obtained to gain insight into protein structure since it uses the dipolar interaction of spins to correlate protons depending on their distance from one another [88]. Through the NOESY spectra obtained, 20 structures with low energy were ultimately determined, but with further conformational analysis, Ball *et al.* were able to determine its best-quality structure, illustrated in ***Figure 1.7*** [84]. This structure showed that apo-daptomycin has an extended conformation, with the majority of the side chains in the cyclic head protruding out

and away from the cyclic core [84]. It was also shown that the decanoyl chain has a high degree of conformation freedom [84].

To further test daptomycin's structure, Ball *et al.* also obtained NMR spectra for daptomycin in the presence of calcium at different molar equivalents. Although the resonances of daptomycin were broadened, a close analysis of the data obtained indicated that the addition of calcium ions did not cause any discernable changes to the chemical shifts at each resonance [84]. In particular, at one molar equivalent of calcium, increasing the temperature from 293 K to 313 K narrowed the broadened spectra of daptomycin, indicating less binding to calcium, but when the temperature was brought back to 293 K, the original broad spectra was obtained, indicating the reversible effect of calcium binding to daptomycin [84]. 2D NMR spectra were also obtained and showed that daptomycin did not go through any conformational changes upon binding to calcium and that the stoichiometry of Ca^{2+} binding to daptomycin is 1:1 [84].

A similar study was done in 2005, where another best-quality structure of apo-daptomycin was suggested [91]. Though overall this structure was similar to the one presented by Ball *et al.*, this group suggested that clustering was existent between amino acid residues Trp-1 and Kyn-13. More thorough analysis and investigation from this group resulted in a higher quality and informative structure of apo-daptomycin that is comparable to the one shown in ***Figure 1.7***. As seen with the previous study, this structure shows that the backbone amide groups seem to be shielded from solvent, which is likely to play a role in enhancing the lipophilicity of daptomycin and thus its penetration into a cell membrane's hydrophobic environment [91].

After the three-dimensional structure had been determined, more focus was placed on the effect of calcium on the structure of daptomycin. Previous studies had shown that calcium led to line broadening in NMR spectra which indicated daptomycin aggregation [84, 91], but a study by Ho *et al.* in 2008 focused on the effect of divalent cations (calcium and magnesium) on daptomycin's structure and aggregation state. Through NMR techniques, the 1:1 stoichiometric ratio for calcium binding to daptomycin was confirmed and it was determined that a 5 Mg^{2+} : 2 DAP

stoichiometric ratio for magnesium ions was required for daptomycin aggregation [92]. Minimum inhibitory concentrations (MICs) for daptomycin were also determined using a microtitre broth dilution method for different divalent cations. The results show that the MIC increased by at least 32-fold when a divalent cation other than calcium was used, signifying much weaker interactions between those cations versus calcium with daptomycin [92]. However, there were also similarities when substituting calcium with other divalent cations. When comparing the structural changes between calcium or magnesium ions binding to daptomycin, there was very little change between those spectra and that of apo-daptomycin [92]. Also, when either of the divalent cations were added to daptomycin, the formation of micelles was observed in both cases, which makes sense due to daptomycin's amphiphilic properties [92, 93].

Various other studies have also been done to further elucidate daptomycin's structure and its conformation in different scenarios through the use of different techniques [83, 84, 86, 91-94]. One study involved the determination of pKa values for ionizable amino acids residues in daptomycin [86]. Another recent study used various methods to evaluate daptomycin's aggregation in the presence of calcium [94]. Fluorescence spectroscopy analyzes the fluorescence of a sample through the emission of light after excitation [95]. In this study by Qiu *et al.*, they exploited the fluorescence resonance energy transfer (FRET) between the two fluorophores, Trp-1 (donor) and Kyn-13 (acceptor), to determine the critical aggregation concentration of daptomycin at various pH levels, which were confirmed by NMR spectroscopy and dynamic light scattering. Of significance is their data obtained at physiological conditions of pH with varying calcium and daptomycin concentrations. Their results showed that daptomycin aggregated when concentrations of 0.06 mM daptomycin and 1.0 mM calcium ions were used at a pH of 7.4 [94]. This means that daptomycin does aggregate under normal physiological conditions and may be a part of its mechanism of action.

Although it is important to understand the structure of daptomycin, it is of even more importance that we understand how that structure is connected to its activity or mechanism of action. With us beginning to understand the three-dimensional structure of daptomycin, more

questions arise as to how it actually aggregates and how these structures interact with the bacterial membrane to carry out their bactericidal role.

1.3.4.2 Membrane Interaction Studies

Since daptomycin's development, there has always been one puzzling question that has plagued researchers studying this novel antimicrobial peptide: how exactly does daptomycin work? In 2003, Silverman *et al.* proposed a multistep model for daptomycin's mechanism of action after studying the correlation between daptomycin's bactericidal activity and the dissipation of membrane potential on bacterial membranes. With their interest triggered by a previous study about how daptomycin could reduce the membrane potential of *Staphylococcus aureus* [96], Silverman's group decided to re-evaluate daptomycin's effect on membrane potential through the use of fluorimetry and flow cytometry techniques. In the former, a fluorescent probe $DiSC_3$ was used as it is sensitive to membrane potentials, being attracted to the surface of polarized cells. A depolarized environment would not allow the dye to partition to the surface of the membrane, releasing it into the medium and increasing the fluorescence signal [97]. Accordingly, membrane depolarization will be observed as an increase in fluorescence intensity. This was exactly the case with daptomycin when 5 μg/mL of daptomycin were incubated for 0, 15, 30 and 60 minutes; $DiSC_3$ fluorescence intensity at 670 nm increased very strongly [61]. Flow cytometry and cell viability testing were also performed to confirm the results of the fluorimetric assay. All three tests showed that daptomycin indeed dissipates the membrane potential in *Staphylococcus aureus* cells, with full membrane depolarization being observed between 30 to 60 minutes [61]. Further testing by this group involved determining what would cause membrane depolarization. It must have been some kind of ion movement across the cytoplasmic membrane, so they added a potassium-sensitive fluorescent probe PBFI to a suspension of *S. aureus* cells to test potassium efflux due to daptomycin [61]. Both a signal increase and cell viability decrease were observed upon addition of daptomycin to the bacterial cells, suggesting

that potassium efflux plays a role in daptomycin's mechanism of action [61]. However, this does not mean that the membrane pores are K^+-selective.

A new study has shown that sodium influx is the primary cause of depolarization under typical *in vivo* conditions, complementing the potassium efflux upon daptomycin insertion [98]. This group used fluorescence spectroscopy to study the permeability of liposomes for different cations and anions, in which they found that daptomycin permeabilized the liposome membranes in a cation-selective fashion and that the pores could discriminate between different cations according to size.

Recently, there have been various studies focusing on the interaction of daptomycin with model membranes. In one study, fluorescence spectroscopy was used to examine daptomycin's insertion into membranes [81]. Since daptomycin contains two aromatic residues that are intrinsically fluorescent (Trp-1 and Kyn-13), these properties can be exploited in fluorescence experiments. It is also important to note that upon the insertion of these residues into a less polar environment (such as that of a phospholipid membrane), an increased intensity has been observed from previous experiments [99, 100]. As a result, when determining whether daptomycin inserts into a model membrane, an increase in fluorescence for either Trp-1 or Kyn-13 would indicate insertion due to its association with a less polar environment. In the 2004 study by Jung *et al.*, an emission wavelength of 465 nm was used and the fluorescence intensity was observed for daptomycin in the presence or absence of calcium. They discovered that in an aqueous solution, daptomycin with and without calcium exhibited low fluorescence intensities, but when exposed to neutral phosphatidylcholine (PC) liposomes, a 5-fold increase in fluorescence intensity was observed for daptomycin in the presence of calcium. When they used a 1:1 PC and PG (phosphatidylglycerol) liposome combination, a 9-fold increase was observed [81]. Not only do these results show that daptomycin does insert into the membrane of lipid models, but also that daptomycin exhibits different membrane interactions with membranes composed of PC/PG and just PC [81]. The group postulated that daptomycin inserted more deeply into the mixed PC/PG liposomes than the PC liposomes.

In the same study, the researchers determined that daptomycin, in the presence of calcium, was able to induce a significant amount of lipid flip-flop in both types of lipid models [81]. This lipid flip-flop occurs when the polar head group of a lipid traverses the hydrophobic core of the membrane, essentially flipping over to the other leaflet of the bilayer membrane [101, 102]. The maximum extent of flip-flop was in correlation with the MIC for daptomycin, between 0.5 to 2.0 μg/mL [81]. With evidence of lipid flip-flop as well as insertion into model lipid membranes, the group decided to test daptomycin's induction of membrane leakage as well, using the liposome-encapsulated dye called calcein to see if it would be released upon the interaction of daptomycin with the membrane. Indeed, calcein leakage was observed at high percentages with the PC/PG liposome, but only at 10% for the PC liposomes [81]. Additional findings brought forth some modifications to the initial multi-step model for daptomycin's mechanism of action by Silverman *et al.* [61]. It was proposed that when calcium binds to daptomycin, a conformational change is induced which increases the complex's amphipathicity while decreasing its charge, allowing it to interact with neutral or acidic membranes [81]. It was proposed that once daptomycin has inserted into these membranes, an additional conformational change occurs, where calcium acts as a bridge between daptomycin and the acidic phospholipids on the lipid membrane to promote deeper insertion [81].

In a subsequent study by the same group, the interaction of daptomycin with neutral and acidic membranes in the presence of calcium ions was examined [103]. Apart from confirming their previous results about daptomycin insertion into the membrane through fluorescence spectroscopy, the phase transitions that phospholipids undergo when the structural organization and dynamics of lipids are changed was studied by differential scanning calorimetry (DSC) [103]. From the endotherms obtained, different transition peak temperatures could be attributed to changes in surrounding electrostatics in the lipid bilayer [103]. In these experiments, the group showed that a combination of electrostatic and hydrophobic interactions occurred when daptomycin was bound to neutral bilayers. Bilayers with acidic lipids primarily involved

electrostatic interactions but led to the formation of non-lamellar lipid phases and membrane fusion [103].

Another group has studied the oligomerization of daptomycin in detail. In 2011, Palmer's group used FRET between native daptomycin and a fluorescently-labelled NBD (7-nitro-2,1,3-benzoxadiazol) daptomycin derivative to prove that membrane-associated oligomers form as part of daptomycin's mechanism of action [68]. Their experiment involved measuring FRET at different ratios of daptomycin (donor) to NBD-daptomycin (acceptor), where the concentration of the latter would be kept constant. FRET efficiency was measured through a decrease in donor emission. With the PC-only lipid membranes, there was no change in FRET between donor-acceptor ratios of 16:1 and 1:1, which meant that no oligomerization occurred. Meanwhile, on the PC/PG membranes, a fourfold reduction in the Kyn-13 lifetime indicated the presence of oligomerization [68]. FRET experiments were also performed in the presence and absence of calcium, with results indicating that FRET only occurred in its presence and therefore is required for membrane binding [68].

To further characterize these membrane oligomerization events, Palmer's group used perylene excimer fluorescence, where a perylene-butanoic acid replaced daptomycin's *N*-terminal side chain [104]. Although possessing only one-third of the original daptomycin's bactericidal activity, the perylene daptomycin was capable of forming excimers (short-lived molecule between two species) to show that neighbouring oligomeric subunits were in direct contact with one another. They showed that daptomycin oligomerizes on live bacterial cells and that there was a high extent of oligomerization on model membranes that signifies these events play a large role in daptomycin's bactericidal effect. Apart from this, their results suggests that neighbouring subunits of the daptomycin oligomer are aligned parallel or at acute angles from one another and that this oligomerization event is mediated by phosphatidylglycerol [104].

In another study by the same group, daptomycin was used together with a semisynthetic derivative of A54145 (CB-182,462), which shares 5 identical and 4 similar amino acid residues

with daptomycin. Through fluorescence spectroscopy and antibacterial activity testing, they determined that the two antibiotics formed hybrid oligomers; however, the antimicrobial activity of these hybrids was reduced. This confirmed that oligomerization is required, but not sufficient for antibacterial activity [105].

Using similar techniques as before, the group also showed that lipid membranes with cardiolipin prevented membrane translocation and permeabilization by daptomycin [106]. Through FRET, it was observed that even with cardiolipin, daptomycin oligomers continued to form, but in groups of four subunits as indicated before with FRET experiments [107], which is half of what was observed on membranes without cardiolipin. They believe that cardiolipin prevents daptomycin from translocating to the inner leaflet of the lipid membrane, thus being unable to form the tetramer (the other half of the subunit) on the other side [106]. Their findings led them to suggest an updated model of daptomycin's mechanism of action (see ***Figure 1.8***) where daptomycin aggregates in tetramers on the outer leaflet of the lipid membrane and then (through lipid flip-flop) translocates to the inner leaflet until such time that an outer tetramer combines with the inner one to form an octameric pore [106].

Expanding from this proposed mechanism where bacterial membrane permeabilization involves the formation of transmembrane pores that are made of six to eight daptomycin subunits, Taylor *et al.* discovered that each daptomycin molecule sequentially binds two calcium ions, which they believe is required for antibacterial activity [108]. It was suggested that the first calcium ion encourages daptomycin to bind to the membrane, and the second calcium ion allows for deeper insertion and incorporation of daptomycin into the bacterial membrane, where it confers its bactericidal activity [108].

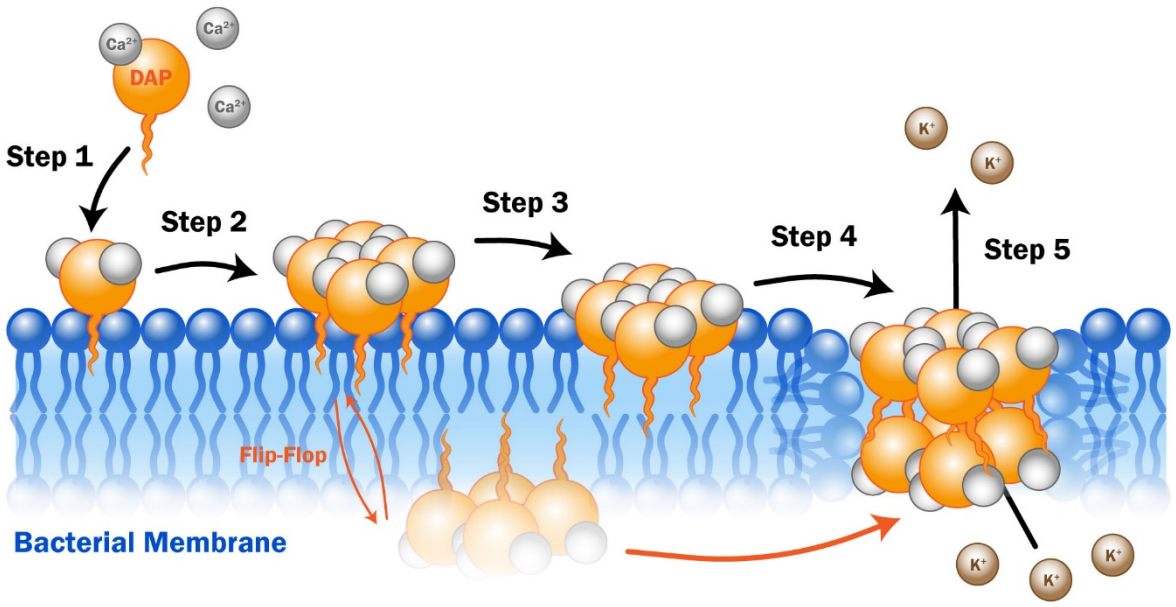

Figure 1.8 Updated model of daptomycin pore formation. This figure presents an updated model of daptomycin's mechanism of membrane insertion, pore formation and structure. (1) Daptomycin binds to calcium and inserts into the membrane as in ***Figure 1.5***, oligomerizing on the surface. (2) Daptomycin forms a tetramer on the outer leaflet of the bacterial cell membrane. (3) This daptomycin tetramer inserts itself into the membrane. (4) The absence of cardiolipin allows for deeper penetration of daptomycin into the membrane, which means that the head group of the daptomycin tetramer may very well cause a localized cave-in of the outer leaflet of the bacterial membrane. (5) Once this tetramer is situated in the membrane, it combines with another tetramer on the other side of the membrane to form an octameric pore which causes potassium ion leakage and subsequent cell death. In order to get a daptomycin tetramer on the other side of the membrane, it is posited that lipid flip-flop may occur, where the tetramer translocates to the inner leaflet. In this figure, lipid flip-flop has occurred for one daptomycin tetramer, represented by the orange arrows [106].

Another group studied daptomycin's effect on the membrane through cell biological assays [109]. They showed that daptomycin induces the formation of randomly-positioned membrane patches that are colocalized with a fluorescent daptomycin derivative. This means that they are a direct result of daptomycin's insertion into the membrane. In addition, evidence is given to show that daptomycin severely alters the shape and peptidoglycan biogenesis of the bacterial cell wall [109]. Another recent study has shown that daptomycin causes a lipid extracting effect when

interacting with giant unilamellar vesicles in the presence of calcium, but no clear conclusions could be made [110]. The group claims that this lipid extraction leads to ion permeation, but further experiments will need to be performed [110]. Transmission electron microscopy has also been used to qualitatively determine that daptomycin does not cause lysis of bacterial cell membranes [111]. Although numerous membrane interaction studies have been completed, there is a lack of these types of studies in relation to complex lipid model membrane systems.

Apart from membrane interaction studies, susceptibility testing also plays a large role in daptomycin research, especially with many questions still to be answered about its organ-specific inhibition in the lungs.

1.3.4.3 Antimicrobial Susceptibility Testing

Although the action mechanism of daptomycin has not been clearly established, there are some certainties to this mystery. First of all, daptomycin's dependency on calcium to carry out its bactericidal activity has been proven in many cases [4-9, 49, 61, 67, 103, 105]. In particular, studies have shown that daptomycin's minimal inhibitory concentration (MIC) increases significantly when calcium is not present [6, 103]. This indicates that calcium is required in order for daptomycin to carry out its bactericidal action. But exactly how much bactericidal action does daptomycin confer? That's where antimicrobial susceptibility testing comes in.

Before FDA approval, a study compared the MIC and minimal bactericidal concentration (MBC) of daptomycin with other pharmaceutical alternatives such as vancomycin and gentamicin [112]. *In vitro* susceptibility tests were performed using microdilution techniques, and it was determined that daptomycin's MIC and MBC for MRSA-67 (methicillin-resistant *Staphylococcus aureus*, strain 67) were 0.125 μg/mL and 0.5 μg/mL respectively [112]. In comparison with the other drugs, daptomycin's MIC was half of theirs while the MBC remained the same [112]. These results were confirmed once again in another study that tested for the MIC and MBC for various drugs,

including linezolid and quinupristin-dalfopristin [72]. Out of all these drugs, daptomycin was the most bactericidal against the highest number of strains, meaning it had a broad range of antibacterial activity as well as efficient bactericidal qualities [72]. Many of the previous drugs had already experienced increasing resistance from the bacteria they were supposed to target.

Table 1.2 MIC values of daptomycin and comparator drugs against PRSP. Select antibiotics have been evaluated for their bactericidal activity against penicillin-resistant *Streptococcus pneumoniae* worldwide. MIC_{50} and MIC_{90} minimal inhibitory concentration values are presented for each antibiotic, as well as susceptibility and resistance of bacterial strains against each antibiotic. Daptomycin has the best combined values with low MIC_{90} and 100% susceptibility (Adapted from [113]).

Antibiotic	MIC_{50} (µg/mL)	MIC_{90} (µg/mL)	Susceptibility[a] (%)	Resistance[b] (%)
Amoxicillin-Clavulanate	≤2	8	79.2	11.9
Ceftriaxone	≤1	1	91.6	4.0
Clindamycin	≤0.06	8	64.0	34.0
Daptomycin	≤0.12	0.25	100.0	0.0
Erythromycin	4	32	25.6	72.9
Levofloxacin	1	1	98.5	1.5
Linezolid	1	1	100.0	---
Quinupristin-Dalfopristin	0.25	0.5	100.0	0.0
Vancomycin	0.25	0.5	100.0	---

[a] Refers to the percentage of strains susceptible to the antibiotic
[b] Refers to the percentage of strains resistant to the antibiotic
* Values of susceptibility and resistance may not add up to 100% due to a subset of strains that are categorized as neither susceptible or resistant to the antibiotic, but rather intermediate (susceptible/resistant only under certain conditions)

In testing daptomycin against various strains of multi-drug resistant Gram-positive strains of bacteria, it was shown that daptomycin had high activity against vancomycin-resistant enterococci (VRE) as well as various resistant strains of staphylococci [111, 113, 114]. The MIC_{90}

(MIC required to kill 90% of bacterial strains) was determined to be 0.25, 1, and 4 μg/mL for *Streptococcus pneumoniae*, *Enterococcus faecium*, and *Enterococcus faecalis* respectively [113]. Daptomycin was recorded to be the most potent compound against *S. pneumoniae* with the lowest MIC_{90} value (see ***Table 1.2***), but an *in vitro* study showed that there was no bactericidal activity against this bacterium in cases of community-acquired pneumonia [10, 113]. It was discovered through microdilution techniques and fluorescence spectroscopy that daptomycin interacts with and is sequestered by the pulmonary surfactant found within the alveoli of the lungs, thus marking a unique example of organ-specific inhibition of an antibiotic [10]. More studies still have to be performed to elucidate this interesting case of daptomycin inhibition inside the lungs.

Nevertheless, daptomycin is still effective against many other Gram-positive infections such as complicated skin and skin structure infections, bacteremia, endocarditis, osteomyelitis, and more [115]. In the first few years of its use, daptomycin has gained much popularity due to its favourable safety and tolerability despite various treatment durations [115]. In fact, apart from its usual dosage of 4 mg/kg/day for most Gram-positive infections, doses between 8 to 12 mg/kg/day have been used for acute cases of infections [116]. Even with these high dosages, no adverse events were reported, indicating its strong efficacy and safety for clinical use [117-120].

Daptomycin has indeed shown a significant potency and activity against many Gram-positive bacteria, including those that are multi-drug resistant. It is no doubt a great alternative to the drugs afflicted by the emergence of resistant bacteria, and has been useful in treating many patients with Gram-positive infections. In fact, daptomycin was found to be active against all 833 isolates of MRSA tested in a recent study to encourage the use of daptomycin in Japan [121]. A worldwide study of daptomycin's activity against 164,457 bacterial isolates from hospitalized patients has also shown its potency against an impressive amount of Gram-positive pathogens [122].

However, with daptomycin increasingly replacing these drugs that are no longer as effective on their bacterial targets, what will happen should daptomycin fall into the same category and resistance starts to rise against it? Unfortunately, the bacterial world adapts quickly to change, and several cases have already reported daptomycin-resistant strains of bacteria.

1.3.4.4 Rising Resistance to Daptomycin

As pathogens receive more exposure to antibiotics, they build stronger resistance towards these drugs, creating barriers to prevent their own demise. MRSA (methicillin-resistant *Staphylococcus aureus*) infections are becoming more frequent, but due to an increase in resistance, it has become increasingly difficult to treat patients who are afflicted by these illnesses [123]. Vancomycin has been used against Gram-positive infections for quite some time, and decreased susceptibility has been reported in various staphylococcal strains, sparking widespread interest to create a "replacement" drug that can be just as efficient as vancomycin, but with zero or minimal resistance. Enter daptomycin, a rapidly bactericidal AMP that is approved for various Gram-positive infections at daily dosages of 4 to 6 mg/kg depending on the type of infection [123].

Although only having been on the market since its FDA approval in 2003, various reports have shown that clinical *S. aureus* strains had increased daptomycin MICs or a loss of its susceptibility [124-127]. Another study had shown that daptomycin resistance has emerged in enterococci as well, specifically *Enterococcus faecium* [128]. With daptomycin's mechanism not well understood, its mechanism of resistance is even less understood. A study by Jones *et al.* in 2008 used fluorescence techniques to compare various membrane parameters between the parental and resistant strains. They showed that the resistant isolates had enhanced membrane fluidity, increased translocation of lysyl-PG from the inner to the outer membrane leaflet, increased net positive surface charge, reduced susceptibility to daptomycin-induced permeabilization and depolarization, decreased surface binding of daptomycin, and increased cross-resistance to other

cationic AMPs [129]. But a precise understanding of daptomycin's non-susceptibility (where the MIC is greater than 1 μg/mL) has yet to be revealed.

Throughout the past decade or so, various studies have focused on the genetics of non-susceptible daptomycin strains [129-135]. Mutations in certain genes, namely: *mprF* (lysyl-PG synthetase), *yycG* (histidine kinase also known as WalK), and *rpoB* and *rpoC* (subunits of RNA polymerase) have been correlated with daptomycin non-susceptibility [130]; *mprF* mutations seemed to favour the repulsion of a functional, calcium-bound daptomycin complex [134]. This reduced drug binding has been attributed to changes in the expression or function of genes associated with cell surface charges, such as dltA, which mediates the D-alanylation of the teichoic acids of the bacterial cell wall [131, 136]. Various other studies have shown that modifications to the cytoplasmic membrane's fluidity and cell wall thickness play a role in non-susceptibility [129, 134]. In a study by Patel *et al.*, it was concluded that multiple genetic changes are associated with daptomycin resistance in Gram-positive pathogens [135]. Cell viability and gene sequencing techniques were used in a couple of experiments to show that substitution mutations in *mprF* and *yycG* induced cell wall thickening on a frequent basis [132, 135]. Such thickening was confirmed by transmission electron microscopy in other studies, which showed that the daptomycin-resistant bacterial isolates produced more cell wall, by weight, than the parental strains [131, 137]. Further studies have confirmed that strains acquire resistance in multiple steps, which include strain-dependent phenotypes, adaptations in metabolic functions and modification of lipid and protein contents of the cell wall and membrane [138]. Some proposed resistance mechanisms include repulsion, where the membrane surface charge and phospholipid content block daptomycin from binding and oligomerizing, and diversion, where cardiolipin clusters or microdomains help to trap daptomycin away from areas prone to pore formation [54].

Apart from genetic mutations, there has also been much discussion about how daptomycin could be inactivated as a mechanism of resistance from any class of bacteria. The first comprehensive analysis of such a mechanism was presented in a study by D'Costa *et al.* in 2011, which discovered

that various types of hydrolases were capable of cleaving the ester linkage of daptomycin's ring structure. Although *S. aureus* has yet to exhibit resistance to daptomycin through enzymatic hydrolysis, this group said that it is highly possible that *S. aureus* could synthesize and secrete extracellular proteases that could hydrolyze daptomycin in the future [139].

A different study focusing on the genetic, genomic and phenotypic analyses of daptomycin-resistant bacterial isolates of *Bacillus subtilis* has suggested that reduced levels of PG in the membrane would decrease the net negative charge of the membrane. As a result, this would weaken the bacterium's interaction with a positively-charged calcium-bound daptomycin complex and increase the chance of its cell survival [140]. Recently, one group proposed an additional model for daptomycin resistance amongst bacteria, specifically that of *Enterococcus faecalis* [141]. Their evidence suggested that vancomycin-resistant enterococci (VRE) use a novel strategy to avoid daptomycin killing by diverting the antibiotic molecules to distinct membrane regions and trapping them there. Fluorescence techniques and TEM were used to elucidate these cell membrane sites, which were discovered to be deficient in PG and rich in other negatively-charged phospholipids [141]. These studies on different methods of daptomycin resistance have led researchers to think about the consequences of this non-susceptibility and whether other drugs and antibiotics can be affected by bacterial evolution as well.

The notion of cross-resistance has also been touched on by several studies. It is unfortunate that when certain antibiotics share similar mechanisms of action, any resistance built up towards one type of antibiotic in that category might cross over to other antibiotics of that type. Although daptomycin has a unique mechanism of action, it still has properties of a cationic AMP once bound to calcium, and even though it may take more time to build a resistance towards daptomycin, it makes sense that this resistance could potentially carry over to cationic AMPs. This is exactly what was reported in a recent study, where it was shown that for MRSA isolates developing reduced susceptibilities to daptomycin, reduced *in vitro* susceptibilities to two other cationic AMPs were observed [132, 133]. Due to the mounting evidence of antibiotic resistance mechanisms, it is clear that future studies will need to involve more precise evaluations of how

such drug-resistance patterns can occur [142]. But in the meantime, there is another alternative to improving daptomycin's bactericidal activity should some resistant bacteria come its way.

1.3.4.5 Combination Treatments

To counter the trend toward increasing resistance to it, daptomycin has more recently been used in combination with various other antibiotics. The synergistic effects of daptomycin with various types of antibiotics have been tested against multi-drug resistant strains of *Staphylococcus aureus* and other Gram-positive bacteria. For example, a study in 2007 tested the activity of daptomycin in combination with gentamicin, another antibiotic used in the treatment of MRSA [143]. Using *in vitro* time-kill studies (a measure of bactericidal activity and killing speed for each individual bacteria or in combination), this group combined daptomycin with gentamicin at sub-MIC levels and observed synergy in 68% of the strains tested. In fact, for these successful results, a marked change in the slope of the killing curve indicated that the combination treatment of daptomycin and gentamicin was more rapidly bactericidal than either antibiotic by itself [143]. Rifampin, ceftriaxone, and some β-lactams have also been tested with daptomycin, yielding favourable results against VRE and other resistant bacteria [112, 143-157].

These results have proven useful, as rifampin has been used as an addition to daptomycin in the successful treatment of daptomycin-resistant MRSA infections such as meningitis and bacteremia [158-161]. Linezolid and gentamicin, each combined with daptomycin, have also been used to successfully treat vancomycin-intermediate *Staphylococcus haemolyticus* and VRE infections [162, 163]. Other studies have proven the efficacy of daptomycin combined with fosfomycin for the treatment of MRSA osteomyelitis and ceftaroline for the treatment of MRSA infections [164, 165]. A recent study incorporated high-dose daptomycin regimens with rifampicin to treat Gram-positive osteoarticular infections [166]. Although the clinical uses of these combination therapies have been successful, questions arise as to how and why daptomycin either enhances or is enhanced by the activity of its partnered drug.

In a study by Berti *et al.* in 2013, several β-lactams such as ampicillin and nafcillin were used in combination with daptomycin to test its relative enhancement of bactericidal activity against MRSA. Since there is high variability in the profiles of penicillin-binding proteins (PBPs) between different β-lactam antibiotics, the goal of this study was to determine whether a specific profile was associated with enhanced daptomycin activity. Using time-kill assays, this group showed that β-lactams indeed possess different potencies in enhancing daptomycin's bactericidal activity against MRSA. Their results indicated that the β-lactams exhibiting PBP1 binding enhanced daptomycin activity more than those with minimal PBP1 binding [167].

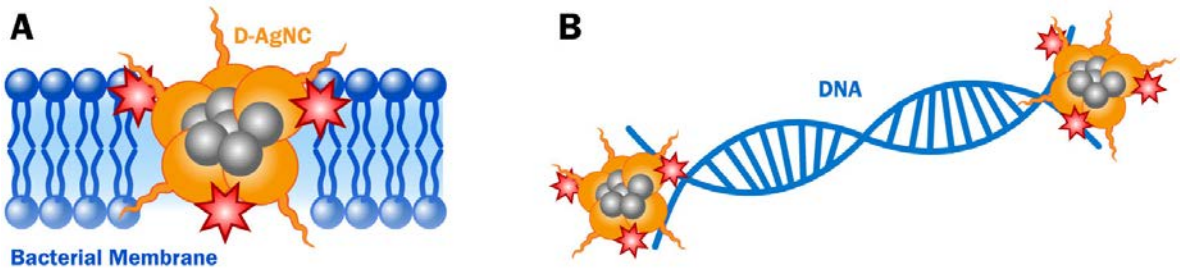

Figure 1.9 Silver nanoclusters packed with daptomycin act as antimicrobial bombs. To improve the efficacy of antimicrobial agents, integrating two bactericides into one entity could be an option for future development. This figure represents the work done by one group in designing an antimicrobial hybrid made of silver nanoclusters (AgNCs) conjugated with daptomycin. These antimicrobial cluster bombs (depicted as D-AgNC in the figure) allow for greater bacterial membrane damage through the (A) creation of larger pores due to its larger size, while (B) localized high reactive oxygen species (ROS) concentrations, shown in red, continuously generate within the bacteria and causes severe DNA damage (Adapted from [168]).

There is also a growing interest in incorporating daptomycin into antimicrobial "cluster bombs", which involve a hybrid of silver nanoclusters with daptomycin (see ***Figure 1.9***) [168]. Since silver (Ag) is known to exert a wide spectrum of bactericidal activity through a multitude of killing mechanisms [169], its combination with the antimicrobial activity of daptomycin should not only allow for enhanced antimicrobial activity but also be less prone to bacterial resistance. The results from this group showed that their novel antimicrobial hybrid obtained through silver nanocluster

and daptomycin conjugation was able to enhance the killing effect for *S. aureus*, suggesting that a synergistic killing mechanism is taking place: localized daptomycin damages the bacterial membrane in its usual way while localized silver nanoclusters can generate reactive oxygen species to oxidize the lipids of the bacterial membrane and help intensify membrane damage [168].

All of these studies reveal that daptomycin's synergistic effects are particular to each drug it is paired up with. Every antibiotic has its own mechanism of action, and the consequences of those interactions may directly promote or reduce daptomycin's bactericidal activity. On the flip side, daptomycin's mechanism of action could do the same for the antibiotic it is partnered with as well. This leads us to believe that the most common type of enhancing interaction between daptomycin and its partnered drugs would involve some kind of coupled or additive response [170]. However, further studies will certainly be required to elucidate each combination's effect on daptomycin's mechanism of action.

1.3.4.6 Daptomycin Derivatives

Various derivatives of daptomycin have been produced by Cubist Pharmaceuticals. After FDA approval of daptomycin in 2003, novel antibiotics related to daptomycin were produced for further antimicrobial screening and drug development [171]. These derivatives are important not only for determining new antibiotics that can be of clinical use, but also in determining daptomycin's mechanism of action and its inhibition by pulmonary surfactant. In one study, daptomycin derivatives were tested along with hybrid molecules of a structurally related lipopeptide called A54145, which is produced by *Streptomyces fradiae* instead of *S. roseosporus* [172]. These hybrids were obtained by swapping the coding sequences of some modules between the daptomycin and A54145 NRPS systems. Subsequently, MIC tests for bactericidal activity against *Staphylococcus aureus* were performed in the absence and presence of 1% bovine pulmonary surfactant [173]. From this study, it was discovered that, although some derivatives could exhibit

antibacterial activity in the presence of pulmonary surfactant, they were less efficient and resulted in higher MIC values. These derivative compounds were CB-182,561, CB-182,575 and A54145D with MIC values of 2, 4, and 4 μg/mL, respectively [173]. When we compare these derivative MICs to the original daptomycin compound with an MIC of 64 μg/mL in the presence of surfactant, this is a great improvement. However, in the case of an environment without surfactant, the MIC increases by 2- or 8-fold as compared to the original, indicating a decrease in bactericidal activity [173]. Experiments have yet to be performed to elucidate the difference in interactions, either action mechanisms or affinity, between daptomycin and these derivatives in the presence of pulmonary surfactant. Such information would provide further insight into daptomycin's usual mechanism of action as well as guidance for future research and development of antimicrobial drugs. In fact, a lot more research still needs to be done in order to answer the many questions we have about daptomycin and how it works.

1.3.4.7 A54145 and CB-182,462

Due to increasing bacterial resistance to daptomycin and lack of bactericidal activity in the presence of lung surfactant, there was an increasing effort to develop various daptomycin derivatives to overcome these obstacles. One study focused on the development of different hybrids between daptomycin and A54145, a calcium-dependent antibiotic that comes from the same A21978C complex as daptomycin [82, 173]. Although homologous to daptomycin, A54145 is known to be toxic [105, 174]. However, numerous hybrids and derivatives of A54145 have proven to exhibit bactericidal activity within the presence of lung surfactant [173].

One such A54145 derivative is CB-182,462 (see ***Figure 1.10***), which was found by Cubist Pharmaceuticals to be potent against *S. pneumoniae* in the presence of lung surfactant; in fact, more potent than most of the naturally-occurring molecules of A54145 (J. Silverman, personal communication). Unfortunately, CB-182,462 caused toxicity in experiments with mice, which developed kidney phospholipidosis when exposed to the drug; accordingly, the development of

462 was stopped (J. Silverman, personal communication). Nevertheless, testing this antibiotic and comparing its mechanism of action with that of daptomycin may help to shed further light into the issue of daptomycin's inhibition by lung surfactant.

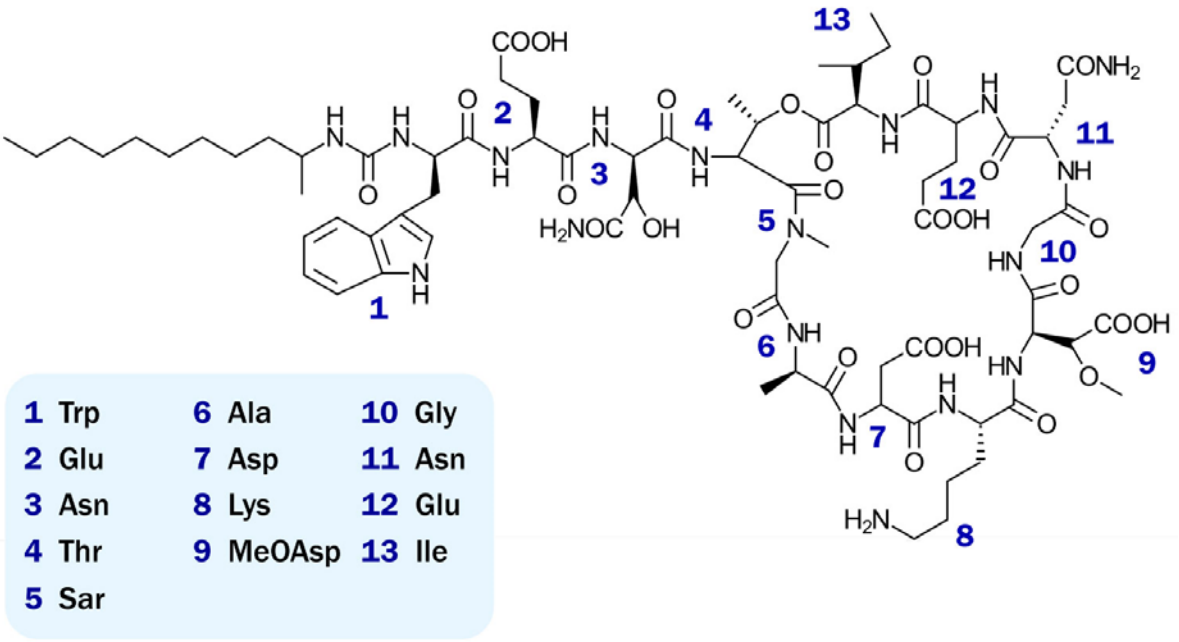

Figure 1.10 Chemical structure of CB-182,462. The compound CB-182,462 is a semisynthetic derivative of the natural compound A54145, which has the same architecture as daptomycin. As a result, CB-182,462 has a 13 amino acid chemical structure.

The structure of CB-182,462 is very similar to that of A54145, but with a substituted alkyl-carbamyl residue replacing the naturally-occurring fatty acyl residue at the *N*-terminus [105]. As it is a semisynthetic derivative of A54145, CB-182,462 will also share a number of structural features with this complex, which in turn will be comparable to daptomycin. This means that CB-182,462 has a 10-member ring, has Asp residues at positions 7 and 9 to form a calcium-binding motif, has achiral amino acids at positions 5 and 10, has D-amino acids at positions 2, 8 and 11, and has the rare amino acid 3mGlu, all structures that are shared with daptomycin. However, this also means that CB-182,462 has different amino acids than daptomycin: D-Asn is

replaced by D-Glu in position 2, L-Asp by L-HO-Asn in position 3, Gly by Sar in position 5, L-Orn by L-Ala in position 6, D-Ala by D-Lys in position 8, L-Asp by L-MeOAsp in position 9, D-Ser by D-Asn in position 11, 3-L-MeGlu by L-Glu in position 12, and finally L-Kyn by L-Ile in position 13.

Only one study has been published regarding CB-182,462, related to its use in forming a hybrid oligomer with daptomycin to test whether daptomycin's antimicrobial activity came from oligomer formation alone or additional steps to confer proper antibacterial activity [105]. There are currently no published studies on just CB-182,462 and its interaction with model membrane systems or in comparison to daptomycin.

CHAPTER 2

2 OVERVIEW OF THESIS

2.1 Research Goals

The primary objective of the research outlined in this thesis is to use advanced biological nanotechnology tools to investigate daptomycin's molecular mechanism of action and gain further insight into its inhibition by pulmonary surfactant when used to treat Gram-positive *Streptococcus pneumoniae* infections within the lung. We are interested in elucidating the interactions of daptomycin with model lipid monolayers and membranes that mimic bacterial membranes (*S. pneumoniae*), human membranes (erythrocytes), and lung surfactant.

Until now, daptomycin's general mechanism of action has been modeled as ion channel formation within the bacterial membrane, which causes membrane depolarization and subsequent cell death. Daptomycin is an extremely potent antimicrobial peptide that acts against all Gram-positive microorganisms, but somehow loses its bactericidal activity when inside the lungs, in the presence of lung surfactant.

Although additional details regarding daptomycin oligomerization and pore formation have been obtained, there is little research done to elucidate daptomycin's inhibition by lung surfactant and

why this would happen. There is a hypothesis that ascribes daptomycin's inhibition to a much greater abundance of lung surfactant than daptomycin, therefore dampening its activity or binding to lung surfactant and preventing it from attacking bacterial cell membranes. Nevertheless, daptomycin's inhibition in the presence of lung surfactant is highly unique as it is the first ever reported case of organ-specific inhibition of an antibiotic within the lungs, and it is still a problem that needs to be solved.

The specific objectives of this thesis are as follows:

1. ***Can we mimic different natural lipid membranes?*** In order to study daptomycin's interaction with different membranes, we must first develop these membrane systems. The first objective is to develop model lipid membrane systems that mimic the lipid membrane composition of *S. pneumoniae*, erythrocytes, and lung surfactant. Bovine lipid extract surfactant (BLES®) will be used as a readily-available tool to validate the lung surfactant lipid model. The development of these lipid models is the focus of ***Chapter 3***.

2. ***Is there strong binding of daptomycin to lung surfactant?*** There is evidence that daptomycin can insert into surfactant, and the widely accepted theory is that there is such a vast abundance of surfactant within the lungs (greater surface area) that daptomycin is incapable of distinguishing between lung surfactant and bacterial pathogens (with a smaller surface area) [10]. However, there is no study that compares the binding of daptomycin to different model lipid systems, specifically those of lung surfactant and bacterial membrane. Experiments that provide additional insight into this area are presented in ***Chapter 5***.

3. ***Can we quantify the changes that daptomycin insertion incurs on different monolayer models?*** Monolayers are useful models for membrane interactions. Since daptomycin can insert into lung surfactant as well as bacterial membranes, what changes

in monolayer properties does daptomycin insertion incur in each monolayer model? Even if we determine whether it has strong binding or not, the question remains as to how daptomycin affects the properties of lung surfactant after it has incorporated itself within this thin film. Thin film compression and insertion assay experiments using the Langmuir-Blodgett trough help elucidate these changes and are presented in ***Chapter 6***.

4. ***Can we visualize the changes that daptomycin insertion incurs on different monolayer models?*** Various scanning probe microscopy methods are excellent nanotechnology tools that allow for high-resolution imaging of nanoscale structures. The goal is to apply atomic force microscopy, phase imaging and Kelvin probe force microscopy techniques to obtain high-resolution topographical, phase and surface potential images of monolayers with and without daptomycin and/or calcium. These experiments will provide novel insight into the qualitative effects of daptomycin on different lipid models and are covered in ***Chapter 7***.

5. ***Can these visualizations be seen using membrane models instead?*** No model system can mimic all the properties of a natural membrane. Although lipid monolayer models are good representatives of lipid bilayers and membranes, we want to take that extra step and use liquid AFM imaging to further visualize daptomycin's interaction with model bacterial membranes and lung surfactant bilayers. This question is examined in ***Chapter 7*** as well.

6. ***How does CB-182,462 differ from daptomycin?*** Since daptomycin exhibits organ-specific inhibition in the lungs, it is a natural response for pharmaceutical companies to modify and create additional analogues of daptomycin and derivatives for testing. Cubist Pharmaceuticals, Inc. (a subsidiary of Merck & Co. since 2015) developed multiple genetically engineered lipopeptide antibiotics related to A54145, a naturally-existing lipopeptide in *Streptomyces fradiae* that has a similar structure to daptomycin [173]. A

compound that was obtained through chemical modifications, labeled CB-182,462, was shown to have potent bactericidal action against *S. pneumoniae* in the presence of lung surfactant (J. Silverman, personal communication). However, there was evidence of kidney toxicity through phospholipidosis, so its development never went forward (J. Silverman, personal communication). Although the development of CB-182,462 has ceased, comparisons of this compound's interactions versus daptomycin's interactions can provide further insight into CB-182,462's mechanism of action and toxicity. Experiments containing these comparisons are described in ***Chapters 5 to 7***.

The combined results of this thesis will help to elucidate the interaction of daptomycin and CB-182,462 with each lipid model system, confirm its calcium-dependent mechanism of action, and provide further details on daptomycin's inhibition by lung surfactant. This knowledge will provide a basis upon which other groups can expand to improve the use of daptomycin and its derivatives to treat community-acquired pneumonia more efficiently. The methods and techniques presented in this thesis can also be carried forth to future research in investigating the mechanisms of action of various different antibiotics and peptides.

2.2 Organization of Thesis

This thesis is organized into eight chapters. ***Chapter 1*** presents background information related to different aspects of the thesis topic. Meanwhile, this ***Chapter 2*** presents the overarching questions that subsequent thesis chapters seek to answer.

Part of my thesis involved the novel design and development of lipid membrane model systems that mimic different types of membranes. Relevant background information, along with rationale behind the design of each model system, is presented in ***Chapter 3***. ***Chapter 4*** presents the different methods and techniques that were used in subsequent chapters to study these lipid

membrane model systems. Appendices are included at the end of this thesis that detail various experimental protocols that were developed for this thesis work.

The thesis research projects are organized into three chapters, *Chapters 5 to 7*. *Chapter 5* looks to provide evidence of daptomycin sequestration by lung surfactant and describes how daptomycin interacts with different membrane model systems. The monolayer studies performed in *Chapter 6* aim to quantify the effect of daptomycin on different lipid model systems, specifically related to a monolayer's compressibility and changes in pressure. Finally, *Chapter 7* looks at the qualitative effect of daptomycin on the different lipid model systems by using AFM and KPFM to study topographical and electrical surface potential changes amongst different samples. Each of these research chapters is formatted as a distinct paper to be submitted for publication in a scientific journal.

All of the thesis projects are summarized in *Chapter 8*, with generalized conclusions and possible avenues for future research.

CHAPTER 3

3 DESIGN & DEVELOPMENT OF LIPID MODELS

Cellular membranes and biological thin films are highly complex, containing not only the lipid molecules that make up the bulk of their fundamental structure, but also many proteins that confer additional functionality to the membrane. Due to their intricate structure and function, biological membranes have been widely studied in an attempt to gain further insight into their capabilities. Throughout time, biological membranes have been the inspiration behind many types of lipid model systems which allow researchers to tailor their size, structure, composition and organization. Common model membranes include vesicles, supported bilayers and bilayer islands wrapped by proteins [175]. Lipid monolayers are also excellent model systems that provide insight into the interactions taking place at model membrane surfaces [176].

All biological membranes are composed of lipids, proteins and carbohydrates, with the bulk of it being a bilayer of amphipathic lipids. According to the updated fluid mosaic model and lipid raft hypothesis, there are specialized, higher-order membrane domains that are enriched in certain lipids (mainly cholesterol and sphingolipids) and proteins that can move across a sea of

lower-order lipids (see ***Figure 3.1***) [177, 178]. The theory behind the formation of these lipid rafts is constantly evolving, as more and more studies shed additional light into their structure and development. The current concept involves a reversible and dynamic process of lipid membrane nanodomains, which can form from the presence of hydrogen bonds, hydrophobic entropic forces, charge pairing, and van der Waals forces [178-184]. When these interactions are strong enough, the small structures created are called lipid rafts, which contain specific lipids or proteins that allow for compartmentalized functional platforms for various cellular functions [178, 185-189].

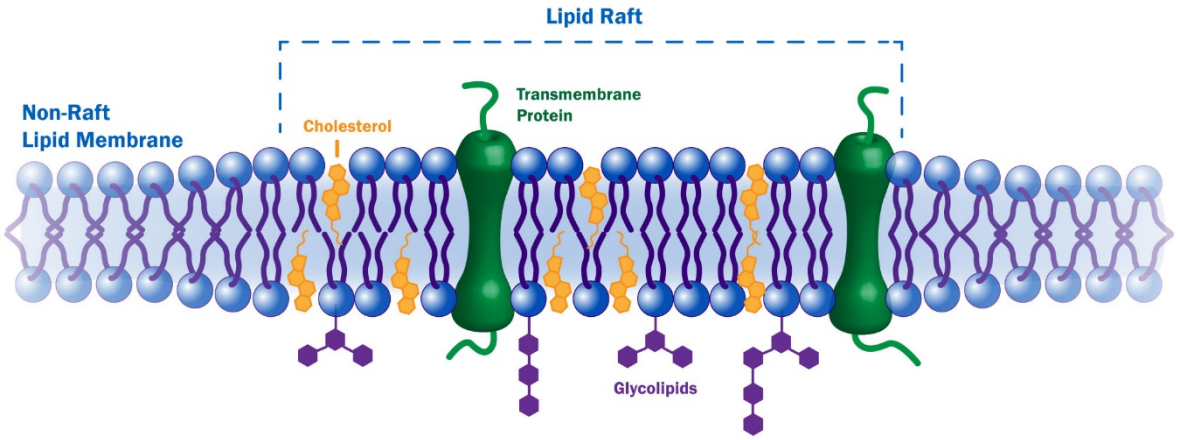

Figure 3.1 Overview of lipid raft organization. The plasma membrane of a cell has an outer leaflet and an inner leaflet. Certain areas of this bilayer are called lipid rafts, specialized membrane domains that tend to compartmentalize cellular processes. These lipid rafts are known to have high concentrations of cholesterol and sphingolipids, but every raft may not be identical due to the specific proteins or lipids contained within them. They are known to play a role in cell signalling and the regulation of membrane bioactivity [190].

The complexity of biological membranes is too much to mimic accurately in lipid membrane models, and we can only hope to mimic the functions, properties, and compositions of isolated areas within these membranes that are related to what we are studying. For my thesis, the primary goal is to further elucidate daptomycin's mechanism of action and inhibition by lung surfactant

in the context of an individual who has community-acquired pneumonia (CAP) caused by *S. pneumoniae*.

Prior to beginning any experimental work on daptomycin's mechanism of action, we must first develop lipid model systems to mimic different lipid membranes relevant to our study. In order to study daptomycin and CB-182,462's interaction with different membranes, we need to determine which types of membranes these antibiotics would interact with in reality and try to mimic these as closely as possible.

Streptococcus pneumoniae, commonly known as pneumococcus, is a leading cause of bacterial CAP [191]. Commonly residing in the upper respiratory tract of health individuals, *S. pneumoniae* can be easily spread to others via inhalation. Once it reaches the lungs (either through the bloodstream or via inhalation), *S. pneumoniae* interacts with alveolar surfaces and lung surfactant to activate inflammatory host responses [192]. Daptomycin and CB-182,462 are both antibiotics that show potent bactericidal activity against *S. pneumoniae*. However, the former is inhibited by lung surfactant and the latter is toxic to mammalian host membranes. In order to compare the effects and interactions that these antibiotics have on CAP patients, three lipid membrane model systems will need to be developed: (1) a bacterial membrane model system that mimics the lipid composition of *S. pneumoniae*, (2) a lung surfactant model system that mimics the lipid composition of human lung surfactant, and (3) a host human membrane model system that mimics the lipid composition of erythrocytes or regular tissues cells that these antimicrobial peptides may come into contact with. Since BLES® (Bovine Lipid Extract Surfactant) is readily available, our lung surfactant lipid model will be compared to our modified BLES® lipid model (the fourth model) to test the relevance of our surfactant model system.

The following sections will cover the four different lipid model systems that will be used throughout the work in this thesis as well as the determination of lipid composition of these models.

3.1 Bacterial Membrane (BM) Lipid Model

The process behind developing our bacterial membrane lipid model is multifold. First, we must understand the disease we wish to study, community-acquired pneumonia, and then look into the leading bacterial causes of this disease. Once that has been established, we can then delve into the properties of this bacterium, *Streptococcus pneumoniae*, and determine the lipid composition of its bacterial membrane. We can then choose relevant lipids and ratios to use for our simplified bacterial membrane model.

3.1.1 Overview of Community-Acquired Pneumonia (CAP)

Community-acquired pneumonia (CAP) is a severe infection of the lungs contracted by an individual that has had little to no contact with the healthcare system; it is the opposite of hospital-acquired pneumonia (HAP), which is contracted when patients spend extended amounts of time in healthcare facilities [193, 194]. CAP is the most common type of pneumonia, affecting people of all ages and walks of life. It causes the lung's alveoli to fill up with fluid due to constant inflammation [195, 196].

For the past two centuries, community-acquired pneumonia has secured its place as one of the leading causes of death due to infectious disease. In the pre-antibiotic era, *Streptococcus pneumoniae* was the culprit behind at least 95% of these cases, with mortality rates ranging from 20 to 40% [191]. In 1995, the United States of America reported over 4 million cases per year, affecting 12 per 1000 adults per year and causing annual costs of about US$23 billion [197]. After years of research and antimicrobial drug development, CAP remains a major cause of complications and death in our world. Specifically, the predominant causative pathogen has remained the same for all of these years. Although *S. pneumoniae* is detected from 5% to 35% of cases nowadays, it still remains the most commonly identified cause of CAP [193]. Other key pathogens associated with

CAP include *Haemophilus influenzae*, *Legionella pneumophila*, *Mycoplasma pneumoniae*, and *Chlamydophila pneumoniae* [193, 197, 198].

3.1.2 Overview of *Streptococcus pneumoniae* (Pneumococcus)

Streptococcus pneumoniae, or pneumococcus, is a Gram-positive bacterium that is not only a leading cause of pneumonia, but can cause numerous diseases such as meningitis, bacteremia, sepsis, endocarditis, cellulitis and brain abscesses [199-201]. It was first isolated and named pneumococcus by Louis Pasteur, a renowned French chemist, as well as U.S. physician George Steinberg in 1881 [202, 203]. As time progressed, the organism was identified as *Diplococcus pneumoniae* from 1920 to 1974, when it was renamed as *Streptococcus pneumoniae* due to its similarities to typical streptococci [204] [205].

In order for bacteria to colonize and spread throughout their hosts, they must first adhere to, multiply and invade a target tissue. As an extremely effective colonizer, *S. pneumoniae* performs these tasks with evolved mechanisms that allow it to not only adhere to respiratory epithelium and mucous, but also form pneumococcal biofilms by aggregating together and creating a protective extracellular matrix with dead cellular debris [206-208]. Although *S. pneumoniae* can exist harmlessly within the host's nasopharynx , colonization can spread to more distant sites like the lung (causing pneumonia) or meninges (causing bacterial meningitis) [201, 209, 210]. Its transition from colonization to infection is not well understood, but studies have shown that the presence of phosphatidylcholine in the bacterial cell wall allows pneumococcal cells to internalize and translocate across epithelial and endothelial cells, and that the production of pneumolysin, a cholesterol-dependent toxin, leads to cell death and desquamation [201, 208, 210-212]. All of these steps give rise to the toxic effect of *S. pneumoniae* to host cells as well as its spread and colonization throughout the host organism. Individuals who are highly susceptible to *S. pneumoniae* invasion, colonization, and infection typically have impaired immune and inflammatory responses [209].

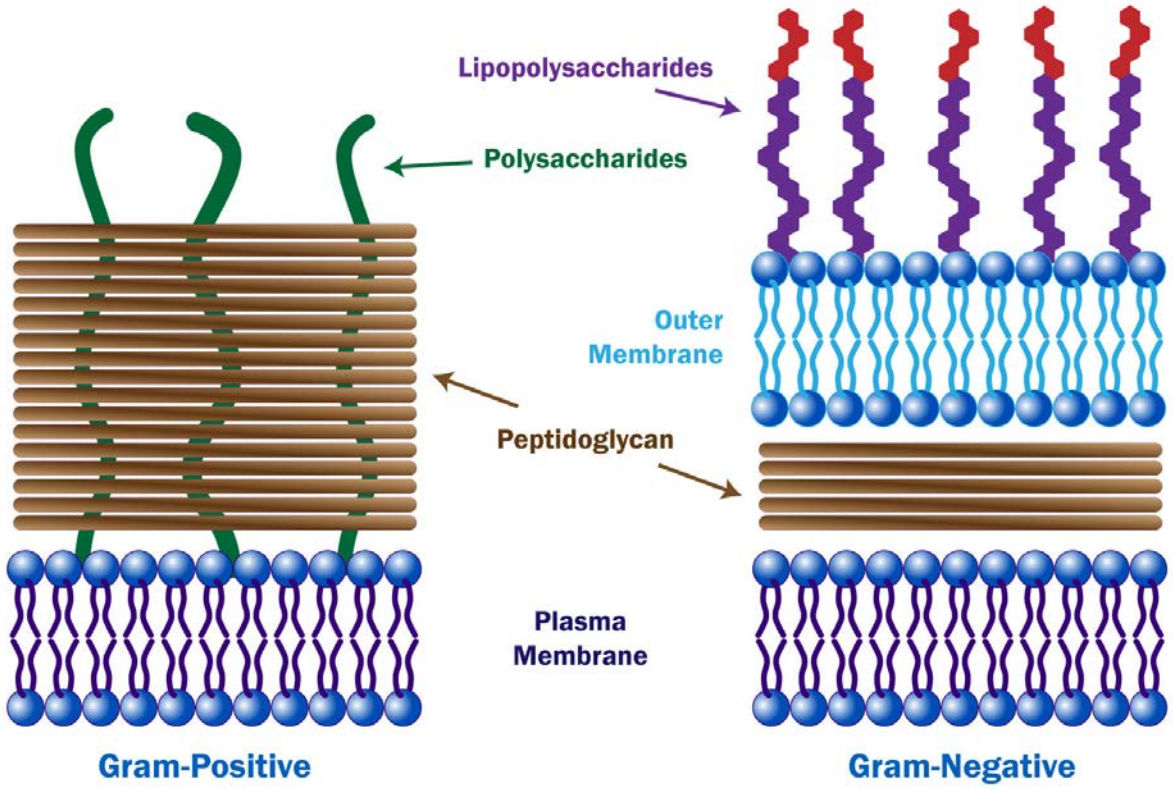

Figure 3.2 Gram-positive versus Gram-negative bacterial cell wall. Gram-positive bacteria have a thick peptidoglycan multilayer as well as teichoic acids that are anchored in the plasma membrane. Gram-negative bacteria have two membranes: the plasma membrane and an outer membrane, separated by a thin layer of peptidoglycan. Lipopolysaccharides occupy the outer envelope in abundance.

Since it is a Gram-positive bacterium, *S. pneumoniae* has a thick peptidoglycan multilayer (versus the thin, single-layer that Gram-negative bacteria have) as well as teichoic acids that form a major constituent of its cell wall. These teichoic acids are cell wall polymers that include wall teichoic acids (WTAs) that are covalently attached to peptidoglycan and lipoteichoic acids (LTAs) that span the peptidoglycan layers and are anchored to the bacterial cell membrane [213-215]. Both types of teichoic acids protrude above the peptidoglycan layer and the phosphodiester groups in the regular repeating units of these polymer chains provides the Gram-positive cell wall with a net negative charge (one negative charge per repeating unit), which is of great significance for bacterial pathogenesis, immune response, and antibiotic attraction [215-221]. Unlike Gram-

negative bacteria, Gram-positives do not have an outer membrane in addition to its inner cytoplasmic cell membrane (see ***Figure 3.2***), which also carries a net negative charge due to its lipid composition [221, 222]. The negatively charged components of both Gram-negative and Gram-positive bacteria drive the electrostatic attraction of cationic AMPs onto the bacterial surface [17].

3.1.3 Lipid Composition

The membrane of *S. pneumoniae* is no doubt very complex, including many types of proteins, carbohydrates, and lipids. However, our primary interest lies in lipid-drug interactions, so we just want to focus on the lipid composition of the cellular membrane. Although membrane proteins are essential to the function of any bacterial cell membrane, they are difficult to incorporate into a lipid model system that will be used for both our monolayer and bilayer studies since a large portion of them require the use of solid supported substrates[223].

Trombe *et al.* showed that pneumococcal membranes contain a large amount of two glycolipids, monoglucosyldiacylglycerol (MGDG) and galactosylglucosyldiacylglycerol (DGDG), two acidic phospholipids: phosphatidylglycerol (PG) and cardiolipin (CL), and a neutral lipid, diacylglycerol (DAG) [224]. A few decades later, Pesakhov *et al.* determined the lipid composition of *S. pneumoniae* under aerobic and anaerobic growth conditions. Under aerobic conditions, it was discovered for various wild type strains of *S. pneumoniae* that there were approximately equal ratios of PG to CL (approximately 15-20% of the total lipid content), while the remainder was made up of neutral molecules including MGDG, DGDG and DAG [225].

For our model, we wish to use only phospholipids and not incorporate the use of glycolipids in membrane models. As a result, we decided to substitute the group of neutral molecules (MGDG, DGDG, and DAG) with the neutral phospholipid phosphatidylethanolamine (PE), which is a principal phospholipid in most bacterial inner membranes, to better mimic the overall charge

density of the bacterial membrane lipid model [226-228]. We can then approximate the reported ratios as 20% phosphatidylglycerol, 20% cardiolipin, and 60% neutral lipids or phosphatidylethanolamine.

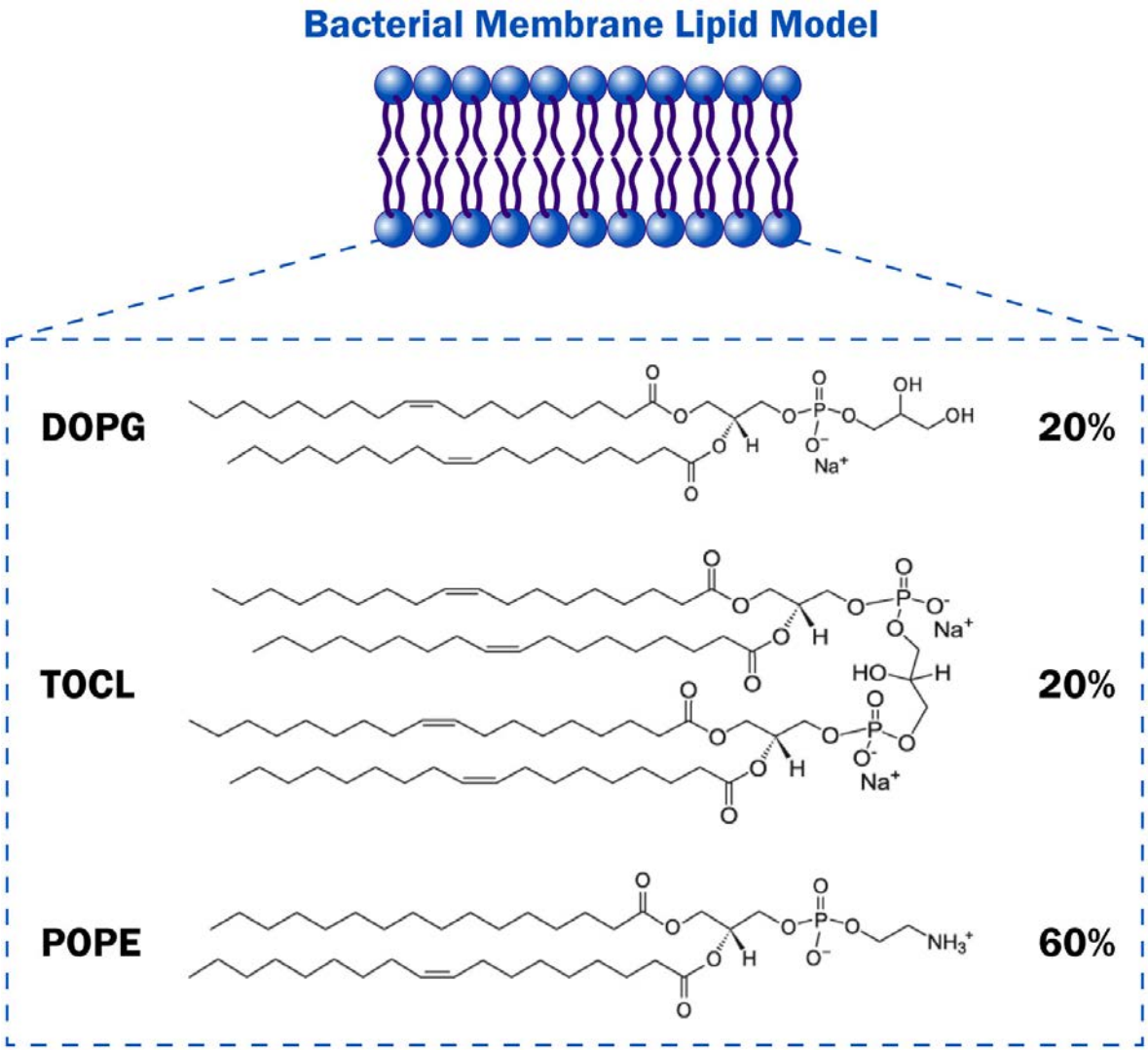

Figure 3.3 Lipid composition of bacterial membrane model system. The bacterial membrane (BM) model is composed of 20% phosphatidylglycerol, 20% cardiolipin, and 60% phosphatidylethanolamine. The chemical structures of the exact lipids used in this thesis are shown: DOPG (1,2-dioleoyl-*sn*-glycero-3-[phosphor-*rac*-(1-glycerol)]), TOCL (1,1'2,2'-tetraoleoyl cardiolipin) and POPE (1-palmitoyl-2-oleoyl-*sn*-glycero-3-phosphoethanolamine).

When looking at this bacterial membrane model of 20:20:60 PG/CL/PE, we can look at each individual lipid to determine an overall net charge for the lipid model system. As seen in ***Figure 3.3***, PG has a negative charge on its phosphate group at neutral pH, making it an anionic lipid. Under the same conditions, cardiolipin can potentially carry two negative charges since it has four acyl groups and two phosphate groups [229]. Since PE is a neutral and zwitterionic lipid at neutral pH (due to its protonated amino group and presence of a phosphate group), the bacterial membrane model carries a net negative charge under physiological conditions.

3.2 Lung Surfactant (LS) Lipid Model

Lung surfactant, or pulmonary surfactant, is a widely studied component of the lung's alveolar surface. Therefore, various models have already been created in previous studies to mimic the lipid composition of lung surfactant. Since daptomycin's bactericidal activity is inhibited in the presence of lung surfactant, it is necessary to use a lung surfactant lipid model in comparison to the other models within this thesis. An overview of pulmonary surfactant will be given in the subsequent section, followed by an overview of the models that have been studied and which one this thesis will focus on.

3.2.1 Pulmonary Surfactant

The adult human breathes in approximately 10 L of air each minute, which contains around 10^7 microorganisms [80]. Since the lung, the body's gas exchange organ, is constantly exposed to air that is contaminated with an abundance of microbes, the presence of a pulmonary innate immunity is crucial to eliminating these pathogens and maintaining an inflammation-free environment [230]. This is especially true when it comes to the lung's alveolar epithelium, where pulmonary surfactant exists at its air-liquid interface to protect it from such threats [231].

Following its synthesis by type II alveolar cells, pulmonary surfactant is stored in lamellar bodies and secreted into the alveolar space to form tubular myelin, which eventually forms a monolayer lipid film that coats the single layer of alveolar epithelial cells [232]. This lung surfactant is a phospholipoprotein complex composed of approximately 10% surfactant proteins, 80% phospholipids (mainly dipalmitoylphosphatidylcholine or DPPC), and 10% neutral lipids [233]. Its components help to fight invading pathogens and stabilize the alveoli by reducing surface tension so that they can inflate and deflate more easily with respiration [234]. More specifically, the phospholipids and hydrophobic surfactant proteins SP-B and SP-C help to promote pulmonary compliance, regulate alveolar size, and prevent alveolar fluid accumulation, while the surfactant proteins SP-A and SP-D play a direct and crucial role in pulmonary host defense [235].

There are four types of surfactant proteins that make up around 10% of lung surfactant: SP-A, SP-B, SP-C and SP-D. SP-A and SP-D are known as lung collectins that mediate innate immunity within the lung [236]. Each protein consists of subunits, each with a cysteine-containing N-terminal and CRD (carbohydrate recognition domain) surrounding a collagenous domain [237]. Three of these subunits make a trimer, which recognizes carbohydrate and charge patterns on pathogens or nonself particles. Moreover, the trimeric CRD can interact with receptor molecules that are present on various immune cells [236]. These general functions and capabilities are carried over to the lung collectins, since SP-A is formed by 6 trimers, while SP-D contains 4 trimers [237]. The key function of these lung collectins is the opsonisation of pathogens, where they bind to viruses, fungi, allergens, and both Gram-positive and Gram-negative bacteria after recognizing them through the binding motifs located on their CRDs [235]. This enhanced phagocytosis is crucial to host defence mechanisms within our lungs [235, 238-240].

SP-B and SP-C are hydrophobic spreading proteins that are essential for pulmonary compliance. SP-B plays a critical role in the reduction of alveolar surface tension to allow for easier inhalation and exhalation of the lungs [241]. Specifically, SP-B is capable of rearranging lipid molecules to reduce surface tension as well as interfere with the attractive forces between water molecules at the air-water interface [242, 243]. Without SP-B, lung conditions will develop, with the most

common being acute respiratory distress syndrome (ARDS), which is highly associated with surfactant dysfunction [244]. To help with pulmonary compliance, SP-C is a highly hydrophobic lipopeptide that inserts into phospholipids to alter their packing and facilitate a rapid spreading of surfactant lipids while imparting monolayer film stability [242, 245-247]. The particular method by which SP-C facilitates this rapid surfactant spreading is through its ability to reversibly transition a monolayer to surface-associated multilayers upon compression and expansion of the lungs [247, 248].

3.2.2 Lipid Composition

Lung surfactant has been widely studied using Langmuir monolayers as model surfactant systems [249]. These model systems tend to use dipalmitoylphosphatidylcholine (DPPC) to represent the saturated lipids and 1,2-dioleoylphosphatidylglycerol (DOPG) as the unsaturated lipids [249]. A general model for lung surfactant that has been widely used contains 70% to 80% phosphatidylcholines, 5% to 10% phosphatidylglycerols, 5% to 10% cholesterol, and additional surfactant-associated proteins [250-252]. It is important to note that, although the presence of cholesterol contributes to membrane fluidity and surfactant spreading, the presence of supraphysiological amounts of cholesterol will impair the self-assembly of lung surfactant into a functional film [252-256]. Studies with commercial surfactant BLES® (Bovine Lipid Extract Surfactant) have shown results comparable to model lipid systems of 80:20 DPPC/DOPG with 5% cholesterol by weight [250, 256-258]. The work in this thesis will also be using this model (see *Figure 3.4*).

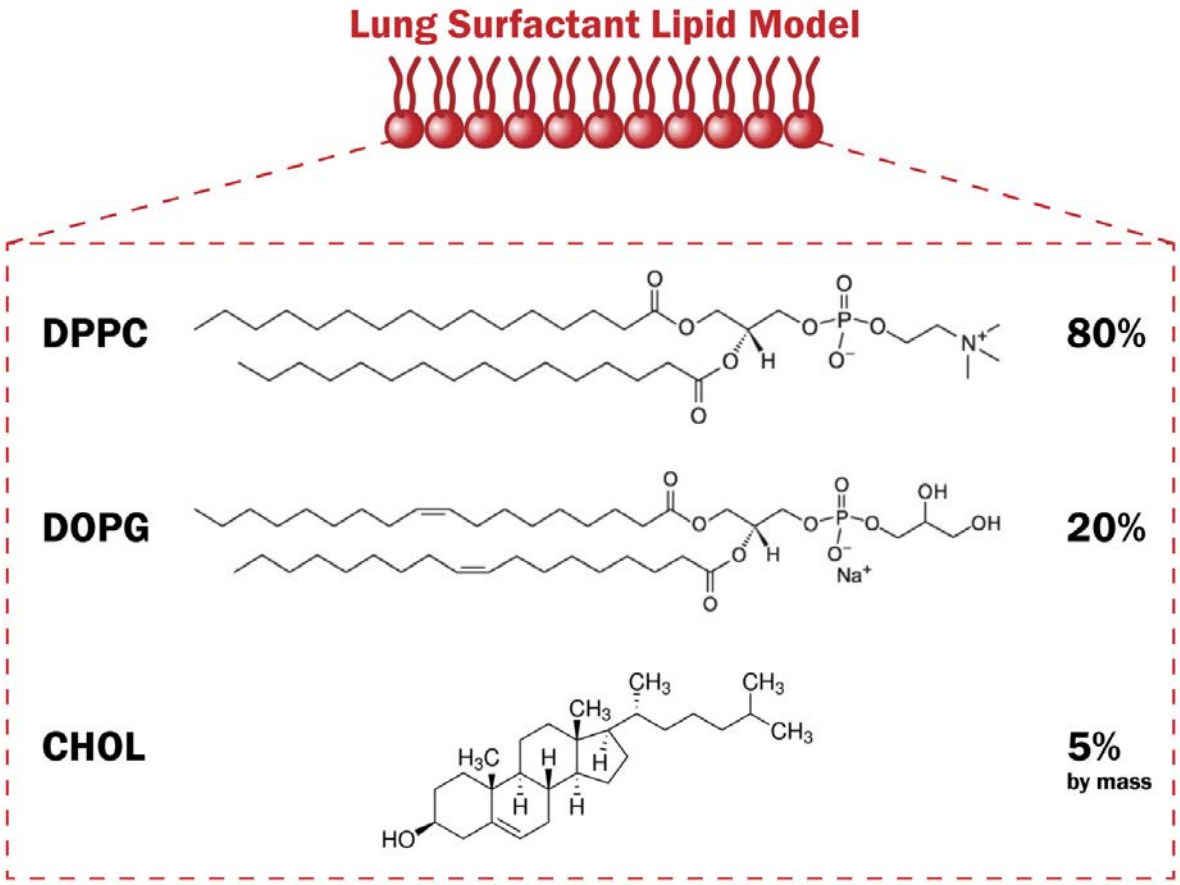

Figure 3.4 Lipid composition of lung surfactant lipid model. The synthetic lung surfactant model is composed of 80% PC and 20% PG with 5% cholesterol by mass. The exact lipids used in this thesis are shown in the figure: DPPC (1,2-dipalmitoyl-*sn*-glycero-3-phosphocholine), DOPG (1,2-dioleoyl-*sn*-glycero-3-[phosphor-*rac*-(1-glycerol)]), and cholesterol from sheep wool.

3.3 BLES® (Bovine Lipid Extract Surfactant)

Various synthetic lipid mixtures and extracts of mammalian lung surfactant have been developed to treat human patients with lung surfactant deficiencies. Natural surfactant preparations are derived from bovine or porcine lungs and contain the hydrophobic surfactant proteins SP-B and SP-C, which help with lung surfactant spreading [259]. One such natural surfactant is BLES®, Bovine Lipid Extract Surfactant, manufactured by BLES Biochemicals Inc. (London, Ontario,

Canada) and is commonly used for neonates affected by RDS [260]. Other modified natural surfactants are Curosurf® by Chiesi Farmaceutici S.p.A (Parma, Italy), Infasurf® by ONY Inc. (Amherst, New York, USA) and Survanta® by Abbott Laboratories Ltd. (Saint-Laurent, Quebec, Canada), just to name a few [261]. Compared to Survanta®, another natural bovine surfactant, BLES® was shown to achieve faster clinical responses for favourable RDS therapeutic outcomes [260]. As a result, BLES® surfactant systems were used in this thesis as a comparison to and test of validity for the purely synthetic lung surfactant lipid model presented in the previous section.

3.3.1 History and Development

BLES® is marketed as a leading treatment option for premature infants suffering from neonatal respiratory distress syndrome. It is unique because there is no generic form of this product and it is solely produced from BLES Biochemicals Inc., a Canadian-owned pharmaceutical company [262].

BLES Biochemicals Inc. was incorporated in 1992 after decades of research at The University of Western Ontario by Dr. Fred Possmayer and colleagues [262]. After years of additional drug development, their streamlined product BLES® obtained Canadian drug approval in 2002. As of 2015, they now have drug approval from India, New Zealand, South Africa (Liposurf as the brand name), Bolivia, Iran, Moldova, Ecuador and Saudi Arabia [262].

BLES® itself is bovine lipid extract surfactant, extracted from lung lavage fluid of slaughtered cows. Their unique manufacturing process involves the removal of hydrophilic proteins (specifically SP-A and SP-D), which allows for the selection of hydrophobic components such as phospholipids and surfactant proteins SP-B and SP-C, which play strong roles in surfactant spreading and fluidity [262].

When used to treat neonatal RDS in infants, BLES® is applied via intratracheal instillation at a recommended dosage of 5 mL/kg at 27 mg of phospholipids per mL [262].

3.3.2 Lipid Composition

BLES® is prepared from lung lavage collected from adult cows being slaughtered [263]. This endotracheal lung fluid is subjected to an organic solvent extraction, resulting in a final lipid composition of approximately 97% phospholipid and 3% cholesterol [264]. The phospholipids within the 97% were phosphatidylcholine at 79%, phosphatidylglycerol at 11%, and smaller amounts of phosphatidylethanolamine, phosphatidylinositol, sphingomyelin, and lyso-bis-phosphatidic acid [264]. Although a chloroform/methanol extraction was performed to remove proteins in the extracted lung lavage, the hydrophobic surfactant proteins were not affected by this extraction and approximately 10% (w/w) of the original protein content remains within the final BLES® solution [263].

Figure 3.5 BLES® surfactant from BLES Biochemicals Inc. The work in this thesis used natural BLES® (bovine lipid extract surfactant) to create a natural lung surfactant model to compare with the synthetic lung surfactant model. The lipid composition of BLES® is fairly similar to the synthetic LS model. Additional lipid extraction and filtration techniques were applied to the natural BLES® solution to create this more complex model of lung surfactant.

For the experiments performed in this thesis, BLES® obtained from BLES Biochemicals Inc. was extracted using a chloroform/methanol mixture and centrifuged a significant number of times to allow for the formation of BLES® lipid vesicles in subsequent steps. As a result, the hydrophobic surfactant proteins SP-B and SP-C would be much less than the original BLES® solution, or be present in insignificant amounts.

3.4 Human Membrane (HM) Lipid Model

Daptomycin is now a popular antibiotic used in the treatment of drug-resistant Gram-positive microorganisms. However, it is inhibited by lung surfactant in the case of community-acquired pneumonia. CB-182,462 was developed by Cubist Pharmaceuticals (prior to their acquisition by Merck & Co.) as an alternative to daptomycin that could potentially work in the presence of lung surfactant, but it failed pre-IND testing due to animal toxicity and was abandoned. This toxicity problem presented itself as renal phospholipidosis, where kidney cells accumulated excessive membrane material within the cytoplasm (J. Silverman, personal communication). However, due to the ability of CB-182,462 to overcome inhibition by lung surfactant, it was interesting to study its mechanism of action as well. For this purpose, a human membrane lipid model was developed to mimic human tissue cells, or erythrocytes. This system will help compare the toxicities of daptomycin versus CB-182,462.

3.4.1 Lipid Composition

There are many different types of host cells, so it is important to choose a type of system to model our human membrane after. As a drug that is to be injected, daptomycin and CB-182,462 will be in contact with red blood cells (erythrocytes) as well as tissue cells.

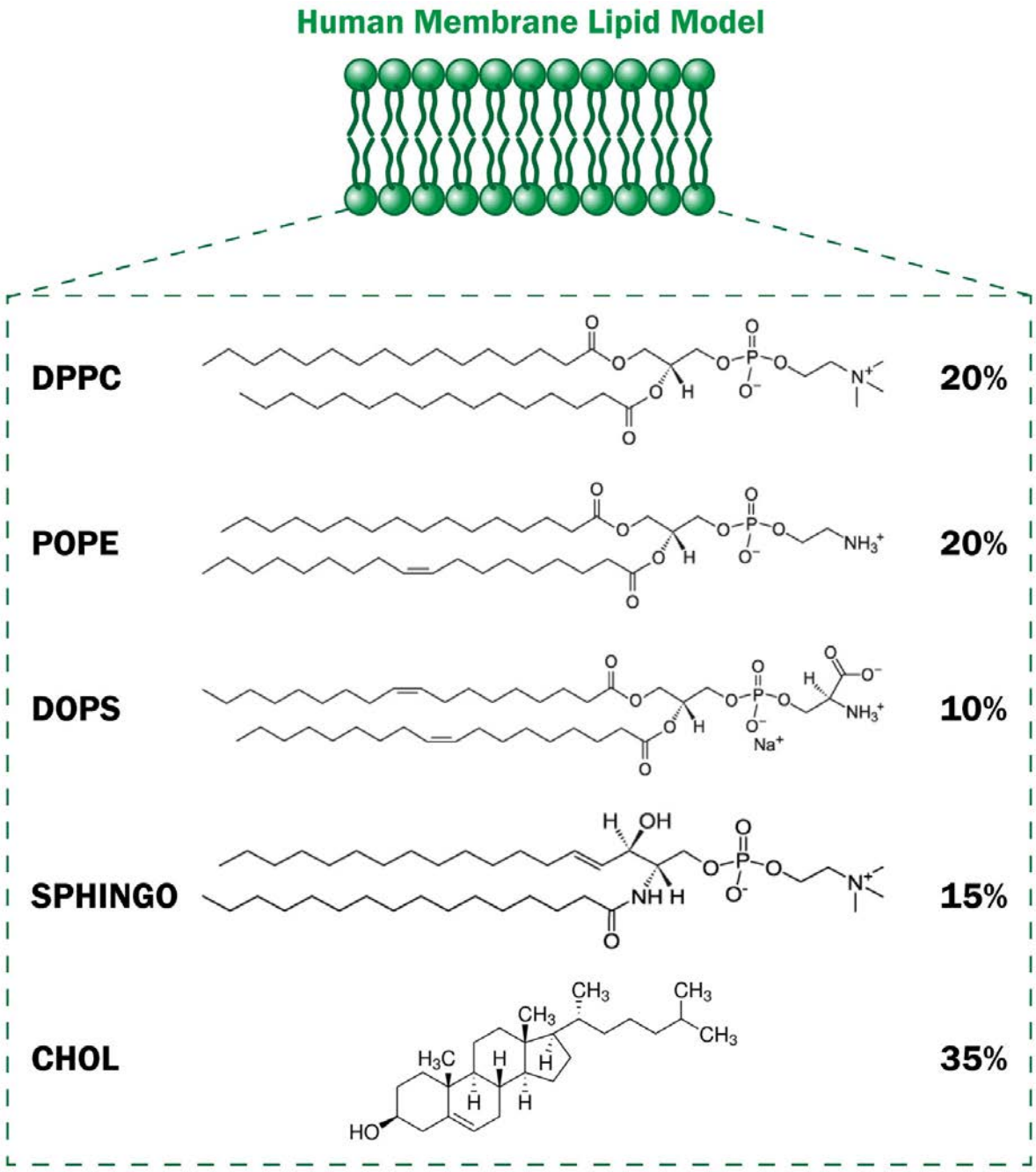

Figure 3.6 Lipid composition of human membrane lipid model. The human membrane (HM) model is comprised of five different components: 20% phosphatidylcholine, 20% phosphatidylethanolamine, 10% phosphatidylserine, 15% sphingomyelin, and 35% cholesterol. The specific lipids used in this thesis are: DPPC (1,2-dipalmitoyl-*sn*-glycero-3-phosphocholine), POPE (1-palmitoyl-2-oleoyl-*sn*-glycero-3-phosphoethanolamine), DOPS (1,2-dioleoyl-*sn*-glycero-3-[phospho-L-serine]), sphingomyelin (egg, chicken) and cholesterol (sheep wool).

The plasma membranes of human epithelial cells contain approximately 35% phosphatidylcholine (PC), 20% phosphatidylethanolamine (PE), 20% sphingomyelin (SM), and the remainder primarily consisting of cholesterol [265]. However, the presence of phosphatidylinositol (PI) and phosphatidylserine (PS) were suggested in a later study [266]. In 1985, another study showed that rat erythrocyte lipid composition consisted of 21% phosphatidylethanolamine, 3% phosphatidylinositol, 3% phosphatidylserine, 32% phosphatidylcholine, 8% sphingomyelin, and 30% cholesterol, with trace amounts of diacylglycerols and lysophosphatidylcholine [267]. In 1998, the phospholipid composition of the human erythrocyte membrane was discovered to be approximately 29.3% PC, 25.5% SM, 14.9% PS, 0.6% PI, and 27.6% PE with traces amounts of other phospholipids [268]. Other studies have also shown similar ratios, but most contain a large amount of cholesterol [269-275].

From the lipid compositions presented in previous studies for mammalian erythrocytes, a simplified human membrane model (see ***Figure 3.6***) was created for use in this thesis, consisting of 20% phosphatidylcholine, 20% phosphatidylethanolamine, 10% phosphatidylserine, 15% sphingomyelin, and 35% cholesterol.

CHAPTER 4

4 METHODS & TECHNIQUES

To study the effect of daptomycin and CB-182,462 on the different lipid membrane models presented in *Chapter 3*, various experimental methods were used to analyze the biological and physical properties of each system. Fluorescence spectroscopy was used to study the binding of these antibiotics to the different model membranes, while the Langmuir-Blodgett trough was used to study monolayer properties and antibiotic insertion. Difference atomic force microscopy methods in air and liquid were then performed to qualitatively observe any changes in physical properties of the monolayers and membranes, respectively.

4.1 Fluorescence Spectroscopy

A fluorophore is a chemical compound, most often aromatic, that absorbs and emits energy at two different wavelengths. When it absorbs an incident photon and is excited into a higher energy state, its emission (or return to a lower energy state) is called fluorescence of a photon

[276-278]. Such processes are usually illustrated through the use of a Jablonski diagram, which typically shows the single ground (S_0), first (S_1) and second (S_2) electronic states of a fluorophore, with each state having possible existence in different vibrational energy levels [276]. Transitions between states are represented by vertical lines.

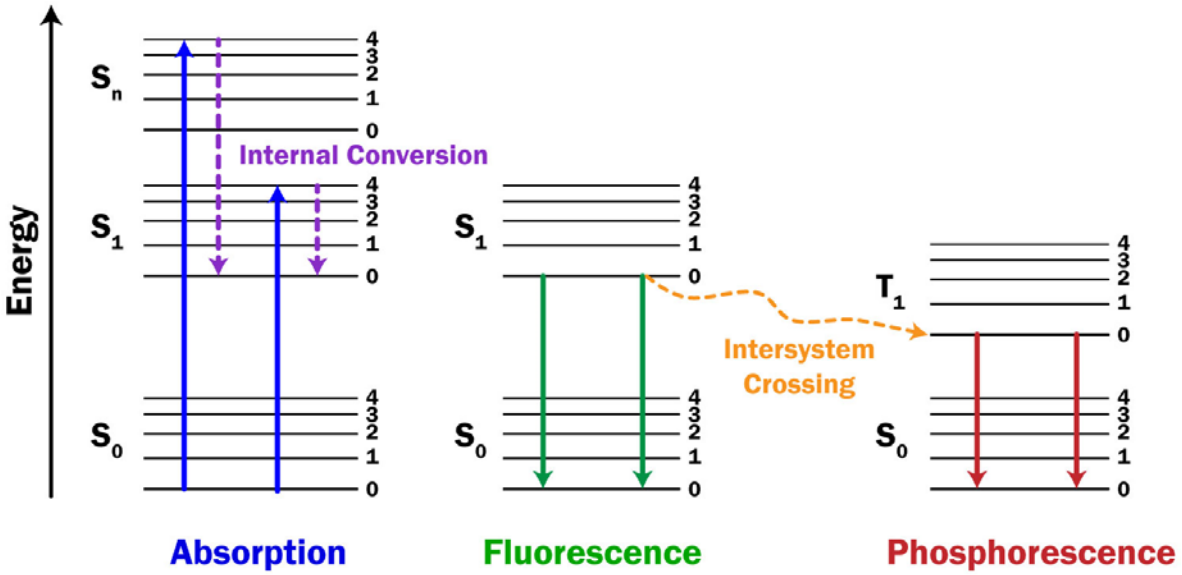

Figure 4.1 Overview of the Jablonski diagram and fluorescence emission. The Jablonski diagram is a graphical depiction of a fluorophore's electronic states and the transitions between those states. When a fluorophore is excited, it goes through a process of absorption and reaches a higher vibrational level (S_n) than its first electronic state. However, the excited fluorophore rapidly relaxes to the lowest vibrational level of its first electronic state (S_1) through a process called internal conversion. From the lowest energy vibrational state of S_1, fluorescence emission occurs as the fluorophore returns to its ground state (S_0). Sometimes, fluorophores that exist in the S_1 state can be converted into a first triplet state (T_1) due to spin conversion, a process called intersystem crossing. When this happens, phosphorescence emission occurs instead of fluorescence emission, taking place at longer wavelengths and lifetimes.

As can be seen in ***Figure 4.1***, following light absorption, a fluorophore can be excited to a higher vibrational level than its first electronic state. Prior to fluorescence emission, the excited fluorophore rapidly relaxes to the lowest vibrational level of its first electronic state through a

process called internal conversion [276-278]. It is from this lowest energy vibrational state of S_1 that fluorescence emission occurs upon the fluorophore's return to the ground state [276, 278]. Sometimes, molecules in the S_1 state convert into a first triplet state (T_1) due to spin conversion, called intersystem crossing [277]. This process results in phosphorescence (from triplet states) at longer wavelengths relative to fluorescence (from singlet states) [277].

Fluorescence spectroscopy (FS) is a type of electromagnetic spectroscopy in which the fluorescence of a sample is measured after it has been excited by a photon source [277]. To observe such phenomena, a spectrofluorometer can be used to record emission spectra from a sample that has been excited at a certain wavelength [278]. Recently, fluorescence spectroscopy has been used to study daptomycin oligomerization and properties [68, 98, 104-108, 174].

The use of fluorescence spectroscopy to study the binding of daptomycin and CB-182,462 to different lipid membrane models involves the preparation of lipid membrane liposomes. Full details on sample preparation and operation of the spectrofluorometer are available in *Appendix B*.

4.2 Langmuir-Blodgett Trough Techniques

Back in 1773, Benjamin Franklin (a Founding Father of the United States of America; 1706-1790) dropped oil onto rough bodies of water and noticed a calming effect on the waves once the oil was added in [279, 280]. What he did not realize was that he had just formed a monomolecular layer of oil on top of the water's surface, something that no one caught onto until Lord Rayleigh (1842-1919) entered the scene over a century later. In 1890, Rayleigh published his findings of the thickness of an olive oil monolayer after he spread it over the entire surface area of a bath to produce a repeatable calming effect on the surface of the water [281, 282]. A self-taught scientist named Agnes Pockels (1862-1935) was fascinated by this discovery and invented a tin trough with small barriers that could measure surface tension through the use

of a small disk on the surface of the subphase [280]. This would later evolve into the Langmuir-Blodgett trough that is now a core nanotechnology tool for membrane biophysicists across the globe.

While working at the General Electric (GE) Research Laboratory in New York, Irving Langmuir (1881-1957) invented the Langmuir trough based on Pockels tin trough specifications, with the addition of a highly sensitive pressure-measuring device attached to a fixed arm, so that the surface tension of the Langmuir film could be measured [283-285]. Later on, Langmuir hired Katherine Blodgett as his assistant, and they both worked together to develop the Langmuir-Blodgett film deposition process, where a preformed monolayer could be deposited onto a solid substrate multiple times to create multilayers of very accurate thickness [285, 286]. Langmuir's work and contributions to surface chemistry garnered him a Nobel Prize in 1932 [282, 285].

Today, Langmuir troughs are used for a wide variety of biophysical and nanotechnology applications to compress amphiphilic molecules into a monolayer and to directly measure surface phenomena resulting from this compression [287]. Although Langmuir troughs can be used to perform compression isotherms and insertion assays, a Langmuir-Blodgett trough is necessary for Langmuir-Blodgett film deposition due to the requirement for a dipping mechanism that a standard Langmuir trough does not have [287]. As the experiments presented in this thesis require the use of the Langmuir-Blodgett film deposition technique, only the Langmuir-Blodgett trough will be considered in subsequent discussions and descriptions.

The typical setup of a Langmuir-Blodgett (LB) trough is presented in ***Figure 4.2***. The frame of the apparatus holds a trough top that contains the liquid subphase where lipids will be deposited [288]. Software-controlled barriers are placed on top of the edges of the trough top, one on each side, which help compress the monolayer at a rate set by the user [288]. The trough top and barrier are usually made of the same hydrophobic material, such as Teflon, to help contain the liquid subphase [288].

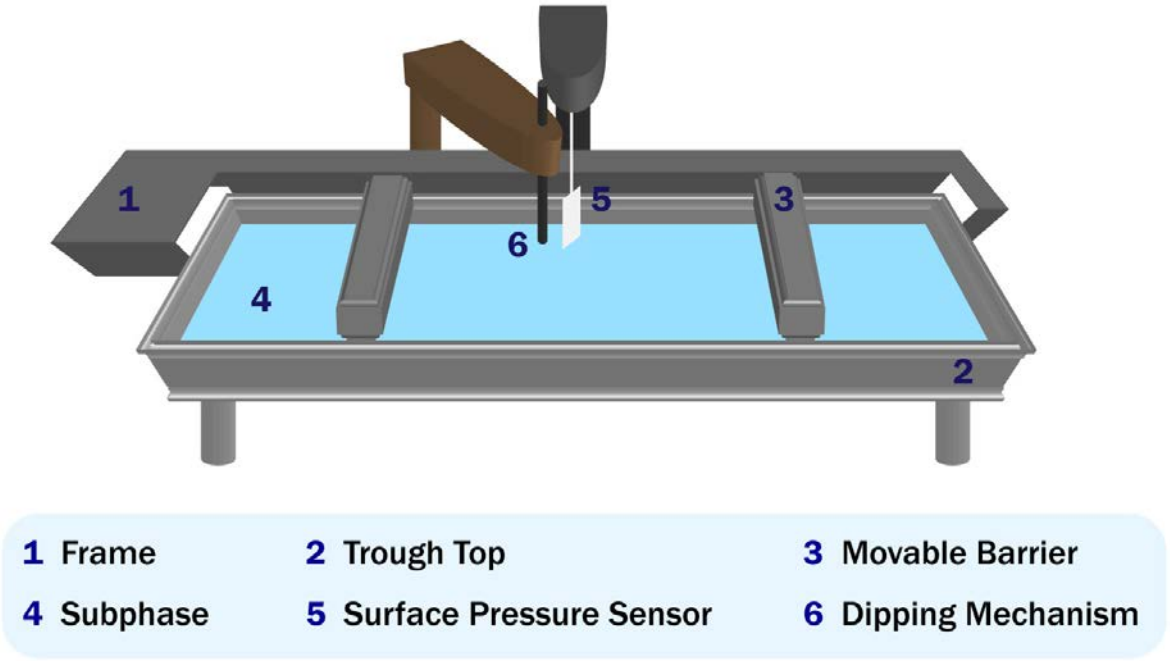

Figure 4.2 Diagram of Langmuir-Blodgett trough. A Langmuir-Blodgett (LB) trough is a trough that is capable of creating Langmuir films (compressed thin films) as well as Langmuir-Blodgett films (thin films deposited on a solid substrate). The only difference between the two is the presence of a dipping mechanism that allows for the depositing of a thin film onto a substrate. Each trough will have a frame, a trough top, movable barriers to compress the thin film with, a surface pressure sensor to sense changes in pressure. The electronic components are controlled by an interface unit specific to the manufacturer.

To measure the surface pressure of each monolayer system, a Wilhelmy plate or Langmuir balance is added to the LB trough apparatus, which consists of a partially-immersed plate that is connected to an electrobalance [289]. This Wilhelmy plate usually comes in the form of filter paper, which is wetted prior to and during any experiment to ensure constant mass. Once it has achieved equilibrium, the Wilhelmy plate detects the downwards force exerted by the meniscus formed by the liquid subphase and allows for the calculation of surface tension [289]. The reduction in surface tension between the ideal or absolute surface tension from Nanopure water (γ_0) and the surface tension achieved after the monolayer sample has been added at the air-water interface (γ) is known as the surface pressure (Π) [289]:

$$\Pi = \gamma_0 - \gamma \qquad \text{(Eq. 1)}$$

The ability of the Langmuir-Blodgett trough instrumentation to calculate the surface pressure of a system at different trough areas and time points allows for various types of experiments to be performed. The first of these are compression isotherms, where the trough barriers compress a monolayer either to the point of collapse, or until the trough barriers cannot close any further. This produces a pressure-area isotherm [289, 290]. The second type of experiment that can be performed is called an insertion assay, where a monolayer is created and sustained at a steady, constant pressure. After a set amount of time, peptides or other molecules can be injected underneath the monolayer to record any changes in surface pressure resulting from interactions with or insertion into the monolayer itself [291]. Finally, the dipper mechanism on the Langmuir-Blodgett trough can be used to deposit a preformed monolayer onto a solid substrate, such as mica (muscovite), for further analysis using other tools such as atomic force microscopy [287, 289].

4.2.1 Monolayer Compression Isotherms

Using the Langmuir-Blodgett trough, a Langmuir film can be compressed at a constant temperature to obtain a pressure vs. area plot, also known as a compression isotherm. When amphiphilic molecules, like phospholipids, are added on top of a liquid subphase, they orientate themselves in a predictable way, such that their hydrophilic (polar) heads face the liquid water subphase and their hydrophobic (non-polar) tails face away from the water at the air-water interface [288].

During the measurement of a compression isotherm (***Figure 4.3***), the molecules within the monolayer organize themselves differently as the available surface area decreases due to the movement of the trough barriers [289]. A typical isotherm starts with the monolayer existing in a two-dimensional gas phase (*G*), where the molecules are disordered, spread far apart and do

not interact with each other. As the surface area of the trough decreases, the monolayer enters into a liquid phase (*L*), where the molecules are now more organized and closely packed together, therefore increasing the surface pressure [289]. When the monolayer is compressed far enough, it will enter into its solid phase (*S*), where the molecules are now tightly packed together into one cohesive structure, creating a spike in surface pressure readings [289]. If the trough barriers continue to compress a solid phase monolayer, a collapse pressure (π_c) will be reached when monolayer packing can no longer be sustained and the molecules will not only become disordered once again, but collapse into three-dimensional structures as molecules are ejected out of the monolayer plane [289].

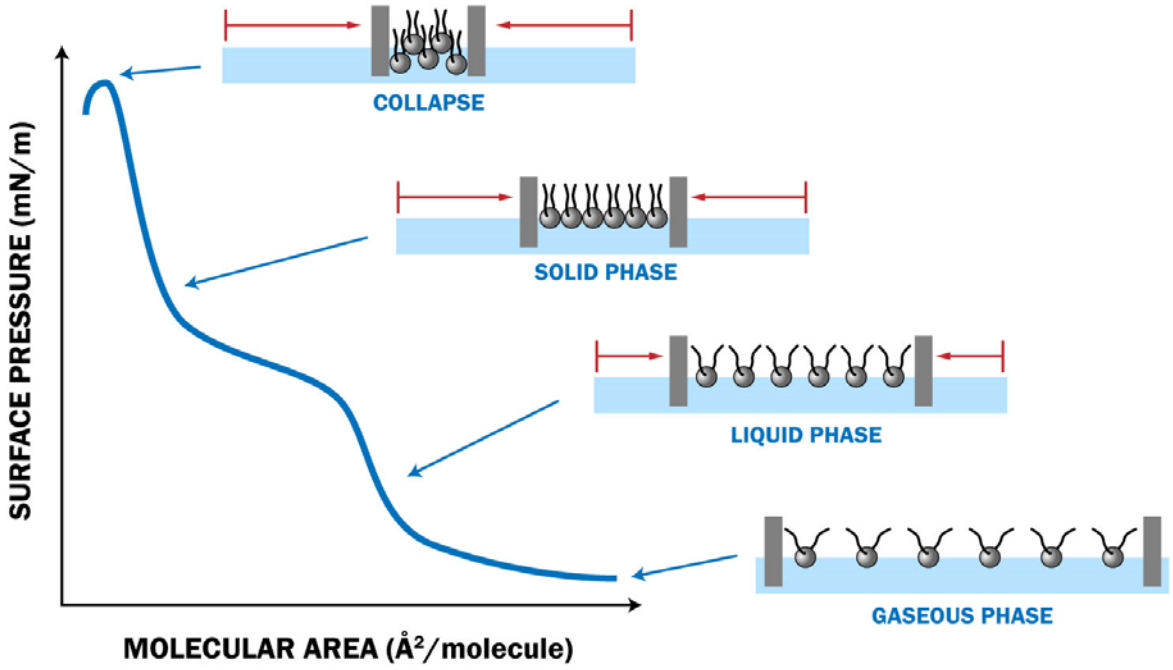

Figure 4.3 Typical surface-area compression isotherm. This plot represents a typical surface pressure vs. molecular area isotherm obtained by compressing a lipid monolayer at an air-water interface. When the lipids are first deposited, they are in a gaseous phase, where they are disordered. As the lipids are compressed, they reach a more ordered, yet still expanded liquid phase, marked by a slight increase in pressure readings. When the lipids are further compressed into a tightly-packed monolayer, it enters a solid phase, and a sharp rise in pressure is recorded. However, too much pressure past a threshold will cause the monolayer to collapse.

Compression isotherms provide insight into a monolayer's physical properties, specifically its packing behaviour and compressibility. Full sample preparation and experimental protocols can be found in *Appendix C1-C3*.

4.2.2 Monolayer Insertion Assays

A Langmuir insertion assay is a method for studying lipid-protein and lipid-peptide interactions by keeping the surface area of the trough or the surface pressure of a monolayer constant [292, 293]. Once a target pressure has been determined that has physiological relevance to the model system being studied, the Langmuir monolayer is compressed until that pressure has been reached. Once that pressure is reached, one of two paths can be taken to continue with the experiment. First, the surface pressure can be kept constant using a feedback loop, and changes in surface area can be monitored to observe peptide interactions with the monolayer. If the peptide inserts into the monolayer, then the surface area should increase, whereas if the peptide causes the lipid monolayer to dissolve into the subphase, the surface area would decrease [291, 293]. Second, the surface area can be kept constant by locking the trough barriers, and changes in surface pressure can be monitored to observe whether the peptide inserts into the monolayer and therefore increase the surface pressure [293]. A Hamilton syringe is used for injection of the peptide from underneath one of the trough barriers to avoid disturbing the lipid monolayer between the barriers [294].

Multiple insertion assay studies have been performed with simple monolayers, where either a constant pressure or surface area is maintained and the change in surface area or surface pressure is measured upon peptide injection, respectively [291, 293, 294]. However, a recent study within our lab has shown that this technique is unreliable due to observed leakage of monolayer material in our trough [295].

Since previously published protocols for peptide insertion assays have not been successful or applicable to the scope of this thesis, a large portion of time was spent developing novel protocols for constant-area insertion assays for the interaction of daptomycin and CB-182,462 with different, complex monolayer lipid models. These protocols have proven to be highly effective and reproducible, and are presented in ***Appendix C4***.

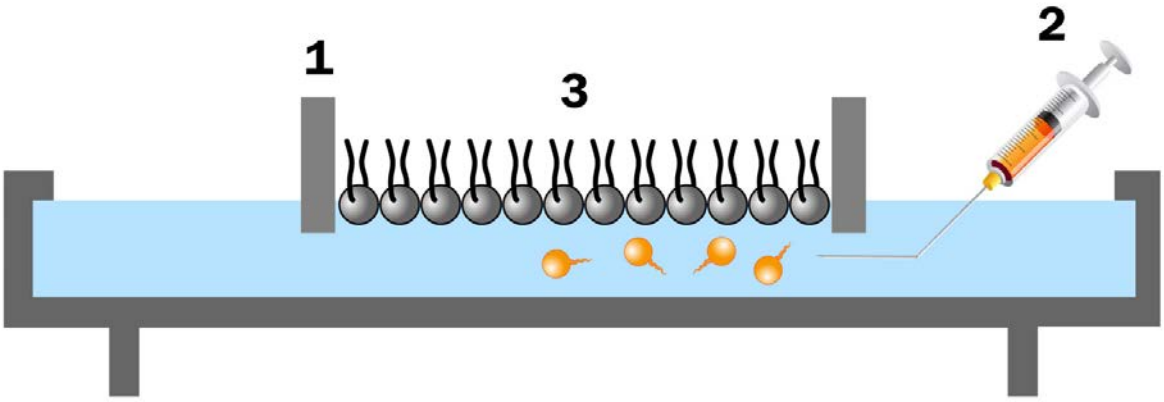

Figure 4.4 Schematic of constant-area monolayer insertion assays. The Langmuir-Blodgett trough can be used to perform insertion assays. These assays can be performed with constant pressure or constant area, the latter of which is depicted in this figure. In constant-area insertion assays, the following steps occur: (1) lipids are deposited onto the trough subphase and compressed to a target pressure, at which point the barriers are locked in place to ensure a constant area; (2) a specific peptide or protein (such as daptomycin or CB-182,462) can be injected using an L-shaped or bent Hamilton syringe that reaches underneath one of the barriers and releases its content underneath the monolayer; (3) pressure readings are recorded throughout these steps to monitor changes in pressure before, during, and after the injection.

The work in this thesis is based on novel protocols for constant-area insertion assays (see ***Figure 4.4***), in which monolayers are compressed to a specific target pressure. Once the monolayer has reached that target pressure, the barriers of the trough are locked in place and the monolayer is "released" from a pressure stabilizer for a few minutes to ensure that the recorded target pressure remains the same without the help of automated controls. After that, a custom-bent L-shaped

Hamilton syringe is used to inject the antibiotic underneath one of the barriers at a consistent force and speed, and the change in surface pressure was monitored over a period of five minutes.

A similar technique is applied when depositing a monolayer onto a solid substrate for imaging purposes.

4.2.3 Monolayer Depositions on Mica Substrates

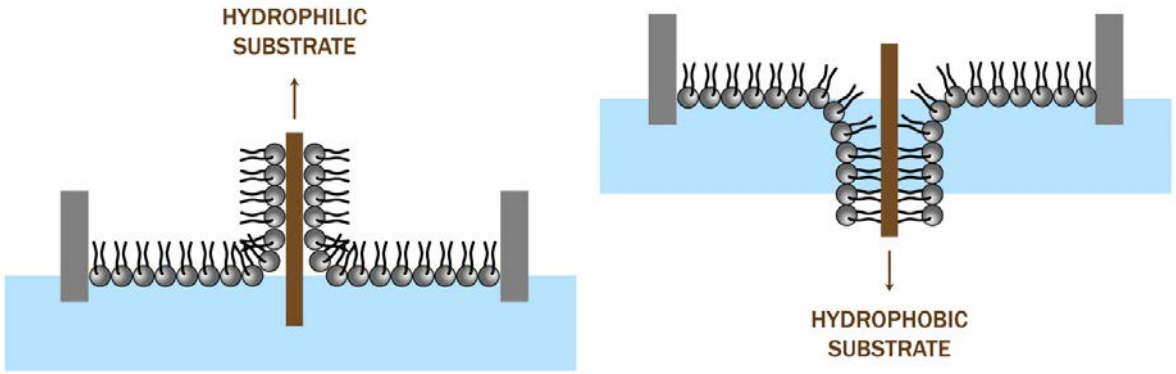

Figure 4.5 Monolayer deposition on different types of substrates. Two types of lipid monolayer depositions can occur depending on the type of substrate being deposited on. If you have a hydrophilic substrate, such as mica, the hydrophilic heads of the lipids will orient themselves so that the heads are facing towards the mica surface. As a result, the substrate is pulled upwards using the Langmuir-Blodgett trough. If you have a hydrophobic substrate, the hydrophobic tails will orient themselves towards the surface of the substrate. This means that the substrate now has to be pulled downwards using the trough.

Apart from compression isotherms and insertion assays, the Langmuir-Blodgett trough can also be used for Langmuir-Blodgett films, which can be deposited onto two types of solid substrates: hydrophobic and hydrophilic (see ***Figure 4.5***). When depositing a monolayer onto a hydrophobic surface, the substrate must travel downwards across the air-water interface, so that the hydrophobic tails can attach to the substrate's hydrophobic surface [289]. On the other hand,

when depositing a monolayer onto a hydrophilic surface, the substrate must already be submerged in the subphase and travel upwards across the air-water interface so that the hydrophilic heads can attach to the substrate's hydrophilic surface [289]. Even if it is unknown whether a substrate's surface is hydrophobic or hydrophilic, it is easy to distinguish by knowing whether the meniscus curves downwards (hydrophobic) or upwards (hydrophilic) when the substrate is partially immersed in the subphase [289].

One of the most common substrates used is muscovite, the most abundant mineral of the mica family [296-298]. Muscovite mica sheets not only cleaves perfectly into thin, flexible, elastic sheets, but it is also an excellent insulator that is chemically inert, dielectric, and hydrophilic [299-302]. Since muscovite mica sheets are hydrophilic, that means that using a mica substrate would require it to be fully submerged and dragged upwards for a monolayer to adhere to its surface.

A detailed overview of monolayer deposition on mica substrates is available in *Appendix C5*.

4.3 Atomic Force Microscopy Techniques

Atomic force microscopy (AFM) is a type of scanning probe microscopy that offers high-resolution imaging of surface topography at nanometer and atomic scales [303-305]. As shown in *Figure 4.6*, a flexible cantilever acts like a spring as it is rastered across the sample's surface. The cantilever's movements alter the deflection of a laser beam reflecting off the cantilever tip and onto a quadrant photodiode. This signal is used to construct an image that reflects the type of interaction being measured by the probe in relation to the surface [303-305]. AFM is a highly versatile technique as it can be used for different life science applications, and imaging can be performed in different modes and environments [306].

AFM has been extensively used to image biological samples, such as bacteria and lipid monolayers and membranes, in the presence of antimicrobial peptides [307, 308]. As a result,

different variations of AFM techniques were used in this thesis to qualitatively observe the interaction of daptomycin and CB-182,462 with different model monolayers and membranes.

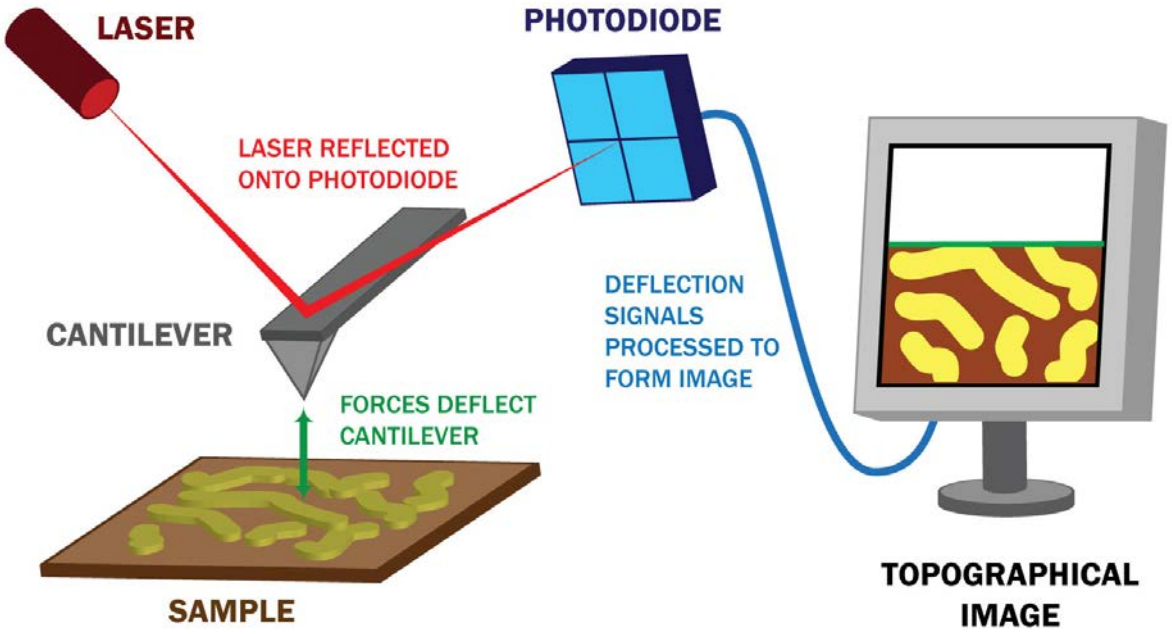

Figure 4.6 Schematic of atomic force microscopy. In atomic force microscopy, a laser is reflected off a cantilever and onto a photodiode. As the cantilever tip scans across the surface of the sample, the forces it experiences will deflect the cantilever, therefore changing the placement of the reflected laser beam on the photodiode. These changes in deflection signals are then processed using AFM operating software into a viewable image of the sample's topography.

4.3.1 Topographical Imaging

In AFM, a flexible cantilever acts like a spring to measure the interactions between the tip and the sample, whilst its deflections are electrically monitored by the reflection of a laser beam that bounces off the cantilever onto a quadrant photodiode. As the tip is rastered across the sample surface, an image is formed from the feedback signals. There are multiple imaging modes of atomic force microscopy that differ in the types of forces between the tip and the surface of the sample [305, 309, 310]. These types of attractive and repulsive forces can be represented by a

generic tip-sample force vs. distance curve as seen in ***Figure 4.7***. As the tip approaches the sample surface from afar, it experiences attractive, long-range forces such as van der Waals and capillary forces [309, 311]. As the tip gets closer to the sample surface, this attraction gives way to a repulsive force governed by short-range interactions as their electron orbitals begin to overlap [305, 311].

The first and most basic imaging mode is contact mode, where a force value of tip repulsion is selected, and the feedback system adjusts the height of the tip to keep this repulsive force constant as the tip raster-scans the surface of the sample [305, 309, 311]. Accordingly, on the generic force curve, contact mode is a single point. In other words, the tip never leaves the surface of the sample when imaging.

In intermittent contact mode, the tip is not always in contact with the surface, but rather oscillates between the attractive and repulsive parts of the force-distance curve [305, 311-313]. As a result, the lateral forces are much lower with this imaging mode, allowing for high-resolution topographical images of soft samples to be obtained [309, 311]. Typically, the cantilever is driven close to the resonance of the system so that phase information can be obtained and a workable amplitude for the oscillation can be used to obtain topographical data from the sample [309, 311]. This makes phase imaging possible, which will be explained in the subsequent section.

Although non-contact mode is another type of AFM imaging mode, it is rarely used because it is difficult to control and monitor the long-range interactions between the tip and sample [305, 311].

No matter which imaging mode is chosen, different cantilevers with different properties will affect its operation. Stiffer cantilevers will have a higher spring constant, which means that stronger forces are required to deflect the tip; these types of cantilevers are good for contact mode imaging [305, 311]. Softer cantilevers have a lower spring constant and therefore require

less force to deflect the tip, which means that they are more suitable for use with softer samples in intermittent contact mode, both in air and in liquid [305, 311-314].

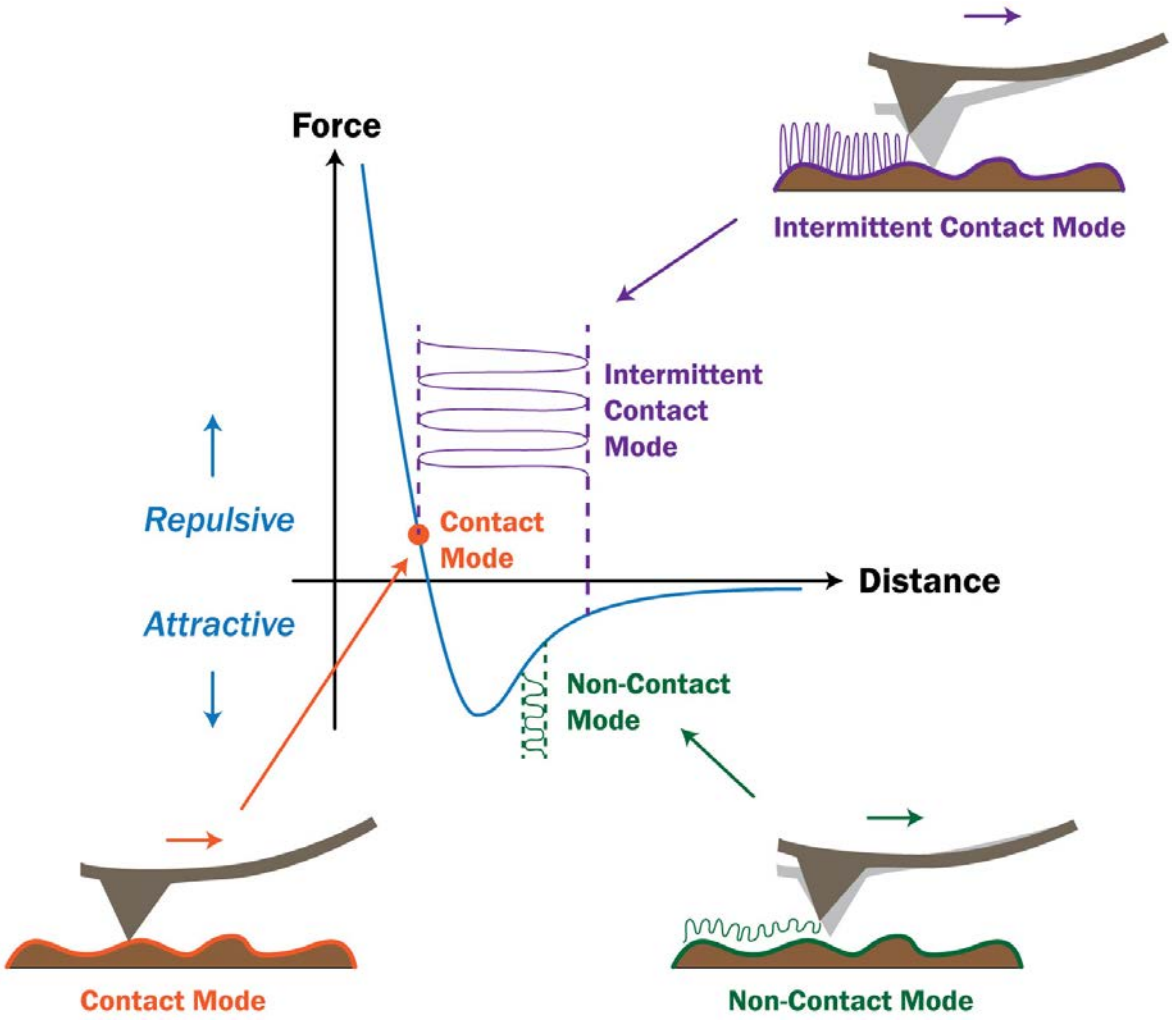

Figure 4.7 Different AFM imaging modes. In an atomic force microscope, as the tip approaches the sample surface, it experiences long-range attractive forces. As it gets closer to the sample surface, this attraction gets converted into a repulsive force and experiences short-range interactions. Various operating modes of the AFM take advantage of these types of interactions. In contact mode, the tip touches the sample surface and experiences repulsive forces. In non-contact mode, the tip depends on short-range attractive forces to detect surface topography. Meanwhile, intermittent contact mode is where the tip is oscillated between repulsive and attractive interactions.

Experimental protocols for AFM imaging in air can be found in ***Appendix D*** while detailed sample preparation and techniques for AFM imaging in liquid can be found in ***Appendix E***.

4.3.2 Phase Imaging

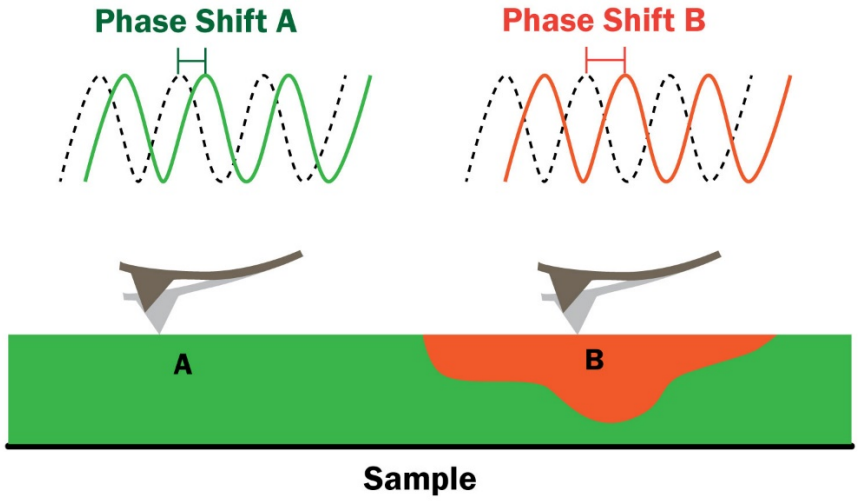

Figure 4.8 Schematic of AFM phase imaging. While an AFM is operating in intermittent contact mode, or tapping mode, the tip is oscillated vertically at its resonance frequency. Apart from tracking the height differences of the sample during a scan, the tip's motion can also be characterized by its phase (solid lines) relative to the piezoelectric driver (dotted lines) of the system. When the tip encounters different phases (such as from material A to B in the figure), the phase signal shifts a certain amount, and different regions can be differentiated from these changes in phase shift.

In intermittent contact mode, the cantilever is oscillated at a particular resonance frequency by the piezoelectric driver of the system [305, 311]. As the tip lightly taps the surface, the amplitude of the oscillation is reduced at that point, and these changes in amplitude provide information on surface topography [311]. Apart from this, the tip's motion can be characterized by its phase in comparison to the piezoelectric driver of the system [311, 315, 316]. This means that phase

shifts can be monitored continuously as the tip scans the surface of the sample, as in ***Figure 4.8*** [311, 316]. These phase shifts are very sensitive to variations in composition, frictions, adhesion, viscoelasticity and surface stiffness, allowing for the detection of surface features and characteristics that may not be seen in a topographical image [311, 315, 316].

4.3.3 Kelvin Probe Force Microscopy

Invented in 1991, Kelvin probe force microscopy (KPFM) is a scanning probe microscopy method, similar to AFM. It involves the use of a conducting probe and conductive substrate to record nanoscale images which contain information on electrostatic interactions between the tip and the substrate [317]. KPFM is regularly used to study the work function differences in metals and electrical surface potential differences in other materials. KPFM can be performed simultaneously with AFM imaging, which allows for the direct comparison of topographical surface structures with electrical surface potential [318-320].

When thin organic films like lipid monolayers, which are polar or charged molecules, are deposited on top of a conductive substrate, the differences in electrical surface potential can be recorded within the monolayer, provided the electrical surface potential of the conductive substrate below is uniform [317, 321]. The electrical surface potential of a lipid film has been defined by the molecular dipoles (μ) that are aligned perpendicular to the interface, the dielectric constant (ε), and the packing density (A) covered by each molecule [322]. When phospholipids are considered, a refined model is used, where the normal components of the dipole moments of the water molecules (μ_1), lipid head groups (μ_2), and lipid tail groups (μ_3) are included [250, 322]:

$$\Delta V = \frac{\mu_{\perp}}{\epsilon_0 \cdot A} = \frac{1}{A \cdot \epsilon_0}\left[\frac{\mu_1}{\epsilon_1} + \frac{\mu_2}{\epsilon_2} + \frac{\mu_3}{\epsilon_3}\right] \qquad \text{(Eq. 2)}$$

In KPFM, an AC bias (V_{AC}) is applied between the tip and the sample while the cantilever is oscillated close to its resonance frequency. As the tip rasters across the sample surface, tip-sample interactions induce changes in oscillation amplitude and electrical forces [323]. The KPFM feedback detects these changes and adjusts a DC bias (V_{DC}) such that the induced changes are nullified, at which point the V_{DC} is equal to the contact potential difference, or CPD (V_{CPD}), between the tip and sample surface. We can then correlate local contact potential difference with surface features. Both voltages and the resonance frequency ω_0 are related through the following equation for the electrostatic force F_ω, where $C(z)$ is the capacitance between the tip and sample surface and the $\pm$ sign depends on whether the bias V_{DC} is applied to the tip (-) or sample (+) [324]:

$$F_\omega = -\frac{\partial C(z)}{\partial z}(V_{DC} \pm V_{CPD})V_{AC}\sin(\omega t) \qquad \text{(Eq. 3)}$$

As a result, a KPFM image of the electrostatic surface potential of the sample can be recorded from the nulling voltage V_{DC} versus the tip's positional coordinate, commonly outputted as (x, y, z, V_{DC}) data points as opposed to the traditional (x, y, z) coordinates in AFM [325].

With KPFM, there are three main operation modes, which are AM (amplitude modulation) and FM (frequency modulation) KPFM that allow for high-resolution imaging, as well as lift mode [317, 324]. Both modes can be performed in a one-pass fashion, where the AFM imaging is done simultaneously with KPFM. It can also be done in a two-pass fashion, where AFM imaging is done in the first trace and KPFM is done in a retrace [326]. In this thesis, AFM images were collected using the latter technique, where AFM images were taken during the first trace and AM-KPFM in the retrace (see ***Figure 4.9***). KPFM imaging can be done in air only.

Due to its ability to measure a sample's electrical surface potential and correlate them with their respective topographical structures, KPFM will be an important and useful method in elucidating electrostatic properties for biological samples. The KPFM experiments performed in this thesis are based on AM-KPFM, and detailed protocols can be found in ***Appendix D***.

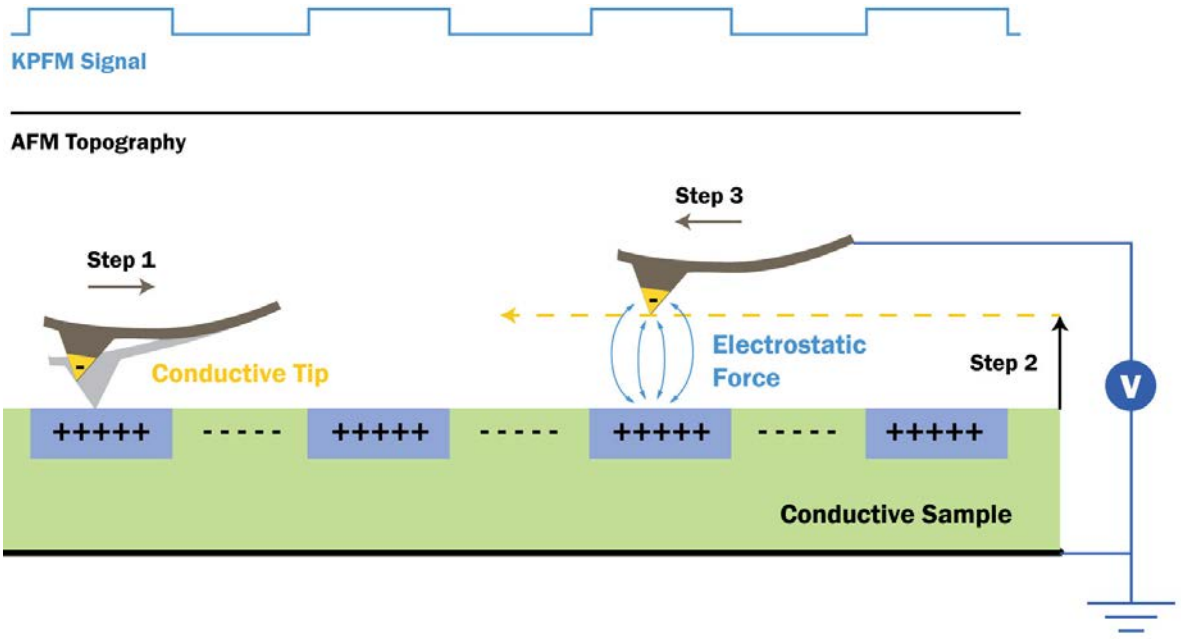

Figure 4.9 Simplified schematic of two-pass KPFM technique. KPFM requires both the sample and the tip to be conductive. In this figure, there is a gold-coated tip and a sample with regions of positive and negative charges. In amplitude-modulation Kelvin probe force microscopy, the imaging technique used in this thesis involves a two-pass method where (1) a conductive tip first takes a topographical AFM scan of the sample's conductive surface, (2) lifts up a certain amount (10 nm setoff distance), and (3) performs a KPFM retrace of the height profile at that setoff distance.

CHAPTER 5

5 FLUORESCENCE SPECTROSCOPY STUDIES: DAPTOMYCIN IS SEQUESTERED BY LUNG SURFACTANT AT PHYSIOLOGICAL CALCIUM CONCENTRATIONS

5.1 Introduction

The prevalence of resistance in Gram-positive pathogens has significantly risen over the past few decades, spurring a demand for novel antibiotics that are effective against multi-resistant bacterial strains [5, 327, 328]. Globally, pneumonia still presents as a serious public health concern and was rated as the eighth most common cause of mortality in the United States as of 2014 [329]. In the same year, the World Health Organization reported *Streptococcus pneumoniae*,

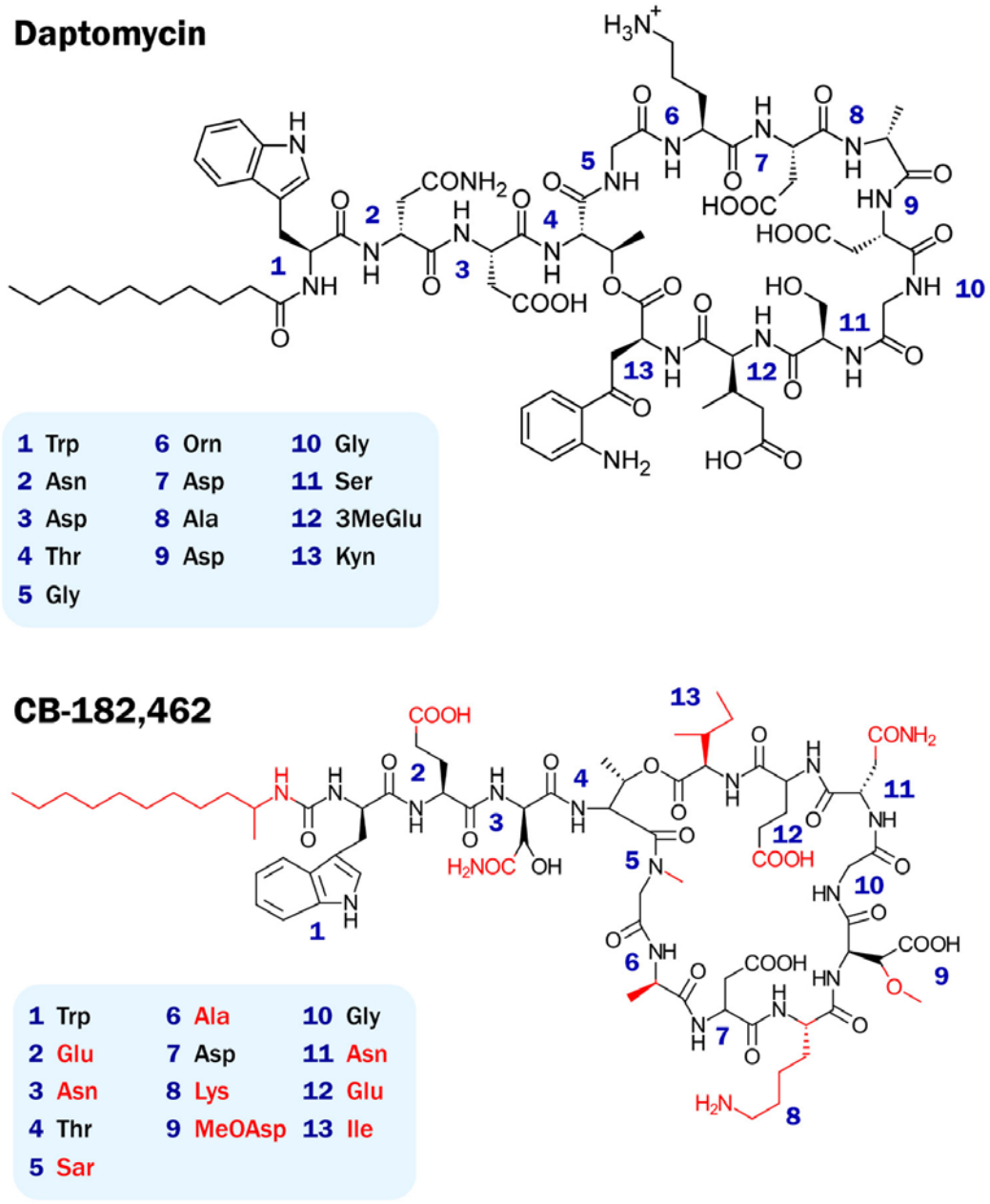

Figure 5.1 Comparison of daptomycin and CB-182,462 chemical structures. Daptomycin and CB-182,462 have similar architecture. Daptomycin is derived from *Streptomyces roseosporus*, while CB-182,462 is derived from *Streptomyces fradiae*. Some core differences in CB-182,462 include its alkyl-carbamyl residue (instead of daptomycin's decanoyl tail) as well as the absence of kynurenine (replaced by isoleucine) and methyl-glutamate (replaced by glutamate). Both compounds are calcium-dependent in their mechanisms of action. The abbreviated names for non-standard amino acids are as follows: Orn for ornithine, MeGlu for methyl-glutamate, Kyn for kynurenine, Sar for sarcosine, and MeOAsp for methoxy-aspartate.

the main causative agent of community-acquired pneumonia (CAP), as one of the nine bacteria that should be of international concern due to its rise in antibiotic resistance [330, 331].

Clinically, a novel lipopeptide antibiotic called daptomycin is used against Gram-positive bacterial infections caused by microorganisms such as *Staphylococcus aureus*, enterococci, and even their strains that are resistant to other drugs [49, 54]. As a fairly young drug, daptomycin has risen to become a widely-used antibiotic due to its role as a last-resort alternative to antibiotics that fail against serious infections [82]. Daptomycin's antimicrobial activity depends on calcium, which promotes the initial insertion and subsequent oligomerization of daptomycin in the bacterial membrane, forming ion channels that disrupt its membrane potential and lead to cell death [61].

Although daptomycin is clinically effective against skin infections, bacteremia, and right-sided endocarditis caused by multi-resistant strains of Gram-positive bacteria, it is ineffective against CAP, which is most commonly caused by *S. pneumoniae,* another Gram-positive pathogen [4]. Its poor efficacy against CAP has been attributed to its inability to distinguish between the immense amount of lung surfactant present in the lungs versus the small surface area of the bacterial pathogens, rendering it sequestered by lung surfactant and therefore inactive against the bacteria [10]. It has been postulated that since lung surfactant contains a considerable fraction of negatively charged phosphatidylglycerol, which is also a main component of the bacterial plasma membrane, daptomycin's insertion into lung surfactant is promoted [10]. In fact, a recent study has shown that the presence of phosphatidylglycerol allows for membrane-bound daptomycin to undergo a structural conformation and not only oligomerize, but insert deeper into the membrane itself [68]. Daptomycin sequestration has been shown through fluorescence studies before [10], but there is no study that compares the binding of daptomycin to lipid models of the relevant systems at hand.

Due to daptomycin's lack of bactericidal activity in the presence of lung surfactant, multiple derivatives and hybrids between daptomycin and A54145 were created in an attempt to find a

better alternative [171, 173]. Although numerous derivatives were proven to exert bactericidal activity within the presence of lung surfactant, all of them stemmed from A54145, which is known to be toxic [105, 174]. One such A54145 derivative is CB-182,462, with more potent bactericidal activity against *S. pneumoniae* than most of the other derivatives (J. Silverman, personal communication). However, CB-182,462 was discovered to be toxic with development of phospholipidosis in the kidneys, so its development was abandoned (J. Silverman, personal communication). As a semisynthetic derivative of A54145, CB-182,462 shares numerous structural features with this complex, which in turn is comparable to daptomycin's structure (***Figure 5.1***). There have also been no studies performed that compare the interaction of CB-182,462 with different lipid membrane models relevant to community-acquired pneumonia.

To elucidate the inhibition of daptomycin by lung surfactant and further understand its mechanism of action, the studies performed in this chapter will compare the interaction of daptomycin versus CB-182,462 in different lipid membrane models that represent the lipid compositions of bacterial membranes, lung surfactant, and human cell membranes. The interaction of these antibiotics with these model liposomes will be compared using fluorescence spectroscopy, taking advantage of their intrinsic fluorescence. The emission intensity and spectral position of the kynurenine and tryptophan residues will be used to determine the insertion of daptomycin and CB-182,462 into each of the model liposomes, respectively. It has been shown that, when these residues transition from an aqueous to a hydrophobic environment such as the bilayer of the liposome, an increase in fluorescence will be observed, allowing their insertion to be determined from the emission spectra acquired [81].

The results obtained from this experiment present novel insight into the inhibition of daptomycin by lung surfactant and provide strong evidence that daptomycin is sequestered by both synthetic and natural models of lung surfactant. Interestingly, it was observed that the binding of daptomycin into the bacterial membrane model increased accordingly with calcium concentration. At both 2 mM and 10 mM calcium concentrations, daptomycin exhibited minimal interaction with the human membrane model. However, CB-182,462 not only bound more

strongly to the human membrane model than it did the other models, but did not experience a blue spectral shift like the other models. CB-182,462 also did not bind strongly to the lung surfactant models, suggesting its function is unhindered by surfactant.

These trends have several significant implications. It is shown here that daptomycin is sequestered by lung surfactant. Specifically, daptomycin has similar affinity for both lung surfactant and bacterial membrane, suggesting that these two membranes play a competitive role in the binding of daptomycin. Increased emission spectra for daptomycin and bacterial membranes at higher concentrations of calcium suggest that calcium may remove the inhibition that cardiolipin places on a late step of daptomycin pore formation. It is also shown that CB-182,462 is not inhibited or sequestered by lung surfactant and exhibits strong binding to bacterial membranes, signifying potent bactericidal activity. However, it also binds strongly to the human membrane model. This suggests that CB-182,462 toxicity can be explained by its reduced selectivity for bacterial versus human cell membranes.

5.2 Materials and Methods

5.2.1 Lipid Models

Four lipid models were used in this study: bacterial membrane lipid model, human endothelial membrane lipid model, synthetic lung surfactant lipid model, and lipid-extracted BLES® model. In molar percentages, the bacterial membrane (BM) lipid model consists of 20% phosphatidylglycerol, 20% cardiolipin, and 60% phosphatidylethanolamine; the human membrane (HM) lipid model consists of 20% phosphatidylcholine, 20% phosphatidylethanolamine, 10% phosphatidylserine, 15% sphingomyelin, and 35% cholesterol; the lung surfactant (LS) lipid model consists of 80% phosphatidylcholine and 20% phosphatidylglycerol, with 5% cholesterol; and the final model is a mixture of lipids extracted from bovine lipid extract surfactant (BLES®), which should have a similar lipid composition as

that of the LS lipid model. The derivation and reasoning behind each of these lipid models can be found in *Chapter 3*.

5.2.2 Liposome Preparation

Prior to preparing the liposomes for fluorescence spectroscopy, stock solutions of 1 mM daptomycin, 1 mM CB-182,462, and 100 mM calcium were made, along with a HEPES buffer (20 mM HEPES, 150 mM NaCl, pH 7.4) for liposome resuspension. See *Appendix A* for detailed procedures.

The following lipids were purchased from Avanti Polar Lipids (Alabaster, Alabama, US) in powder form with >99% purity: 1,2-dipalmitoyl-*sn*-glycero-3-phosphocholine (DPPC), 1,2-dioleoyl-*sn*-glycero-3-[phospho-*rac*-(1-glycerol)] (DOPG), 1-palmitoyl-2-oleoyl-*sn*-glycero-3-phosphoethanolamine (POPE), 1,2-dioleoyl-*sn*-glycero-3-[phospho-L-serine] (DOPS), 1,1'2,2'-tetraoleoyl cardiolipin (TOCL), and sphingomyelin (egg, chicken). Cholesterol was purchased from Sigma-Aldrich (St. Louis, Missouri, US), also with >99% purity.

For fluorescence spectroscopy studies, a 5 mM solution of large unilamellar vesicles (LUVs) was prepared for each membrane lipid model according to their lipid compositions. For each lipid model, specific amounts of lipids were weighed into a round-bottom flask and dissolved in chloroform/methanol (4:1). The solvent mixture was evaporated with nitrogen gas until a thin film formed around the lower-half of the round-bottom flask, which was then further dried overnight under vacuum. The following day, HEPES buffer was added to the dried thin film to rehydrate and resuspend the vesicles within the buffer solution. The resulting solution was passed through a LIPEX™ Thermobarrel Extruder (from Transferra Nanosciences Inc., previously known as Northern Lipids, Burnaby, British Columbia, Canada) at least 15 times using 100 nm polycarbonate filters at a constant physiological temperature of 37°C. The process of extrusion allows the large multilamellar vesicles from the rehydration step to form smaller,

uniformly sized large unilamellar vesicles. Detailed experimental protocols are available in *Appendix B1*.

Note that for preparing lipid mixtures with BLES®, novel protocols had to be designed to extract the lipids from the original surfactant suspension in order to successfully prepare BLES® LUVs. Prior to this, BLES® liposomes have only been prepared as giant unilamellar vesicles. To successfully form BLES® LUVs, specific aliquots of BLES® and chloroform/methanol (4:1) need to be thoroughly mixed together and centrifuged at least eighteen times, each spin lasting for 5 minutes at 2000 RPM. After each spin, a separation of phases can be seen; the bottom phase is saved to another tube for storage while the upper phase and supernatant are spun down again upon further additional of chloroform/methanol (4:1). Full details are available in *Appendix B.1.1.2*.

All fluorescence experiments were repeated a total of three times, with at least 3 emission spectra obtained for each trial and scenario. Emission spectra specific to the daptomycin or CB-182,462 experiments were normalized separately so that the emission peaks of the controls shared a common scale within each group of data. One-way ANOVA (with Tukey's *post hoc* test) was conducted using OriginPro 2016 (proprietary software owned by Origin®, Version b9.3.1.273) to determine statistical significance (α level set to 0.01) and compare the mean emission peaks observed for different lipid membrane models in the presence or absence of calcium ions for daptomycin and CB-182,462 data sets.

5.2.3 Fluorescence Spectroscopy

A Photon Technology International (PTI) QuantaMaster Spectrofluorometer was used to acquire fluorescence emission spectra. Both daptomycin and CB-182,462 (Cubist Pharmaceuticals Inc., Lexington, Massachusetts, USA) have intrinsic fluorescence due to their kynurenine and tryptophan residues, respectively. Accordingly, the samples with daptomycin were excited at 365 nm, with emission spectra recorded from 400 nm to 600 nm, while the

samples with CB-182,462 were excited at 280 nm with emission spectra recorded from 300 nm to 500 nm.

Every lipid model studied had six separate scenarios: the lipid model by itself, in the presence of just calcium, just daptomycin, or just CB-182,462, and with both calcium and daptomycin or CB-182,462. Each 1 mL cuvette that was used for fluorescence measurements was incubated for 3 minutes. The final concentration of daptomycin or CB-182,462 in the cuvette was 4 μM, while calcium was 2 mM or as indicated in the *Results* section, and liposomes were 250 μM total lipid. All solutions and measurements were taken at a temperature of 37°C. A total of three trials with fresh stock solutions and liposomes were performed, and the measurements for each scenario in each trial were taken at least three separate times on different days. Detailed instructions on fluorescence spectroscopy experimental protocols are available in ***Appendix B2***.

5.3 Results

It has been previously shown that daptomycin only binds to bacterial membranes in the presence of calcium, and that the higher the calcium concentration, the stronger the binding [61, 81, 103]. A calcium titration was performed to determine the peak emission signal from a sample of daptomycin and bacterial membrane vesicles with increasing calcium concentrations from 0 mM to 50 mM (see ***Figure 5.2***). A half-maximal increase was observed close to 0.5 mM Ca^{2+}, and it was determined that the emission peaked at around 10 mM of calcium. As a result, initial experiments with fluorescence spectroscopy began at 10 mM of calcium concentration, well above that of physiological extracellular calcium concentration (which is under 2 mM). Subsequent experiments were done at 2 mM of calcium.

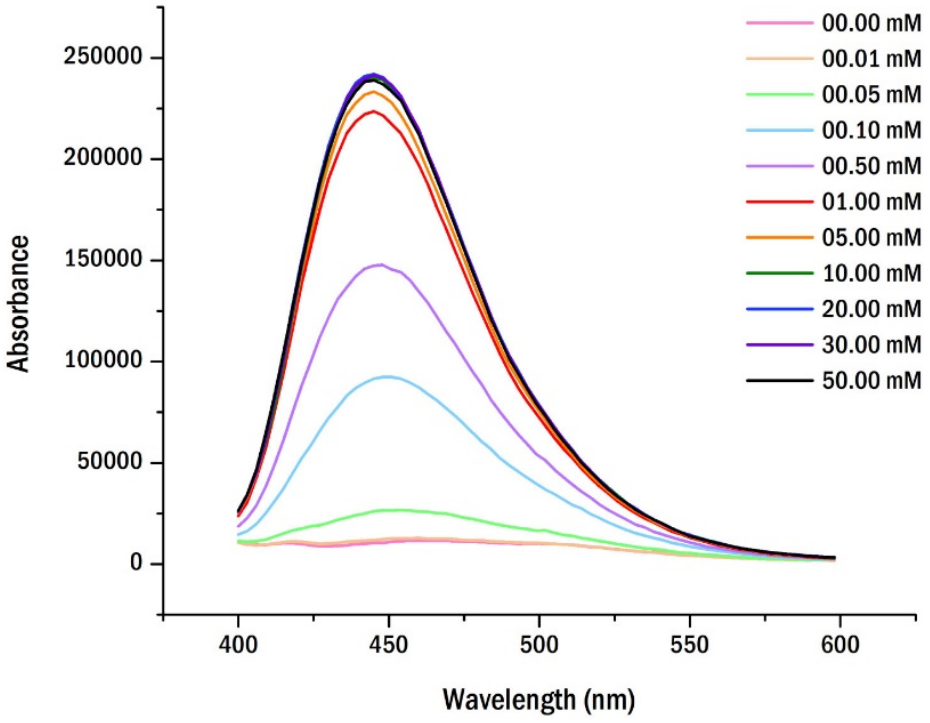

Figure 5.2 Determining emission plateau using calcium titration. A calcium titration of the bacterial membrane model with daptomycin was performed to determine the calcium concentration that provided a peak emission signal from the sample to begin experiments with. It was determined that the emission signal reached a plateau at approximately 10 mM Ca^{2+}.

5.3.1 Interaction of Daptomycin with Membrane Models

5.3.1.1 Fluorescence Spectra of Daptomycin with Membrane Models at 10 mM Ca^{2+}

Using a concentration of 10 mM Ca^{2+}, emission spectra were obtained as preliminary data for each of the membrane lipid models, excluding the BLES® lipid model. In ***Figure 5.3***, we can see a fluorescence vs. wavelength plot of the emission spectra obtained for daptomycin, with its kynurenine residue excited at 365 nm. The results show that there is minimal binding of daptomycin to the human membrane model (in green), which supports the notion that it is nontoxic and does not interact with human membranes. The plot also shows strong binding of

daptomycin to the lung surfactant lipid model (in red), providing preliminary evidence to support the hypothesis that daptomycin is sequestered by lung surfactant due to its lipid composition and presence of phosphatidylglycerol.

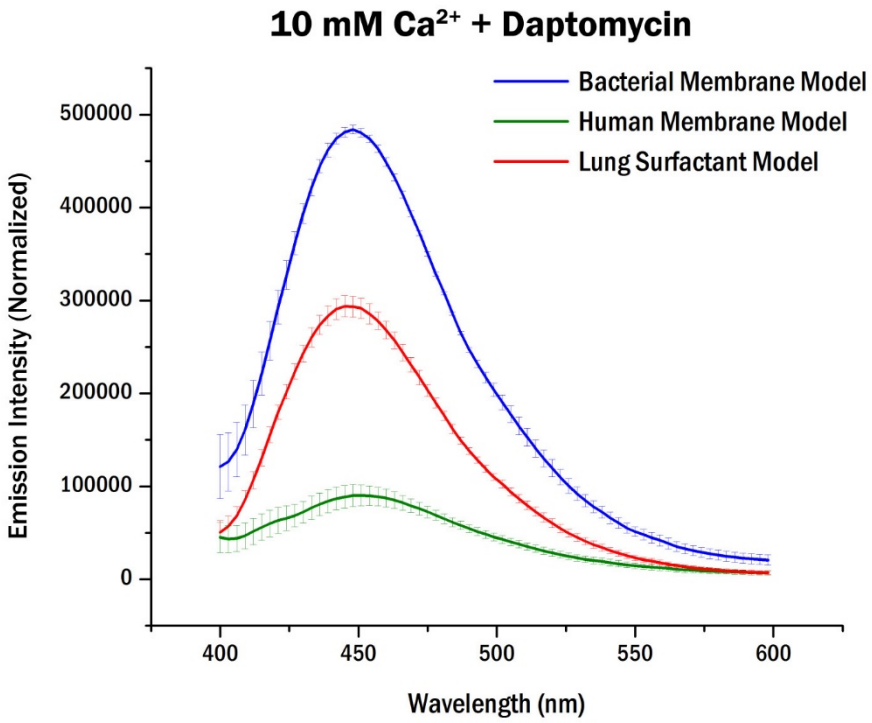

Figure 5.3 Preliminary data obtained for BM, HM, LS models with daptomycin at 10 mM Ca^{2+}. These plots show the normalized emission spectra obtained for daptomycin in the presence of 10 mM Ca^{2+} for different model liposomes (bacterial membrane, human membrane, lung surfactant lipid models). The kynurenine residue on daptomycin was excited at 365 nm, and the emission spectra were acquired from 400 - 600 nm. Each measurement was repeated at least 3 times in each of the 3 trials.

5.3.1.2 Fluorescence Spectra of Daptomycin with Membrane Models at 2 mM Ca^{2+}

In order to better understand the inhibition of daptomycin by lung surfactant and elucidate daptomycin's mechanism of action, experiments were performed close to a physiological calcium concentration of 2 mM to give our data more physiological relevance. This particular calcium

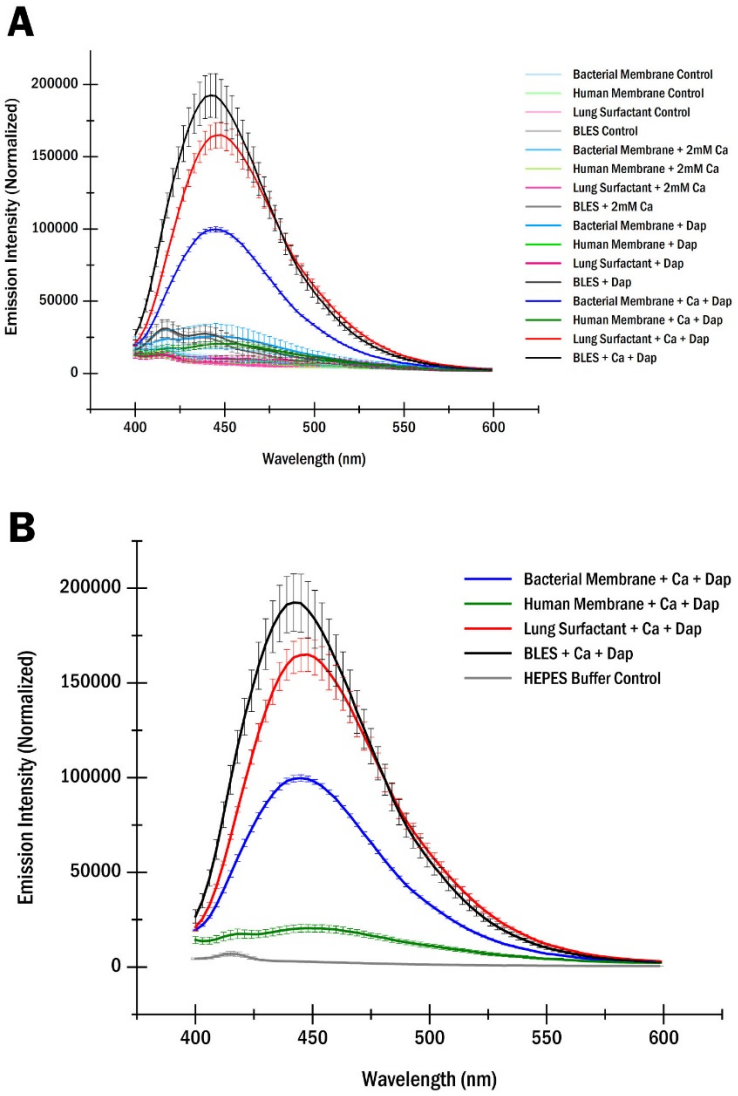

Figure 5.4 Emission spectra for 2 mM Ca^{2+} daptomycin experiments. The plots presented here represent the data obtained for all four lipid models in four different scenarios: the model itself as a control, the model with just calcium as another control, the model with just the antibiotic as a third control, and the model with both the antibiotic and calcium. (A) Emission spectra were obtained from 400 – 600 nm for a full set of experiments for daptomycin with excitation wavelength at 365 nm for kynurenine. Each membrane model is designated by a different set of hues: blue for the BM model, green for the HM model, red for the LS lipid model, and black for the BLES® lipid model. (B) Averaged emission spectra for different membrane models (BM, HM, LS, BLES®) in the presence of 2 mM Ca^{2+} and daptomycin. Both the LS and BLES® models have similar peaks and spectra, and it can be seen that daptomycin binds more strongly to the LS models than to the BM model. A HEPES buffer control is presented with no liposomes, daptomycin or calcium.

concentration has been widely used in various studies [332-336]. Each set of experiments involved studying daptomycin in four different scenarios for each of the membrane models: the membrane itself, the membrane with only calcium or daptomycin, and the membrane with both calcium and daptomycin included. Full sets of data are presented in ***Figure 5.4A***, where the buffer, membrane, membrane with only calcium and membrane with only daptomycin (or CB-182,462) samples acted as negative controls for the experiment. It can be seen that the controls (membrane with just calcium or daptomycin) have low readings for emission intensity, similar to the HM + Ca^{2+} + DAP spectra.

Selected results are presented in ***Figure 5.4B*** for a clearer comparison between membrane models. As previously observed in ***Figure 5.4A***, there is minimal interaction of daptomycin to the human membrane model (in green) as its emission spectra are comparable to the emission spectra obtained from the controls. However, the relative order of emission intensity for both the bacterial membrane (in blue) and lung surfactant lipid models (in red for synthetic; black for natural) at 2 mM Ca^{2+} have essentially become reversed from the trends seen at 10 mM Ca^{2+}. Instead of higher emission peaks for bacterial membrane liposomes, daptomycin now induces higher emission peaks with the lung surfactant lipid models at 445 nm. When compared to the BLES® lipid model, even stronger emission intensities were observed. Both lung surfactant models had emission intensities almost twice as strong as that of the bacterial membrane model. One-way ANOVA and Tukey's *post hoc* test were used to determine these averaged peak emission values as statistically significant ($p < 0.0001$). Note that the emission spectra obtained for both the LS and BLES® lipid models correlate well with each other.

5.3.1.3 Effect of Increasing Calcium Concentration on Daptomycin's Interaction with BM, LS, and BLES® Model Liposomes

From the previous experiments performed, it seems that daptomycin interacts more strongly with lung surfactant than with bacterial membrane at low calcium concentrations, and then shifts

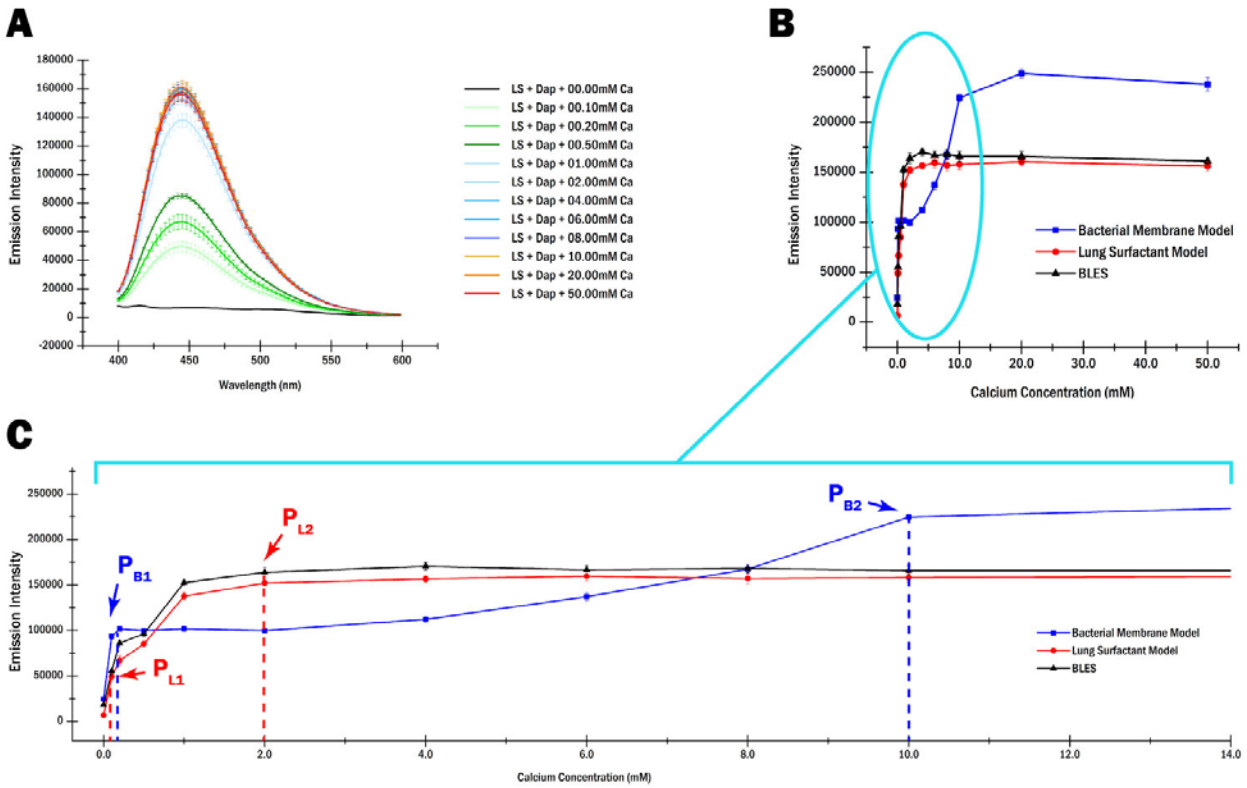

Figure 5.5 Comparison of daptomycin insertion into BM and LS models at different calcium concentrations. (A) A calcium titration from 0 – 50 mM Ca^{2+} was performed for daptomycin and three models (bacterial membrane, lung surfactant, and BLES®), with the LS® results shown here. (B) Averaged peaks of absorbance at 345 nm for emission spectra obtained at 0 – 50 mM Ca^{2+}. Each point on a coloured line represents the average absorbance of at least 9 absorbance peaks (taken from at least 3 emission spectra of 3 trials) for a singular model. (C) Zoomed-in plot of (B) from 0 – 14 mM Ca^{2+} to visualize the trends within this range of calcium concentrations. Daptomycin insertion into the two lung surfactant models reaches an initial plateau (P_{L1}) just before 0.1 mM Ca^{2+} and a final plateau (P_{L2}) at approximately 2 mM Ca^{2+}; daptomycin insertion into the BM model reaches an initial plateau (P_{B1}) at 0.1 mM Ca^{2+} and then a secondary plateau (P_{B2}) at 10 mM Ca^{2+}. The degree of daptomycin insertion into BM surpasses that of P_L at 8 mM Ca^{2+}.

at some higher calcium concentration to interact more strongly to bacterial membrane instead of lung surfactant. To further elucidate this odd behaviour, a full calcium titration experiment was performed to pinpoint what calcium concentrations these points of inflection are occurring at.

Emission spectra were obtained for three models (bacterial membrane, lung surfactant and BLES®) in the presence of daptomycin and calcium ranging from 0 mM to 50 mM (***Figure 5.5A***). At least three trials were performed, with three repeats or measurements each, and the emission peaks at 345 nm were averaged for each scenario and plotted onto a graph, as seen in ***Figures 5.5B and 5.5C***. By looking at the full plot from 0 mM to 50 mM Ca^{2+}, it can be seen that no significant changes occur past about 15 mM Ca^{2}. For both the bacterial membrane and lung surfactant models, an initial plateau (P_{B1} and P_{L1}) is reached at approximately 0.1 mM Ca^{2+}. Daptomycin's emission intensity increases immediately afterwards for the lung surfactant model until a secondary plateau (P_{L2}) is reached at 2 mM Ca^{2+}. Meanwhile, the intensity for the bacterial membrane model does not start to increase again until about 4 mM Ca^{2+}, reaching a 50% increase at 6 mM Ca^{2+} until a final plateau (P_{B2}) is reached at 10 mM Ca^{2+}.

The trends presented in this calcium titration provide information on why two different results were seen in the first two experiments with 2 mM and 10 mM Ca^{2+}. With lung surfactant, the second plateau is reached much sooner than that of the bacterial membranes, so stronger intensities are observed for lung surfactant at lower calcium concentrations. However, when comparing final plateaus of intensity, bacterial membrane has a greater value of emission intensity, so when this plateau is reached at higher calcium concentrations, greater emission intensity will be observed for bacterial membrane models versus the lung surfactant models. These results also show the strong correlation between the two lung surfactant models.

5.3.2 Interaction of CB-182,462 with Membrane Models

A second set of experiments were performed alongside those for daptomycin; these experiments focused on CB-182,462 instead. Similar to daptomycin, experiments were performed first at 10 mM of calcium and then 2 mM of calcium.

5.3.2.1 Fluorescence Spectra of CB-182,462 with Membrane Models at 10 mM Ca^{2+}

In ***Figure 5.6***, preliminary emission spectra were obtained for the tryptophan present in CB-182,462 at a calcium concentration of 10 mM. Very low emission peaks were observed for the

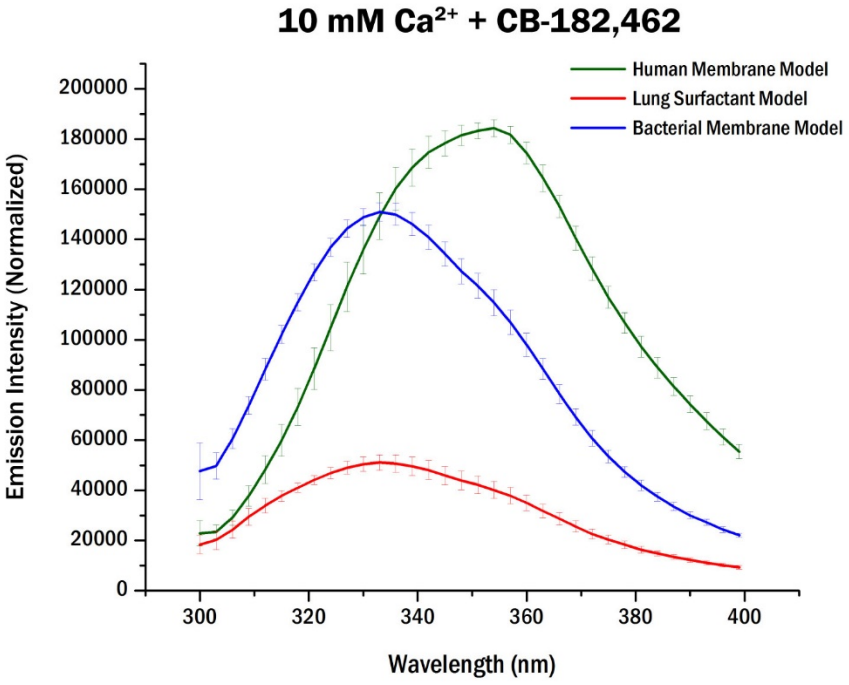

Figure 5.6 Preliminary data obtained for BM, HM, LS models with CB-182,462 at 10 mM Ca^{2+}. These plots show the normalized emission spectra obtained for CB-182,462 in the presence of 10 mM Ca^{2+} for different model liposomes (bacterial membrane, human membrane, lung surfactant lipid models). The tryptophan residue on CB-182,462 was excited at 280 nm, and emission spectra were acquired from 300 - 400 nm. Each measurement was repeated at least 3 times in each of the 3 trials.

interaction of CB-182,462 to the lung surfactant liposomes (in red), suggesting that this semisynthetic derivative may not interact much with or be inhibited by lung surfactant. Meanwhile, CB-182,462 induced greater emission intensities in the bacterial membrane model (in blue) and human membrane model (in green), suggesting it binds to and inserts with both types of membranes. Interestingly, for the human membrane model, a noticeable spectral shift in its emission spectrum was observed in the presence of calcium and CB-182,462, relative to the lung surfactant and bacterial membrane model emission spectra. This supports our hypothesis that CB-182,462 interacts with the human membrane model differently than other models, potentially causing toxic effects. To elucidate this spectral shift and determine whether any noticeable differences occurred at different calcium concentrations, further experiments and controls were performed at a 2 mM concentration of calcium to better mimic a physiological environment.

5.3.2.2 Fluorescence Spectra of CB-182,462 with Membrane Models at 2 mM Ca^{2+}

Emission spectra were obtained for CB-183,462 with different membrane models at 2 mM of calcium. If we look at ***Figure 5.7B***, the trends for CB-182,462 are fairly similar to those we saw in the 10 mM Ca^{2+} set of experiments, so different calcium concentrations do not seem to play a role in the trends observed between models.

The emission spectra for both the LS and BLES models are almost identical, showing great correlation with similar peak emission intensities at 333 nm, while the peak emission intensity for BM was at least twice this value. Interestingly, a blue-shift of 21 nm is observed in the emission spectra of the LS/BLES® and BM models, relative to their emission spectra in the absence of calcium (at 354 nm). For the HM model, the peak of the emission spectra is now wider than that of the BM model, and its peak emission intensity is slightly higher than that of the BM model and at a wavelength of 354 nm, which means that no blue shift is observed from the controls. These differences were statistically significant ($p < \alpha$).

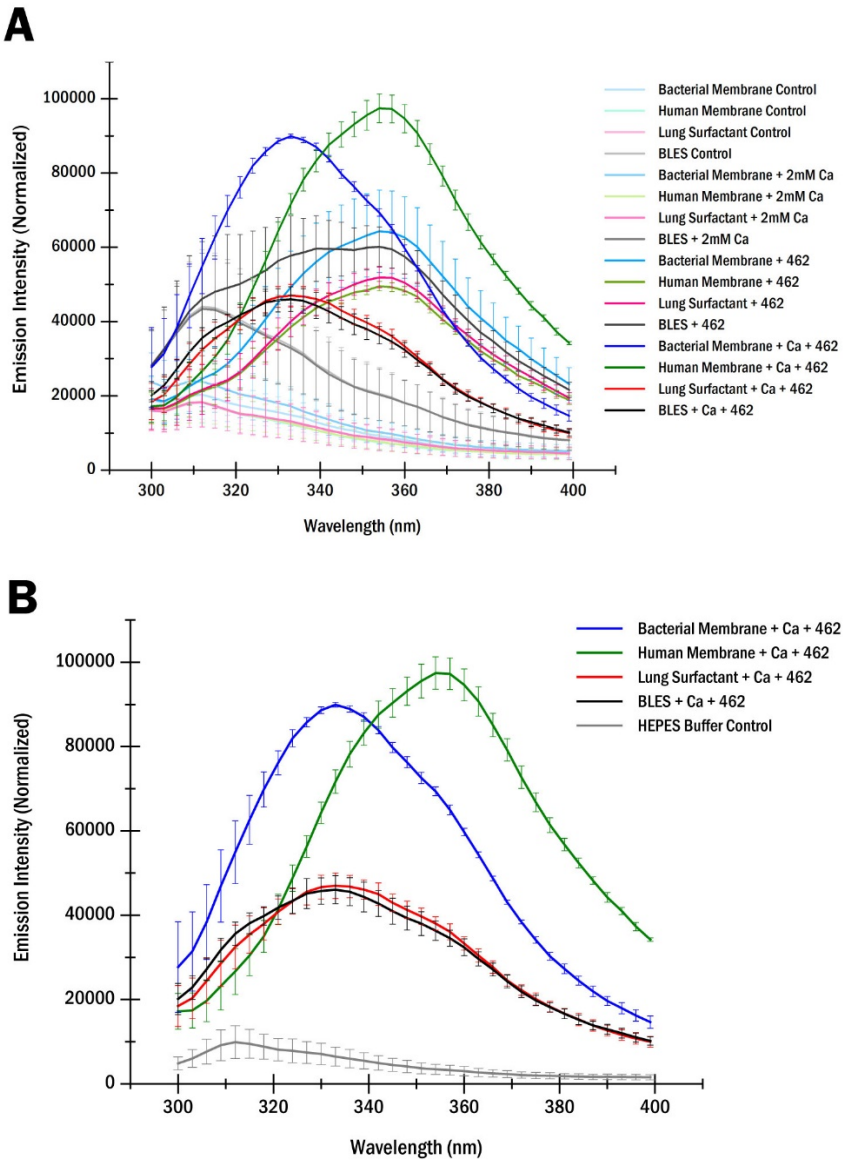

Figure 5.7 Emission spectra for 2 mM Ca^{2+} CB-182,462 experiments. (A) Emission spectra were obtained from 300 – 400 nm for a full set of experiments for CB-182,462 with excitation wavelength at 280 nm for tryptophan. Similar to the daptomycin set of experiments in ***Figure 5.4***, the same set of hues were used to designate each model. (B) Averaged emission spectra for each membrane models in the presence of calcium and CB-182,462, presented with a buffer control. There is less exhibited insertion of CB-182,462 in the LS/BLES® models as compared to the BM model, but there is strong insertion in the HM model. A blue shift relative to the liposome controls with CB-182,462, seen in (A), is observed for the LS/BLES® and BM models in the presence of 462 and Ca^{2+}. For all experiments, three trials were performed with at least 3 emission spectra obtained for each trial and scenario.

These results show that CB-182,462 does not interact with LS, which explains why LS does not inhibit its antibacterial activity. Moreover, they provide additional evidence that our synthetic LS liposomes are excellent models of natural BLES surfactant due to their similar findings. Moreover, although CB-182,462 can interact strongly with bacterial membranes, it is also toxic and not only interacts more into human membranes, but also does not experience the blue shift that other models do, which may signify other conformational or electrostatic changes are at play in its action mechanism.

5.4 Discussion

Model membranes have been used in a variety of studies to mimic biological structures and provide us with details on their interactions with different molecules, such as cationic peptides [337]. Liposome models for bacterial membranes, human cell membranes and both synthetic and natural lung surfactant were developed and used in this study. The bacterial membrane of a generic bacterium was modeled with a 20:20:60 ratio of DOPG/TOCL/POPE, while the human membrane was modeled with a 20:20:10:15:35 ratio of DPPC/POPE/DOPS/sphingomyelin/ cholesterol. Lung surfactant was represented by creating a liposome containing an 80:20 ratio of DPPC/DOPG with 5% cholesterol, a model which has been successfully used with previous studies [250, 258]. To test the validity of this synthetic lung surfactant lipid model, BLES® natural bovine surfactant was used to create a natural BLES® lung surfactant model following additional lipid extraction procedures. Large unilamellar vesicles of BLES® were successfully created and reported for the first time as previous studies have only been performed with giant unilamellar vesicles [338-340]. Lipid extraction had to be performed at least 18 times to be able to form working BLES® vesicles that could pass through an extruder and it is assumed that the original BLES® suspension contained too many large proteins (most likely surfactant proteins SP-B and SP-C that help in surfactant spreading) that hindered the formation of smaller lipid vesicles. However, it is important to note

that due to the large number of extractions performed, it is highly likely that the lipid composition of BLES® will be affected on top of the removal of these large proteins. As a result, our natural BLES® surfactant can only be considered a more complex lung surfactant model compared to our synthetic one. The results obtained for our synthetic lung surfactant lipid model and natural BLES® lipid model liposomes correlated extremely well with each other, which suggests that our lung surfactant lipid model with an 80:20 ratio of DPPC/DOPG with 5% cholesterol can act as a substitute for natural lung surfactant in modelling studies.

5.4.1 Daptomycin Binds to Lung Surfactant and Bacterial Membranes with Similar Affinity

In this study, fluorescence spectroscopy was used to evaluate the interaction of daptomycin with four model liposomes. In particular, the main goal of this study was to determine the interaction of daptomycin with bacterial membranes versus lung surfactant because direct experimental evidence of daptomycin's sequestration by lung surfactant is lacking.

The fluorescence spectroscopy data presented in *Chapter 5.3.1* allow us to draw several conclusions when comparing daptomycin's interaction with the different membrane models. In every experiment, the addition of daptomycin and calcium to the human membrane model did not result in a significant fluorescence increase compared to the controls, suggesting that daptomycin does not interact with the human membrane. Meanwhile, the addition of calcium and daptomycin to the bacterial membrane model induced a significant fluorescence increase. The high emission intensities observed for daptomycin's interaction with bacterial membrane at 2 mM Ca^{2+} indicate that the kynurenine residue is located within an environment with low polarity, which suggests a deeper insertion of kynurenine into the bacterial membrane. Although we can correlate emission intensity with the degree of interaction of daptomycin with the membrane, it is hard to pinpoint the type of interaction being experienced: daptomycin could be inserting more deeply into the membrane, there could be conformational changes brought

upon by varying membrane polarity, and it may be that daptomycin resides at the same depth of insertion in the same conformation while both membranes differ in polarity at that level. However, numerous studies have shown this increase in fluorescence, and there is a general consensus that the increase in emission intensity observed when daptomycin and calcium are added to bacterial membrane liposomes indicates the binding and insertion of daptomycin into the membrane [61, 68]. Our data provide additional evidence for daptomycin's dependence on calcium as part of its mechanism of action.

Interestingly, an increase in fluorescence was also observed when daptomycin and calcium were added to both the synthetic and natural lung surfactant models. This suggests that daptomycin does bind or insert into lung surfactant, and that this action is dependent on the presence of calcium. What is even more intriguing is that the initial binding of daptomycin to both the lung surfactant models and bacterial membrane occur very early on at approximately 0.1 mM Ca^{2+}. This suggests daptomycin has a similar affinity to lung surfactant and bacterial membrane, and that, when both are present in the same compartment, lung surfactant will effectively compete with bacterial membranes for the binding of daptomycin. This scenario would apply to the lung tissue in community-acquired pneumonia and can readily explain why daptomycin is not therapeutically effective in this disease.

Previous studies have shown that daptomycin's bactericidal activity against *S. pneumoniae* is extremely potent *in vitro* (MIC_{90} at 0.06 μg/mL), but greatly diminished *in vivo* due to the presence of lung surfactant [10, 341]. This inhibition has also been confirmed by *in vitro* antibacterial assays, where daptomycin was shown to interact with bovine-derived lung surfactant extract aggregates and exhibit increased MIC (minimal inhibitory concentration) values in a calcium-dependent manner [10]. It has been postulated that because lung surfactant and bacterial membranes share some of the same lipid composition, primarily phosphatidylglycerol (PG), daptomycin is capable of inserting into lung surfactant. It has also been shown that daptomycin requires the presence of PG in order to oligomerize and subsequently insert into the bacterial membrane to exert bactericidal activity [68, 104, 140, 342-344]. Although lung surfactant

contains somewhat less PG than bacterial membranes, the vast amount of surfactant outweighs the small, collective surface area of the exposed bacterial membranes, suggesting that daptomycin would be sequestered by lung surfactant. Our data not only confirm that the binding of daptomycin to lung surfactant is calcium-dependent, but provides evidence of the sequestration of daptomycin by lung surfactant due to possible competition between lung surfactant and bacteria to bind daptomycin. In fact, since it has been shown that daptomycin oligomerization occurs on membranes with PC and PG [68], we hypothesize that this sequestration of daptomycin may not just be driven by a strong binding affinity to lung surfactant, but also an oligomerization event which may lead to deeper membrane insertion.

5.4.2 Higher Calcium Concentrations may Remove Inhibited Late Step of Daptomycin Pore Formation in Bacterial Membranes

Apart from elucidating daptomycin's interaction with lung surfactant, our fluorescence spectroscopy data also show that calcium concentration has a powerful effect on the emission intensity of daptomycin with bacterial membrane. As seen in ***Figure 5.5C***, at lower calcium concentrations, daptomycin reaches an intensity plateau with bacterial membrane at about 0.1 mM Ca^{2+}. However, emission starts to rise again and reaches a second plateau at around 10 mM Ca^{2+}. The calcium concentration that elicited an approximate 50% fluorescence increase from the initial plateau is 6 mM Ca^{2+}, suggesting that the supplementation of additional calcium causes some sort of conformational change in either daptomycin or the bacterial membrane.

A pronounced effect of high calcium concentrations has also been observed in a recent study by Lohani *et al.*, where the MIC of daptomycin against *B. subtilis* (1046) was reduced from 0.75 μg/mL at 5 mM $CaCl_2$ to 0.5 μg/mL at 25 mM and 100 mM $CaCl_2$ [345, 346]. However, their results only compared MIC values for three separate calcium concentrations. Our study expands on their findings by presenting a clear trend in increasing daptomycin insertion into bacterial membrane model liposomes with increasing calcium concentrations. Although the mechanism

by which this transition occurs needs to be elucidated in further studies, we know that the primary difference between our two models is their lipid composition.

A previous study by Zhang *et al.* has shown that the presence of cardiolipin within the membrane can prevent a late step in daptomycin's mechanism of pore formation [106]. Their suggested mechanism of action is presented in ***Figure 1.8***, where (1) daptomycin binds to the outer leaflet of the target membrane, (2) four molecules of daptomycin form a tetramer in the outer leaflet, (3) this tetramer translocates to the inner leaflet of the membrane, and (4) two aligned tetramers from opposite leaflets form an octameric and functional pore. In their study, they showed that daptomycin bound to PG and CL more than PC in their lipid membrane models. This group also provided evidence that membranes containing both PG and CL can induce the oligomerization of daptomycin [106]. However, they hypothesized that the third step, the translocation of tetramers to the inner leaflet, is inhibited on membranes that contain cardiolipin at low calcium concentrations [106]. According to our results, we observe two intensity plateaus with bacterial membrane model. It may very well be that this translocation step correlates with the second plateau, and that a higher calcium concentration could overcome the inhibition placed upon it by cardiolipin. Further studies will need to be performed to elucidate this.

Since there is evidence of two plateaus (P_{B1} and P_{B2} from ***Figure 5.5C***) for the bacterial membrane model, with P_{B2} being much greater than the insertion plateau reached by daptomycin insertion into lung surfactant, we also speculate that the bactericidal activity of daptomycin against *S. pneumoniae* may increase with localized calcium supplementation in the presence of lung surfactant. Of course, it is harmful to increase the *in vivo* concentration of calcium to such high values, so additional avenues of research should be pursued to determine whether it is possible to localize such exposures to high calcium concentrations.

5.4.3 CB-182,462 Binds to Human and Bacterial Membrane Models

Fluorescence spectroscopy studies were also performed to elucidate CB-182,462's mechanism of action and the difference in interaction between different membrane models. In ***Chapter 5.3.2***, the trends in emission spectra for 2 mM and 10 mM Ca^{2+} did not change for CB-182,462 and the four membrane models. It was shown that both the synthetic and natural lung surfactant models had the lowest emission intensity with calcium and CB-182,462, comparable to that of the membrane controls. This not only suggests that our LS model is a good substitute for BLES®, but that CB-182,462 may not interact much with surfactant, and is therefore uninhibited by it. However, a noticeable blue shift of 21 nm is observed between the membrane and CB-182,462 controls and LS/BLES + Ca^{2+} + 462. Additional controls will need to be examined in further experiments to determine whether this blue shift is a result of just calcium binding to CB-182,462, or whether it is due to a membrane interaction of some nature. Nevertheless, we hypothesize that because calcium induces daptomycin aggregation, that it may also induce CB-182,462 aggregation, which would in turn produce a blue shift in the emission spectra.

If we look at CB-182,462's interaction with the bacterial membrane model in the presence of calcium, we see a similar blue shift as with the lung surfactant models with 462 and calcium, but much greater emission intensity. Red-shifts in tryptophan fluorescence have been reported in solutions with higher polarity [347-349]. In terms of bilayers, tryptophan residues buried deep into a bilayer have shown larger blue-shifts than those that are exposed to lipid and oligomerized at the surface of a bilayer leaflet [350-354]. The combination of a blue shift and increase in emission intensity suggest that multiple events are occurring, which may include the transition of CB-182,462 into a less polar environment as observed with previous studies on tryptophan, or some kind of membrane interaction. CB-182,462's strong binding with the bacterial membrane model suggests that it can exhibit strong potency against bacteria in the presence of lung surfactant. This was already confirmed during pre-IND (Investigational New Drug) testing (J. Silverman, personal communication).

Interestingly, when CB-182,462 is added to the human membrane model with calcium, there is no longer a blue shift, but the emission intensity is even higher than that of the bacterial membrane. There are two possible explanations for this. First, the lack of a blue shift may indicate that the human membrane interaction of CB-182,462 may be incomplete or modified compared its interaction with bacterial membranes. Since this blue-shift was not observed for the human membrane model with calcium and 462, relative to its calcium-free counterpart, we believe that CB-182,462 does not insert more deeply into the human membrane model liposome, but rather localizes more onto the surface of the membrane; this may or may not be accompanied by the formation of oligomers. Second, CB-182,462 still binds to the human membrane and may trigger some form of perturbation that will ultimately result in tissue damage. The mechanism for this damage will need to be studied further, and future research should involve permeability studies to determine whether membrane permeabilization is required for toxicity, or whether this toxicity can be attributed to binding events.

The oligomerization of CB-182,462 onto human membrane model liposomes and its strong insertion into bacterial membrane versus lung surfactant lipid models in the presence of calcium constitute the first of such evidence.

5.5 Conclusion

Direct experimental evidence of daptomycin sequestration by lung surfactant is currently lacking. It has been speculated that daptomycin is inhibited by lung surfactant due to the vast abundance of lung surfactant versus the small presence of bacterial cells, and therefore daptomycin would be trapped in this lung surfactant and not be free to exert its bactericidal effect on *S. pneumoniae* within the lungs.

In this study, we have shown that fluorescence spectroscopy can be used to compare the extent of binding and insertion of an antimicrobial peptide into different lipid membrane models.

BLES® surfactant was also transformed into large unilamellar vesicles for the first time using novel protocols developed for this experiment.

The results from this study provide strong evidence to support the theory that daptomycin is inhibited by lung surfactant not only because of the vast abundance of the surfactant, but also because it has a similar affinity to bind to lung surfactant as it does to bacterial membrane. This potential competition may exacerbate its inhibition by lung surfactant. Additional evidence was also obtained to verify daptomycin's dependency on calcium to exert its mechanism of action. Our results also suggest that increasing the calcium concentration may help remove the inhibition that cardiolipin places upon a late step of daptomycin pore formation in bacterial membranes, which is related to its translocation to the inner membrane leaflet.

Meanwhile, the semisynthetic antibiotic CB-182,462 was shown to exhibit strong binding to the human membrane model liposomes at all concentrations of calcium, providing a possible explanation for its toxicity where it binds to and causes some form of membrane damage.

Overall, our studies present a good correlation of *in vitro* versus *in vivo* observations. Our lung surfactant models can be used for the rapid screening of novel daptomycin derivatives to test for surfactant-driven inhibition, while our human membrane models can be used to test for toxicity potential.

Future studies that may help provide additional insight into daptomycin's inhibition by lung surfactant in cases of pneumococcal infection could involve competitive binding assays that test daptomycin's preference in binding between lung surfactant lipid models and bacterial membrane models. It will also be useful to determine whether daptomycin oligomerizes when inserting into lung surfactant, and if so, how many daptomycin molecules form this oligomer. Studies could also be performed in testing daptomycin's bactericidal activity against *S. pneumoniae* in the presence of lung surfactant at different calcium concentrations, as stronger binding to bacterial membrane model liposomes was observed in this study at higher calcium concentrations. Another study related to daptomycin may involve laurdan fluorescence intensity

experiments to determine how daptomycin can change membrane phase properties for both bacterial membranes and lung surfactant due to its sensitivity to polarity within the bilayer. This would provide insight into whether daptomycin causes changes in membrane polarity and structure in the presence of calcium. CB-182,462 can be studied further using permeability testing to elucidate its mechanism of toxicity.

CHAPTER 6

6 LANGMUIR-BLODGETT MONOLAYER STUDIES: DAPTOMYCIN STRONGLY INSERTS INTO AND DECREASES THE COMPRESSIBILITY OF LUNG SURFACTANT

6.1 Introduction

Daptomycin (*Figure 1.3*) is a lipopeptide antibiotic that has a 13 amino acid residues, 10 of which are arranged cyclically and 3 on an exocyclic tail [67, 355]. Its action mechanism is distinct from that of most other clinically used antibiotics, which means that it is unaffected by resistance mechanisms that are specific for the latter. Therefore, it can be used against resistant strains of Gram-positive pathogens, such as MRSA and VRE [4, 8, 9]. Consistent reports have shown that daptomycin's mechanism of action involves depolarization of the bacterial membrane [61, 62,

96, 356], while other molecular targets and modes of actions have been suggested, such as the inhibition of peptidoglycan synthesis [65, 357]. Apart from its mechanism of action not being fully understood, even more peculiar is its inhibition by lung surfactant in the context of pneumococcal pneumonia caused by *Streptococcus pneumoniae* [10]. The study performed in ***Chapter 5*** has shown evidence of daptomycin sequestration by lung surfactant at physiological calcium concentrations. However, daptomycin's mechanism of inhibition by lung surfactant may very well be multifaceted and not as straightforward as having a binding affinity to surfactant.

Although model membranes such as vesicles and supported bilayers may be used to study daptomycin's effect, it is important to note that lipid monolayers are also excellent model systems that have provided a great deal of insight into surface interactions taking place on a single membrane leaflet [175, 176, 337]. This study aims to provide further insight into the effect of daptomycin on lung surfactant monolayer properties using Langmuir-Blodgett monolayer techniques. The data obtained from our daptomycin experiments will be compared with another set of experiments performed with CB-182,462 (see ***Figure 1.10***), a semisynthetic derivative similar to daptomycin that is not inhibited by lung surfactant and still presents potent bactericidal activity, but causes kidney phospholipidosis (J. Silverman, personal communication). Although CB-182,462 was never brought to clinical trials due to its toxicity problems, comparing its effect on monolayer properties with that of daptomycin may prove useful in understanding their differences. The four lipid models that will be used in this study are related to systems that these two antibiotics would encounter in the case of a patient presenting with pneumonia caused by *S. pneumoniae*: a bacterial membrane model will be based off of the lipid composition of *S. pneumoniae*, a human membrane model will be based off of erythrocyte endothelial cell membranes, and both synthetic and natural lung surfactant models will be used.

Compression isotherms were taken of each monolayer model by itself as a control and in the presence of calcium, daptomycin/CB-182,462 or both. These compression isotherms are obtained when the Langmuir-Blodgett trough barriers compress the monolayer until the minimum trough area is reached and provide data on monolayer compressibility at any chosen

pressure. Our results show that at a pressure of 40 mN/m, the elastic area compressibility modulus of our synthetic and natural lung surfactant monolayers increased significantly, which directly translated into reduced monolayer compressibility.

Insertion assays were also performed for each monolayer model in the same scenarios as those presented in the compression isotherm studies. Here, the monolayers were compressed to a lower pressure of 20 mN/m and either daptomycin or CB-182,462 was injected underneath the monolayer to record any changes in pressure; any increase in pressure would represent a greater amount of insertion into the monolayer being studied. Our results strongly correlate with the fluorescence spectroscopy data obtained in *Chapter 5*.

The studies presented in this chapter provide further insight into the behaviour of daptomycin in the presence of lung surfactant. From our results, it can be seen that daptomycin does not just insert more into lung surfactant than bacterial membrane lipid monolayers, but it also decreases the compressibility of lung surfactant significantly, especially in the case of BLES® natural bovine surfactant extract. This leads us to suggest a new model of daptomycin sequestration by lung surfactant, where daptomycin is not just inserted into the lung surfactant, but may help confer certain surfactant-spreading properties that promote the function of lung surfactant. This means that the lung surfactant may be able to form multilayers at lower pressures than normal, effectively trapping daptomycin within these layers of lung surfactant and reinforcing its sequestration.

6.2 Materials and Methods

6.2.1 Lipid Models

There were four lipid models used in this study. The bacterial membrane (BM) lipid model consisted of 20% PG, 20% CL, and 60% PE while the human membrane (HM) lipid model was composed of 20% PC, 20% PE, 10% PS, 15% sphingomyelin, and 35% cholesterol. Modified

natural BLES® lung surfactant was used as our natural lung surfactant model while a synthetic lung surfactant (LS) model was made from 80% PC and 20% PG with 5% cholesterol by mass. Additional details regarding each of these models area available in ***Chapter 3***.

6.2.2 Solution Preparation

The majority of the lipids used in each of the models were purchased from Avanti Polar Lipids (Alabaster, Alabama, US) in powder form with >99% purity: 1,2-dipalmitoyl-*sn*-glycero-3-phosphocholine (DPPC), 1,2-dioleoyl-*sn*-glycero-3-[phospho-*rac*-(1-glycerol)] (DOPG), 1-palmitoyl-2-oleoyl-*sn*-glycero-3-phosphoethanolamine (POPE), 1,2-dioleoyl-*sn*-glycero-3-[phospho-L-serine] (DOPS), 1,1'2,2'-tetraoleoyl cardiolipin (TOCL), and sphingomyelin (egg, chicken). Cholesterol (>99% purity) was purchased from Sigma-Aldrich (St. Louis, Missouri, US).

Prior to starting experiments on the Langmuir-Blodgett trough, 1 mM mixed lipid stock solutions had to be made for each of the models being studied (see ***Appendix C1*** for detailed protocols). Stock solutions of 1 mM daptomycin, 1 mM CB-182,462 and 100 mM $CaCl_2$ were also prepared (see ***Appendix A*** for detailed procedures).

6.2.3 Langmuir-Blodgett Trough Techniques

6.2.3.1 Monolayer Compression Isotherms

A Langmuir-Blodgett micro-trough from NIMA Technology Ltd. (Coventry, England) was used for the monolayer experiments in this study. Trough cleaning procedures are available in ***Appendix C2***.

For compression isotherms, the surface pressure of Langmuir monolayers was continuously measured as the area of the trough decreased to create a pressure-area isotherm. The trough was filled with a set amount of Milli-Q® ultrapure water (resistivity greater than 18.2 MΩ·cm) and, depending on whether calcium was incorporated into the solution, the final calcium concentration in the ultrapure water subphase was 2 mM. During the acquisition of compression isotherms, the chosen model lipid mixture (stock solution in 4:1 ratio of chloroform/methanol) was added on top of the subphase in between the two trough barriers and left for at least 10 minutes to let the solvent evaporate. A Hamilton® gastight syringe (Reno, Nevada, United States of America) with a precision-machined PTFE plunger tip and leak-free seal was used for depositing lipid solutions. The trough barriers were then set at a speed of 20 cm^2/min to compress the Langmuir monolayer on the surface of the subphase. A set amount of daptomycin, CB-182,462 or ultrapure water (for control runs without either antibiotic) was injected underneath the monolayer prior to the start of compression. The final concentration of daptomycin or CB-182,462 in the subphase was 4 μM (slightly higher than their MIC). For a detailed explanation of experimental protocols for compression isotherms, please refer to *Appendix C3*.

Once the compression isotherms were recorded, the resulting plot had pressure (mN/m) on the *y*-axis and absolute area (cm^2) on the *x*-axis. In order to calculate the elastic area compressibility modulus, this *x*-axis had to be converted to molecular area, or area per molecule ($Å^2$/molecule) using the following equation [358], where a_m is the molecular area, A is the absolute area, M_w is the average molecular weight of all lipids in the mixture (g/mol), c is the concentration of the lipid mixture (mg/mL), N_A is Avogadro's number (molecules/mol), and V is the volume of lipid mixture added atop the subphase (μL):

$$a_m = \frac{(A)(M_W)}{(c)(N_A)(V)} \qquad \text{(Eq. 4)}$$

From here, we can obtain a pressure versus molecular area isotherm, which can be directly used to calculate the elastic area compressibility modulus. A particular pressure is chosen at which the most changes are observed between slopes across all isotherms. In our case, a pressure of 40 mN/m was chosen as clear differences in slope were qualitatively observed between each model and scenario. To calculate the elastic area compressibility modulus or C_s^{-1}, the following equation was used, where A is molecular area, and Π is the surface pressure [290, 359, 360]. Note that higher C_s^{-1} values correspond to lower monolayer compressibility [290, 360].

$$C_s^{-1} = -A\left(\frac{d\Pi}{dA}\right) \qquad \text{(Eq. 5)}$$

A minimum of three compression isotherms were taken for at least three trials and variance was analyzed using one-way ANOVA with Tukey's *post hoc* test for statistical significant ($\alpha = 0.01$)

6.2.3.2 Monolayer Insertion Assays

Using the same Langmuir-Blodgett micro-trough, constant-area insertion assays were performed. Each monolayer was prepared on an ultrapure water subphase (with or without 2 mM Ca^{2+}) and compressed to a target pressure of 20 mN/m at a compression speed of 20 cm^2/min. Once this pressure was reached, the trough barriers were locked in place. Using a Hamilton® syringe (Reno, Nevada, United States of America) and a 22-gauge, 2-inch needle that was custom-bent into an L-shape, a set amount of either daptomycin, CB-182,462 or ultrapure water (as a control) was injected gently and carefully underneath one of the trough barriers under the preformed monolayer using uniform force and speed. After injection, the Hamilton® syringe was carefully removed and the pressure readings were taken for at least 5 minutes until a steady plateau was reached. Detailed instructions for Langmuir-Blodgett trough operation and experimental protocols are available in ***Appendix C4***.

At least 3 insertion assays were performed for each of the three trials, with fresh stock and lipid solutions made for each trial. The final pressure was recorded for each of the runs and averaged to obtain a mean pressure for each scenario. One-way ANOVA was used to test for variance and statistical significance, while Tukey's *post hoc* test was used to compare individual scenarios.

6.3 Results

6.3.1 Daptomycin Significantly Decreases the Compressibility of Lung Surfactant

Our previous studies (see ***Chapter 5***) have shown that daptomycin inserts strongly into our synthetic and natural lung surfactant models, while CB-182,462 does not. However, we are interested in elucidating the mechanism of inhibition that lung surfactant imposes on daptomycin. Since monolayers are good representatives of one leaflet of a membrane bilayer, monolayer studies were performed to monitor the effect of daptomycin and CB-182,462 on monolayer properties for each of our membrane lipid models.

Compression isotherms were gathered for each model monolayer (BM, HM, LS, and BLES® lipid models). Since it was not possible to enter the molecular weight of more than two different lipids and their ratios into the Langmuir-Blodgett trough control software, pressure versus absolute area isotherms were initially obtained so that proper calculations and conversion of the *x*-axis to molecular area could be completed using Eq. 3. Each lipid model had its own unique conversion rate due to their differing lipid ratios and molecular weights; the molecular weight used for Eq. 3 consisted of a weighted average of the molecular weights of each of the lipids within a particular model. After conversion of absolute area to molecular area, the compression isotherms were replotted onto a pressure versus molecular area graph (see ***Figure 6.1***).

From these compression isotherms, it can be seen that each monolayer follows a particular curve, and the slope of that curve at certain pressures is what sets each monolayer apart in terms of compressibility. In general, each monolayer starts off in a two-dimensional gas phase, where the

lipid molecules are disordered and do not really interact with each other as they are far apart. As the area decreases, the lipids are pushed closer together and enter into a liquid phase, which increases the pressure. As the pressure continues to rise, the lipids enter into a solid phase where the molecules are packed tightly together into one continuous and stable monolayer. Qualitatively, it can be seen that for both the LS and BLES® compression isotherms with daptomycin and calcium, the slope of the curve at the liquid-solid phase is much steeper compared to the slope of the curve for the BM and HM compression isotherms. Meanwhile, it seems that the slope for LS compression isotherm in the presence of calcium and CB-182,462 seems to be a bit steeper than the other models. However, qualitative observations are not enough to perceive the differences between these compression isotherms.

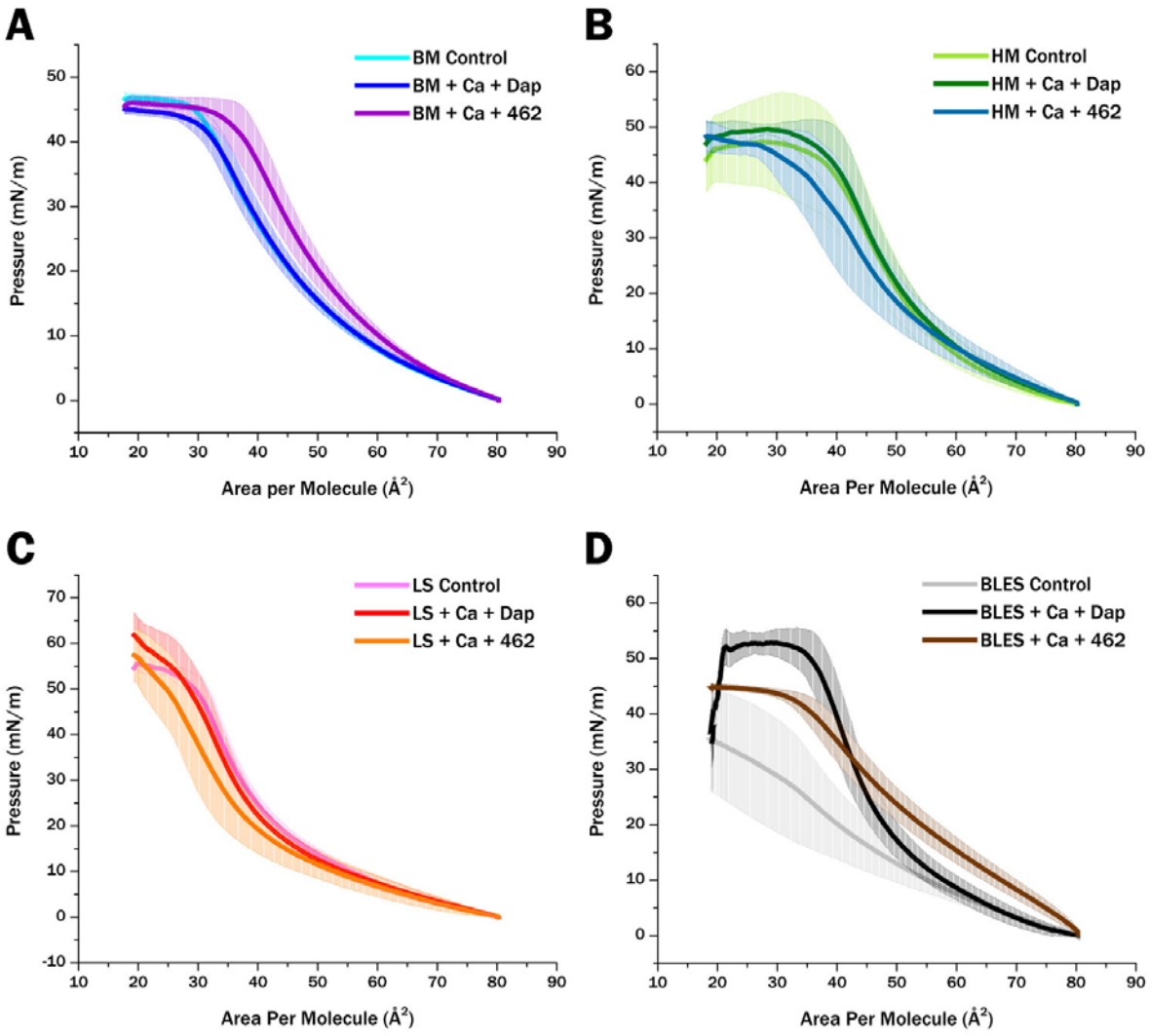

Figure 6.1 Pressure vs. molecular area graphs of compression isotherms. Compression isotherms were performed on each of the four membrane models: (A) bacterial membrane, (B) human membrane, (C) lung surfactant, and (D) BLES®. This data was then plotted using pressure versus molecular area. Each data point was obtained from at least 9 measurements spanning across three trials; error bars are shown for each measurement (shaded areas).

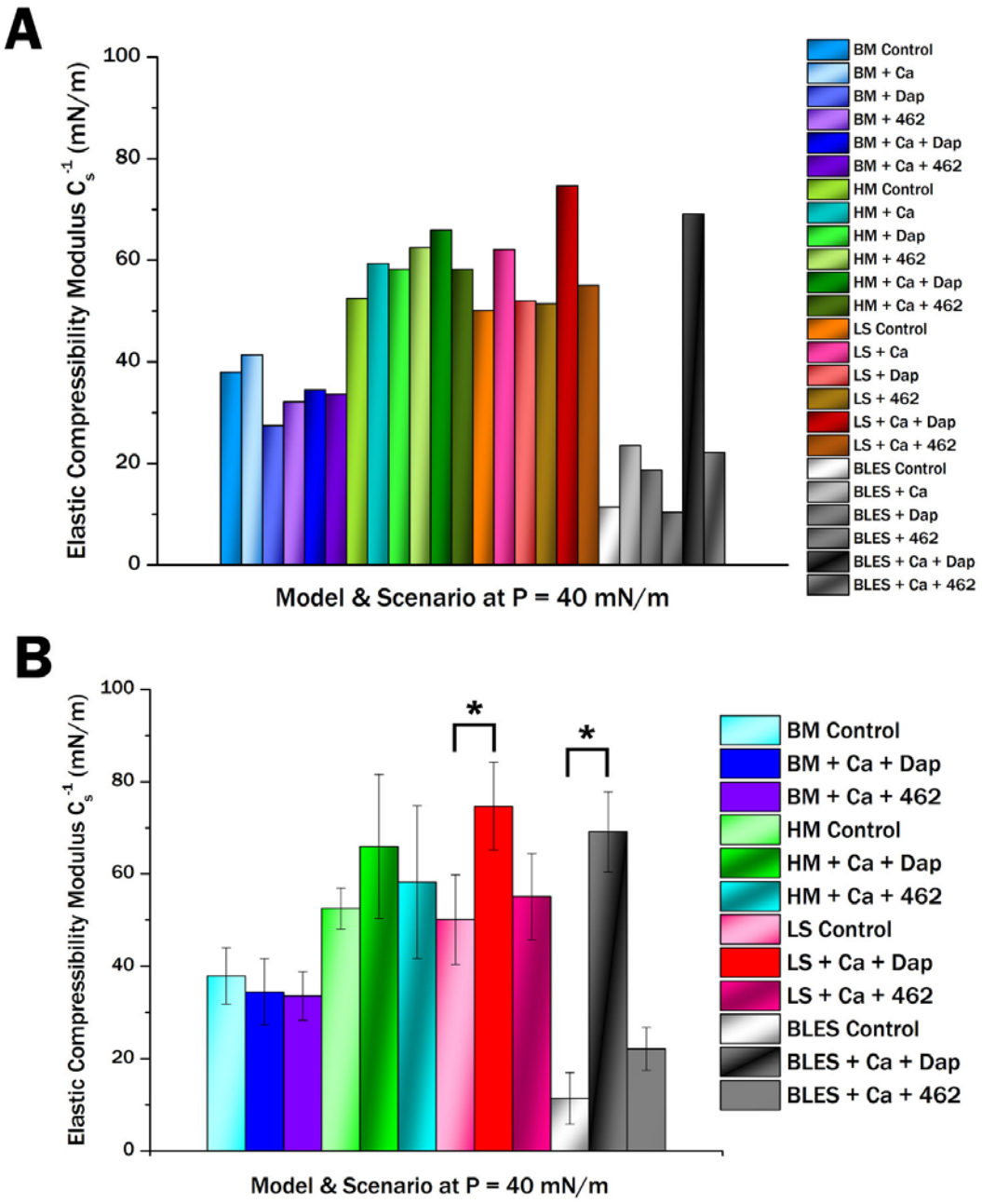

Figure 6.2 Comparison of C_s^{-1} for different models and scenarios. The elastic area compressibility modulus (C_s^{-1}) was calculated for each compression isotherm at a chosen pressure of 40 mN/m and plotted in a bar graph (see ***Table 6.1*** for values). In (A), the C_s^{-1} values for each model monolayer (BM, HM, LS, BLES®) in each scenario are shown. In (B), select compressibility moduli are shown for the controls of each monolayer model as well as in the presence of both Ca^{2+} and an antibiotic (DAP or 462). Statistical significance ($p < 0.01$) between means are depicted by an asterisk.

To calculate the elastic area compressibility modulus (C_s^{-1}) for each compression isotherm, a set pressure must be chosen for this comparison. Since each of the isotherms had their steepest slope near their solid phase, a pressure of 40 mN/m was chosen and the elastic area compressibility modulus of each isotherm was calculated using Eq. 4. ***Figure 6.2A*** shows each value obtained for C_s^{-1}, while ***Figure 6.2B*** shows the final results of these calculations for each model monolayer's control isotherm as well as the compression isotherms obtained in the presence of calcium and either daptomycin or CB-182,462. If we look at ***Figure 6.2B***, we can see that the compressibility of the BM or HM monolayers do not change much upon addition of calcium and daptomycin or CB-182,462. However, a significant change in compressibility is noticed for the lung surfactant monolayers. The synthetic LS monolayer has a base compressibility modulus of about 50.1 mN/m ± 9.7 mN/m, which increases to 74.7 mN/m ± 9.5 mN/m in the presence of calcium and daptomycin. That represents an approximately 50% increase in compressibility modulus of the synthetic lung surfactant monolayer, or in other words, an approximate 33% decrease in monolayer compressibility.

Remarkably, these changes are much more pronounced in the BLES® natural lung surfactant monolayer compressibility values. The control BLES® monolayer has a very low initial compressibility modulus of 11.4 mN/m ± 5.6 mN/m. However, in the presence of calcium and daptomycin, it experiences a six-fold increase and has a compressibility modulus of 69.1 mN/m ± 8.8 mN/m, meaning its monolayer compressibility has decreased significantly. The stark difference between these two models may very well be due to the fact that the synthetic lung surfactant model does not have any surfactant-associated proteins present, while the natural BLES® model may still have some surfactant-associated proteins incorporated within the monolayer that were not extracted during sample preparation.

From these results, it can be seen that daptomycin severely affects the compressibility of lung surfactant monolayers. However, additional monolayer properties could be tested using insertion assays, which would not only provide information on the insertion of either daptomycin or CB-

182,462 into these monolayers, but provide data on the stability of these monolayers as well after insertion events.

Table 6.1 Compressibility moduli of select models and scenarios. The elastic area compressibility modulus (mN/m) is presented for each model monolayer system (BM, HM, LS, and BLES®) at a pressure of 40 mN/m and select scenarios: monolayer control, monolayer with both calcium and daptomycin, and monolayer with both calcium and CB-182,462. Each value was obtained from at least 9 measurements.

Model & Scenario	Elastic Area Compressibility Modulus (mN/m)
BM Control	37.93 ± 6.06
BM + Ca^{2+} + Daptomycin	34.46 ± 7.26
BM + Ca^{2+} + CB-182,462	33.60 ± 5.22
HM Control	52.53 ± 4.42
HM + Ca^{2+} + Daptomycin	65.97 ±15.61
HM + Ca^{2+} + CB-182,462	58.25 ± 16.56
LS Control	50.11 ± 9.71
LS + Ca^{2+} + Daptomycin	74.67 ± 9.52
LS + Ca^{2+} + CB-182,462	55.08 ± 9.33
BLES® Control	11.38 ± 5.58
BLES® + Ca^{2+} + Daptomycin	69.11 ± 8.69
BLES® + Ca^{2+} + CB-182,462	22.12 ± 4.71

6.3.2 Daptomycin Inserts More into Lung Surfactant than Bacterial Membrane

Insertion assays with and without calcium were performed on each monolayer model in combination with a control injection (ultrapure water) or injections of either daptomycin or CB-182,462. Once a monolayer was compressed to a target pressure of 20 mN/m (assumed to be

in a liquid-condensed phase for the lipid models used), it was left to equilibrate for about 2 minutes prior to injection at t = 180 seconds. The resulting changes in pressure were then monitored for at least 5 minutes until t = 500 seconds. ***Figure 6.3*** compares the insertion assays performed for each monolayer model with either DAP or 462 in the presence of calcium.

In ***Figure 6.3A***, it can be seen that daptomycin, in the presence of calcium, does not insert into the human membrane model monolayer; the observed trace resembles the wide range of controls obtained for these sets of experiments (cases where no calcium is added or just ultrapure water instead of daptomycin). Meanwhile, daptomycin inserts strongly into the bacterial membrane model monolayer, reaching a pressure of about 23.5 mN/m ± 0.4 mN/m. Similar to previous findings reported in ***Chapter 5***, daptomycin experiences greater insertion into the lung surfactant models, reaching a final pressure of 26.10 mN/m ± 0.6 mN/m for the synthetic LS monolayer and 25.7 mN/m ± 0.3 mN/m for the natural BLES® monolayer. In the context of insertion, these results show us that our synthetic and natural lung surfactant models experience similar trends.

In ***Figure 6.3B***, the results for the CB-182,462 insertion assays can be observed. Once again, the lung surfactant monolayers have comparable results, and do not experience a significant degree of insertion from CB-182,462 in the presence of calcium (final pressure of 20.8 mN/m ± 0.2 mN/m for the LS monolayer and 20.5 mN/m ± 0.2 mN/m for the BLES® monolayer). This is expected because CB-182,462 functions in the presence of lung surfactant, and therefore should not bind to it. However, this is not the case with the bacterial membrane or human membrane models. Since CB-182,462 should exhibit strong bactericidal activity, strong insertion should be seen, and this is shown in our results with a pressure increase to 24.1 mN/m ± 0.4 mN/m at t = 500 seconds. Similar to the fluorescence experiments in ***Chapter 5***, CB-182,462 displays a strong interaction with the human membrane model, showing a great amount of insertion into the HM monolayer until a pressure of 25.1 mN/m ± 0.5 mN/m is reached. ***Figure 6.3C*** shows a bar graph of select scenarios and their corresponding final pressures, while ***Table 6.2*** shows the values corresponding to all scenarios.

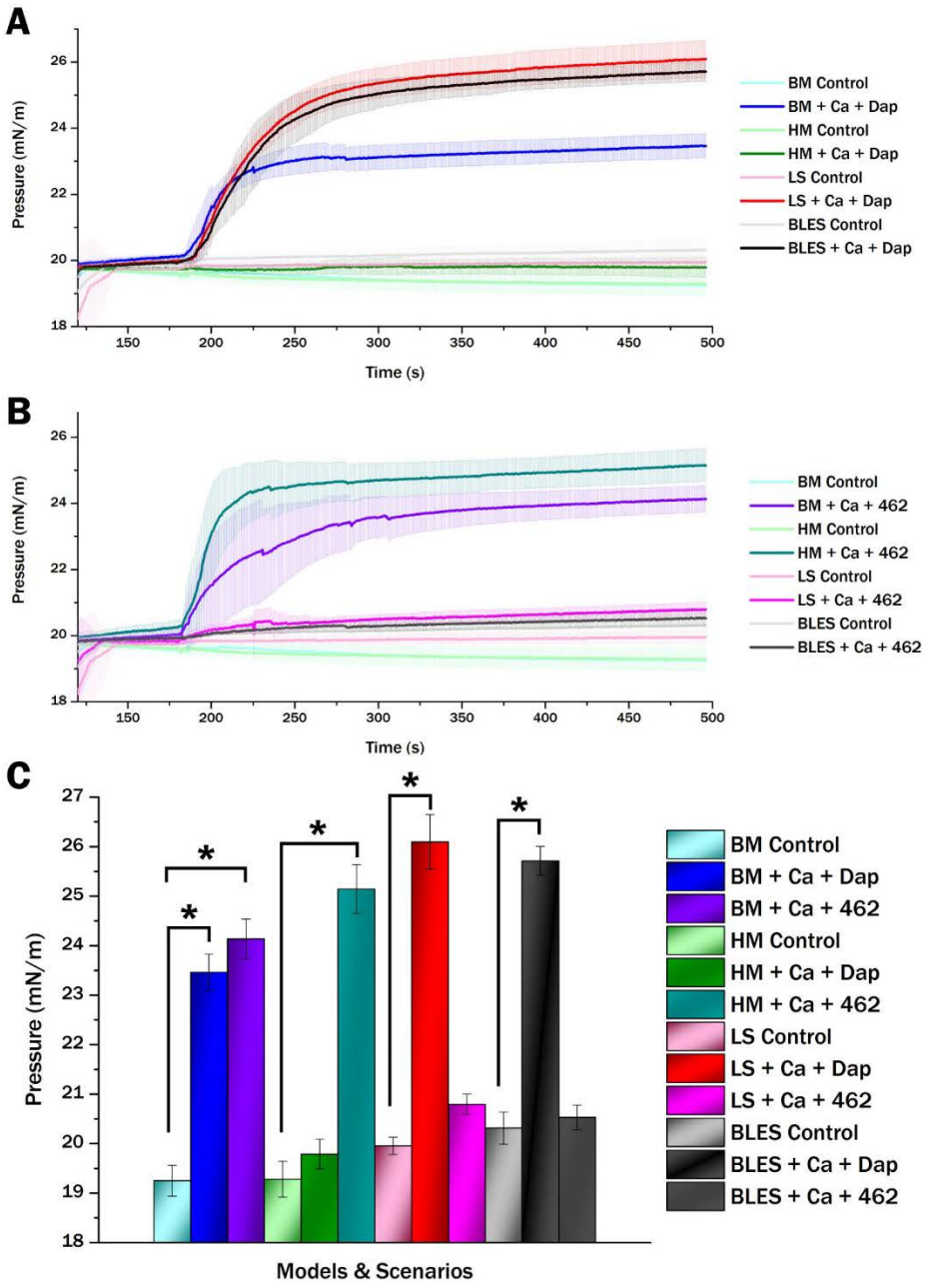

Figure 6.3 Insertion assay results for all model monolayers. Insertion assays were performed on each monolayer model (BM, HM, LS, BLES®) in different scenarios. Each monolayer was compressed to a target pressure of 20 mN/m, the trough barriers were locked in place, and an injection of either nanopure water (control), daptomycin, or CB-182,462 was made and the pressure changes recorded for a total of 5 minutes. At least 9 assays were performed per scenario. Plot (A) represents the insertion assays for the daptomycin experiments, plot (B) represents those for the CB-182,462 experiments, and plot (C) represents the pressure reached at $t = 500$ seconds. Statistical significance ($p < 0.01$) between groups is indicated by asterisks.

Table 6.2 Final surface pressure readings for insertion assay experiments. For each insertion assay experiment, the final surface pressure reading was taken at a time of 500 seconds. These readings are presented in this table, with each reading being an average of 9 measurements.

Model & Scenario	Surface Pressure @ t = 500 s (mN/m)
BM Control	19.25 ± 0.31
BM + Ca^{2+}	20.30 ± 0.15
BM + Daptomycin	20.09 ± 0.43
BM + CB-182,462	20.06 ± 0.30
BM + Ca^{2+} + Daptomycin	23.46 ± 0.37
BM + Ca^{2+} + CB-182,462	24.14 ± 0.40
HM Control	19.28 ± 0.37
HM + Ca^{2+}	19.42 ± 0.39
HM + Daptomycin	19.08 ± 0.15
HM + CB-182,462	19.32 ± 0.39
HM + Ca^{2+} + Daptomycin	19.79 ± 0.30
HM + Ca^{2+} + CB-182,462	25.14 ± 0.49
LS Control	19.95 ± 0.18
LS + Ca^{2+}	19.71 ± 0.25
LS + Daptomycin	19.99 ± 0.16
LS + CB-182,462	19.70 ± 0.27
LS + Ca^{2+} + Daptomycin	26.10 ± 0.55
LS + Ca^{2+} + CB-182,462	20.79 ± 0.20
BLES® Control	20.31 ± 0.33
BLES + Ca^{2+}	20.53 ± 0.18
BLES + Daptomycin	20.56 ± 0.20
BLES + CB-182,462	20.48 ± 0.14
BLES® + Ca^{2+} + Daptomycin	25.71 ± 0.29
BLES® + Ca^{2+} + CB-182,462	20.53 ± 0.25

6.4 Discussion

The Langmuir-Blodgett (LB) monolayer technique has been widely used to study monolayer lipid films at the air-water interface [184, 258, 361-364]. These lipid monolayers have been shown to be excellent, simplified models that allow us to study complex lipid systems [365]. In this study, monolayers of each of our lipid model systems were successfully formed. Compression isotherms and insertion assays were obtained to help elucidate the inhibition of daptomycin by lung surfactant.

The interaction of daptomycin with lung surfactant is important to understand, and is still relevant in cases of bacterial pneumonia, such as CAP. These causative bacteria have been shown to cause changes in lung surfactant: the bacteria may interact directly with secreted surfactant to change its physical properties (eg. density and surface tension), while others can indirectly affect surfactant by interacting with type II alveolar cells (eg. abnormal surfactant production and lipid composition) [366]. Although severe cases of pneumonia result in fluid-filled alveolar sacs with severely impaired surfactant, lung surfactant plays a significant role in the initial clearance of pneumococci during early stages of infection due to the lung's innate immunity, made possible by surfactant proteins SP-A and SP-D [367, 368]. As the disease progresses, decreased SP-A, PG, and PC levels are observed [369, 370]. Therefore, lung surfactant is still present and functional during early stags of pneumococcal infection.

The elastic area compressibility modulus (C_s^{-1}) of a lipid monolayer is a measurement of its resistance to area expansion or compression [371]. Meanwhile, the term 'compressibility' is used to describe the ability of a specific lipid film in lowering surface tension during surface area reduction [372]. In other words, higher values of C_s^{-1} refer to lower degrees of monolayer compressibility. Good surfactants have low compressibility because of their ability to lower surface tension significantly during surface area reduction [372]. With regards to lung surfactant, the surfactant-associated proteins SP-B and SP-C have strong surface activity, because they allow the surfactant to reduce its surface tension upon film compression [372, 373]. Removing these

surfactant proteins has been shown to significantly increase monolayer compressibility, which reduces lung compliance as low compressibility is required for the easy reduction of surface tension [374]. A squeeze-out model has been proposed and modified throughout the years, suggesting that during the compression of a good surfactant, gel-phase phospholipids are retained in the primary surfactant layer, while fluid-phase lipids are expelled to form additional monolayers attached to the primary layer, effectively creating bilayers and multilayers at reduced surface areas [375, 376].

The compression isotherm experiments performed in this study provide interesting results regarding the interaction of daptomycin with lung surfactant. In general, daptomycin decreased the compressibility of the lung surfactant monolayers, as it increased their C_s^{-1} values by a significant amount compared to the controls. These properties correlate with those of a good surfactant, where low compressibility allows for greater reduction in surface tension at lower surface areas. It is then plausible that daptomycin helps to confer surface activity, similar to the function of both SP-B and SP-C, allowing the surfactant to have greater flexibility in rearranging its lipids to achieve lower surface tensions upon compression.

It is most interesting that the addition of daptomycin decreased the compressibility of the natural BLES® surfactant monolayer (from C_s^{-1} = 11.4 mN/m ± 5.6 mN/m in BLES® control to C_s^{-1} = 69.1 mN/m ± 8.7 mN/m with calcium and daptomycin) much more than it did the synthetic LS monolayer (from C_s^{-1} = 50.1 mN/m ± 9.7 mN/m in BLES® control to C_s^{-1} = 74.7 mN/m ± 9.5 mN/m with calcium and daptomycin). Part of the reason why there was such a drastic difference in compressibility between the control monolayers and their respective monolayers with calcium and daptomycin is that the BLES® control monolayer had a very low elastic area compressibility modulus compared to the other controls amongst all models. Since our modified BLES® is natural surfactant with most of it surfactant-associated proteins removed, and has a slightly more complex lipid composition that the simplified LS model, it can be conceived that the absence of most of these proteins has significantly impaired its ability to reduce surface tension, thus increasing its compressibility. However, upon the addition of daptomycin, its

compressibility decreased significantly by about six-fold, most likely because daptomycin may help to confer surface activity similar to what the hydrophobic surfactant proteins do. As a result, it is our belief that daptomycin not only associates itself with lung surfactant, but also plays a role in lowering its compressibility, making it an even better surfactant that can reduce surface tension at even lower surface areas than before. This suggests that at higher surface pressures and reduced surface areas, daptomycin would be more effectively sequestered within the lung surfactant, especially after multilayers have formed with daptomycin trapped within them.

BLES® and other clinical surfactant films have been shown to undergo a monolayer-to-multilayer transition plateau at around 40-50 mN/m, where the pressure slowly increases during monolayer compression [251]. However, our studies use a modified version of BLES® with most of its surfactant-spreading proteins removed; it would be considered more of a simplified lipid model derived from natural surfactant. When we performed compression isotherms, the slope of the curve was steeper in the synthetic LS model versus the BLES® model, suggesting that the surfactant-spreading properties of our BLES® monolayer may have been somewhat impaired from successive lipid extractions performed in its preparation. Nevertheless, their curves seem to correlate with typical isotherm collected for surfactant models, both synthetic and natural [251, 261]. However, upon the addition of calcium and daptomycin, we see a significant change in both surfactant models (especially in the BLES® model), where a very steep slope is observed, beginning at lower pressures. This suggests that daptomycin and calcium may alter the surface activity of lung surfactant, but the questions remain as to how much it changes surfactant function, and whether this monolayer-to-multilayer transition occurs at lower pressures.

Insertion assays were used to study the insertion of peptides and molecules into lipid monolayers, but primarily using the constant-pressure technique where the changes in molecular area are measured and the target pressure is kept constant [293, 377-379]. A previous study used a constant-area technique for insertion assays, testing the effect of daptomycin on equal fractions of PC and PG monolayers with varying concentrations of cardiolipin [106]. Due to the various different lipid model systems being used, it was more suitable to use the constant-area technique

in our case so that the area could be held constant at a specific initial pressure, and the change in pressure compared afterwards for each scenario.

The insertion assays obtained provide data that correlate nicely with the previous results obtained in ***Chapter 5***, where fluorescence spectroscopy was used to study the insertion of daptomycin or CB-182,462 into model liposomes. In this study, monolayers were used instead of bilayers, and the similarities in results illustrate that monolayers are great models for membrane systems. Here, it was shown that daptomycin does not insert into the HM model monolayer, suggesting it does not interact with this model and supporting the fact that it is not as toxic as CB-182,462, which inserts significantly into the HM model monolayer. Both daptomycin and CB-182,462 are known to exhibit strong bactericidal activity against *S. pneumoniae*, and these results show that they insert strongly into the BM model monolayers, with CB-182,462 inserting a little bit more strongly on average. The main difference comes with the lung surfactant models. For both the LS and BLES® model monolayers, daptomycin inserts strongly into each model, about 3 to 4 mN/m more than it does with the BM model monolayer. This supports our theory that daptomycin is strongly sequestered by lung surfactant. Meanwhile, since CB-182,462 is supposed to work in the lungs, minimal insertion is observed with both the lung surfactant models.

6.5 Conclusion

This study provides the first reported evidence of daptomycin affecting the physical properties of lung surfactant upon binding to it in the presence of calcium. Through our studies with monolayer insertion assays and compression isotherms, we provide novel evidence that daptomycin not only inserts and integrates strongly into the lung surfactant monolayer (due to a greater increase in pressure readings as compared to other lipid monolayer models), but also severely decreases the compressibility of the lung surfactant monolayer.

From these findings, we now present a new model of daptomycin inhibition by lung surfactant. We hypothesize that (1) daptomycin recognizes the lung surfactant and is most likely attracted to it, (2) daptomycin binds to and strongly inserts into the lung surfactant, whether it is in monolayer or multilayer form, effectively sequestering it, and (3) daptomycin reduces the compressibility of lung surfactant, allowing it to possibly form multilayers more easily at lower pressures and thus reinforce its sequestration.

Interestingly, the development of the semisynthetic antibiotic CB-182,462 was halted due to manifested toxicity, specifically related to phospholipidosis within the kidneys. Our results provide supporting evidence to the fluorescence studies presented in ***Chapter 5***, where CB-182,462 strongly inserts into the human membrane lipid model. This suggests that a strong electrostatic attraction and subsequent insertion into erythrocytes or other tissue cells may be one of the first steps in the mechanism of action of CB-182,462 in relation to its toxicity.

Much focus has been directed towards the effect of lung surfactant on daptomycin and how it can inhibit its bactericidal activity. Our study has effectively shown that the inhibition of daptomycin involves an alteration of lung surfactant on top of daptomycin's ability to bind to the surfactant. Additional studies will need to be performed to focus on the effect of daptomycin on lung surfactant. Our study has also shown that constant-area insertion assays are highly reproducible and can be used as a good basis to compare the insertion of a peptide or molecule between different monolayer models.

CHAPTER 7

7 AFM & KPFM IMAGING STUDIES: DAPTOMYCIN AND CALCIUM INDUCE LUNG SURFACTANT MULTILAYER FORMATION

7.1 Introduction

Daptomycin, commonly known as Cubicin® (Cubist Pharmaceuticals, a subsidiary of Merck & Co.), is a novel lipopeptide antibiotic that is rapidly bactericidal against major Gram-positive pathogens [7, 35, 49, 55, 58, 61, 69, 72, 96]. This antimicrobial peptide has a distinct proposed mechanism of action: it disrupts the membrane potential of a bacterial plasma membrane, ultimately leading to cell death [61, 81, 83, 84]. This mechanism of action has not been fully elucidated, and even more intriguing is its complete inhibition by lung surfactant in the case of pneumococcal-based pneumonia, such as community-acquired pneumonia [10]. One would think that, since *Streptococcus pneumoniae* is a Gram-positive bacterium (and one that is becoming

more resistant to conventional antibiotics), daptomycin would be a good antibiotic to combat this pathogen. However, this is not the case, since even though daptomycin is highly bactericidal against *S. pneumoniae* by itself, it is inhibited by lung surfactant [10, 82].

Due to this inhibition of daptomycin by lung surfactant, additional derivatives and alternatives to daptomycin have been created to try and overcome this complication [171, 173]. Cubist Pharmaceuticals themselves created a semisynthetic derivative called CB-182,462, which was found to be very potent against Gram-positive pathogens, even in the presence of lung surfactant, but unfortunately was found to be toxic due to the potential development of phospholipidosis within the kidneys (J. Silverman, personal communication). Accordingly, it is important that daptomycin's inhibition by lung surfactant be studied in an attempt to clarify its mode of action in the presence of lung surfactant.

Our previous studies in ***Chapters 5 and 6*** have shown that daptomycin inserts strongly into lung surfactant at physiological calcium concentrations and decreases its compressibility, suggesting an increase in the surfactant's ability to reduce surface tension or form multilayers at lower surface pressures than the norm. The Langmuir-Blodgett compression isotherm and insertion assay studies performed in ***Chapter 6*** allowed us to discover that daptomycin affected the properties of lung surfactant. The LB trough can also be used to prepare supported lipid monolayers on solid substrates for subsequent imaging. In this study, atomic force microscopy was used to try and visualize the effect of daptomycin on model monolayers. It is our hypothesis that at a physiologically relevant surface pressure, lung surfactant should exhibit greater multilayer formation in the presence of daptomycin and calcium than a control.

Atomic force microscopy has been frequently used to study lipid monolayers of both simple and complex lipid mixtures [376, 380-388]. During AFM imaging of mixed lipid monolayers and bilayers, one can observe topographical features called domains [389, 390]. Domains are topographical features of a monolayer that arise because of the different composition of lipids within a mixture [391-394]. Each lipid mixture has its own ratio of different lipids, and their

properties (such as size, phase, polarity, etc.) will affect how they are organized when forming a solid monolayer [389]. Meanwhile, pores can help determine the depth of each monolayer or bilayer if they are present. Phase imaging is usually performed simultaneously with atomic force microscopy imaging and provides a powerful tool for mapping material differences within a sample's surface and associating those with surface structures [395-399].

Kelvin probe force microscopy (KPFM), a subset of atomic force microscopy, has also been used to study the electrostatic and physicochemical properties of lipid monolayers [250, 380, 400]. Similar to phase imaging, KPFM can be performed simultaneously with AFM, which allows for the correlation of electrical surface potential with topographical surface structures [380, 401-404]. We hypothesize that, should there be any changes to the monolayer due to daptomycin or CB-182,462, a noticeable change in local electrostatic potential should be observed, especially in the case with lung surfactant and possible multilayer formation. Although AFM, phase, and KPFM imaging can all be done simultaneously to help correlate structural features with material differences and electrostatic potential, one core disadvantage to KPFM is that it does not work in aqueous solutions. As a result, all of the simultaneous AFM, phase and KPFM images were obtained in air using conductive monolayer samples.

Since KPFM imaging cannot be performed in biologically relevant conditions (in aqueous solutions), AFM liquid imaging was also performed with lipid bilayers to further mimic a physiologically suitable environment. These supported bilayer samples were created using vesicle fusion on top of a mica substrate and hydrated with an aqueous buffer solution during imaging.

The images obtained in this study present compelling support for our new theory of daptomycin inhibition by lung surfactant. Not only do the synthetic and natural lung surfactant monolayer show increased multilayer formation upon the addition of calcium and daptomycin, but their corresponding membranes also show increased multi-bilayer formation. This strongly suggests that daptomycin helps confer surfactant-spreading properties to lung surfactant in the presence of calcium, causing it to be fully sequestered and rendered inactive by the surfactant.

7.2 Materials and Methods

7.2.1 Lipid Models

Mixed lipid monolayers and bilayers were prepared for this study using four different lipid membrane model systems: bacterial membrane (BM) lipid model, human endothelial membrane (HM) lipid model, synthetic lung surfactant (LS) lipid model, and extracted lipid BLES® model. The BM lipid model consisted of 20% phosphatidylglycerol, 20% cardiolipin, and 60% phosphatidylethanolamine; the HM model with 20% phosphatidylcholine, 20% phosphatidylethanolamine, 10% phosphatidylserine, 15% sphingomyelin, and 35% cholesterol; the LS model had 80% phosphatidylcholine and 20% phosphatidylglycerol with 5% cholesterol by mass; and the BLES® model consisted of modified natural bovine lipid extract surfactant that had gone through further lipid extraction protocols. More details regarding each of these lipid model systems can be found in ***Chapter 3***.

7.2.2 Solution Preparation

Cholesterol was purchased from Sigma-Aldrich (St. Louis, Missouri, US), and the following lipids were purchased from Avanti Polar Lipids (Alabaster, Alabama, US) in powder form: 1,2-dipalmitoyl-*sn*-glycero-3-phosphocholine (DPPC), 1,2-dioleoyl-*sn*-glycero-3-[phospho-*rac*-(1-glycerol)] (DOPG), 1-palmitoyl-2-oleoyl-*sn*-glycero-3-phosphoethanolamine (POPE), 1,2-dioleoyl-*sn*-glycero-3-[phospho-L-serine] (DOPS), 1,1'2,2'-tetraoleoyl cardiolipin (TOCL), and sphingomyelin (egg, chicken).

The procedures for preparing supported lipid monolayer and bilayer substrates are quite different. However, stock solutions of 1 mM daptomycin, 1 mM CB-182,462, and 100 mM $CaCl_2$ as well as a HEPES buffer (20 mM HEPES, 150 mM NaCl, pH 7.4) were prepared for use in both experiments. ***Appendix A*** has detailed procedures on stock solution preparation.

For monolayer experiments (imaging in air), 1 mM mixed lipid stock solutions were made for each of the models being studied, as explained in *Appendix C1*. For membrane experiments (imaging in liquid), 5 mM liposome solutions were prepared with an extruder (see *Appendix E1*) and further diluted to a concentration of 1 mM using HEPES buffer. Prior to imaging in liquid, the liposome solutions were sonicated to reagitate the solution.

7.2.3 Monolayer Sample Preparation for Air Imaging

The Langmuir-Blodgett trough is widely used to prepare solid supported lipid monolayers on solid substrates. Here, mixed lipid monolayers for each model system (with or without calcium and with or without daptomycin or CB-182,462) were deposited onto freshly cleaved mica substrates to be imaged in air. A Langmuir-Blodgett micro-trough was used from NIMA Technology (Coventry, England).

To deposit a lipid monolayer onto a mica substrate, the freshly cleaved piece of mica was submerged into the LB trough well prior to monolayer formation. Once the monolayer was compressed to a targeted pressure of 20 mN/m at a speed of 20 cm^2/min, the pressure was held constant while the mica was very slowly withdrawn from the well. A pressure of 20 mN/m was chosen because surface pressures between ~15 to ~30 mN/m create conditions in monolayers that are similar to those within a lipid membrane [394, 405]. As the mica is withdrawn, the lipid monolayer deposits itself onto both sides of the mica, with the hydrophilic heads facing the hydrophilic surface of the mica substrate and the hydrophobic tails exposed to the air. See *Appendix C5* for full details and procedures regarding the LB monolayer deposition technique.

Once the lipid monolayer was deposited onto the mica substrate, it was left to air-dry for about 30 minutes prior to being placed in a desiccator for at least 48 hours. Afterwards, the sample had to be processed for KPFM imaging as mica by itself is an insulator and non-conductive. As a result, modifications had to be made to the mica substrate to give it conductive properties. This

involved attaching a conductive substrate (aluminum foil) to the bottom of the mica using double-sided conductive tape. The excess aluminum foil around the edge of the mica was then folded over and secured in each corner with an additional sliver of conductive tape (holding it in place to the mica surface). A detailed explanation of this procedure is available in *Appendix D1*.

7.2.4 Supported Bilayer Sample Preparation for Liquid Imaging

As indicated in *Chapter 7.2.2*, 1 mM liposomes were prepared for use in preparing supported bilayer samples. Mica was chosen to be the solid substrate, as it is chemically inert and hydrophilic. Since the JPK NanoWizard® II AFM from JPK Instruments AG (Berlin, Germany) has a liquid cell, this apparatus was used to prepare the supported bilayers using vesicle fusion.

In our vesicle fusion procedures, a vesicle or liposome solution is added to a freshly cleaved piece of mica substrate (placed inside the liquid cell) and incubated for 15 minutes to allow the vesicles to adhere to the mica. During this time, the vesicles will eventually reach a threshold concentration that ruptures the vesicles, allowing them to fuse and form a supported bilayer on top of the mica substrate. After 15 minutes, calcium and either daptomycin or CB-182,462 can be added, to be incubated for another 3 minutes. After this allotted amount of time, the sample is gently rinsed 10 to 15 times with small aliquots of HEPES buffer; each time, approximately 100 μL of the original solution is removed by a pipette and 100 μL of HEPES buffer is added to the substrate with another pipette. This effectively removes excess free and unbound vesicles from the solution to prevent vesicle deposits on top of the supported bilayer. The sample is then ready to be imaged and is stable for approximately 48 hours under constant hydration with HEPES buffer. Detailed protocols for vesicle fusion are available in *Appendix E2*.

7.2.5 AFM, Phase and KPFM Imaging in Air

Atomic force microscopy, phase, and Kelvin probe force microscopy imaging were done in air using the SmartSPM™ 1000 fully-automated scanning probe microscope from Advanced Integrated Scanning Tools for Nano-Technology or AIST-NT™ (Novato, California, US). A MikroMasch® HQ:NSC14 Au coated conductive cantilever tip was used to obtain each of the images. These gold-coated cantilevers have a tip radius of ~35 nm, resonance frequency of 160 kHz, length of 125 μm ± 5 μm, and force constant of 5 N/m.

Each set of images for AFM, phase and KPFM were obtained simultaneously. Typically, a preliminary scan had to be performed first using the SmartSPM™ 1000's QScan Mode to ensure a high-quality AFM and phase image could be obtained. Next, the SmartSPM™ 1000 was set to Kelvin mode to perform two-pass amplitude-modulation (AM) KPFM imaging, where a tip is scanned across a surface in the first pass to get a topographical and phase image and in the second pass to obtain an image of the surface's contact potential difference. A detailed overview of using the AIST-NT™ SmartSPM™ 1000 is available in *Appendix D2*.

For each model system and their respective scenarios, at least three samples were made from fresh stock solution. For each scenario (a particular monolayer with or without daptomycin or CB-182,462 in the absence or presence of calcium), at least 10 images (mixture of 2 μm by 2 μm and 5 μm by 5 μm images) were obtained in total amongst the multiple samples made. Image analysis and processing was performed on each of the images using either Gwyddion image processing (non-proprietary and free online software, Version 2.47) or AIST-NT™ IAPro image analysis and processing (proprietary software, Version 3.3.4). These images were first processed using a plane correction to eliminate any unwanted tilt in the image. When necessary, the z-range (scale) was adjusted on an image and filtered accordingly to improve the quality of the image. Surface roughness analysis was done using the IAPro statistical analysis features while cross-sectional statistical analyses were performed manually by taking at least 100 measurements of cross-sections for different observed structural features within a sample to find the average

height of these features as well as their distribution. Statistical significance of reported values were tested with one-way ANOVA with Tukey's *post hoc* test to compare means.

7.2.6 AFM Imaging in Liquid

AFM imaging of supported lipid bilayers was done in liquid using the JPK NanoWizard® II from JPK Instruments AG (Berlin, Germany). For liquid imaging, non-conductive silicon nitride probes from Bruker AFM Probes Americas (Camarillo, California, US) were used: DNP-S10 sharpened, high-resolution triangular probes with a tip radius of >10 nm, resonance frequency of 56 kHz, spring constant of 0.24 N/m, and length of 205 μm.

Proper care must be employed when setting up the liquid cell for imaging. After the liquid cell was placed in position and the NanoWizard® II apparatus and associated software for AFM imaging were set up, the liquid cell was left to equilibrate for approximately 15 to 20 minutes. Images were then taken using intermittent contact mode in liquid. A detailed overview of using the JPK NanoWizard® II is available in *Appendix E3*.

Each model membrane system was tested by itself or with a combination of calcium and either daptomycin or CB-182,462. For each scenario, at least three supported bilayer samples were prepared, and at least 5 images in total were obtained for each of those samples. Image analysis, processing and statistical analysis were performed using the JPK image processing software (proprietary software from JPK Instruments AG) and SPIP™ Version 6.6.4 from Image Metrology (Hørsholm, Denmark). Each image was plane-corrected and leveled using a polynomial fit, with adjustment of z-range and filters to improve image quality whenever necessary. Large artefacts were removed and surface roughness analysis was performed using the SPIP™ software on every image. Cross-sectional analyses of different surface features were taken on representative images to obtain approximate height differences of these features.

7.3 Results & Discussion

In order to study the effect of daptomycin and CB-182,462 on different membrane systems, numerous samples had to be prepared and imaged. For each of the four model membrane systems, 6 monolayer samples (each sample representing one scenario) for air imaging were made in triplicate: the model monolayer by itself, the monolayer with only calcium or daptomycin or CB-182,462, and the monolayer with both calcium and either daptomycin or CB-182,462. Since each of these model membrane systems consisted of at least three different lipids (with the LS and BM models made up of 3 different lipids, the HM model made up of 5 different lipids, and the BLES® model being the most complex), the structure and arrangement of these lipids within a monolayer can be quite complex, and may very well involve the formation of more than one

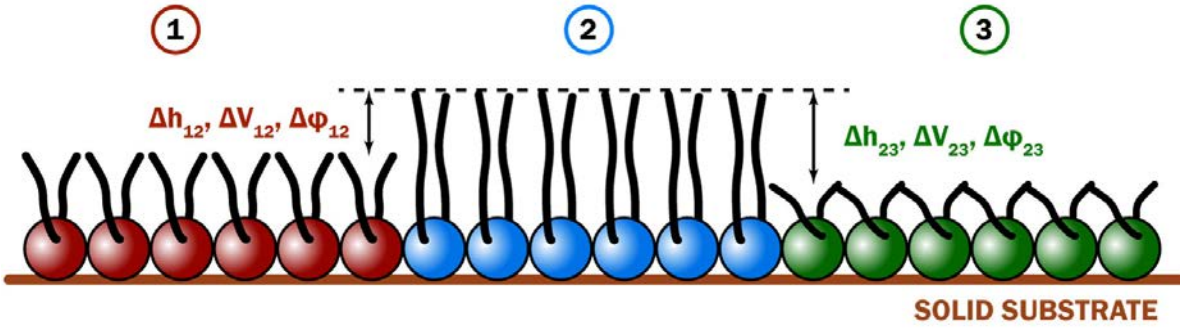

Figure 7.1 Simplified overview of monolayer domains in a model lipid system. This figure represents a theoretical model of domain separation in a three-component model lipid system that is not to scale. These lipids have been attached to a hydrophilic, solid substrate (such as mica), and due to their different levels of saturation, the acyl tail length of each type of lipid differs slightly. Depending on how the lipids interact with each other and how they are arranged in the monolayer, there will be different regions (domains) of these lipids which can be detected using various types of imaging methods. Atomic force microscopy allows for topographical imaging of the monolayer, and height differences ($\angle h$) can be detected between these different domains (notice the first domain below lower in height than the second domain, and the third domain being lower in height than both the first and second types of domains). Phase imaging can also provide information on the phase shift between two different domains ($\angle \varphi$), which allows us to map material differences in the monolayer. Kelvin probe force microscopy allows for the mapping of electrical surface potential, where different domains may have different changes in electrical surface potential ($\angle V$).

type of domain within the monolayer. ***Figure 7.1*** shows a general overview of how these different domains can be distinguished from each other using cross-sectional analysis of AFM, phase, and KPFM images, which can provide us with quantitative values of domain height differences ($\angle h$), phase lag differences ($\angle \varphi$), and electrical surface potential differences ($\angle V$) respectively.

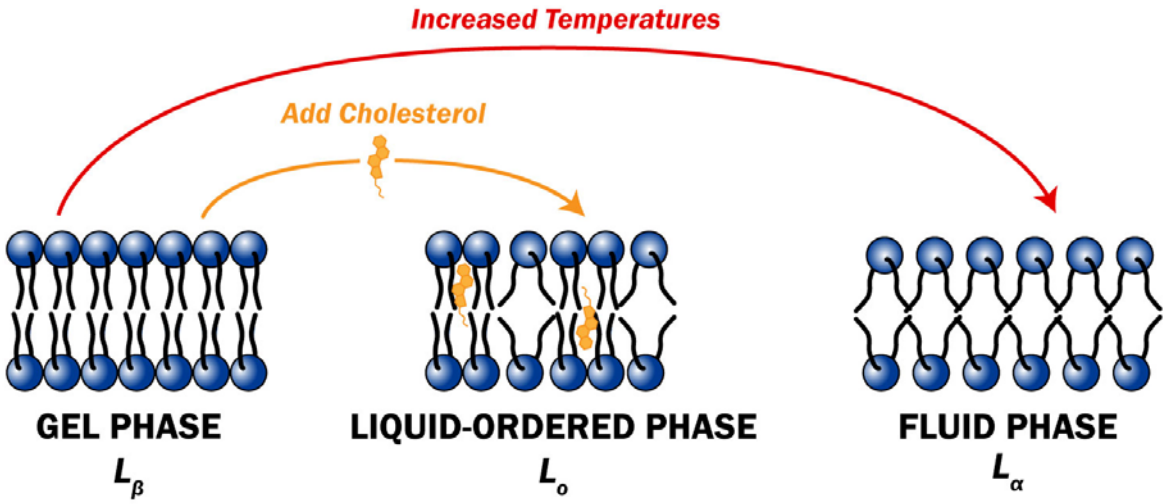

Figure 7.2 Effect of cholesterol and temperature on lipid membrane phase. Normally, a bilayer can exist in two main phases: a gel phase at lower temperatures and a fluid phase at higher temperatures. The transition from a gel phase to a fluid phase increases the fluidity of the membrane significantly. However, when cholesterol is introduced to the lipid bilayer system, an intermediate state is created between the gel phase and fluid phase, called the liquid-ordered phase. This phase occurs because cholesterol is able to alter the conformation of lipid acyl chains while increasing the fluidity of the bilayer.

The formation of domains is strongly tied to the properties of the individual lipid molecules within a lipid mixture, specifically their phase [406]. A lipid's phase is highly dependent on the length of the lipid's acyl chain (increased chain lengths correspond to increased transition temperatures), its degree of saturation (increased presence of double- and triple-bonds in the acyl chain corresponds to a decreased degree of saturation and therefore a decreased transition

temperature), its headgroup size, and the presence of other lipids [184, 185, 407, 408]. In general (***Figure 7.2***), a bilayer can exist in two phases: a gel-phase (L_β) at lower temperatures and a fluid-phase (L_α) at higher, physiologically relevant temperatures [394, 407, 409, 410]. However, in the presence of a sterol (mainly cholesterol), an intermediate state between the gel- and fluid-phases can form, called the liquid-ordered phase (L_o) [394, 411-413]. This occurs because cholesterol is able to induce conformational changes in the acyl chains of neighbouring lipids without reducing the fluidity of the bilayer [388, 407, 414-419]. Understanding the properties of each lipid will help provide insight into the results obtained in this study.

7.3.1 Daptomycin Enhances Lung Surfactant Multilayer Formation on Monolayer Samples

AFM, phase, and KPFM images were taken of each lipid model in six different scenarios: by itself, with only calcium, with only DAP, with only 462, with both Ca^{2+} and DAP, and with both Ca^{2+} and 462. A collection of all topographical images can be found in ***Appendix F***, while only relevant AFM, phase, and KPFM images and their respective cross-sections are presented here.

The bacterial membrane model system was studied first, which consisted of 20% DOPG, 20% TOCL, and 60% POPE. Each of the monolayer samples was imaged using AFM, phase, and KPFM imaging techniques. ***Figure 7.3*** shows representative images for the BM monolayer control as well as in combination with both calcium and daptomycin or CB-182,462. A qualitative analysis of each of these images shows that there are multiple types of domains visible, some that are more prominent or taller than others, and some that seem to be larger than what one would assume would be a domain. In the BM monolayer control (***Figure 7.3A-7.3C***), there are two types of visible, elliptically-shaped domains with an average surface roughness R_a = 0.32 ± 0.03 nm and approximate dimensions of 70 × 60 nm. The lower domains have $\angle h$ = 1.17 ± 0.20 nm, $\angle \varphi$ = 10.23 ± 2.06° and $\angle V$ = 21.36 ± 2.43 mV, while the higher domains have $\angle h$ = 1.76 ± 0.30 nm, $\angle \varphi$ = 9.24 ± 0.29° and $\angle V$ = 30.23 ± 2.11 mV. These different domains

correspond to lipid molecules in different phases, and it is suspected that the lower domains correspond to DOPG molecules, while the higher domains correspond to TOCL molecules. The POPE molecule has a polar head group with a cationic amine residue and an anionic phosphate residue, making POPE zwitterionic (see ***Figure 3.3***). These POPE molecules can therefore form hydrogen bonds with each other, forming a compact and rigid head-group network at the air-water interface [420, 421]. Meanwhile, DOPG molecules interact with each other using an extensive network of hydrogen bonds, ionic bonds and co-ordination bonds, suggesting a more ordered phase that is thicker than the POPE molecules [422, 423]. Cardiolipin is a fairly compact molecule that has a double-glycerophospholipid structure that is connected to a glycerol residue [424]. Its small polar head group allows for a tight packing of acyl chains between the TOCL molecules, but most likely cannot interact with the tight network or DOPG molecules, which would effectively cause patches of TOCL molecules to form [393]. As a result, it seems that the BM model monolayer has DOPG domains that contain localized domains of TOCL.

When daptomycin or CB-182,462 are added with calcium, a third type of "domain" is observed, which is higher than the two domains seen in the control. In the BM + Ca^{2+} + Daptomycin monolayers (see ***Figure 7.3D-7.3F***), the surface roughness is now higher at 0.44 ± 0.05 nm, which can be explained by the presence of additional types of domains. The lower domains have

Figure 7.3 AFM, phase and KPFM images of BM monolayer samples. Every row of images and their associated cross-sections are representative images of one particular BM monolayer sample. Images A-C represent the topography, phase, and electrical surface potential of a 20% DOPG, 20% TOCL, and 60% POPE monolayer sample, respectively. Images D-F represent the BM monolayer in the presence of 2 mM Ca^{2+} and 4 μM daptomycin, while images G-I represent the BM monolayer in the presence of 2 mM Ca^{2+} and 4 μM CB-182,462. By comparing the AFM images for each sample, it can be seen that additional, higher domains are visible in the monolayer samples with either DAP or 462, and these domains can be differentiated from each other by looking at the phase images as well. The KPFM images show that higher domains are associated with larger differences in electrical surface potential. All corresponding sets of AFM, phase and KPFM images (in other words, images in each row) were taken simultaneously and scanned in air under ambient conditions. The images presented here are all 1 μm by 1 μm.

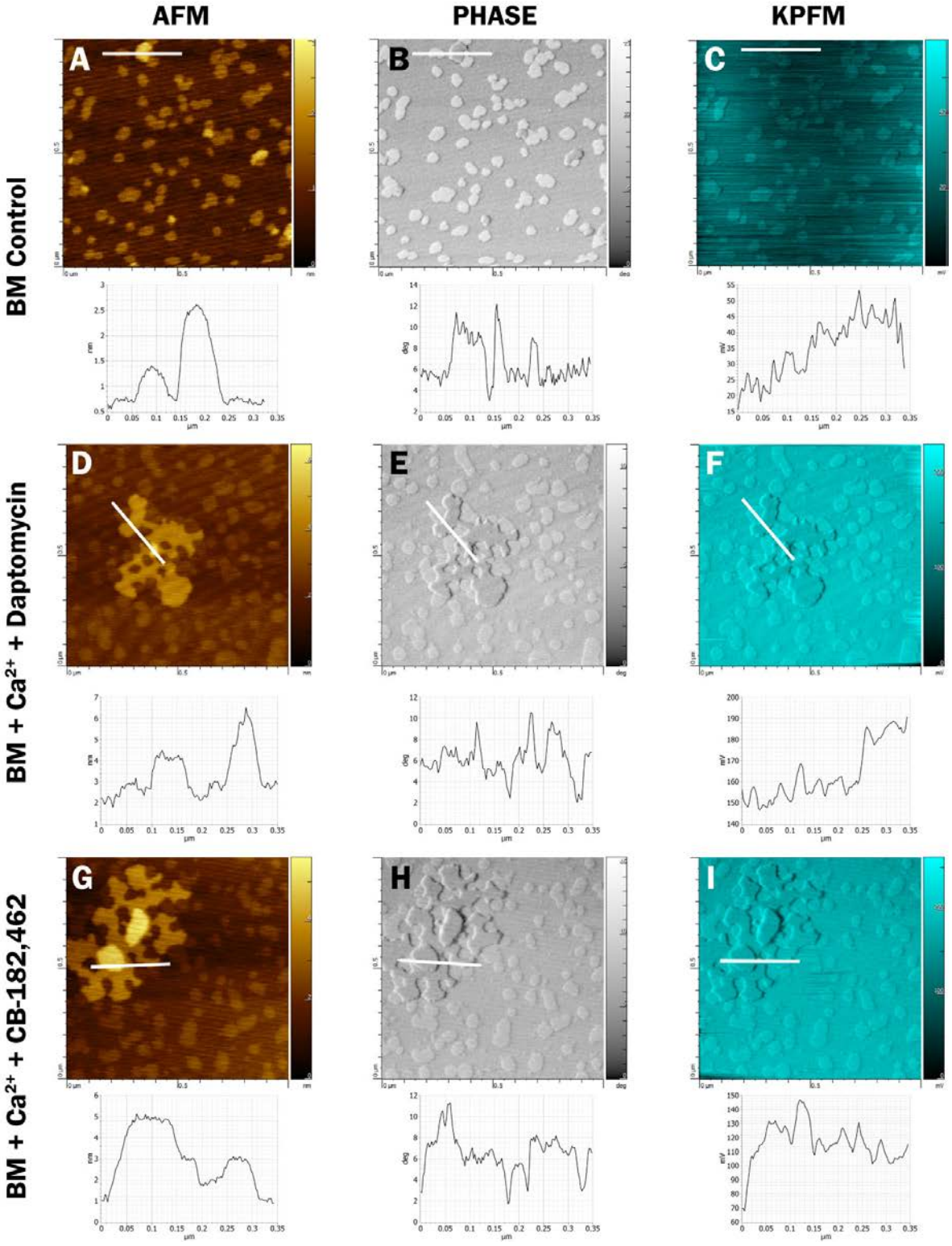
AFM
PHASE
KPFM
BM Control
BM + Ca2+ + Daptomycin
BM + Ca2+ + CB-182,462
A
B
C
D
E
F
G
H
I

averages of $\angle h$ = 1.10 ± 0.31 nm, $\angle \varphi$ = 2.93 ± 0.50° and $\angle V$ = 44.07 ± 0.44 mV, the mid-sized domains have averages of $\angle h$ = 2.31 ± 0.20 nm, $\angle \varphi$ = 8.55 ± 1.93° and $\angle V$ = 58.65 ± 0.49 mV, and the higher "domains" have averages of $\angle h$ = 4.87 ± 0.58 nm, $\angle \varphi$ = 8.91 ± 0.47° and $\angle V$ = 62.36 ± 0.47 mV. It is hypothesized that the lower domains of these monolayers are POPE molecules that have bound to either calcium or daptomycin, thus changing its fluidity and forming patches within the monolayer. The mid-sized domains, which we suspect to be DOPG or TOCL, are now much larger (occurring in patches with dimensions of about 500 × 600 nm) and remain at approximately the same height difference (slightly higher than the control monolayer's lower domains), but the electrostatic surface potential difference has changed drastically, increasing by approximately 28 mV. These increased values are likely caused by the binding of calcium and daptomycin to the DOPG lipid molecules, which has been known to occur [68]. They can also be correlated with patches of TOCL that are assumed to be expelled from DOPG patches since they cannot interact with their tight network [393]. The higher "domains" in this daptomycin monolayer are 4.87 ± 0.20 nm, which is highly unusual for a typical domain. As a result, we suspect that these higher "domains" are actually regions of lipids that have been bound to daptomycin and are raised up due to daptomycin's cyclic head (see ***Figure 7.4***). We believe that this orientation of daptomycin in the lipid monolayer occurs because during sample preparation, the monolayer is created at an air-water interface, where the polar heads are facing the water subphase. When daptomycin is injected into this water subphase, insertion of the tail into the monolayer (representative of one side of the bilayer leaflet) would occur in such an orientation. The deposition of these daptomycin-bound monolayers onto mica means that the hydrophilic heads of the lipid monolayer will face the hydrophilic surface of the mica substrate. These results imply that daptomycin, in the presence of calcium, induces significant changes in the bacterial membrane monolayer, which are characterized by increased height profiles of lipid domains as well as enhanced electrical surface potential.

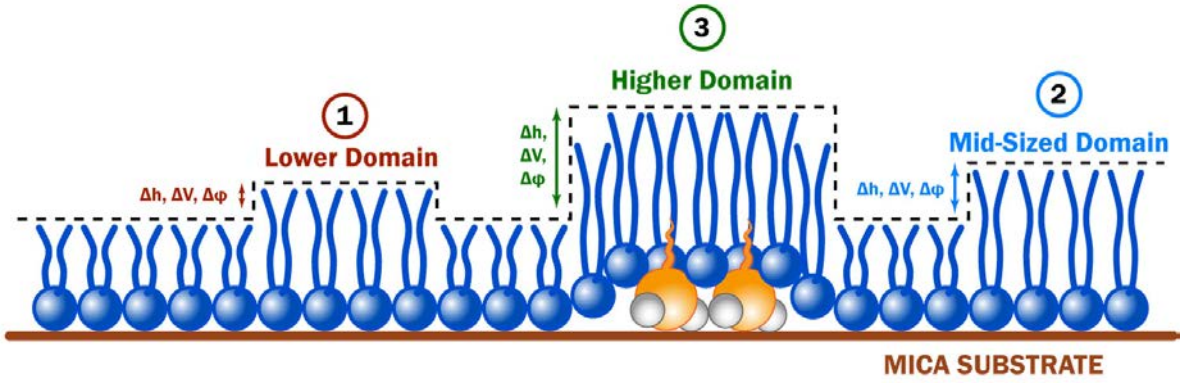

Figure 7.4 Schematic of proposed arrangement of lipids and surface features on bacterial lipid monolayer with calcium and daptomycin. The AFM, phase and KPFM images of the BM monolayer + 2 mM calcium + 4 μM daptomycin samples showed three different surface features assumed to be different regions of lipid domains. It is possible that the lower and mid-sized domains are regions of lipids which are more saturated, while the higher domains are regions of lipids that are raised up due to daptomycin bound to its head groups.

When calcium and CB-182,462 are added to the BM monolayer, similar effects comparable to its daptomycin counterpart are observed. The surface roughness is greater for the CB-182,462 BM monolayers with calcium, with a value of 0.53 ± 0.02 nm, and this is primarily due to the presence of larger mid-sized domains (most likely DOPG) that are highly irregular in shape and reach sizes of up to 700 × 1300 nm. Higher domains, similar in height to those observed with calcium and daptomycin, are also seen sporadically throughout the monolayer, suggesting that these regions have CB-182,462 bound to them (similar to how daptomycin binds to the monolayer in ***Figure 7.4***). The average values for R_a, Δh, $\Delta \varphi$, and ΔV are summarized for each sample in ***Table 7.1***.

Next, the human membrane model system was studied (which was composed of 20% DPPC, 20% POPE, 10% DOPS, 15% sphingomyelin, and 35% cholesterol). In the HM monolayer control sample, the surface roughness is 0.35 ± 0.03 and only one type of domain can be observed with an average height profile of 1.48 ± 0.21 nm, phase difference of 8.13 ± 1.89°, and ΔV of 50.55 ± 2.09 mV. It is highly likely that these domains consist of cholesterol,

sphingomyelin, and DPPC, effectively forming lipid rafts (see ***Figure 3.1***) that are elevated compared to the rest of the monolayer composed of unsaturated and kinked phospholipids. In these domains, cholesterol can insert itself in between phospholipids within the raft, filling up any void molecular space between the associated lipids and therefore forces them into a tighter alignment [425]. As can be seen in ***Figure 7.5A-7.5C***, the HM monolayer control sample has domains that are more irregularly-shaped and larger than the lower domains seen in the BM monolayer samples.

When calcium and daptomycin are added into the HM monolayer (see ***Figure 7.5D-7.5F***), the sample is slightly smoother with R_a = 0.24 ± 0.04 nm, and the domains are larger, while the average height and phase differences are comparable to the control. Although the average difference in electrical surface potential increases by about 17 mV, this value is seen across other controls (with just calcium, daptomycin or CB-182,462; see ***Appendix F***), which means that the addition of daptomycin and calcium have caused the surface charge to fluctuate and increase.

However, when we look at the HM monolayer with calcium and CB-182,462, radical changes are observed, starting with the height profile and shape of the domains (see ***Figure 7.5G-7.5I***). No longer do we see large, smooth domains, but rather multiple circular patches of smaller domains with different height profiles. As a result, the surface roughness has increased to 0.46 ± 0.05 nm. The lower domains (about 40 nm in diameter) have an average $\measuredangle h$ = 1.14 ± 0.37 nm, average $\measuredangle \varphi$ = 3.13 ± 0.52° and average $\measuredangle V$ = 16.31 ± 0.35 mV, the mid-sized domains (about 60 nm in diameter) have an average $\measuredangle h$ = 1.37 ± 0.64 nm, average $\measuredangle \varphi$ = 8.49 ± 0.64° and average $\measuredangle V$ = 36.47 ± 2.98 mV, while the largest domains (about 120 nm in diameter) have an average $\measuredangle h$ = 4.11 ± 2.03 nm, average $\measuredangle \varphi$ = 16.55 ± 2.0° and average $\measuredangle V$ = 107.49 ± 4.06 mV. The reduction of overall domain size and the significant increase in $\measuredangle V$ of these larger, circular domains (at least 50 mV above the control samples' domains) tells us that CB-182,462 not only disrupts the formation of lipid domains, but also interacts with them to form thicker structures. These thicker structures may very well be caused by the binding of CB-182,462 to the lipids and subsequent insertion into them, thus raising the height of these regions to see the

higher domains through AFM imaging. Since CB-182,462 is presumed to be toxic to human membranes and may cause phospholipidosis within the kidneys, it is evident here that CB-182,462 does affect the structural organization, aggregation and/or clustering of these lipids within a human membrane model system, which may play a role in its toxic mode of action. More studies will need to be performed to elucidate this mechanism of action.

With regards to lung surfactant, both the synthetic lung surfactant lipid model system and the natural BLES® surfactant model system were examined. The LS model system was made up of 80% DPPC and 20% DOPG with 5% cholesterol by mass. In the LS monolayer control sample, the surface roughness was 0.97 ± 0.04 nm with large, irregularly-shaped domains spanning the surface with average differences of $\angle h$ = 1.87 ± 0.21 nm, $\angle \varphi$ = 57.03 ± 1.91 ° and $\angle V$ = 30.30 ± 2.06 mV. These domains also seem slightly porous in nature, as this characteristic is visible in all three images (*Figure 7.6A-7.6C*). Previous studies using a similar LS model system have shown similar features and heights in their domains, but compressed at much higher pressures of 45-50 mN/m, where multilayer formation is seen as well [250, 258]. Since the samples used in this study were compressed to a final pressure of 20 mN/m, multilayers for control samples should not form. Similar to the HM model, it is suspected that these domains primarily consist

Figure 7.5 AFM, phase and KPFM images of HM monolayer samples. Representative topographical, phase, and electrical surface potential images for each human membrane model monolayer sample are presented in each row, along with their associated cross-sections. Images A-C represent the AFM, phase, and AM-KPFM images of a 20% DPPC, 20% POPE, 10% DOPS, 15% sphingomyelin and 35% cholesterol monolayer sample, respectively. Images D-F are representative images of the HM monolayer in the presence of 2 mM calcium and 4 μM daptomycin, and G-I are images of the HM monolayer with 2 mM calcium and 4 μM CB-182,462. When looking at the AFM images for each sample, we can see that the surface topography drastically changes in the case of CB-182,462, where not only the domain size and shape of the monolayer are disrupted, but also the height profile and the emergence of different types of spherical domains which look like clusters of lipids. The phase and KPFM images show greater phase shifts and larger surface potential readings for higher domains. All corresponding sets of 1 μm by 1 μm AFM, phase and KPFM images were simultaneously scanned in air under ambient conditions.

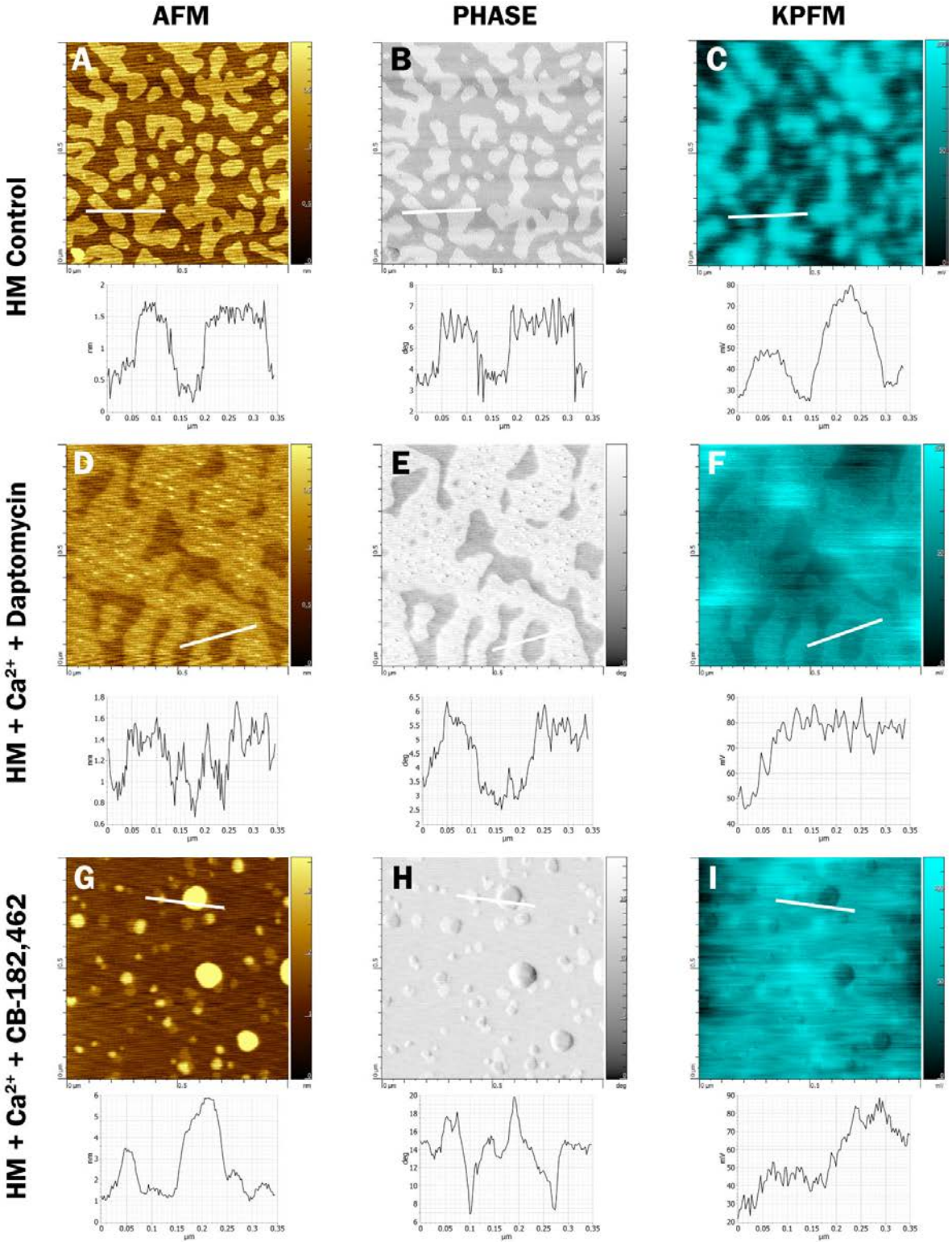
AFM
PHASE
KPFM
HM Control
HM + Ca2+ + Daptomycin
HM + Ca2+ + CB-182,462
A
B
C
D
E
F
G
H
I

of unsaturated DPPC and cholesterol.

Upon the addition of calcium and daptomycin (see ***Figure 7.6D-7.6F***), not only does the shape of the domains change significantly, but also their height profiles. Although the domains are still spread across the surface of the sample, they are much more porous and randomly arranged. Most intriguing is the average height difference of Δh = 7.30 ± 1.94 nm and average electrical surface potential difference of ΔV = 96.53 ± 2.09 mV, suggesting daptomycin (in the presence of calcium) strongly binds to and inserts into the LS monolayer and promotes multilayer formation, a phenomenon that is only seen at higher surface pressures for lung surfactant alone [263]. Since the height difference of these so-called domains is 7.30 ± 1.94 nm, it is most probable that they contain an additional bilayer of 5 to 6 nm in height that rests on top of the lipid monolayer. ***Figure 7.7*** provides a schematic of the possible organization of lung surfactant multilayers in the presence of daptomycin and calcium, where bound daptomycin acts as an anchor between each monolayer. These data correlate with the findings from ***Chapters 5 and 6*** of this thesis and the new model presented of daptomycin's inhibition by lung surfactant (***Figure 8.1***) . This new model suggests that strong binding of daptomycin to lung surfactant, in the

Figure 7.6 AFM, phase and KPFM images of synthetic LS monolayer samples. Every row of images and their associated cross-sections are representative 1 μm by 1 μm images of a specific lung surfactant monolayer sample taken in air under ambient conditions. Images A-C represent the atomic force microscope, phase, and Kelvin probe force microscopy images of a 80% DPPC, 20% DOPG with 5% cholesterol lung surfactant monolayer sample, respectively. Images D-F represent the LS monolayer with 2 mM calcium and 4 μM daptomycin, while Images G-I represent the LS monolayer with CB-182,462 instead of daptomycin. In the control sample, the monolayer domains are about 1.87 ± 0.21 nm, but upon addition of calcium and daptomycin, the height of the visible domains increase to about 7.30 ± 1.94 nm. Minor topographical changes are observed in the LS monolayer sample with 462 and calcium, but rather a greater presence of very larger surface artifacts and debris. Higher topographical domains correspond to larger phase shifts and larger differences in contact potential in the phase and KPFM images, respectively.

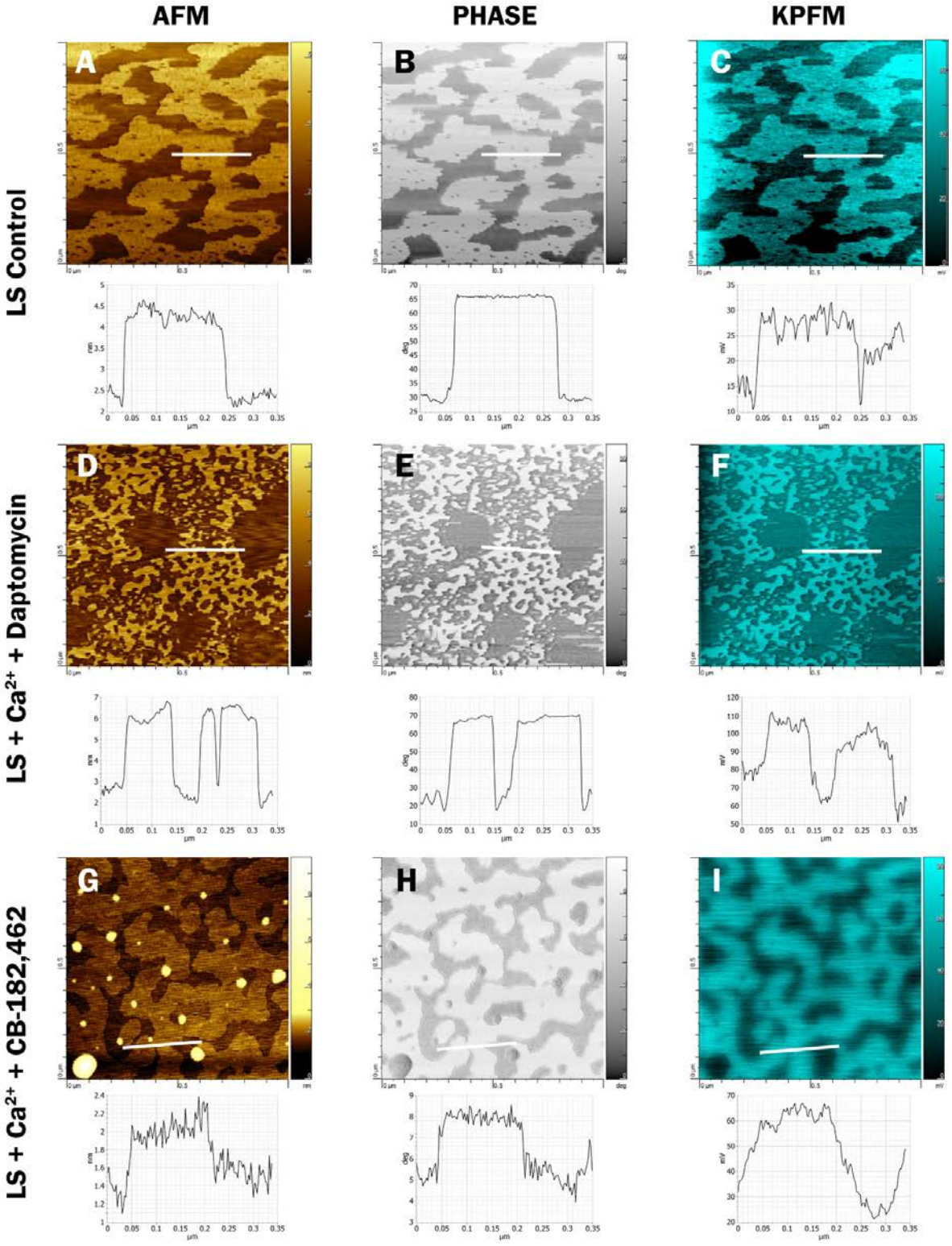
AFM
PHASE
KPFM
LS Control
LS + Ca2+ + Daptomycin
LS + Ca2+ + CB-182,462
A
B
C
D
E
F
G
H
I

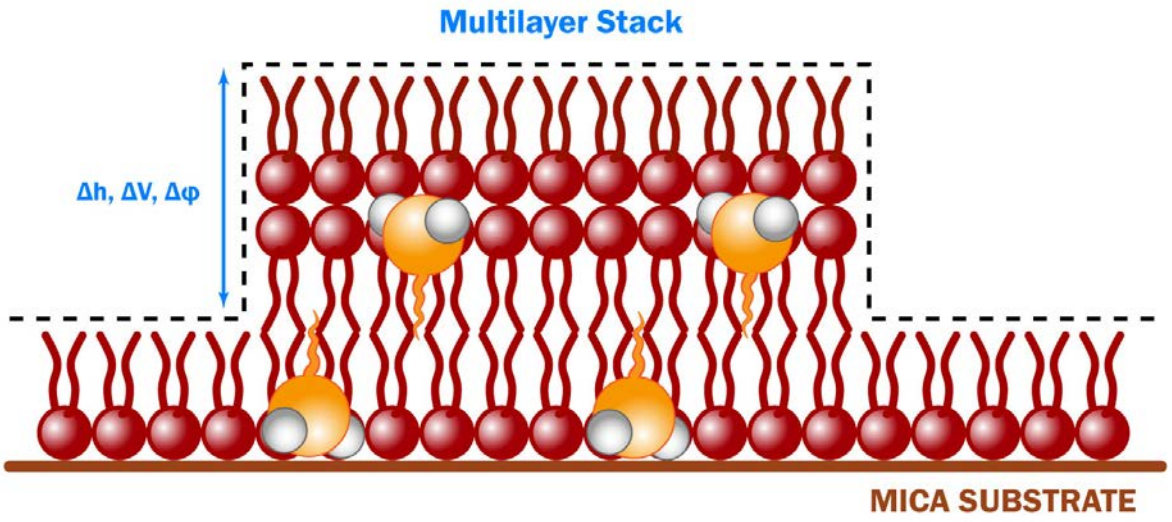

Figure 7.7 Schematic of proposed multilayer formation of lipids in lung surfactant monolayer models due to daptomycin and calcium. Very tall and flat surface features above 7 nm in height were observed for the lung surfactant monolayer models. This schematic shows a potential multilayer stack comprised of three layers of lipids, each bound to the next because of the presence of calcium-bound daptomycin, which is proposed to insert into lung surfactant and help connect these layers together. Such an arrangement will help explain the height differences observed in the AFM topographical images, suggesting an additional bilayer of lipids rests on top of the original lung surfactant monolayer.

presence of calcium, not only allows it to be sequestered, but also exhibit surfactant-spreading properties that allow the lung surfactant to achieve multilayer formation at lower pressures than normal.

When CB-182,462 is added to the LS monolayer with calcium, the results are fairly consistent with the control samples with just the monolayer or with only calcium, daptomycin or CB-182,462. As can be seen in ***Figure 7.6G-7.6I*** and ***Table 7.1***, the LS + Ca^{2+} + CB-182,462 samples are smoother with R_a = 0.20 ± 0.03 (comparable to the controls with just daptomycin and CB-182,462), and the average ΔV is a bit higher at 52.31 ± 4.13 mV while the height profile does not change much. This suggests that CB-182,462 does not bind to or change the properties

of the LS monolayer, implying that the minor fluctuations seen are a result of the addition of charged calcium ions and CB-182,462 molecules into the monolayer.

Contrary to the LS model, the BLES® model system's exact composition is not known, but can be considered more complex than the LS model system due to the possible presence of multiple other neutral and charged lipids in lower concentrations. As a result, it is expected that differences are seen between the LS and BLES® monolayers. For the BLES® monolayer control samples (***Figure 7.8A-7.8C***), the average values for the domains are $\angle h$ = 1.26 ± 0.21 nm, $\angle \varphi$ = 6.91 ± 2.05 ° and $\angle V$ = 36.63 ± 2.04 mV, with the surface quite smooth at R_a = 0.20 ± 0.02 nm and the general size of the domains larger than those in the LS monolayer. Similar to the LS control, these domains are most likely regions of unsaturated phospholipids (such as DPPC) with cholesterol. The presence of larger, spherical structures with height profiles greater than 5-10 nm were observed in most of the images with the BLES® monolayer. We suspect that these non-lipid components from the natural BLES® surfactant that were unsuccessfully filtered out during our sample preparation, such as proteins.

When daptomycin and calcium are added to the BLES® monolayers, the results are quite comparable to those of the LS monolayers in this scenario. In general, the observed domains, which are actually multilayers, are much larger in lateral size than those observed in the LS monolayers, but the height profiles are very similar with the average $\angle h$ = 7.51 ± 2.02 nm, indicating the presence of an additional bilayer on top of the original monolayer (see ***Figure***

Figure 7.8 AFM, phase and KPFM images of BLES® monolayer samples. Each row contains representative images of a specific sample's surface topography, phase shift, and electrical surface potential and their associated cross-sections. Images A-C represent the AFM, phase and KPFM images of a BLES® bovine natural lung surfactant monolayer, respectively. Images D-F represent the BLES® monolayer in the presence of 2 mM Ca^{2+} and 4 μM daptomycin, while images G-I represent the monolayer with 4 μM CB-182,462 instead. Similar to the LS images, the domains seen in the BLES® control are quite flat, but in the presence of calcium and daptomycin, larger and higher domains emerge. The images presented are all 1 μm by 1 μm in size, with images taken under ambient conditions and scanned in air.

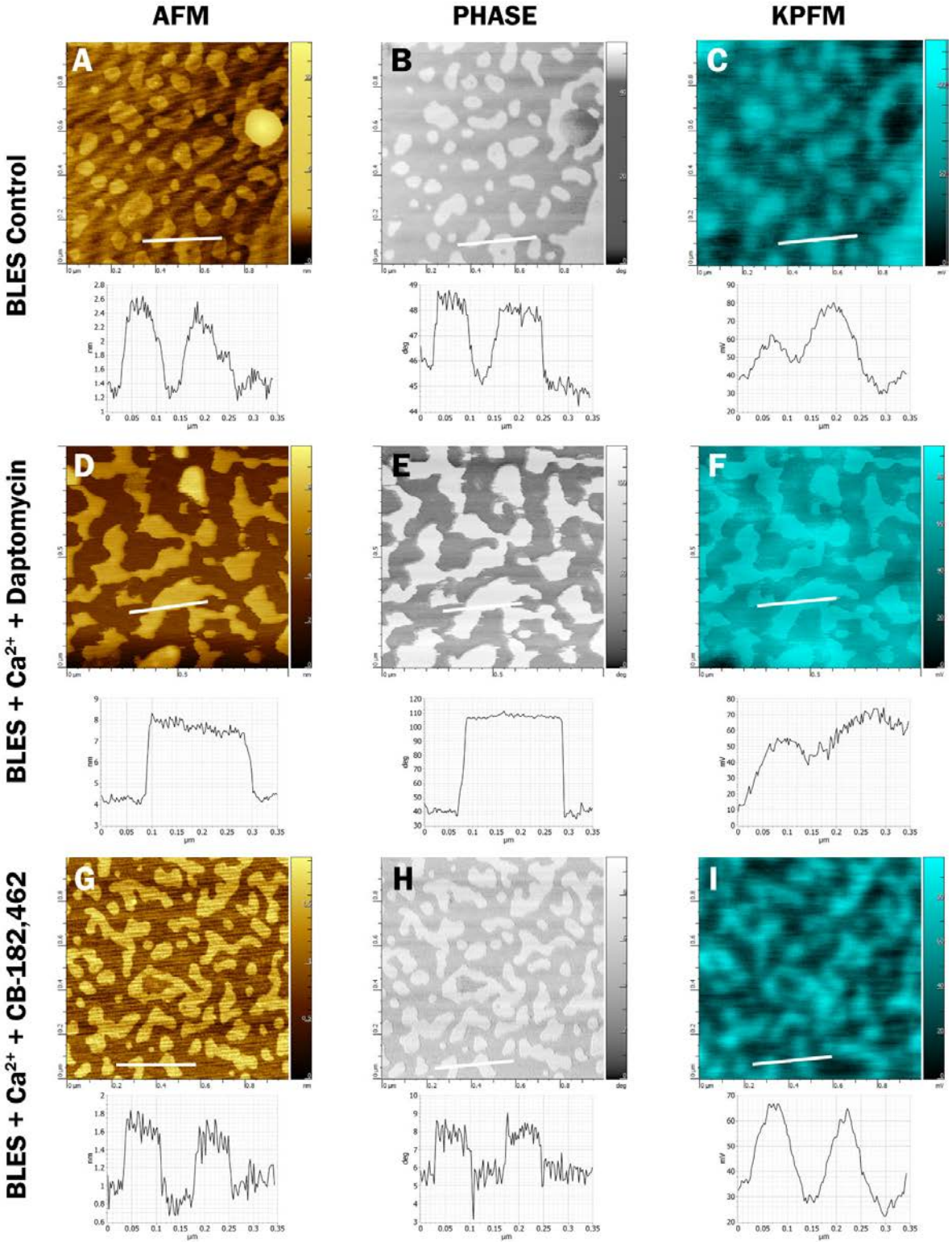
AFM
PHASE
KPFM
BLES Control
BLES + Ca2+ + Daptomycin
BLES + Ca2+ + CB-182,462
A
B
C
D
E
F
G
H
I

7.8D-7.8F). The average difference in electrical surface potential is ΔV = 84.42 ± 2.07 mV, which means that daptomycin and calcium together have a measurable effect on lung surfactant's electrostatic non-homogeneity. These results are in alignment with the new model presented for daptomycin inhibition as well, presented in ***Chapters 5 and 6.***

In the presence of calcium and CB-182,462, the BLES® monolayers have a surface roughness of 0.30 ± 0.04 nm and the domains experience more phase separation amidst being smaller in lateral size (see ***Figure 7.8G-7.8I***). In this scenario, although the KPFM image shows us that the electrical surface potential has an average value of ΔV = 51.02 ± 5.10 mV (which is similar to the controls), the AFM and phase images show us that the size and shape of the domains has changed significantly from the controls. What this means is that even though CB-182,462 does not impart any electrostatic effects onto natural lung surfactant, it may very well still effect the distribution and ordering of the lipids within the surfactant.

From these AFM, phase, and KPFM images, it is possible to visualize the effects of daptomycin and CB-182,462 on different model systems in the presence of calcium. Our results show that daptomycin's effect is dependent on the presence of calcium, and that together, they promote the formation of multilayers within lung surfactant. From the images, it seems plausible that three-layer multilayer stacks are formed when daptomycin and calcium incorporate themselves

Table 7.1 Table of values for roughness, differences in height, phase shift, and electrical surface potential for AFM, phase, and KPFM images for each monolayer sample. Each model is separated by a different colour scheme (blue for bacterial membrane, green for human membrane, red for synthetic lung surfactant, and black for BLES®). For each model, 6 different scenarios were tested: the monolayer by itself, the monolayer with just 2 mM calcium, the monolayer with 4 μM daptomycin, the monolayer with 4 μM CB-182,462, the monolayer with both calcium and daptomycin, and the monolayer with both calcium and CB-182,462. For each scenario, at least 3 monolayer samples were prepared, and from those samples, at least 10 images were obtained in total. From these AFM, phase, and KPFM images, at least 100 height, phase shift, and electrical surface potential measurements were taken for each type of domain observed, respectively. These measurements were then averaged and presented here in this table.

Model & Scenario	R_a (nm)	Δh (nm)	$\Delta \varphi$ (deg)	ΔV (mV)
Bacterial Membrane (BM) Model				
BM Control	0.32 ± 0.03			
Lower Domains		1.17 ± 0.20	10.23 ± 2.06	21.36 ± 2.43
Higher Domains		1.76 ± 0.30	9.24 ± 0.29	30.23 ± 2.11
BM + Ca^{2+}	0.25 ± 0.03			
Lower Domains		1.08 ± 0.21	5.04 ± 0.58	22.15 ± 1.36
Higher Domains		5.17 ± 1.52	8.74 ± 1.94	36.04 ± 2.02
BM + Daptomycin	0.33 ± 0.04			
Lower Domains		1.35 ± 0.20	8.21 ± 0.58	22.12 ± 1.53
Higher Domains		2.82 ± 0.53	9.31 ± 2.01	37.35 ± 1.96
BM + CB-182,462	0.31 ± 0.05			
Lower Domains		1.25 ± 0.22	5.53 ± 0.72	35.84 ± 2.05
Higher Domains		2.57 ± 0.35	9.21 ± 2.19	39.76 ± 0.68
BM + Ca^{2+} + Daptomycin	0.44 ± 0.05			
Lower Domains		1.10 ± 0.31	2.93 ± 0.50	44.07 ± 0.44
Mid-sized Domains		2.31 ± 0.20	8.55 ± 1.93	58.65 ± 0.49
Higher Domains		4.87 ± 0.58	8.91 ± 0.47	62.36 ± 0.47
BM + Ca^{2+} + CB-182,462	0.53 ± 0.02			
Lower Domains		1.80 ± 0.47	3.17 ± 0.54	48.77 ± 0.65
Mid-sized Domains		2.79 ± 0.23	9.13 ± 1.97	59.78 ± 0.66
Higher Domains		4.63 ± 0.43	12.76 ± 0.64	59.57 ± 0.73
Human Membrane (HM) Model				
HM Control	0.35 ± 0.03	1.48 ± 0.21	8.13 ± 1.89	50.55 ± 2.09
HM + Ca^{2+}	0.30 ± 0.04	1.41 ± 0.21	11.16 ± 1.97	47.41 ± 1.90
HM + Daptomycin	0.32 ± 0.04	1.48 ± 0.20	6.08 ± 1.98	47.15 ± 3.96
HM + CB-182,462	0.27 ± 0.03	1.46 ± 0.20	9.82 ± 2.04	67.26 ± 2.07
HM + Ca^{2+} + Daptomycin	0.24 ± 0.04	1.51 ± 0.21	7.12 ± 1.95	67.06 ± 4.99
HM + Ca^{2+} + CB-182,462	0.46 ± 0.05			
Lower Domains		1.14 ± 0.37	3.13 ± 0.52	16.31 ± 0.35
Mid-sized Domains		1.37 ± 0.64	8.49 ± 0.64	36.47 ± 2.98
Higher Domains		4.11 ± 2.03	16.55 ± 2.02	107.49 ± 4.06
Lung Surfactant (LS) Model				
LS Control	0.97 ± 0.04	1.87 ± 0.21	57.03 ± 1.91	30.30 ± 2.06
LS + Ca^{2+}	0.95 ± 0.04	1.77 ± 0.20	44.16 ± 2.09	31.96 ± 4.08
LS + Daptomycin	0.35 ± 0.04	1.66 ± 0.19	25.41 ± 2.02	40.83 ± 1.99
LS + CB-182,462	0.27 ± 0.05	1.78 ± 0.19	30.40 ± 2.02	49.43 ± 2.98
LS + Ca^{2+} + Daptomycin	1.50 ± 0.04	7.30 ± 1.94	51.50 ± 2.98	96.53 ± 2.09
LS + Ca^{2+} + CB-182,462	0.20 ± 0.03	1.67 ± 0.20	8.21 ± 1.99	52.31 ± 4.13
Bovine Lipid Extract Surfactant (BLES®) Model				
BLES Control	0.20 ± 0.02	1.26 ± 0.21	6.91 ± 2.05	36.63 ± 2.04
BLES + Ca^{2+}	0.25 ± 0.02	1.34 ± 0.20	11.84 ± 2.99	40.55 ± 3.06
BLES + Daptomycin	0.37 ± 0.04	1.81 ± 0.20	21.01 ± 1.88	46.05 ± 1.92
BLES + CB-182,462	0.48 ± 0.03	2.22 ± 0.19	28.84 ± 2.08	49.25 ± 3.94
BLES + Ca^{2+} + Daptomycin	1.52 ± 0.02	7.51 ± 2.02	64. 93 ± 2.05	84.42 ± 2.07
BLES + Ca^{2+} + CB-182,462	0.30 ± 0.04	1.45 ± 0.20	8.74 ± 2.04	51.02 ± 5.10

into the lung surfactant monolayer at a pressure of 20 mN/m. The data shows that the total height difference of these stacks atop the monolayer was at least 7 nm in height, which is greater than the typical thickness of a bilayer, about 5 to 6 nm [426-428]. However, when preparing multilayers at an air-water interface (like we did using the LB trough), multilayers must have an odd number of layers as the polar heads must face the water and the tails must face the air. Therefore, it is more plausible that a daptomycin-bound area with a height of 7 nm is one bilayer with daptomycin in between each monolayer. This corresponds to our theory that daptomycin is sequestered by lung surfactant due to an intense attraction to the lipids within the model and subsequent folding of monolayers on top of each other, reinforcing this sequestration.

These images also provide us with additional evidence to support the toxic mechanism of action of CB-182,462 with human tissue cells and erythrocytes. Our previous studies have shown that CB-182,462 strongly binds and inserts into the human membrane model system. This study shows that CB-182,462 not only interacts with the lipids, but completely changes the organization of lipid domains, and may very well cause clumping of lipids in regions where there is a high concentration of CB-182,462.

7.3.2 Daptomycin Causes Multi-Bilayer Formation on LS/BLES Model Bilayers

Since the monolayer experiments showed that daptomycin had a profound effect on the lipid organization and orientation in lung surfactant, the next step was to see whether these effects could be seen using membranes instead of monolayers. Due to daptomycin's proven interaction with lung surfactant, it is believed that it will also interact with the lipids in a lung surfactant bilayer to form additional bilayers. Since daptomycin is also known to insert into and depolarize bacterial membranes, we assume that topographical differences can be observed as well.

In order to image membrane samples, vesicles were first made for each of the four lipid model systems we are studying: bacterial membrane, human membrane, lung surfactant and BLES®.

Once these vesicles were formed, supported bilayer samples were prepared on mica using vesicle fusion and subsequently imaged in liquid using atomic force microscopy. By imaging within a liquid environment, it is possible to measure the surface roughness of the membrane, the height profile of various features, as well as visualize any topographical differences that either daptomycin or CB-182,462 may impart on the membrane. ***Figures 7.9 – 7.12*** present representative AFM images of each of the model membranes by itself or with calcium and daptomycin/CB-182,462. Corresponding surface roughness measurements are summarized in ***Table 7.2***.

In the bacterial membrane control (***Figure 7.9A***), the surface roughness of the membrane is 0.36 ± 0.03 nm, which is fairly smooth considering there are not a lot of surface features. The image represents full surface coverage of the membrane on mica, and there are some circular deposits that can be associated with unruptured vesicles, which has been shown to occur with AFM imaging in liquid [429, 430]. Sometimes these vesicles do not rupture and are adsorbed or trapped atop the membrane [426]. In the BM control, each of these small vesicles are approximately 10-20 nm in height, with a lateral diameter of 150-200 nm. Since the vesicle solutions were stored in the fridge and sonicated prior to vesicle fusion, it is highly likely that these vesicles (of various shapes and sizes ranging from approximately 50-150 nm) spontaneously fuse to form larger vesicles due to the high degree of curvature within the membranes [431]. When calcium and daptomycin are added to the sample, the surface roughness increases drastically to 3.36 ± 0.83 nm, suggesting the presence of more surface structures and aggregates. If we look at ***Figure 7.9B***, we can see that apart from the large spherical deposits ranging from diameters of 100-300 nm, there is an elevated domain with an average height profile of 8.08 ± 0.83 nm. Within these elevated domains are additional elevated areas that are slightly larger than the size and height profiles of the large spherical deposits. This suggests that the elevated domains are an additional bilayer patch that has formed on top of the original supported bilayer. Since daptomycin has been previously shown to bind and insert into our

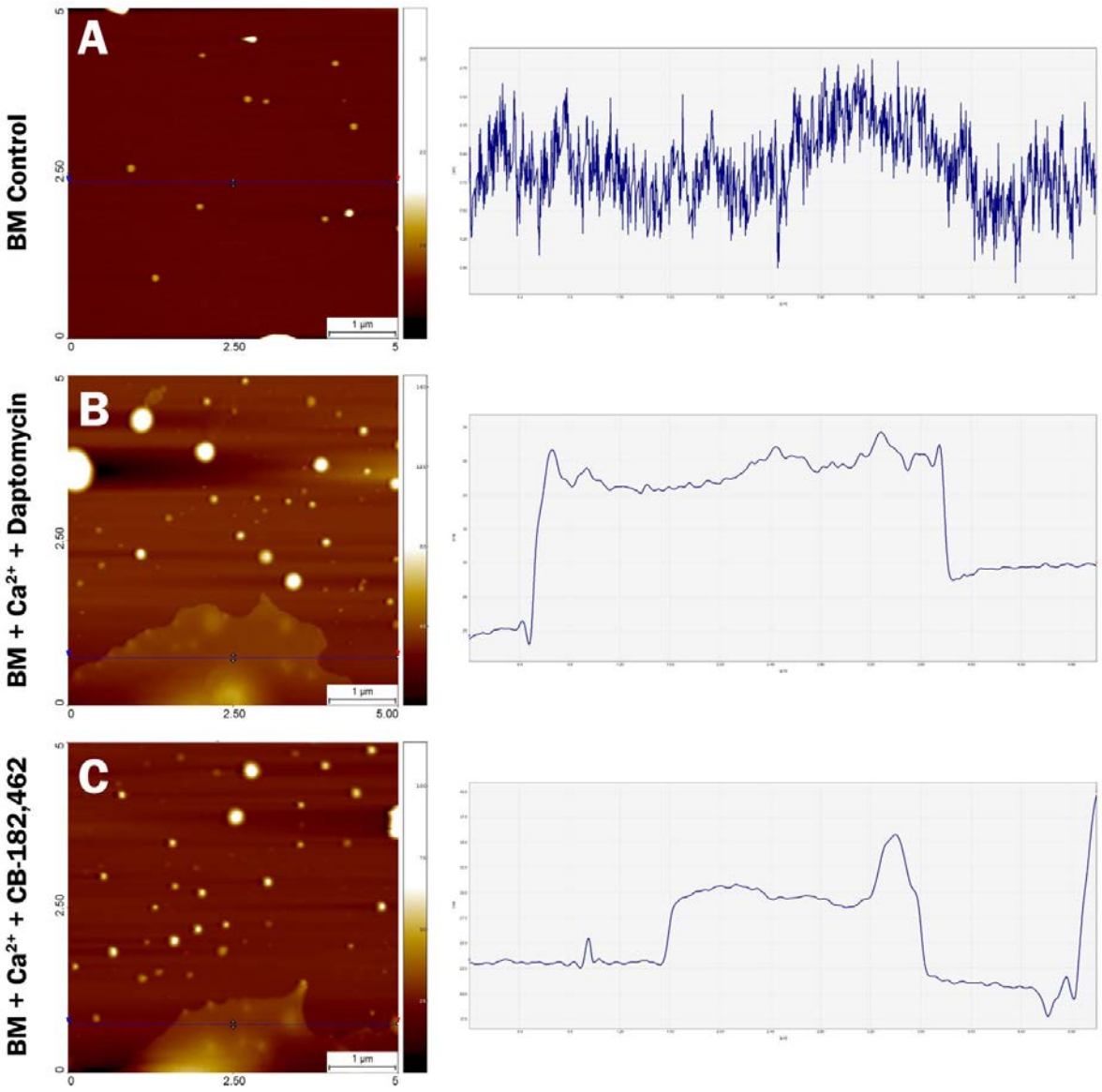

Figure 7.9 Liquid AFM images of BM model membrane. Bacterial membrane model vesicles, made of 20% DOPG, 20% TOCL, and 60% POPE, were deposited onto mica substrates and imaged using an atomic force microscope in an aqueous environment. Image A represents the bacterial membrane control, which is fairly smooth and void of any large defects. Image B and C represent the BM membrane with 2 mM of Ca^{2+} and 4 μM of daptomycin or CB-182,462, respectively. Both of these membranes have large domains and spherical artefacts (most likely unruptured vesicles) that span the surface of the membrane. All images are 5 μm by 5 μm.

bacterial membrane model, it can be construed that these bilayer patches are highly concentrated in membrane-bound daptomycin, extending the bilayer height above normal values. This daptomycin-rich area further attracts additional vesicles, where they rupture and fuse to form an additional bilayer on top. A similar effect can be seen with the BM + Ca^{2+} + CB-182,462 AFM image (***Figure 7.9C***), where an additional patch of bilayer with an average height profile of 6.20 ± 0.72 nm can be seen amongst the flatter part of the membrane. The surface roughness here is 2.42 ± 0.15 nm, which is somewhat smoother than the daptomycin sample, but still prevalent with a wide range of topographical features.

In the human membrane control, the surface roughness is 0.44 ± 0.02 nm. Similar to the bacterial membrane model, the control membrane (see ***Figure 7.10A***) is fairly smooth with the exception of spherical deposits that range in height from 10 to 100 nm with diameters of approximately 120 nm. These are indicative of unruptured vesicles that are trapped or adsorbed to the surface, respectively. When daptomycin and calcium are added to the HM sample, the surface roughness has now increased to 3.53 ± 0.17 nm due to the presence of additional unruptured vesicles (***Figure 7.10B***). The reason for this increase in unruptured vesicles is unknown, but we postulate that it may be due to slight variations in vesicle incubation times and speed of washing the solutions during sample preparation. However, when the HM sample is combined with calcium and CB-182,462, bilayer patches appear with an average height profile of 9.81 ± 0.78 nm (see ***Figure 7.10C***). The surface roughness is now 6.60 ± 0.14 nm, which is significantly higher than both the control and that of the daptomycin sample. This increase in surface roughness is partially due to the presence of unruptured vesicles and bilayer patches, but also additional rounded areas of elevation within each bilayer patch that reach heights of up to 40 nm. It may be that these bilayer patches form on top of large, unruptured vesicles to achieve this curved effect. Since CB-182,462 is known to insert into and bind strongly to our human membrane model, it makes sense that membrane-bound CB-182,462 may attract additional vesicles to a certain area, which cause them to rupture and form an additional bilayer above the original HM model membrane.

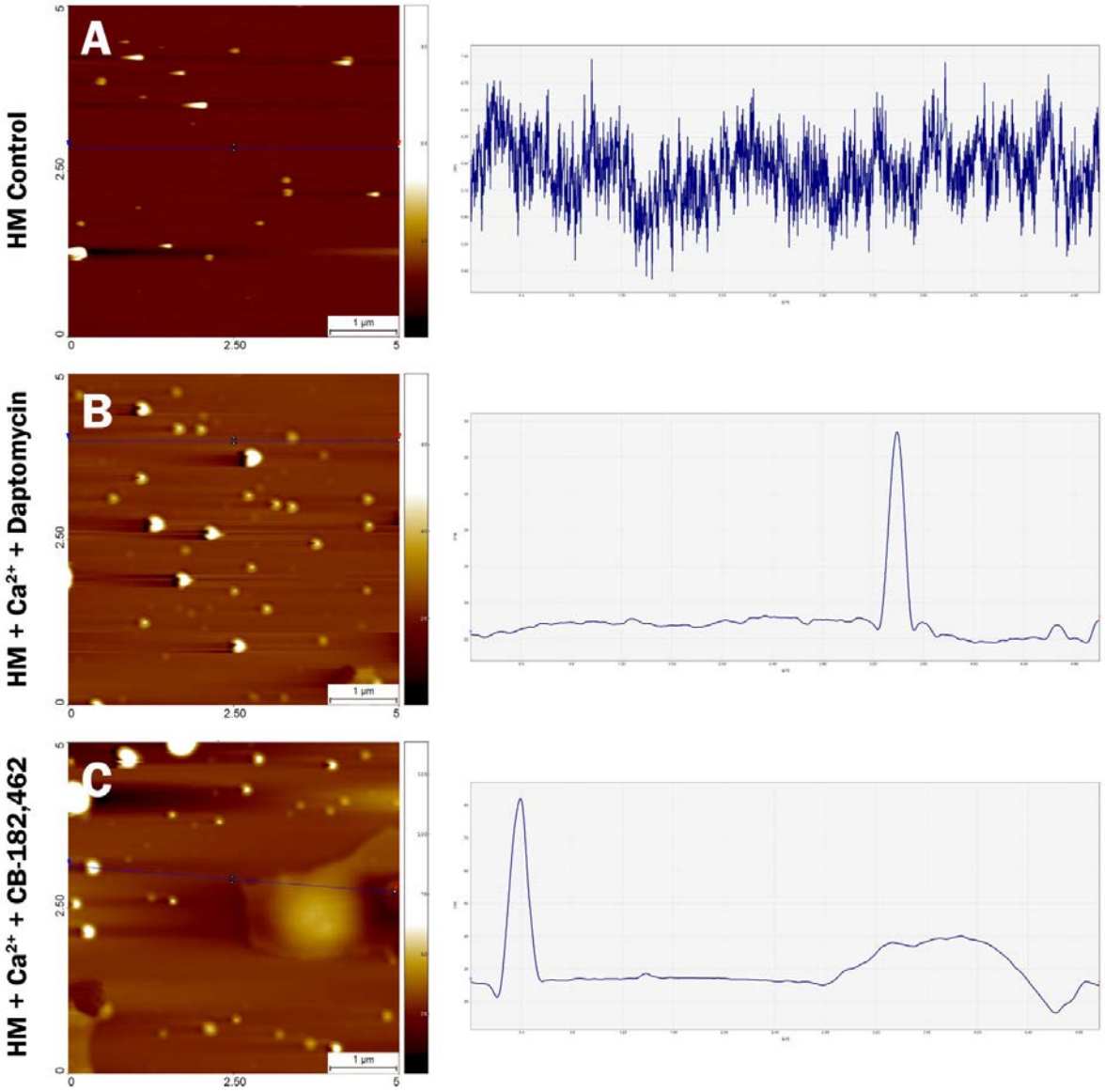

Figure 7.10 Liquid AFM images of HM model membranes. Human endothelial membrane model vesicles, made of 20% DPPC, 20% POPE, 10% DOPS, 15% sphingomyelin and 35% cholesterol, were deposited onto mica substrates using vesicle fusion. Atomic force microscopy was used to obtain 5 µm by 5 µm images under a liquid environment. Image A represents the HM control, which is smooth and void of larger surface artefacts. Both Image A and B represent the HM membrane in the presence of 2 mM Ca^{2+} and either DAP or 462. However, while both contain spherical surface artefacts (presumed to be unruptured vesicles), the 462 sample contains additional large, surface-spanning domains on top of the primary membrane

The lung surfactant membrane by itself was shown to have a surface roughness of 1.25 ± 0.02 nm, which is higher than the other control samples for BM and HM. This is due to the fact that there are additional bilayer patches approximately 5-6 nm high located sporadically across the membrane, and within those patches are additional bilayer patches approximately 5-6 nm in height (see ***Figure 7.11A***). We believe that because lung surfactant forms multilayers when highly compressed, the process of vesicle fusion ensures that a high pressure is reached in order for the vesicles to rupture, essentially forming multi-bilayers due to lung surfactant's low compressibility properties. However, when calcium and daptomycin are added to lung surfactant, these effects are significantly enhanced (***Figure 7.11B***). The surface roughness is now 6.07 ± 0.03 nm because of the formation of extensive, irregular multi-bilayers that cover most of the membrane surface. If we look closely at this sample, there are indistinct layers visible behind the more prominent ones. These lower domains are multilayer patches that are already about 9 nm in height. On top of these patches are additional bilayer patches of approximately 5-6 nm in height. In other areas where there are unruptured 50-150 nm diameter vesicles, the total height can reach up to 70 nm. These results are in agreement with our findings from our monolayer experiments. It is believed that calcium and daptomycin bind to lung surfactant, and due to its strong attraction (and therefore sequestration by lung surfactant), additional LS vesicles are attracted to areas heavily bound to daptomycin, allowing these vesicles to rupture and form additional bilayers on top of preformed ones. In addition, since lung surfactant is thought to reduce the compressibility of lung surfactant, it facilitates the formation of multilayers at lower pressures. In summary, daptomycin and calcium together allow for lung surfactant vesicles to form additional bilayers on top of the original lung surfactant bilayer, and because of the reduced compressibility, a more extensive network of these additional bilayers can be seen across the sample surface. If we look at ***Figure 7.11C***, the addition of calcium and CB-182,462 does not affect the structure of the bilayer much and is quite similar to the corresponding control. The surface roughness is 2.69 ± 0.09 nm, and there are slightly larger, more uniform bilayer patches of about 5 nm in height along with a large number of unruptured vesicles.

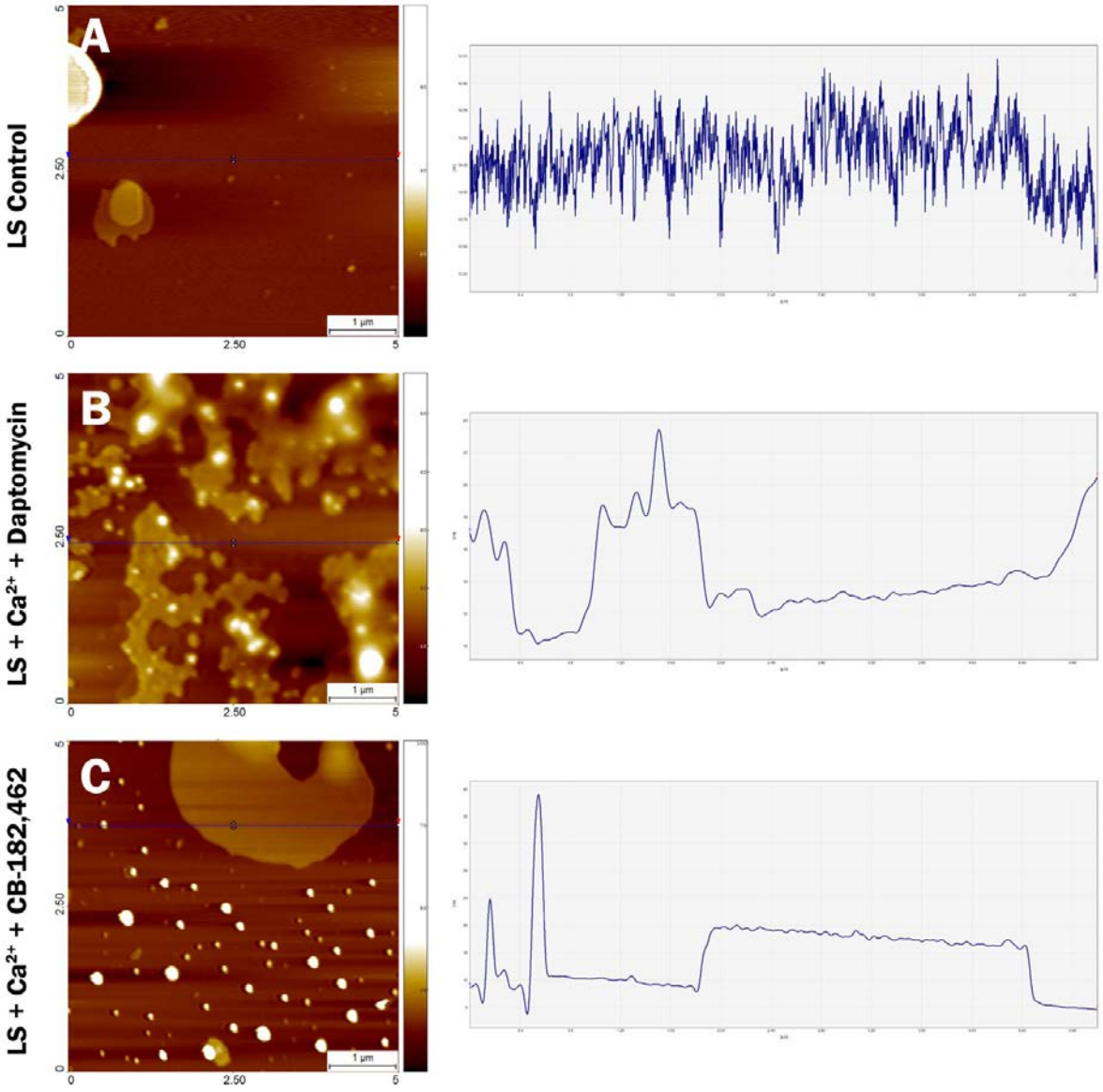

Figure 7.11 Liquid AFM images of synthetic LS membranes. 5 µm by 5 µm AFM images were taken of lung surfactant model vesicles in liquid. Image A represents the LS membrane, made of 80% DPPC and 20% DOPG with 5% cholesterol. For the most part, the membrane surface is very smooth, with some additional smaller patches of membranes (possibly from the rupture of vesicles that were not fused with the primary membrane). However, when 2 mM calcium and 4 µM daptomycin are added to the vesicle solution, the resulting membrane has multiple layers of membranes on top of the primary membrane. This is not the case with the 462 sample (Image C), which only has large, spherical surface artefacts representative of unruptured vesicles.

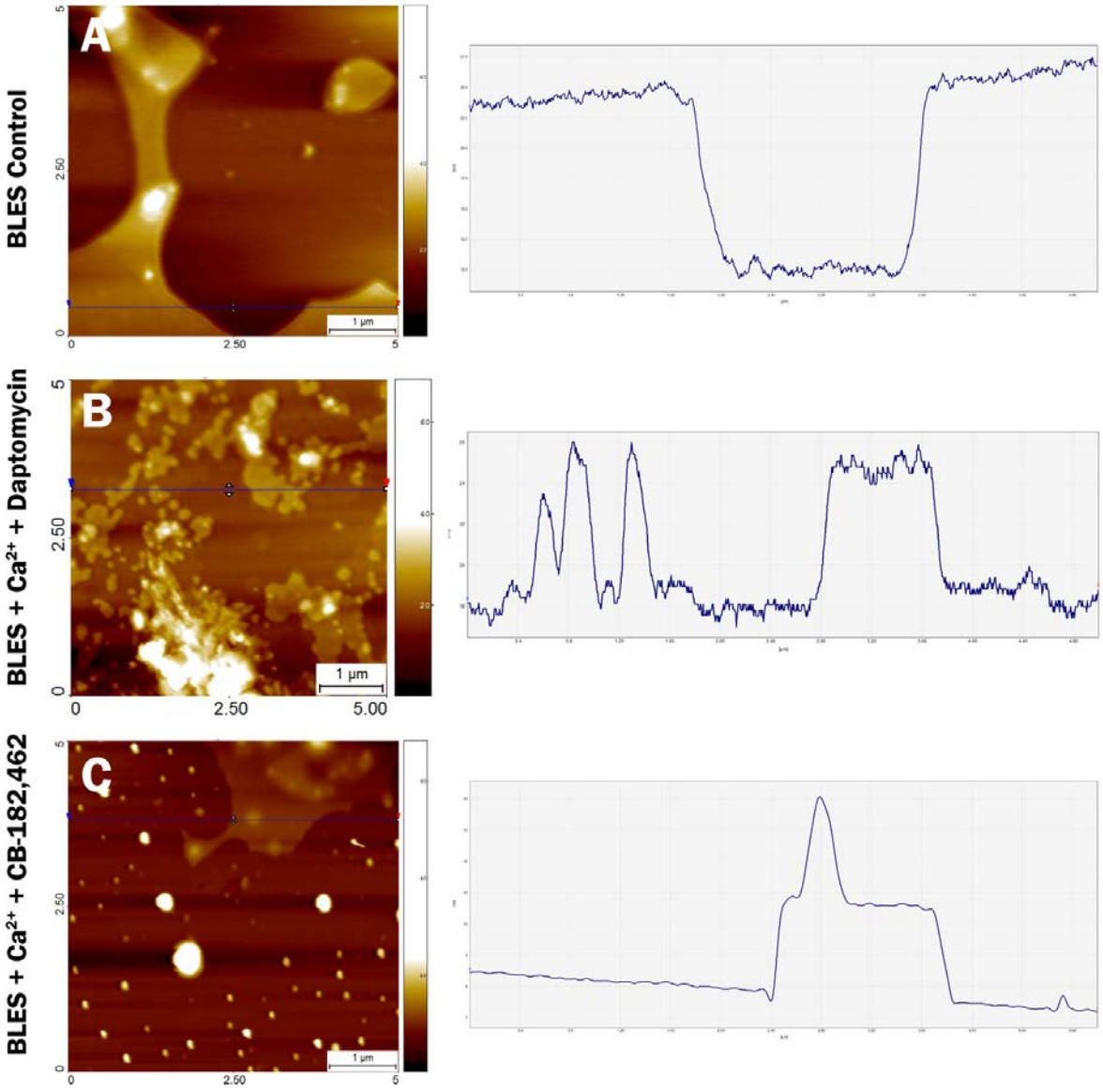

Figure 7.12 Liquid AFM images of BLES® membranes. BLES® vesicles were prepared and deposited onto mica substrates using vesicle fusion. These samples were then imaged in liquid using atomic force microscopy to obtain multiple 5 µm by 5 µm images. Image A represents the BLES® membrane control, which contains larger domains on top of the primary membrane compared to its synthetic LS counterpart. Image B represents the membrane with calcium and DAP, and similar to its LS counterpart, has many more, smaller domains stacked on top of each other, suggesting multi-bilayer formation. Image C represents the membrane with calcium and 462, and although it has some patches of monolayers and bilayers on the surface, it is primarily riddled with presumably unruptured vesicles.

Table 7.2 Average surface roughness of different membrane models and scenarios. The average surface roughness, R_a is presented for every model and its associated three scenarios: the membrane by itself, the membrane with 2 mM calcium and 4 μM daptomycin, and the membrane with both calcium and CB-182,462. Each average value was obtained from no less than 5 liquid AFM images.

Model & Scenario	R_a (nm)
Bacterial Membrane (BM) Model	
BM Control	0.32 ± 0.03
BM + Ca^{2+} + Daptomycin	0.44 ± 0.05
BM + Ca^{2+} + CB-182,462	0.53 ± 0.02
Human Membrane (HM) Model	
HM Control	0.35 ± 0.03
HM + Ca^{2+} + Daptomycin	0.24 ± 0.04
HM + Ca^{2+} + CB-182,462	0.46 ± 0.05
Lung Surfactant (LS) Model	
LS Control	0.97 ± 0.04
LS + Ca^{2+} + Daptomycin	1.50 ± 0.04
LS + Ca^{2+} + CB-182,462	0.20 ± 0.03
Bovine Lipid Extract Surfactant (BLES®) Model	
BLES Control	0.20 ± 0.02
BLES + Ca^{2+} + Daptomycin	1.52 ± 0.02
BLES + Ca^{2+} + CB-182,462	0.30 ± 0.04

Since the LS model is a synthetic one, comparing it with a natural surfactant model will give us further insight and physiological relevance to our findings. A quick glance at the BLES® membrane samples shows us that the results are very similar to those observed in the LS membrane samples. In the BLES® control membrane, the surface roughness is 3.56 ± 0.30 nm, which is rougher than the LS control, but explainable due to the large bilayer patches visible in the sample. These bilayer patches are approximately 8 nm in height (see ***Figure 7.12A***). Since BLES® is supposed to have some remaining hydrophobic surfactant proteins, it is highly possible that it spreads more easily than its synthetic counterpart. In the presence of calcium and daptomycin, multi-bilayers are once again observed with a surface roughness of 6.00 ± 0.26 nm (see ***Figure 7.12B***), this time with bilayer patches reaching 40-60 nm in height in different areas of the sample. This supports our hypothesis that daptomycin helps confer additional surfactant

spreading properties, and that the inclusion of daptomycin allows lung surfactant (BLES®) to continuously form multilayers and spread more easily across the surface of the membrane, effectively sequestering daptomycin in layers of lung surfactant. Meanwhile, no significant differences are observed when calcium and CB-182,462 are added as the surface roughness is 4.27 ± 0.33 nm, which is very similar to the control sample, only that there are more unruptured vesicles present (*Figure 7.12C*).

Overall, these AFM images of our membrane models have allowed us to substantiate our findings from the monolayer experiments. In the presence of calcium and daptomycin, lung surfactant is hypothesized to achieve lower compressibility upon binding of these molecules, thus allowing it to more easily form multilayers and effectively sequester daptomycin and render it inactive.

7.4 Summary & Conclusion

Our study has shown that daptomycin physically affects the lung surfactant monolayer or membrane by allowing for multilayer formation of either monolayers or bilayers, respectively. KPFM studies also showed enhanced electrostatic domains associated with additional multilayer formation on lung surfactant monolayers. This correlates with our previous findings in *Chapters 5 and 6* and our new proposed model of daptomycin inhibition by lung surfactant, where daptomycin is not only attracted to and inserts strongly into lung surfactant, but also reduces its compressibility and makes it easier for it to form multilayers, effectively reinforcing its sequestration. This study also marks the first atomic force microscopy and Kelvin probe force microscopy study of daptomycin and its effect on model monolayers and membranes.

Although it was not possible to resolve the oligomerization or insertion of daptomycin on monolayer or membrane surfaces, it was possible to visualize the effect of daptomycin on these surfaces using atomic force microscopy. The fact that daptomycin has such a significant effect

on lung surfactant suggests that further studies should be done on their interaction with each other. It would be good to compare the effect of daptomycin on lung surfactant held at different pressures and then relate those results to a lung surfactant control at various pressures. This would allow us to determine the degree of surface activity enhancement that daptomycin confers to lung surfactant.

CHAPTER 8

8 CONCLUSIONS & FUTURE RESEARCH

8.1 Summary & Conclusion

The general objective of this thesis was to provide additional insight into daptomycin's inhibition by pulmonary surfactant as well as its molecular mechanism of action. Although daptomycin is a potent antibiotic against serious Gram-positive infections, even those that are highly resistant against most antibiotics, it is inhibited when combatting Gram-positive pathogens within the lungs. Specifically, it cannot be used to treat infections caused by *Streptococcus pneumoniae*, the primary cause of community-acquired pneumonia.

At the beginning of this thesis in ***Chapter 2***, we outlined the specific objectives of our work in elucidating daptomycin's inhibition by pulmonary surfactant. The studies that have been done before have used generic or simplified model membrane systems to examine daptomycin's mechanism of action. In order to gain insight into daptomycin's inhibition by pulmonary

surfactant in the case of community-acquired pneumonia, we wanted to closely mimic the different types of membranes that daptomycin would encounter. These lipid model systems include those of *S. pneumoniae*, erythrocytes or tissue cells, as well as synthetic and natural lung surfactant. We successfully developed these lipid models in ***Chapter 3***, and have used these models throughout each of the experiments in this thesis.

Once these models had been developed, we wanted to see whether daptomycin would strongly bind to lung surfactant. There is evidence that shows daptomycin is capable of inserting into lung surfactant, which has brought forth a widely accepted theory that the vast abundance of surfactant within the lungs can sequester the antibiotic. However, there have been no binding studies done which compare the degree of binding or insertion of daptomycin to different model systems. In ***Chapter 5***, we performed fluorescence spectroscopy experiments to test the binding and insertion of daptomycin into all four model membrane systems. It was discovered that daptomycin inserted more strongly into lung surfactant liposomes than the bacterial membrane liposomes at lower, physiologically-relevant concentrations of calcium (2 mM). Even more intriguing was the opposite effect that was observed when the calcium concentration was increased to 10 mM. At higher concentrations of calcium, it was shown that daptomycin interacted more with the bacterial membrane than it did with lung surfactant. During this study, we developed novel protocols to create modified BLES® (bovine lipid extract surfactant) liposomes, or large unilamellar vesicles of approximately 100 nm in diameter, which has not been successfully accomplished before. The results we obtained for the synthetic lung surfactant liposomes and the BLES® liposomes correlated very nicely together, validating our BLES® protocols as well as showing that the synthetic model is a good and simplified representation of the real thing.

With the insertion of daptomycin into lung surfactant proven to be very strong, the next step was to quantify the changes that daptomycin's insertion incurs on lung surfactant as well as other model systems. In ***Chapter 6***, we performed Langmuir-Blodgett monolayer experiments to help collect data on whether daptomycin can change the properties of each monolayer model in the

presence of calcium. The compression isotherms obtained showed that daptomycin significantly increased the elastic area compressibility modulus of lung surfactant, which translates into reduced compressibility. This means that with daptomycin and calcium, lung surfactant is less compressible and more prone to the formation of multilayers at lower surface pressures and smaller changes in surface area. Subsequently, Langmuir monolayer insertion assays were performed to directly compare the insertion of daptomycin into each of the different lipid model monolayers in the presence of calcium. The results showed that daptomycin inserts into lung surfactant more than it does any other lipid model, verifying our results from *Chapter 5*. In this study, we presented a new model of daptomycin inhibition by lung surfactant, where daptomycin binds more strongly to lung surfactant than bacterial membrane (encouraging its sequestration), and lowers the compressibility of lung surfactant, possibly allowing it to confer surfactant-spreading properties similar to those of other hydrophobic surfactant proteins.

The next set of questions we posed involved being able to visualize the changes that daptomycin may cause on both model monolayer systems as well as model membrane systems. In *Chapter 7*, we performed scanning probe microscopy studies to obtain atomic force microscopy, phase, and Kelvin probe force microscopy images in air for each monolayer model in different scenarios. From these images, it was clear that daptomycin (in the presence of calcium) promotes the formation of multilayers in lung surfactant. The images showed that daptomycin and calcium changed the shape and arrangement of the lipid domains significantly, with increased height profiles reminiscent of bilayers on top of monolayers (and therefore termed 'multilayers') associated with larger differences in electrical surface potential. Afterwards, supported bilayers on mica substrates were prepared for AFM imaging in liquid. The AFM images showed multi-bilayer formation in the lung surfactant bilayer samples in the presence of calcium and daptomycin, substantiating the results obtained from the monolayer samples.

Throughout all of these experiments, a semisynthetic antibiotic derivative called CB-182,462 was tested along with daptomycin. CB-182,462 was under development to help overcome daptomycin's inhibition by lung surfactant, and it was shown to be unhindered by lung surfactant

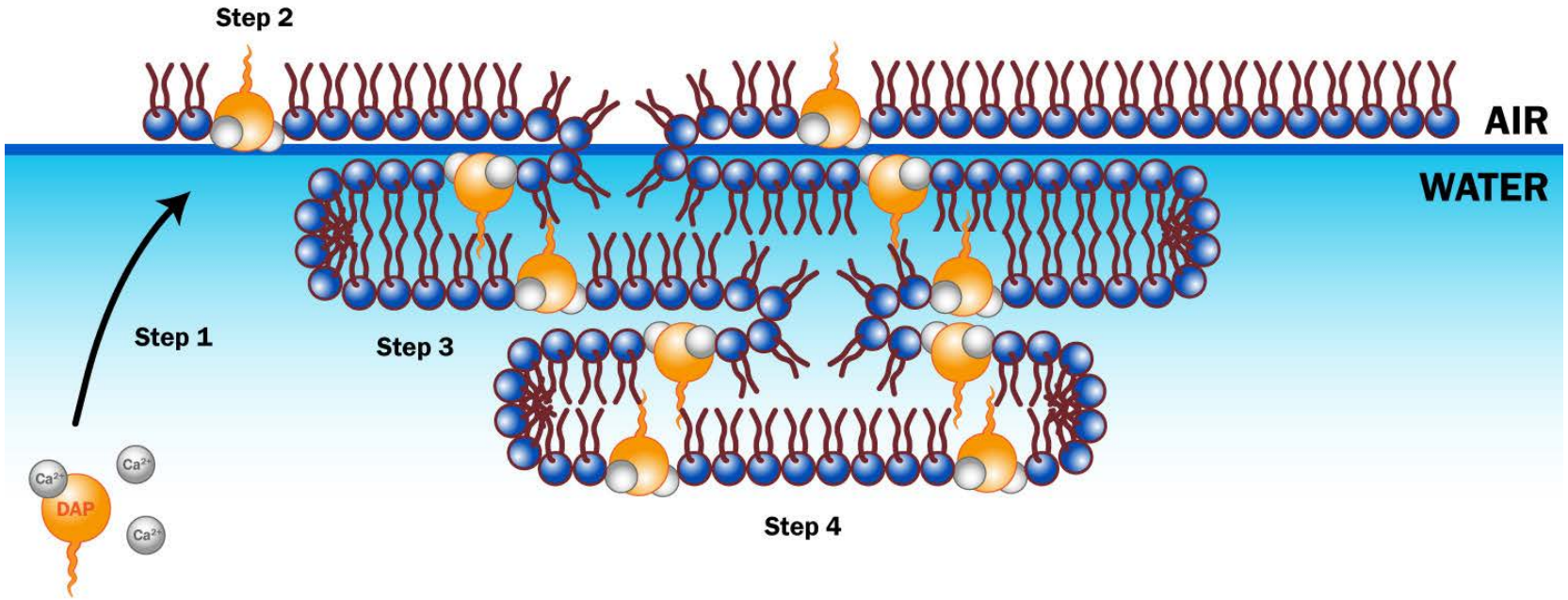

Figure 8.1 New proposed model of daptomycin interaction with lung surfactant. It was previously thought that daptomycin was sequestered by lung surfactant through binding interactions. From the experiments in this thesis, we have shown this binding to be true, and additional experiments have allowed us to propose a more detailed model of daptomycin inhibition by lung surfactant. Step 1: In the presence of calcium, daptomycin (of unknown specific quantity) is attracted to the lung surfactant monolayer and therefore binds to it quite strongly. Step 2: Once inserted into the monolayer, daptomycin confers surfactant-spreading properties, similar to the function of surfactant-spreading proteins SP-B and SP-C, and reduces the compressibility of the lung surfactant. Step 3: Due to this reduction in compressibility, the lung surfactant can more easily form multilayers at lower pressures than before, folding in on itself multiple times. Step 4: With each fold of the monolayer, daptomycin becomes more "trapped" within the depths of the lung surfactant multilayer, effectively sequestering it and reinforcing its inhibition and inability to free itself.

during cell viability studies. However, due to possible toxicity, its development was permanently ceased. The experiments performed through *Chapter 5 to Chapter 7* have provided additional insight into CB-182,462's mechanism of action as well, suggesting its toxicity is due to its strong binding and insertion to the human membrane model as well as its ability to severely alter the physical structure and organization of lipid domains.

From the results obtained throughout this thesis, we were able to present a new model of daptomycin inhibition by lung surfactant (*Figure 8.1*) that is more robust than its predecessor. This new model suggests that (1) daptomycin requires the presence of calcium to strongly insert into lung surfactant, (2) daptomycin confers surfactant-spreading properties by decreasing the compressibility of lung surfactant, (3) this reduction in compressibility allows lung surfactant to fold in on itself at lower pressures to form multilayers, and (4) daptomycin is further sequestered within these multilayers and effectively inhibited.

This thesis successfully provides additional insight into daptomycin's inhibition by lung surfactant. The lipid model systems, experimental protocols, and hypotheses presented in this thesis can also be beneficial to future studies not limited to daptomycin, but other molecules and systems as well.

8.2 Future Research

Microorganisms are constantly evolving and growing more resistant to typical antibiotic regimens. As a result, it is in our interest to continue studying effective antibiotics that can help us gain some ground in the arms race against these resistant strains of bacteria. One such antibiotic is daptomycin, which is highly effective against severely resistant Gram-positive pathogens such as MRSA and VRE. Since *Streptococcus pneumoniae* is a bacteria that is quickly growing in resistance, it is even more imperative that we elucidate daptomycin's inhibition by lung surfactant.

The findings presented in this thesis provide intriguing results that can be expanded upon with further studies. Competitive binding assays can be used to test daptomycin's preference in binding between lung surfactant lipid models and bacterial membrane models. Since daptomycin binds less to lung surfactant at higher calcium concentrations, it may be a good option to test daptomycin's bactericidal activity against *S. pneumoniae* at these higher levels of calcium ions. With the emergence of advanced nanotechnology tools, studies regarding daptomycin delivery to the diseased lung and targeted binding to *S. pneumoniae* or generic lipoteichoic acids may prove to be very useful as well.

Apart from elucidating daptomycin's inhibition by lung surfactant, the results obtained in this thesis present a different question, one that is somewhat reversed: *how does daptomycin affect lung surfactant?* The focus of this thesis has been placed on why daptomycin is inhibited by lung surfactant, but the results have shown that daptomycin may confer surfactant-spreading properties for lung surfactant. There may be possible merits to studying whether daptomycin could have beneficial properties and be able to play a different role in respiratory physiology.

The models and methods developed in this thesis can also be applied to many other studies. Lung surfactant, erythrocytes or tissue cells, and bacterial membranes are common systems that need to be studied, and the models presented here can be used in many other ways outside the scope of this thesis, for other diseases, antibiotics, bacteria, or peptide interaction studies. The protocols and experimental procedures developed through our work will also be very useful for future studies and applications in the field of membrane biophysics.

REFERENCES

[1] Drews J (2000) Drug discovery: a historical perspective. *Science* **287**, 1960-1964.

[2] Ayliffe GA (1997) The progressive intercontinental spread of methicillin-resistant Staphylococcus aureus. *Clin Infect Dis* **24 Suppl 1**, S74-79.

[3] Bozdogan B, Esel D, Whitener C, Browne FA, Appelbaum PC (2003) Antibacterial susceptibility of a vancomycin-resistant Staphylococcus aureus strain isolated at the Hershey Medical Center. *J Antimicrob Chemother* **52**, 864-868.

[4] Cottagnoud P (2008) Daptomycin: a new treatment for insidious infections due to gram-positive pathogens. *Swiss Med Wkly* **138**, 93-99.

[5] Enoch DA, Bygott JM, Daly ML, Karas JA (2007) Daptomycin. *J Infect* **55**, 205-213.

[6] Hawkey PM (2008) Pre-clinical experience with daptomycin. *J Antimicrob Chemother* **62 Suppl 3**, iii7-14.

[7] Tally FP, DeBruin MF (2000) Development of daptomycin for gram-positive infections. *J Antimicrob Chemother* **46**, 523-526.

[8] Vilhena C, Bettencourt A (2012) Daptomycin: a review of properties, clinical use, drug delivery and resistance. *Mini Rev Med Chem* **12**, 202-209.

[9] Baltz RH (2009) Daptomycin: mechanisms of action and resistance, and biosynthetic engineering. *Curr Opin Chem Biol* **13**, 144-151.

[10] Silverman JA, Mortin LI, Vanpraagh AD, Li T, Alder J (2005) Inhibition of daptomycin by pulmonary surfactant: in vitro modeling and clinical impact. *J Infect Dis* **191**, 2149-2152.

[11] Fox JL (2013) Antimicrobial peptides stage a comeback. *Nat Biotechnol* **31**, 379-382.

[12] Ageitos JM, Sanchez-Perez A, Calo-Mata P, Villa TG (2016) Antimicrobial peptides (AMPs): Ancient compounds that represent novel weapons in the fight against bacteria. *Biochem Pharmacol.*

[13] Brogden KA (2005) Antimicrobial peptides: pore formers or metabolic inhibitors in bacteria? *Nat Rev Microbiol* **3**, 238-250.

[14] Wang G, Li X, Wang Z (2009) APD2: the updated antimicrobial peptide database and its application in peptide design. *Nucleic Acids Res* **37**, D933-937.

[15] Yount NY, Yeaman MR (2013) Peptide antimicrobials: cell wall as a bacterial target. *Ann N Y Acad Sci* **1277**, 127-138.

[16] Papagianni M (2003) Ribosomally synthesized peptides with antimicrobial properties: biosynthesis, structure, function, and applications. *Biotechnol Adv* **21**, 465-499.

[17] Malanovic N, Lohner K (2016) Antimicrobial Peptides Targeting Gram-Positive Bacteria. *Pharmaceuticals* **9**, 59.

[18] Ehrenstein G, Lecar H (1977) Electrically gated ionic channels in lipid bilayers. *Quarterly Reviews of Biophysics* **10**, 1-34.

[19] He K, Ludtke SJ, Huang HW, Worcester DL (1995) Antimicrobial peptide pores in membranes detected by neutron in-plane scattering. *Biochemistry* **34**, 15614-15618.

[20] Spaar A, Munster C, Salditt T (2004) Conformation of peptides in lipid membranes studied by x-ray grazing incidence scattering. *Biophys J* **87**, 396-407.

[21] Yang L, Harroun TA, Weiss TM, Ding L, Huang HW (2001) Barrel-stave model or toroidal model? A case study on melittin pores. *Biophys J* **81**, 1475-1485.

[22] Omardien S, Brul S, Zaat SAJ (2016) Antimicrobial Activity of Cationic Antimicrobial Peptides against Gram-Positives: Current Progress Made in Understanding the Mode of Action and the Response of Bacteria. *Frontiers in Cell and Developmental Biology* **4**, 111.

[23] Lee MT, Chen FY, Huang HW (2004) Energetics of pore formation induced by membrane active peptides. *Biochemistry* **43**, 3590-3599.

[24] Matsuzaki K, Murase O, Fujii N, Miyajima K (1996) An antimicrobial peptide, magainin 2, induced rapid flip-flop of phospholipids coupled with pore formation and peptide translocation. *Biochemistry* **35**, 11361-11368.

[25] Melo MN, Ferre R, Castanho MARB (2009) Antimicrobial peptides: linking partition, activity and high membrane-bound concentrations. *Nat Rev Micro* **7**, 245-250.

[26] Hallock KJ, Lee DK, Ramamoorthy A (2003) MSI-78, an analogue of the magainin antimicrobial peptides, disrupts lipid bilayer structure via positive curvature strain. *Biophys J* **84**, 3052-3060.

[27] Bechinger B (1999) The structure, dynamics and orientation of antimicrobial peptides in membranes by multidimensional solid-state NMR spectroscopy. *Biochim Biophys Acta* **1462**, 157-183.

[28] Ladokhin AS, White SH (2001) 'Detergent-like' permeabilization of anionic lipid vesicles by melittin. *Biochim Biophys Acta* **1514**, 253-260.

[29] Oren Z, Shai Y (1998) Mode of action of linear amphipathic alpha-helical antimicrobial peptides. *Biopolymers* **47**, 451-463.

[30] Pouny Y, Rapaport D, Mor A, Nicolas P, Shai Y (1992) Interaction of antimicrobial dermaseptin and its fluorescently labeled analogues with phospholipid membranes. *Biochemistry* **31**, 12416-12423.

[31] Shai Y (1999) Mechanism of the binding, insertion and destabilization of phospholipid bilayer membranes by alpha-helical antimicrobial and cell non-selective membrane-lytic peptides. *Biochim Biophys Acta* **1462**, 55-70.

[32] Yamaguchi S, Huster D, Waring A, Lehrer RI, Kearney W, Tack BF, Hong M (2001) Orientation and dynamics of an antimicrobial peptide in the lipid bilayer by solid-state NMR spectroscopy. *Biophys J* **81**, 2203-2214.

[33] Bierbaum G, Sahl HG (1987) Autolytic system of Staphylococcus simulans 22: influence of cationic peptides on activity of N-acetylmuramoyl-L-alanine amidase. *J Bacteriol* **169**, 5452-5458.

[34] Mishra B, Wang G (2012) The Importance of Amino Acid Composition in Natural AMPs: An Evolutional, Structural, and Functional Perspective. *Front Immunol* **3**, 221.

[35] Abbanat D, Macielag M, Bush K (2003) Novel antibacterial agents for the treatment of serious Gram-positive infections. *Expert Opin Investig Drugs* **12**, 379-399.

[36] Millan X, Muggia V, Ostrowsky B (2014) Antimicrobial agents, drug adverse reactions and interactions, and cancer. *Cancer Treat Res* **161**, 413-462.

[37] Rybak JM, Barber KE, Rybak MJ (2013) Current and prospective treatments for multidrug-resistant gram-positive infections. *Expert Opin Pharmacother* **14**, 1919-1932.

[38] Segreti J (2005) Efficacy of current agents used in the treatment of Gram-positive infections and the consequences of resistance. *Clin Microbiol Infect* **11 Suppl 3**, 29-35.

[39] Woodford N, Livermore DM (2009) Infections caused by Gram-positive bacteria: a review of the global challenge. *J Infect* **59 Suppl 1**, S4-16.

[40] Rybak M, Lomaestro B, Rotschafer JC, Moellering R, Jr., Craig W, Billeter M, Dalovisio JR, Levine DP (2009) Therapeutic monitoring of vancomycin in adult patients: a consensus review of the American Society of Health-System Pharmacists, the Infectious Diseases Society of America, and the Society of Infectious Diseases Pharmacists. *Am J Health Syst Pharm* **66**, 82-98.

[41] Tenover FC (2006) Mechanisms of antimicrobial resistance in bacteria. *Am J Med* **119**, S3-10; discussion S62-70.

[42] Badger N (2010) Evaluation of the Treatment of MRSA Infections. *US Pharmacist* **35**, HS2-HS4.

[43] Schaechter M, Engleberg NC, DiRita VJ, Dermody TS (2012) *Schaechter's Mechanisms of Microbial Disease*, Wolters Kluwer Health.

[44] Damodaran SE, Madhan S (2011) Telavancin: A novel lipoglycopeptide antibiotic. *Journal of Pharmacology & Pharmacotherapeutics* **2**, 135-137.

[45] Kirst HA (2013) Developing new antibacterials through natural product research. *Expert Opin Drug Discov* **8**, 479-493.

[46] Nailor MD, Sobel JD (2011) Antibiotics for gram-positive bacterial infection: vancomycin, teicoplanin, quinupristin/dalfopristin, oxazolidinones, daptomycin, telavancin, and ceftaroline. *Med Clin North Am* **95**, 723-742, vii.

[47] Anstead GM, Cadena J, Javeri H (2014) Treatment of infections due to resistant Staphylococcus aureus. *Methods Mol Biol* **1085**, 259-309.

[48] Shoemaker DM, Simou J, Roland WE (2006) A review of daptomycin for injection (Cubicin) in the treatment of complicated skin and skin structure infections. *Ther Clin Risk Manag* **2**, 169-174.

[49] Tally FP, Zeckel M, Wasilewski MM, Carini C, Berman CL, Drusano GL, Oleson FB, Jr. (1999) Daptomycin: a novel agent for Gram-positive infections. *Expert Opin Investig Drugs* **8**, 1223-1238.

[50] Eliopoulos GM, Willey S, Reiszner E, Spitzer PG, Caputo G, Moellering RC, Jr. (1986) In vitro and in vivo activity of LY 146032, a new cyclic lipopeptide antibiotic. *Antimicrob Agents Chemother* **30**, 532-535.

[51] Fass RJ, Helsel VL (1986) In vitro activity of LY146032 against staphylococci, streptococci, and enterococci. *Antimicrob Agents Chemother* **30**, 781-784.

[52] Jones RN, Barry AL (1987) Antimicrobial activity and spectrum of LY146032, a lipopeptide antibiotic, including susceptibility testing recommendations. *Antimicrob Agents Chemother* **31**, 625-629.

[53] Silva M, Jacobus NV, Gorbach SL (1988) In vitro activity of LY146032 against gram-positive bacteria. *Diagn Microbiol Infect Dis* **9**, 79-85.

[54] Miller WR, Bayer AS, Arias CA (2016) Mechanism of Action and Resistance to Daptomycin in Staphylococcus aureus and Enterococci. *Cold Spring Harb Perspect Med* **6**.

[55] King A, Phillips I (2001) The in vitro activity of daptomycin against 514 Gram-positive aerobic clinical isolates. *J Antimicrob Chemother* **48**, 219-223.

[56] Woodford N (2003) Novel agents for the treatment of resistant Gram-positive infections. *Expert Opin Investig Drugs* **12**, 117-137.

[57] Raja A, LaBonte J, Lebbos J, Kirkpatrick P (2003) Daptomycin. *Nat Rev Drug Discov* **2**, 943-944.

[58] Oleson FB, Jr., Berman CL, Kirkpatrick JB, Regan KS, Lai JJ, Tally FP (2000) Once-daily dosing in dogs optimizes daptomycin safety. *Antimicrob Agents Chemother* **44**, 2948-2953.

[59] Arbeit RD, Maki D, Tally FP, Campanaro E, Eisenstein BI (2004) The safety and efficacy of daptomycin for the treatment of complicated skin and skin-structure infections. *Clin Infect Dis* **38**, 1673-1681.

[60] Wright BM, Eiland EH (2011) Retrospective Analysis of Clinical and Cost Outcomes Associated with Methicillin-Resistant Staphylococcus aureus Complicated Skin and Skin Structure Infections Treated with Daptomycin, Vancomycin, or Linezolid. *Journal of Pathogens* **2011**.

[61] Silverman JA, Perlmutter NG, Shapiro HM (2003) Correlation of daptomycin bactericidal activity and membrane depolarization in Staphylococcus aureus. *Antimicrob Agents Chemother* **47**, 2538-2544.

[62] Allen NE, Hobbs JN, Alborn WE, Jr. (1987) Inhibition of peptidoglycan biosynthesis in gram-positive bacteria by LY146032. *Antimicrob Agents Chemother* **31**, 1093-1099.

[63] Boaretti M, Canepari P (1995) Identification of daptomycin-binding proteins in the membrane of Enterococcus hirae. *Antimicrob Agents Chemother* **39**, 2068-2072.

[64] Boaretti M, Canepari P, Lleo MM, Satta G (1993) The activity of daptomycin on Enterococcus faecium protoplasts: indirect evidence supporting a novel mode of action on lipoteichoic acid synthesis. *J Antimicrob Chemother* **31**, 227-235.

[65] Canepari P, Boaretti M, Lleo MM, Satta G (1990) Lipoteichoic acid as a new target for activity of antibiotics: mode of action of daptomycin (LY146032). *Antimicrob Agents Chemother* **34**, 1220-1226.

[66] Laganas V, Alder J, Silverman JA (2003) In vitro bactericidal activities of daptomycin against Staphylococcus aureus and Enterococcus faecalis are not mediated by inhibition of lipoteichoic acid biosynthesis. *Antimicrob Agents Chemother* **47**, 2682-2684.

[67] Steenbergen JN, Alder J, Thorne GM, Tally FP (2005) Daptomycin: a lipopeptide antibiotic for the treatment of serious Gram-positive infections. *J Antimicrob Chemother* **55**, 283-288.

[68] Muraih JK, Pearson A, Silverman J, Palmer M (2011) Oligomerization of daptomycin on membranes. *Biochim Biophys Acta* **1808**, 1154-1160.

[69] Barry AL, Fuchs PC, Brown SD (2001) In vitro activities of daptomycin against 2,789 clinical isolates from 11 North American medical centers. *Antimicrob Agents Chemother* **45**, 1919-1922.

[70] Counter FT, Allen NE, Fukuda DS, Hobbs JN, Ott J, Ensminger PW, Mynderse JS, Preston DA, Wu CY (1990) A54145 a new lipopeptide antibiotic complex: microbiological evaluation. *J Antibiot (Tokyo)* **43**, 616-622.

[71] Eliopoulos GM, Thauvin C, Gerson B, Moellering RC, Jr. (1985) In vitro activity and mechanism of action of A21978C1, a novel cyclic lipopeptide antibiotic. *Antimicrob Agents Chemother* **27**, 357-362.

[72] Fuchs PC, Barry AL, Brown SD (2002) In vitro bactericidal activity of daptomycin against staphylococci. *J Antimicrob Chemother* **49**, 467-470.

[73] Cha R, Rybak MJ (2004) Influence of protein binding under controlled conditions on the bactericidal activity of daptomycin in an in vitro pharmacodynamic model. *J Antimicrob Chemother* **54**, 259-262.

[74] Snydman DR, Jacobus NV, McDermott LA, Lonks JR, Boyce JM (2000) Comparative In vitro activities of daptomycin and vancomycin against resistant gram-positive pathogens. *Antimicrob Agents Chemother* **44**, 3447-3450.

[75] Pereira JM, Teixeira-Pinto A, Basilio C, Sousa-Dias C, Mergulhao P, Paiva JA (2013) Can we predict pneumococcal bacteremia in patients with severe community-acquired pneumonia? *J Crit Care* **28**, 970-974.

[76] Goerke J (1998) Pulmonary surfactant: functions and molecular composition. *Biochim Biophys Acta* **1408**, 79-89.

[77] Vermehren C, Frokjaer S, Aurstad T, Hansen J (2006) Lung surfactant as a drug delivery system. *Int J Pharm* **307**, 89-92.

[78] White DC, Frerman FE (1967) Extraction, characterization, and cellular localization of the lipids of Staphylococcus aureus. *J Bacteriol* **94**, 1854-1867.

[79] Ariki S, Nishitani C, Kuroki Y (2012) Diverse functions of pulmonary collectins in host defense of the lung. *J Biomed Biotechnol* **2012**, 532071.

[80] Palaniyar N, Clark H, Nadesalingam J, Shih MJ, Hawgood S, Reid KB (2005) Innate immune collectin surfactant protein D enhances the clearance of DNA by macrophages and minimizes anti-DNA antibody generation. *J Immunol* **174**, 7352-7358.

[81] Jung D, Rozek A, Okon M, Hancock RE (2004) Structural transitions as determinants of the action of the calcium-dependent antibiotic daptomycin. *Chem Biol* **11**, 949-957.

[82] Taylor SD, Palmer M (2016) The action mechanism of daptomycin. *Bioorg Med Chem*.

[83] Micklefield J (2004) Daptomycin structure and mechanism of action revealed. *Chem Biol* **11**, 887-888.

[84] Ball L-J, Goult CM, Donarski JA, Micklefield J, Ramesh V (2004) NMR structure determination and calcium binding effects of lipopeptide antibiotic daptomycin. *Organic & Biomolecular Chemistry* **2**, 1872-1878.

[85] Debono M, Barnhart M, Carrell CB, Hoffmann JA, Occolowitz JL, Abbott BJ, Fukuda DS, Hamill RL, Biemann K, Herlihy WC (1987) A21978C, a complex of new acidic peptide antibiotics: isolation, chemistry, and mass spectral structure elucidation. *J Antibiot (Tokyo)* **40**, 761-777.

[86] Qiu J, Yu L, Kirsch LE (2011) Estimated pKa values for specific amino acid residues in daptomycin. *J Pharm Sci*.

[87] Fioroni M, Dworeck T, Rodriguez-Ropero F (2014) Biophysical characterization. *Adv Exp Med Biol* **794**, 41-67.

[88] Marion D (2013) An introduction to biological NMR spectroscopy. *Mol Cell Proteomics* **12**, 3006-3025.

[89] Simmler C, Napolitano JG, McAlpine JB, Chen SN, Pauli GF (2014) Universal quantitative NMR analysis of complex natural samples. *Curr Opin Biotechnol* **25**, 51-59.

[90] Harris RK, Hodgkinson P, Pickard CJ, Yates JR, Zorin V (2007) Chemical shift computations on a crystallographic basis: some reflections and comments. *Magn Reson Chem* **45 Suppl 1**, S174-186.

[91] Rotondi KS, Gierasch LM (2005) A well-defined amphipathic conformation for the calcium-free cyclic lipopeptide antibiotic, daptomycin, in aqueous solution. *Biopolymers* **80**, 374-385.

[92] Ho SW, Jung D, Calhoun JR, Lear JD, Okon M, Scott WR, Hancock RE, Straus SK (2008) Effect of divalent cations on the structure of the antibiotic daptomycin. *Eur Biophys J* **37**, 421-433.

[93] Scott WR, Baek SB, Jung D, Hancock RE, Straus SK (2007) NMR structural studies of the antibiotic lipopeptide daptomycin in DHPC micelles. *Biochim Biophys Acta* **1768**, 3116-3126.

[94] Qiu J, Kirsch LE (2014) Evaluation of lipopeptide (daptomycin) aggregation using fluorescence, light scattering, and nuclear magnetic resonance spectroscopy. *J Pharm Sci* **103**, 853-861.

[95] Bachmann L, Zezell DM, Ribeiro AdC, Gomes L, Ito AS (2006) Fluorescence Spectroscopy of Biological Tissues—A Review. *Applied Spectroscopy Reviews* **41**, 575-590.

[96] Alborn WE, Jr., Allen NE, Preston DA (1991) Daptomycin disrupts membrane potential in growing Staphylococcus aureus. *Antimicrob Agents Chemother* **35**, 2282-2287.

[97] Wu M, Hancock RE (1999) Interaction of the cyclic antimicrobial cationic peptide bactenecin with the outer and cytoplasmic membrane. *J Biol Chem* **274**, 29-35.

[98] Zhang T, Muraih JK, MacCormick B, Silverman J, Palmer M (2014) Daptomycin forms cation- and size-selective pores in model membranes. *Biochim Biophys Acta* **1838**, 2425-2430.

[99] Lakey JH, Maget-Dana R, Ptak M (1989) The lipopeptide antibiotic A21978C has a specific interaction with DMPC only in the presence of calcium ions. *Biochim Biophys Acta* **985**, 60-66.

[100] Lakey JH, Ptak M (1988) Fluorescence indicates a calcium-dependent interaction between the lipopeptide antibiotic LY146032 and phospholipid membranes. *Biochemistry* **27**, 4639-4645.

[101] Goni FM (2014) The basic structure and dynamics of cell membranes: an update of the Singer-Nicolson model. *Biochim Biophys Acta* **1838**, 1467-1476.

[102] Lichtenberg D, Ahyayauch H, Goni FM (2013) The mechanism of detergent solubilization of lipid bilayers. *Biophys J* **105**, 289-299.

[103] Jung D, Powers JP, Straus SK, Hancock RE (2008) Lipid-specific binding of the calcium-dependent antibiotic daptomycin leads to changes in lipid polymorphism of model membranes. *Chem Phys Lipids* **154**, 120-128.

[104] Muraih JK, Harris J, Taylor SD, Palmer M (2012) Characterization of daptomycin oligomerization with perylene excimer fluorescence: stoichiometric binding of phosphatidylglycerol triggers oligomer formation. *Biochim Biophys Acta* **1818**, 673-678.

[105] Zhang T, Muraih JK, Mintzer E, Tishbi N, Desert C, Silverman J, Taylor S, Palmer M (2013) Mutual inhibition through hybrid oligomer formation of daptomycin and the semisynthetic lipopeptide antibiotic CB-182,462. *Biochim Biophys Acta* **1828**, 302-308.

[106] Zhang T, Muraih JK, Tishbi N, Herskowitz J, Victor RL, Silverman J, Uwumarenogie S, Taylor SD, Palmer M, Mintzer E (2014) Cardiolipin prevents membrane translocation and permeabilization by daptomycin. *J Biol Chem* **289**, 11584-11591.

[107] Muraih JK, Palmer M (2012) Estimation of the subunit stoichiometry of the membrane-associated daptomycin oligomer by FRET. *Biochim Biophys Acta* **1818**, 1642-1647.

[108] Taylor R, Butt K, Scott B, Zhang T, Muraih JK, Mintzer E, Taylor S, Palmer M (2016) Two successive calcium-dependent transitions mediate membrane binding and oligomerization of daptomycin and the related antibiotic A54145. *Biochimica et Biophysica Acta (BBA) - Biomembranes* **1858**, 1999-2005.

[109] Pogliano J, Pogliano N, Silverman JA (2012) Daptomycin-mediated reorganization of membrane architecture causes mislocalization of essential cell division proteins. *J Bacteriol* **194**, 4494-4504.

[110] Chen YF, Sun TL, Sun Y, Huang HW (2014) Interaction of Daptomycin with Lipid Bilayers: A Lipid Extracting Effect. *Biochemistry*.

[111] Cotroneo N, Harris R, Perlmutter N, Beveridge T, Silverman JA (2008) Daptomycin exerts bactericidal activity without lysis of Staphylococcus aureus. *Antimicrob Agents Chemother* **52**, 2223-2225.

[112] Akins RL, Rybak MJ (2000) In vitro activities of daptomycin, arbekacin, vancomycin, and gentamicin alone and/or in combination against glycopeptide intermediate-resistant Staphylococcus aureus in an infection model. *Antimicrob Agents Chemother* **44**, 1925-1929.

[113] Sader HS, Streit JM, Fritsche TR, Jones RN (2004) Antimicrobial activity of daptomycin against multidrug-resistant Gram-positive strains collected worldwide. *Diagn Microbiol Infect Dis* **50**, 201-204.

[114] Sader HS, Watters AA, Fritsche TR, Jones RN (2007) Daptomycin antimicrobial activity tested against methicillin-resistant staphylococci and vancomycin-resistant enterococci isolated in European medical centers (2005). *BMC Infect Dis* **7**, 29.

[115] Gonzalez-Ruiz A, Beiras-Fernandez A, Lehmkuhl H, Seaton RA, Loeffler J, Chaves RL (2011) Clinical experience with daptomycin in Europe: the first 2.5 years. *J Antimicrob Chemother* **66**, 912-919.

[116] Wu G, Abraham T, Rapp J, Vastey F, Saad N, Balmir E (2011) Daptomycin: evaluation of a high-dose treatment strategy. *Int J Antimicrob Agents* **38**, 192-196.

[117] Cunha BA, Krol V, Kodali V (2008) Methicillin-resistant Staphylococcus aureus (MRSA) mitral valve acute bacterial endocarditis (ABE) in a patient with Job's

syndrome (hyperimmunoglobulin E syndrome) successfully treated with linezolid and high-dose daptomycin. *Heart Lung* **37**, 72-75.

[118] De Rosa FG, Mollaretti O, Cometto C, Pagani N, Montrucchio C, Di Perri G (2009) Early experience with high-dosage daptomycin for prosthetic infections. *Clin Infect Dis* **49**, 1772-1773.

[119] Lichterfeld M, Ferraro MJ, Davis BT (2010) High-dose daptomycin for the treatment of endocarditis caused by Staphylococcus aureus with intermediate susceptibility to glycopeptides. *Int J Antimicrob Agents* **35**, 96.

[120] Schutt AC, Bohm NM (2009) Multidrug-resistant Enterococcus faecium endocarditis treated with combination tigecycline and high-dose daptomycin. *Ann Pharmacother* **43**, 2108-2112.

[121] Yoshizumi A, Ishii Y, Iwata M, Murakami H, Yumoto S, Yasui K, Maehara C, Fukuzawa S, Enokizono K, Tateda K (2014) Daptomycin susceptibility of 833 strains of Gram-positive cocci from a university hospital in Japan (2009-2011). *Diagn Microbiol Infect Dis*.

[122] Sader HS, Farrell DJ, Flamm RK, Jones RN (2014) Daptomycin activity tested against 164457 bacterial isolates from hospitalised patients: summary of 8 years of a Worldwide Surveillance Programme (2005-2012). *Int J Antimicrob Agents* **43**, 465-469.

[123] Boucher HW, Sakoulas G (2007) Perspectives on Daptomycin resistance, with emphasis on resistance in Staphylococcus aureus. *Clin Infect Dis* **45**, 601-608.

[124] Hayden MK, Rezai K, Hayes RA, Lolans K, Quinn JP, Weinstein RA (2005) Development of Daptomycin resistance in vivo in methicillin-resistant Staphylococcus aureus. *J Clin Microbiol* **43**, 5285-5287.

[125] Mangili A, Bica I, Snydman DR, Hamer DH (2005) Daptomycin-resistant, methicillin-resistant Staphylococcus aureus bacteremia. *Clin Infect Dis* **40**, 1058-1060.

[126] Marty FM, Yeh WW, Wennersten CB, Venkataraman L, Albano E, Alyea EP, Gold HS, Baden LR, Pillai SK (2006) Emergence of a clinical daptomycin-resistant Staphylococcus aureus isolate during treatment of methicillin-resistant Staphylococcus aureus bacteremia and osteomyelitis. *J Clin Microbiol* **44**, 595-597.

[127] Skiest DJ (2006) Treatment failure resulting from resistance of Staphylococcus aureus to daptomycin. *J Clin Microbiol* **44**, 655-656.

[128] Montero CI, Stock F, Murray PR (2008) Mechanisms of resistance to daptomycin in Enterococcus faecium. *Antimicrob Agents Chemother* **52**, 1167-1170.

[129] Jones T, Yeaman MR, Sakoulas G, Yang SJ, Proctor RA, Sahl HG, Schrenzel J, Xiong YQ, Bayer AS (2008) Failures in clinical treatment of Staphylococcus aureus Infection with daptomycin are associated with alterations in surface charge, membrane phospholipid asymmetry, and drug binding. *Antimicrob Agents Chemother* **52**, 269-278.

[130] Friedman L, Alder JD, Silverman JA (2006) Genetic changes that correlate with reduced susceptibility to daptomycin in Staphylococcus aureus. *Antimicrob Agents Chemother* **50**, 2137-2145.

[131] Bertsche U, Weidenmaier C, Kuehner D, Yang SJ, Baur S, Wanner S, Francois P, Schrenzel J, Yeaman MR, Bayer AS (2011) Correlation of daptomycin resistance in a clinical Staphylococcus aureus strain with increased cell wall teichoic acid production and D-alanylation. *Antimicrob Agents Chemother* **55**, 3922-3928.

[132] Mishra NN, McKinnell J, Yeaman MR, Rubio A, Nast CC, Chen L, Kreiswirth BN, Bayer AS (2011) In vitro cross-resistance to daptomycin and host defense cationic antimicrobial peptides in clinical methicillin-resistant Staphylococcus aureus isolates. *Antimicrob Agents Chemother* **55**, 4012-4018.

[133] Mishra NN, Yang SJ, Chen L, Muller C, Saleh-Mghir A, Kuhn S, Peschel A, Yeaman MR, Nast CC, Kreiswirth BN, Cremieux AC, Bayer AS (2013) Emergence of daptomycin resistance in daptomycin-naive rabbits with methicillin-resistant Staphylococcus aureus prosthetic joint infection is associated with resistance to host defense cationic peptides and mprF polymorphisms. *PLoS One* **8**, e71151.

[134] Mishra NN, Yang SJ, Sawa A, Rubio A, Nast CC, Yeaman MR, Bayer AS (2009) Analysis of cell membrane characteristics of in vitro-selected daptomycin-resistant strains of methicillin-resistant Staphylococcus aureus. *Antimicrob Agents Chemother* **53**, 2312-2318.

[135] Patel D, Husain M, Vidaillac C, Steed ME, Rybak MJ, Seo SM, Kaatz GW (2011) Mechanisms of in-vitro-selected daptomycin-non-susceptibility in Staphylococcus aureus. *Int J Antimicrob Agents* **38**, 442-446.

[136] Yang SJ, Kreiswirth BN, Sakoulas G, Yeaman MR, Xiong YQ, Sawa A, Bayer AS (2009) Enhanced expression of dltABCD is associated with the development of daptomycin nonsusceptibility in a clinical endocarditis isolate of Staphylococcus aureus. *J Infect Dis* **200**, 1916-1920.

[137] Bayer AS, Schneider T, Sahl HG (2013) Mechanisms of daptomycin resistance in Staphylococcus aureus: role of the cell membrane and cell wall. *Ann N Y Acad Sci* **1277**, 139-158.

[138] Fischer A, Yang SJ, Bayer AS, Vaezzadeh AR, Herzig S, Stenz L, Girard M, Sakoulas G, Scherl A, Yeaman MR, Proctor RA, Schrenzel J, Francois P (2011) Daptomycin resistance mechanisms in clinically derived Staphylococcus aureus strains assessed by a combined transcriptomics and proteomics approach. *J Antimicrob Chemother* **66**, 1696-1711.

[139] D'Costa VM, Mukhtar TA, Patel T, Koteva K, Waglechner N, Hughes DW, Wright GD, De Pascale G (2012) Inactivation of the lipopeptide antibiotic daptomycin by hydrolytic mechanisms. *Antimicrob Agents Chemother* **56**, 757-764.

[140] Hachmann AB, Sevim E, Gaballa A, Popham DL, Antelmann H, Helmann JD (2011) Reduction in membrane phosphatidylglycerol content leads to daptomycin resistance in Bacillus subtilis. *Antimicrob Agents Chemother* **55**, 4326-4337.

[141] Tran TT, Panesso D, Mishra NN, Mileykovskaya E, Guan Z, Munita JM, Reyes J, Diaz L, Weinstock GM, Murray BE, Shamoo Y, Dowhan W, Bayer AS, Arias CA (2013) Daptomycin-resistant Enterococcus faecalis diverts the antibiotic molecule from the division septum and remodels cell membrane phospholipids. *MBio* **4**.

[142] Kelley WL, Lew DP, Renzoni A (2012) Antimicrobial peptide exposure and reduced susceptibility to daptomycin: insights into a complex genetic puzzle. *J Infect Dis* **206**, 1153-1156.

[143] Credito K, Lin G, Appelbaum PC (2007) Activity of daptomycin alone and in combination with rifampin and gentamicin against Staphylococcus aureus assessed by time-kill methodology. *Antimicrob Agents Chemother* **51**, 1504-1507.

[144] Anastasiou DM, Thorne GM, Luperchio SA, Alder JD (2006) In vitro activity of daptomycin against clinical isolates with reduced susceptibilities to linezolid and quinupristin/dalfopristin. *Int J Antimicrob Agents* **28**, 385-388.

[145] Cilli F, Aydemir S, Tunger A (2006) In vitro activity of daptomycin alone and in combination with various antimicrobials against Gram-positive cocci. *J Chemother* **18**, 27-32.

[146] Debbia E, Pesce A, Schito GC (1988) In vitro activity of LY146032 alone and in combination with other antibiotics against gram-positive bacteria. *Antimicrob Agents Chemother* **32**, 279-281.

[147] John AK, Baldoni D, Haschke M, Rentsch K, Schaerli P, Zimmerli W, Trampuz A (2009) Efficacy of daptomycin in implant-associated infection due to methicillin-resistant Staphylococcus aureus: importance of combination with rifampin. *Antimicrob Agents Chemother* **53**, 2719-2724.

[148] Kuli B, de Barbeyrac B, Dauchy FA, Dutronc H, Bebear C, Megraud F, Dupon M (2009) In vitro activities of daptomycin, tigecycline, linezolid and eight other antibiotics, alone and in combination, against 41 Staphylococcus spp. clinical isolates from bone and joint infections. *Int J Antimicrob Agents* **33**, 491-493.

[149] LaPlante KL, Rybak MJ (2004) Impact of high-inoculum Staphylococcus aureus on the activities of nafcillin, vancomycin, linezolid, and daptomycin, alone and in combination with gentamicin, in an in vitro pharmacodynamic model. *Antimicrob Agents Chemother* **48**, 4665-4672.

[150] Mandell GL, Moorman DR (1980) Treatment of experimental staphylococcal infections: effect of rifampin alone and in combination on development of rifampin resistance. *Antimicrob Agents Chemother* **17**, 658-662.

[151] Miro JM, Garcia-de-la-Maria C, Armero Y, Soy D, Moreno A, del Rio A, Almela M, Sarasa M, Mestres CA, Gatell JM, Jimenez de Anta MT, Marco F (2009) Addition of gentamicin or rifampin does not enhance the effectiveness of daptomycin in treatment of experimental endocarditis due to methicillin-resistant Staphylococcus aureus. *Antimicrob Agents Chemother* **53**, 4172-4177.

[152] Pankey G, Ashcraft D, Patel N (2005) In vitro synergy of daptomycin plus rifampin against Enterococcus faecium resistant to both linezolid and vancomycin. *Antimicrob Agents Chemother* **49**, 5166-5168.

[153] Rand KH, Houck H (2004) Daptomycin synergy with rifampicin and ampicillin against vancomycin-resistant enterococci. *J Antimicrob Chemother* **53**, 530-532.

[154] Rand KH, Houck HJ (2004) Synergy of daptomycin with oxacillin and other beta-lactams against methicillin-resistant Staphylococcus aureus. *Antimicrob Agents Chemother* **48**, 2871-2875.

[155] Snydman DR, McDermott LA, Jacobus NV (2005) Evaluation of in vitro interaction of daptomycin with gentamicin or beta-lactam antibiotics against Staphylococcus aureus and Enterococci by FIC index and timed-kill curves. *J Chemother* **17**, 614-621.

[156] Tsuji BT, Rybak MJ (2005) Short-course gentamicin in combination with daptomycin or vancomycin against Staphylococcus aureus in an in vitro pharmacodynamic model with simulated endocardial vegetations. *Antimicrob Agents Chemother* **49**, 2735-2745.

[157] Tsuji BT, Rybak MJ (2006) Etest synergy testing of clinical isolates of Staphylococcus aureus demonstrating heterogeneous resistance to vancomycin. *Diagn Microbiol Infect Dis* **54**, 73-77.

[158] Ahmad NM, Rojtman AD (2010) Successful treatment of daptomycin-nonsusceptible methicillin-resistant Staphylococcus aureus bacteremia with the addition of rifampin to daptomycin. *Ann Pharmacother* **44**, 918-921.

[159] Gould IM, Miro JM, Rybak MJ (2013) Daptomycin: the role of high-dose and combination therapy for Gram-positive infections. *Int J Antimicrob Agents* **42**, 202-210.

[160] Kelesidis T, Humphries R, Ward K, Lewinski MA, Yang OO (2011) Combination therapy with daptomycin, linezolid, and rifampin as treatment option for MRSA meningitis and bacteremia. *Diagn Microbiol Infect Dis* **71**, 286-290.

[161] Sakoulas G, Moise PA, Casapao AM, Nonejuie P, Olson J, Okumura CY, Rybak MJ, Kullar R, Dhand A, Rose WE, Goff DA, Bressler AM, Lee Y, Pogliano J, Johns S, Kaatz GW, Ebright JR, Nizet V (2014) Antimicrobial Salvage Therapy for Persistent Staphylococcal Bacteremia Using Daptomycin Plus Ceftaroline. *Clin Ther*.

[162] Le J, Bookstaver PB, Rudisill CN, Hashem MG, Iqbal R, James CL, Sakoulas G (2010) Treatment of meningitis caused by vancomycin-resistant Enterococcus faecium: high-dose and combination daptomycin therapy. *Ann Pharmacother* **44**, 2001-2006.

[163] Porter KB, Lynch B, Mani CS (2010) The Use of Daptomycin and Linezolid to Treat Vancomycin-Intermediate Staphylococcus haemolyticus Infection in a Premature Infant. *J Pediatr Pharmacol Ther* **15**, 297-300.

[164] Chen LY, Huang CH, Kuo SC, Hsiao CY, Lin ML, Wang FD, Fung CP (2011) High-dose daptomycin and fosfomycin treatment of a patient with endocarditis caused by daptomycin-nonsusceptible Staphylococcus aureus: case report. *BMC Infect Dis* **11**, 152.

[165] Rose WE, Schulz LT, Andes D, Striker R, Berti AD, Hutson PR, Shukla SK (2012) Addition of ceftaroline to daptomycin after emergence of daptomycin-nonsusceptible Staphylococcus aureus during therapy improves antibacterial activity. *Antimicrob Agents Chemother* **56**, 5296-5302.

[166] Jugun K, Vaudaux P, Garbino J, Pagani L, Hoffmeyer P, Lew D, Uckay I (2013) The safety and efficacy of high-dose daptomycin combined with rifampicin for the treatment of Gram-positive osteoarticular infections. *Int Orthop* **37**, 1375-1380.

[167] Berti AD, Sakoulas G, Nizet V, Tewhey R, Rose WE (2013) beta-Lactam antibiotics targeting PBP1 selectively enhance daptomycin activity against methicillin-resistant Staphylococcus aureus. *Antimicrob Agents Chemother* **57**, 5005-5012.

[168] Zheng K, Setyawati MI, Lim TP, Leong DT, Xie J (2016) Antimicrobial Cluster Bombs: Silver Nanoclusters Packed with Daptomycin. *ACS Nano* **10**, 7934-7942.

[169] Dakal TC, Kumar A, Majumdar RS, Yadav V (2016) Mechanistic Basis of Antimicrobial Actions of Silver Nanoparticles. *Front Microbiol* **7**, 1831.

[170] Steenbergen JN, Mohr JF, Thorne GM (2009) Effects of daptomycin in combination with other antimicrobial agents: a review of in vitro and animal model studies. *J Antimicrob Chemother* **64**, 1130-1138.

[171] Nguyen KT, Ritz D, Gu JQ, Alexander D, Chu M, Miao V, Brian P, Baltz RH (2006) Combinatorial biosynthesis of novel antibiotics related to daptomycin. *Proc Natl Acad Sci U S A* **103**, 17462-17467.

[172] Alexander DC, Rock J, Gu JQ, Mascio C, Chu M, Brian P, Baltz RH (2011) Production of novel lipopeptide antibiotics related to A54145 by Streptomyces fradiae mutants blocked in biosynthesis of modified amino acids and assignment of lptJ, lptK and lptL gene functions. *J Antibiot (Tokyo)* **64**, 79-87.

[173] Nguyen KT, He X, Alexander DC, Li C, Gu JQ, Mascio C, Van Praagh A, Mortin L, Chu M, Silverman JA, Brian P, Baltz RH (2010) Genetically engineered lipopeptide antibiotics related to A54145 and daptomycin with improved properties. *Antimicrob Agents Chemother* **54**, 1404-1413.

[174] Zhang T, Taylor SD, Palmer M, Duhamel J (2016) Membrane Binding and Oligomerization of the Lipopeptide A54145 Studied by Pyrene Fluorescence. *Biophys J* **111**, 1267-1277.

[175] Chan Y-HM, Boxer SG (2007) Model Membrane Systems and Their Applications. *Current opinion in chemical biology* **11**, 581-587.

[176] Brezesinski G, Möhwald H (2003) Langmuir monolayers to study interactions at model membrane surfaces. *Advances in Colloid and Interface Science* **100–102**, 563-584.

[177] Sonnino S, Prinetti A (2013) Membrane Domains and the Lipid Raft Concept. *Current Medicinal Chemistry* **20**, 4-21.

[178] Nicolson GL (2014) The Fluid—Mosaic Model of Membrane Structure: Still relevant to understanding the structure, function and dynamics of biological membranes after more than 40 years. *Biochimica et Biophysica Acta (BBA) - Biomembranes* **1838**, 1451-1466.

[179] Quinn PJ, Wolf C (2009) The liquid-ordered phase in membranes. *Biochimica et Biophysica Acta (BBA) - Biomembranes* **1788**, 33-46.

[180] Quinn PJ (2012) Lipid–lipid interactions in bilayer membranes: Married couples and casual liaisons. *Progress in Lipid Research* **51**, 179-198.

[181] Simons K, Sampaio JL (2011) Membrane organization and lipid rafts. *Cold Spring Harb Perspect Biol* **3**, a004697.

[182] Mouritsen OG (2011) Model Answers to Lipid Membrane Questions. *Cold Spring Harbor Perspectives in Biology* **3**, a004622.

[183] Aittoniemi J, Niemelä PS, Hyvönen MT, Karttunen M, Vattulainen I (2007) Insight into the Putative Specific Interactions between Cholesterol, Sphingomyelin, and Palmitoyl-Oleoyl Phosphatidylcholine. *Biophysical Journal* **92**, 1125-1137.

[184] Ohvo-Rekilä H, Ramstedt B, Leppimäki P, Peter Slotte J (2002) Cholesterol interactions with phospholipids in membranes. *Progress in Lipid Research* **41**, 66-97.

[185] van Meer G, Voelker DR, Feigenson GW (2008) Membrane lipids: where they are and how they behave. *Nat Rev Mol Cell Biol* **9**, 112-124.

[186] Simons K, Vaz WLC (2004) Model Systems, Lipid Rafts, and Cell Membranes. *Annual Review of Biophysics and Biomolecular Structure* **33**, 269-295.

[187] Edidin M (2003) The State of Lipid Rafts: From Model Membranes to Cells. *Annual Review of Biophysics and Biomolecular Structure* **32**, 257-283.

[188] Lingwood D, Simons K (2009) Lipid Rafts As a Membrane-Organizing Principle. *Science* **327**, 46.

[189] Jacobson K, Mouritsen OG, Anderson RGW (2007) Lipid rafts: at a crossroad between cell biology and physics. *Nat Cell Biol* **9**, 7-14.

[190] Simons K, Sampaio JL (2011) Membrane Organization and Lipid Rafts. *Cold Spring Harbor Perspectives in Biology* **3**, a004697.

[191] Musher DM, Thorner AR (2014) Community-Acquired Pneumonia. *New England Journal of Medicine* **371**, 1619-1628.

[192] Humann J, LeMessurier K, Tuomanen E (2013) Streptococcus pneumoniae: The Prototype of Lung Responses in Pneumonia In *Mucosal Immunology of Acute Bacterial Pneumonia*, Prince A, ed. Springer New York, New York, NY, pp. 213-238.

[193] Sethi S (2016) *Respiratory Infections*, CRC Press.

[194] José RJ, Periselneris JN, Brown JS (2015) Community-acquired pneumonia. *Current Opinion in Pulmonary Medicine* **21**, 212-218.

[195] Niederman MS (2015) Community-acquired pneumonia. *Annals of Internal Medicine* **163**, ITC1.

[196] Falguera M, Ramírez MF (2015) Community-acquired pneumonia. *Revista Clínica Española (English Edition)*.

[197] Bartlett JG, Mundy LM (1995) Community-Acquired Pneumonia. *New England Journal of Medicine* **333**, 1618-1624.

[198] File Jr TM (2003) Community-acquired pneumonia. *The Lancet* **362**, 1991-2001.

[199] Ryan KJ, Ray CG (2003) *Sherris Medical Microbiology*, Mcgraw-hill.

[200] Siemieniuk RA, Gregson DB, Gill MJ (2011) The persisting burden of invasive pneumococcal disease in HIV patients: an observational cohort study. *BMC Infect Dis* **11**, 314.

[201] Bogaert D, de Groot R, Hermans PWM (2004) Streptococcus pneumoniae colonisation: the key to pneumococcal disease. *The Lancet Infectious Diseases* **4**, 144-154.

[202] Sternberg GM (1881) *A Fatal Form of Septicaemia in the Rabbit Produced by the Subcutaneous Injection of Human Saliva: An Experimental Research*, John Murphy & Company.

[203] Plotkin SA, Orenstein W, Offit PA (2012) *Vaccines*, Elsevier Health Sciences.

[204] Winslow CEA, Broadhurst J, Buchanan RE, Krumwiede C, Rogers LA, Smith GH (1920) The Families and Genera of the Bacteria: Final Report of the Committee of the Society of American Bacteriologists on Characterization and Classification of Bacterial Types. *Journal of Bacteriology* **5**, 191-229.

[205] Wainer H (2013) *Medical Illuminations: Using Evidence, Visualization and Statistical Thinking to Improve Healthcare*, OUP Oxford.

[206] Barthelson R, Mobasseri A, Zopf D, Simon P (1998) Adherence of Streptococcus pneumoniae to respiratory epithelial cells is inhibited by sialylated oligosaccharides. *Infect Immun* **66**, 1439-1444.

[207] Feldman C, Read R, Rutman A, Jeffery PK, Brain A, Lund V, Mitchell TJ, Andrew PW, Boulnois GJ, Todd HC, et a (1992) The interaction of Streptococcus pneumoniae with intact human respiratory mucosa in vitro. *European Respiratory Journal* **5**, 576.

[208] Price KE, Camilli A (2009) Pneumolysin Localizes to the Cell Wall of Streptococcus pneumoniae. *Journal of Bacteriology* **191**, 2163-2168.

[209] Kadioglu A, Weiser JN, Paton JC, Andrew PW (2008) The role of Streptococcus pneumoniae virulence factors in host respiratory colonization and disease. *Nat Rev Micro* **6**, 288-301.

[210] Hirst RA, Kadioglu A, O'Callaghan C, Andrew PW (2004) The role of pneumolysin in pneumococcal pneumonia and meningitis. *Clinical and Experimental Immunology* **138**, 195-201.

[211] Talbot UM, Paton AW, Paton JC (1996) Uptake of Streptococcus pneumoniae by respiratory epithelial cells. *Infect Immun* **64**, 3772-3777.

[212] Martner A, Dahlgren C, Paton JC, Wold AE (2008) Pneumolysin released during Streptococcus pneumoniae autolysis is a potent activator of intracellular oxygen radical production in neutrophils. *Infect Immun* **76**, 4079-4087.

[213] Brown S, Santa Maria JP, Walker S (2013) Wall Teichoic Acids of Gram-Positive Bacteria. *Annual review of microbiology* **67**, 10.1146/annurev-micro-092412-155620.

[214] Reichmann NT, Gründling A (2011) Location, synthesis and function of glycolipids and polyglycerolphosphate lipoteichoic acid in Gram-positive bacteria of the phylum Firmicutes. *Fems Microbiology Letters* **319**, 97-105.

[215] Brown L, Wolf JM, Prados-Rosales R, Casadevall A (2015) Through the wall: extracellular vesicles in Gram-positive bacteria, mycobacteria and fungi. *Nat Rev Micro* **13**, 620-630.

[216] Tang YW, Sussman M, Liu D, Poxton I, Schwartzman J (2014) *Molecular Medical Microbiology*, Elsevier Science.

[217] Strelkauskas A, Strelkauskas J, Moszyk-Strelkauskas D (2009) *Microbiology: A Clinical Approach*, Taylor & Francis Group.

[218] Wilson M, McNab R, Henderson B (2002) *Bacterial Disease Mechanisms: An Introduction to Cellular Microbiology*, Cambridge University Press.

[219] Wheelis M, Wheelis UCDM (2011) *Principles of Modern Microbiology*, Jones & Bartlett Learning, LLC.

[220] Shagam J (2006) *Introduction to Microbiology*, Pearson Education, Limited.

[221] Malanovic N, Lohner K (2016) Gram-positive bacterial cell envelopes: The impact on the activity of antimicrobial peptides. *Biochimica et Biophysica Acta (BBA) - Biomembranes* **1858**, 936-946.

[222] Silhavy TJ, Kahne D, Walker S (2010) The Bacterial Cell Envelope. *Cold Spring Harbor Perspectives in Biology* **2**, a000414.

[223] Khan MS, Dosoky NS, Williams JD (2013) Engineering Lipid Bilayer Membranes for Protein Studies. *International Journal of Molecular Sciences* **14**, 21561-21597.

[224] Trombe M-C, Lanéelle M-A, Lanéelle G (1979) Lipid composition of aminopterin-resistant and sensitive strains of Streptococcus pneumoniae. Effect of aminopterin inhibition. *Biochimica et Biophysica Acta (BBA) - Lipids and Lipid Metabolism* **574**, 290-300.

[225] Pesakhov S, Benisty R, Sikron N, Cohen Z, Gomelsky P, Khozin-Goldberg I, Dagan R, Porat N (2007) Effect of hydrogen peroxide production and the Fenton reaction on membrane composition of Streptococcus pneumoniae. *Biochimica et Biophysica Acta (BBA) - Biomembranes* **1768**, 590-597.

[226] Epand RF, Savage PB, Epand RM (2007) Bacterial lipid composition and the antimicrobial efficacy of cationic steroid compounds (Ceragenins). *Biochimica et Biophysica Acta (BBA) - Biomembranes* **1768**, 2500-2509.

[227] Epand RM, Epand RF (2009) Lipid domains in bacterial membranes and the action of antimicrobial agents. *Biochimica et Biophysica Acta (BBA) - Biomembranes* **1788**, 289-294.

[228] Murzyn K, Róg T, Pasenkiewicz-Gierula M (2005) Phosphatidylethanolamine-Phosphatidylglycerol Bilayer as a Model of the Inner Bacterial Membrane. *Biophysical Journal* **88**, 1091-1103.

[229] Olofsson G, Sparr E (2013) Ionization Constants pKa of Cardiolipin. *PLOS ONE* **8**, e73040.

[230] Forbes LR, Haczku A (2010) SP-D and regulation of the pulmonary innate immune system in allergic airway changes. *Clin Exp Allergy* **40**, 547-562.

[231] Walters RW, Jenq RR, Hall SB (2000) Distinct steps in the adsorption of pulmonary surfactant to an air-liquid interface. *Biophys J* **78**, 257-266.

[232] Crouch EC (1998) Collectins and pulmonary host defense. *Am J Respir Cell Mol Biol* **19**, 177-201.

[233] Nkadi PO, Merritt TA, Pillers DA (2009) An overview of pulmonary surfactant in the neonate: genetics, metabolism, and the role of surfactant in health and disease. *Mol Genet Metab* **97**, 95-101.

[234] Cockshutt AM, Weitz J, Possmayer F (1990) Pulmonary surfactant-associated protein A enhances the surface activity of lipid extract surfactant and reverses inhibition by blood proteins in vitro. *Biochemistry* **29**, 8424-8429.

[235] Wright JR (2005) Immunoregulatory functions of surfactant proteins. *Nat Rev Immunol* **5**, 58-68.

[236] Nayak A, Dodagatta-Marri E, Tsolaki AG, Kishore U (2012) An Insight into the Diverse Roles of Surfactant Proteins, SP-A and SP-D in Innate and Adaptive Immunity. *Front Immunol* **3**, 131.

[237] Crouch E, Hartshorn K, Ofek I (2000) Collectins and pulmonary innate immunity. *Immunol Rev* **173**, 52-65.

[238] Haslett C (1999) Granulocyte apoptosis and its role in the resolution and control of lung inflammation. *Am J Respir Crit Care Med* **160**, S5-11.

[239] Savill JS, Wyllie AH, Henson JE, Walport MJ, Henson PM, Haslett C (1989) Macrophage phagocytosis of aging neutrophils in inflammation. Programmed cell death in the neutrophil leads to its recognition by macrophages. *J Clin Invest* **83**, 865-875.

[240] Dransfield I, Buckle AM, Savill JS, McDowall A, Haslett C, Hogg N (1994) Neutrophil apoptosis is associated with a reduction in CD16 (Fc gamma RIII) expression. *J Immunol* **153**, 1254-1263.

[241] Schicht M, Knipping S, Hirt R, Beileke S, Sel S, Paulsen F, Brauer L (2013) Detection of surfactant proteins A, B, C, and D in human nasal mucosa and their regulation in chronic rhinosinusitis with polyps. *Am J Rhinol Allergy* **27**, 24-29.

[242] Hawgood S, Derrick M, Poulain F (1998) Structure and properties of surfactant protein B. *Biochim Biophys Acta* **1408**, 150-160.

[243] Weaver TE, Conkright JJ (2001) Function of surfactant proteins B and C. *Annu Rev Physiol* **63**, 555-578.

[244] Wert SE, Whitsett JA, Nogee LM (2009) Genetic disorders of surfactant dysfunction. *Pediatr Dev Pathol* **12**, 253-274.

[245] Glasser SW, Senft AP (2011) Use of transgenic mouse models to understand the origins of familial pulmonary fibrosis. *Curr Pharm Biotechnol* **12**, 1447-1454.

[246] Whitsett JA, Weaver TE (2002) Hydrophobic surfactant proteins in lung function and disease. *N Engl J Med* **347**, 2141-2148.

[247] Ding J, Takamoto DY, von Nahmen A, Lipp MM, Lee KY, Waring AJ, Zasadzinski JA (2001) Effects of lung surfactant proteins, SP-B and SP-C, and palmitic acid on monolayer stability. *Biophys J* **80**, 2262-2272.

[248] Wang L, Cai P, Galla H-J, He H, Flach CR, Mendelsohn R (2005) Monolayer–multilayer transitions in a lung surfactant model: IR reflection–absorption spectroscopy and atomic force microscopy. *European Biophysics Journal* **34**, 243-254.

[249] Selladurai SL, Miclette Lamarche R, Schmidt R, DeWolf CE (2016) Model Lung Surfactant Films: Why Composition Matters. *Langmuir*.

[250] Hane F, Moores B, Amrein M, Leonenko Z (2009) Effect of SP-C on surface potential distribution in pulmonary surfactant: Atomic force microscopy and Kelvin probe force microscopy study. *Ultramicroscopy* **109**, 968-973.

[251] Zhang H, Wang YE, Fan Q, Zuo YY (2011) On the low surface tension of lung surfactant. *Langmuir* **27**, 8351-8358.

[252] Veldhuizen R, Milos S, Ruehlicke J, Yamashita C (2016) The Effect of Cholesterol on the Biophysical Inhibition of Pulmonary Surfactant by Albumin. *The FASEB Journal* **30**, 1297.1292-1297.1292.

[253] Gómez-Gil L, Pérez-Gil J, Goormaghtigh E (2009) Cholesterol modulates the exposure and orientation of pulmonary surfactant protein SP-C in model surfactant membranes. *Biochimica et Biophysica Acta (BBA) - Biomembranes* **1788**, 1907-1915.

[254] Notter RH (2000) *Lung Surfactants: Basic Science and Clinical Applications*, Taylor & Francis.

[255] Vockeroth D, Gunasekara L, Amrein M, Possmayer F, Lewis JF, Veldhuizen RAW (2009) Role of cholesterol in the biophysical dysfunction of surfactant in ventilator-induced lung injury. *American Journal of Physiology - Lung Cellular and Molecular Physiology* **298**, L117.

[256] Leonenko Z, Gill S, Baoukina S, Monticelli L, Doehner J, Gunasekara L, Felderer F, Rodenstein M, Eng LM, Amrein M (2007) An elevated level of cholesterol impairs self-assembly of pulmonary surfactant into a functional film. *Biophys J* **93**, 674-683.

[257] Gunasekara L, Schurch S, Schoel WM, Nag K, Leonenko Z, Haufs M, Amrein M (2005) Pulmonary surfactant function is abolished by an elevated proportion of cholesterol. *Biochim Biophys Acta* **1737**, 27-35.

[258] Hane F, Drolle E, Leonenko Z (2010) Effect of cholesterol and amyloid-beta peptide on structure and function of mixed-lipid films and pulmonary surfactant BLES: an atomic force microscopy study. *Nanomedicine* **6**, 808-814.

[259] Sachdeva A, Dutta A (2012) *Advances in Pediatrics*, Jaypee Brothers,Medical Publishers Pvt. Limited.

[260] Lam BC, Ng YK, Wong KY (2005) Randomized trial comparing two natural surfactants (Survanta vs. bLES) for treatment of neonatal respiratory distress syndrome. *Pediatr Pulmonol* **39**, 64-69.

[261] Zuo YY, Veldhuizen RAW, Neumann AW, Petersen NO, Possmayer F (2008) Current perspectives in pulmonary surfactant — Inhibition, enhancement and evaluation. *Biochimica et Biophysica Acta (BBA) - Biomembranes* **1778**, 1947-1977.

[262] BLES Biochemicals Inc, BLES (Bovine Lipid Extract Surfactant), http://blesbiochem.com/, Accessed December 12, 2016.

[263] Zhang H, Fan Q, Wang YE, Neal CR, Zuo YY (2011) Comparative study of clinical pulmonary surfactants using atomic force microscopy. *Biochimica et biophysica acta* **1808**, 1832-1842.

[264] Yu S, Harding PG, Smith N, Possmayer F (1983) Bovine pulmonary surfactant: chemical composition and physical properties. *Lipids* **18**, 522-529.

[265] Gray GM, Yardley HJ (1975) Lipid compositions of cells isolated from pig, human, and rat epidermis. *Journal of Lipid Research* **16**, 434-440.

[266] Spector AA, Yorek MA (1985) Membrane lipid composition and cellular function. *Journal of Lipid Research* **26**, 1015-1035.

[267] Christie WW (1985) Rapid separation and quantification of lipid classes by high performance liquid chromatography and mass (light-scattering) detection. *Journal of Lipid Research* **26**, 507-512.

[268] Virtanen JA, Cheng KH, Somerharju P (1998) Phospholipid composition of the mammalian red cell membrane can be rationalized by a superlattice model. *Proceedings of the National Academy of Sciences of the United States of America* **95**, 4964-4969.

[269] De Gier J, Mandersloot JG, Van Deenen LLM (1968) Lipid composition and permeability of liposomes. *Biochimica et Biophysica Acta (BBA) - Biomembranes* **150**, 666-675.

[270] Garnier M, Attali JR, Valensi P, Delatour-Hanss E, Gaudey F, Koutsouris D (1990) Erythrocyte deformability in diabetes and erythrocyte membrane lipid composition. *Metabolism* **39**, 794-798.

[271] Marcus AJ, Ullman HL, Safier LB (1969) Lipid composition of subcellular particles of human blood platelets. *Journal of Lipid Research* **10**, 108-114.

[272] McLaughlin J, Engel W (1979) Lipid composition of erythrocytes: Findings in duchenne's muscular dystrophy and myotonic atrophy. *Archives of Neurology* **36**, 351-354.

[273] Nelson GJ (1967) Lipid composition of erythrocytes in various mammalian species. *Biochimica et Biophysica Acta (BBA) - Lipids and Lipid Metabolism* **144**, 221-232.

[274] Nelson GJ (1967) Composition of neutral lipids from erythrocytes of common mammals. *Journal of Lipid Research* **8**, 374-379.

[275] Owen JS, Bruckdorfer KR, Day RC, McIntyre N (1982) Decreased erythrocyte membrane fluidity and altered lipid composition in human liver disease. *Journal of Lipid Research* **23**, 124-132.

[276] Albani JR (2008) *Principles and Applications of Fluorescence Spectroscopy*, Wiley.

[277] Lakowicz JR (2013) *Principles of Fluorescence Spectroscopy*, Springer US.

[278] Weiss S (1999) Fluorescence Spectroscopy of Single Biomolecules. *Science* **283**, 1676.

[279] Franklin B, Brownrigg W, Farish M (1774) Of the Stilling of Waves by means of Oil. Extracted from Sundry Letters between Benjamin Franklin, LL. D. F. R. S. William Brownrigg, M. D. F. R. S. and the Reverend Mr. Farish. *Philosophical Transactions* **64**, 445-460.

[280] Tanford C (2004) *Ben Franklin Stilled the Waves:An Informal History of Pouring Oil on Water with Reflections on the Ups and Downs of Scientific Life in General: An Informal History of Pouring Oil on Water with Reflections on the Ups and Downs of Scientific Life in General*, OUP Oxford.

[281] Rayleigh L (1889) Measurements of the Amount of Oil Necessary in Order to Check the Motions of Camphor upon Water. *Proceedings of the Royal Society of London* **47**, 364-367.

[282] Wang D-N, Stieglitz H, Marden J, Tamm Lukas K (2013) Benjamin Franklin, Philadelphia's Favorite Son, was a Membrane Biophysicist. *Biophysical Journal* **104**, 287-291.

[283] Langmuir I (1917) THE CONSTITUTION AND FUNDAMENTAL PROPERTIES OF SOLIDS AND LIQUIDS. II. LIQUIDS.1. *Journal of the American Chemical Society* **39**, 1848-1906.

[284] Langmuir I (1917) The Shapes of Group Molecules Forming the Surfaces of Liquids. *Proc Natl Acad Sci U S A* **3**, 251-257.

[285] Roberts G (2013) *Langmuir-Blodgett Films*, Springer US.

[286] Blodgett KB (1940) Gen Electric.

[287] Petty MC (1996) *Langmuir-Blodgett Films: An Introduction*, Cambridge University Press.

[288] Ah-Fat NMW, Craig DQM, Taylor KMG (1994) An investigation into the effects of surfactants on phospholipid monolayers using a Langmuir-Blodgett film balance. *International Journal of Pharmaceutics* **107**, 239-242.

[289] Martin P, Szablewski M (2004) *Langmuir-Blodgett Troughs Operating Manual*, Nima Technology Ltd.

[290] Choi Y, Attwood SJ, Hoopes MI, Drolle E, Karttunen M, Leonenko Z (2014) Melatonin directly interacts with cholesterol and alleviates cholesterol effects in dipalmitoylphosphatidylcholine monolayers. *Soft Matter* **10**, 206-213.

[291] Ishitsuka Y, Pham DS, Waring AJ, Lehrer RI, Lee KYC (2006) Insertion selectivity of antimicrobial peptide protegrin-1 into lipid monolayers: Effect of head group electrostatics and tail group packing. *Biochimica et Biophysica Acta (BBA) - Biomembranes* **1758**, 1450-1460.

[292] Hanakam F, Gerisch G, Lotz S, Alt T, Seelig A (1996) Binding of hisactophilin I and II to lipid membranes is controlled by a pH-dependent myristoyl-histidine switch. *Biochemistry* **35**, 11036-11044.

[293] Ege C, Lee KYC (2004) Insertion of Alzheimer's Aβ40 Peptide into Lipid Monolayers. *Biophysical Journal* **87**, 1732-1740.

[294] Maskarinec SA, Lee KYC (2003) Comparative Study of Poloxamer Insertion into Lipid Monolayers. *Langmuir* **19**, 1809-1815.

[295] Choi Y (2014) Nanoscale Characterization of Melatonin and Amyloid Beta in Model Membranes- in Relation to Alzheimer's Disease. *PhD Thesis, University of Waterloo, Ontario, Canada.*

[296] Claesson PM, Blom CE, Herder PC, Ninham BW (1986) Interactions between water—stable hydrophobic Langmuir—Blodgett monolayers on mica. *Journal of Colloid and Interface Science* **114**, 234-242.

[297] Kessel CR, Granick S (1991) Formation and characterization of a highly ordered and well-anchored alkylsilane monolayer on mica by self-assembly. *Langmuir* **7**, 532-538.

[298] Liu Y, Wu T, Evans DF (1994) Lateral Force Microscopy Study on the Shear Properties of Self-Assembled Monolayers of Dialkylammonium Surfactant on Mica. *Langmuir* **10**, 2241-2245.

[299] Bhushan B (2004) *Springer Handbook of Nanotechnology*, Springer Berlin Heidelberg.

[300] Kiss E, Gölander CG (1990) Chemical derivatization of muscovite mica surfaces. *Colloids and Surfaces* **49**, 335-342.

[301] Sides PJ, Faruqui D, Gellman AJ (2009) Dynamics of Charging of Muscovite Mica: Measurement and Modeling. *Langmuir* **25**, 1475-1481.

[302] Yang H, Fung S-Y, Pritzker M, Chen P (2007) Modification of Hydrophilic and Hydrophobic Surfaces Using an Ionic-Complementary Peptide. *PLoS ONE* **2**, e1325.

[303] Binnig G, Quate CF, Gerber C (1986) Atomic Force Microscope. *Physical Review Letters* **56**, 930-933.

[304] Radmacher M, Tillamnn RW, Fritz M, Gaub HE (1992) From molecules to cells: imaging soft samples with the atomic force microscope. *Science* **257**, 1900.

[305] JPK Instruments (2012) The NanoWizard AFM Handbook, Version 2.2a.

[306] Hansma HG, Hoh JH (1994) Biomolecular Imaging with the Atomic Force Microscope. *Annual Review of Biophysics and Biomolecular Structure* **23**, 115-140.

[307] Li A, Ho B, Ding JL, Lim CT (2010) Use of atomic force microscopy as a tool to understand the action of antimicrobial peptides on bacteria. *Methods Mol Biol* **618**, 235-247.

[308] Meincken M, Holroyd DL, Rautenbach M (2005) Atomic force microscopy study of the effect of antimicrobial peptides on the cell envelope of Escherichia coli. *Antimicrob Agents Chemother* **49**, 4085-4092.

[309] Hoh JH, Hansma PK (1992) Atomic force microscopy for high-resolution imaging in cell biology. *Trends in Cell Biology* **2**, 208-213.

[310] Giessibl FJ (2003) Advances in atomic force microscopy. *Reviews of Modern Physics* **75**, 949-983.

[311] Morris VJ, Kirby AR, Gunning AP (2009) *Atomic Force Microscopy for Biologists*.

[312] García R, San Paulo A (1999) Attractive and repulsive tip-sample interaction regimes in tapping-mode atomic force microscopy. *Physical Review B* **60**, 4961-4967.

[313] Putman CAJ, Van der Werf KO, De Grooth BG, Van Hulst NF, Greve J (1994) Tapping mode atomic force microscopy in liquid. *Applied Physics Letters* **64**, 2454-2456.

[314] Kindt JH, Sitko JC, Pietrasanta LI, Oroudjev E, Becker N, Viani MB, Hansma HG (2002) Methods for biological probe microscopy in aqueous fluids. *Methods Cell Biol* **68**, 213-229.

[315] Argaman M, Golan R, Thomson NH, Hansma HG (1997) Phase imaging of moving DNA molecules and DNA molecules replicated in the atomic force microscope. *Nucleic Acids Res* **25**, 4379-4384.

[316] Magonov SN, Elings V, Whangbo MH (1997) Phase imaging and stiffness in tapping-mode atomic force microscopy. *Surface Science* **375**, L385-L391.

[317] Moores B, Hane F, Eng L, Leonenko Z (2010) Kelvin probe force microscopy in application to biomolecular films: frequency modulation, amplitude modulation, and lift mode. *Ultramicroscopy* **110**, 708-711.

[318] Nonnenmacher M, O'Boyle MP, Wickramasinghe HK (1991) Kelvin probe force microscopy. *Applied Physics Letters* **58**, 2921-2923.

[319] Mohn F, Gross L, Moll N, Meyer G (2012) Imaging the charge distribution within a single molecule. *Nat Nano* **7**, 227-231.

[320] Li G, Mao B, Lan F, Liu L (2012) Practical aspects of single-pass scan Kelvin probe force microscopy. *Review of Scientific Instruments* **83**, 113701.

[321] Henning A, Günzburger G, Jöhr R, Rosenwaks Y, Bozic-Weber B, Housecroft CE, Constable EC, Meyer E, Glatzel T (2013) Kelvin probe force microscopy of nanocrystalline TiO(2) photoelectrodes. *Beilstein Journal of Nanotechnology* **4**, 418-428.

[322] Oliveira Jr. ON, Riul Jr. A, Leite VBP (2004) Water at interfaces and its influence on the electrical properties of adsorbed films. *Brazilian Journal of Physics* **34**, 73-83.

[323] Kawai S, Glatzel T, Hug HJ, Meyer E (2010) Atomic contact potential variations of Si(111)-7 x 7 analyzed by Kelvin probe force microscopy. *Nanotechnology* **21**, 245704.

[324] Melitz W, Shen J, Kummel AC, Lee S (2011) Kelvin probe force microscopy and its application. *Surface Science Reports* **66**, 1-27.

[325] Nony L, Foster AS, Bocquet F, Loppacher C (2009) Understanding the Atomic-Scale Contrast in Kelvin Probe Force Microscopy. *Physical Review Letters* **103**, 036802.

[326] Ma ZM, Kou L, Naitoh Y, Li YJ, Sugawara Y (2013) The stray capacitance effect in Kelvin probe force microscopy using FM, AM and heterodyne AM modes. *Nanotechnology* **24**, 225701.

[327] Smith R, Coast J (2013) The true cost of antimicrobial resistance. *BMJ : British Medical Journal* **346**.

[328] Rice LB (2006) Antimicrobial resistance in gram-positive bacteria. *American Journal of Infection Control* **34**, S11-S19.

[329] Arias E, Kochanek KD, Xu J, Murphy S (2015) Mortality in the United States, 2014. *NCHS data brief*, 1.

[330] Cilloniz C, Martin-Loeches I, Garcia-Vidal C, San Jose A, Torres A (2016) Microbial Etiology of Pneumonia: Epidemiology, Diagnosis and Resistance Patterns. *International Journal of Molecular Sciences* **17**.

[331] Organization WH (2014) Antimicrobial resistance global report on surveillance: 2014 summary.

[332] Rausche G, Igelmund P, Heinemann U (1990) Effects of changes in extracellular potassium, magnesium and calcium concentration on synaptic transmission in area CA1 and the dentate gyrus of rat hippocampal slices. *Pflügers Archiv* **415**, 588-593.

[333] Chen N, Murphy TH, Raymond LA (2000) Competitive inhibition of NMDA receptor-mediated currents by extracellular calcium chelators. *J Neurophysiol* **84**, 693-697.

[334] Zima AV, Blatter LA (2006) Redox regulation of cardiac calcium channels and transporters. *Cardiovascular Research* **71**.

[335] ThomasAndrew P (2000) Sharing calcium opens new avenues of signalling. *Nat Cell Biol* **2**, E126-E127.

[336] Wippel C, Förtsch C, Hupp S, Maier E, Benz R, Ma J, Mitchell TJ, Iliev AI (2011) Extracellular Calcium Reduction Strongly Increases the Lytic Capacity of Pneumolysin From Streptococcus Pneumoniae in Brain Tissue. *The Journal of Infectious Diseases* **204**, 930-936.

[337] Zhang L, Rozek A, Hancock RE (2001) Interaction of cationic antimicrobial peptides with model membranes. *J Biol Chem* **276**, 35714-35722.

[338] Bagatolli LA (2003) Direct observation of lipid domains in free standing bilayers: from simple to complex lipid mixtures. *Chemistry and Physics of Lipids* **122**, 137-145.

[339] de la Serna JB, Perez-Gil J, Simonsen AC, Bagatolli LA (2004) Cholesterol Rules DIRECT OBSERVATION OF THE COEXISTENCE OF TWO FLUID PHASES IN NATIVE PULMONARY SURFACTANT MEMBRANES AT PHYSIOLOGICAL TEMPERATURES. *Journal of Biological Chemistry* **279**, 40715-40722.

[340] Nag K, Pao J-S, Harbottle RR, Possmayer F, Petersen NO, Bagatolli LA (2002) Segregation of Saturated Chain Lipids in Pulmonary Surfactant Filmsand Bilayers. *Biophysical Journal* **82**, 2041-2051.

[341] He Y, Li J, Yin N, Herradura PS, Martel L, Zhang Y, Pearson AL, Kulkarni V, Mascio C, Howland K, Silverman JA, Keith DD, Metcalf CA (2012) Reduced pulmonary surfactant interaction of daptomycin analogs via tryptophan replacement with alternative amino acids. *Bioorganic & Medicinal Chemistry Letters* **22**, 6248-6251.

[342] Mishra NN, Bayer AS (2013) Correlation of cell membrane lipid profiles with daptomycin resistance in methicillin-resistant Staphylococcus aureus. *Antimicrobial agents and chemotherapy* **57**, 1082-1085.

[343] Hachmann A-B, Angert ER, Helmann JD (2009) Genetic analysis of factors affecting susceptibility of Bacillus subtilis to daptomycin. *Antimicrobial agents and chemotherapy* **53**, 1598-1609.

[344] da Cunha Camargo ILB, Neoh H-M, Cui L, Hiramatsu K (2008) Serial daptomycin selection generates daptomycin-nonsusceptible Staphylococcus aureus strains with a heterogeneous vancomycin-intermediate phenotype. *Antimicrobial agents and chemotherapy* **52**, 4289-4299.

[345] Lohani CR, Taylor R, Palmer M, Taylor SD (2015) Solid-phase total synthesis of daptomycin and analogs. *Org Lett* **17**, 748-751.

[346] Lohani CR, Taylor R, Palmer M, Taylor SD (2015) Solid-phase synthesis and in vitro biological activity of a Thr4-->Ser4 analog of daptomycin. *Bioorg Med Chem Lett* **25**, 5490-5494.

[347] Vivian JT, Callis PR (2001) Mechanisms of Tryptophan Fluorescence Shifts in Proteins. *Biophysical Journal* **80**, 2093-2109.

[348] Moon CP, Fleming KG (2011) Using tryptophan fluorescence to measure the stability of membrane proteins folded in liposomes. *Methods in enzymology* **492**, 189-211.

[349] Ghisaidoobe ABT, Chung SJ (2014) Intrinsic Tryptophan Fluorescence in the Detection and Analysis of Proteins: A Focus on Förster Resonance Energy Transfer Techniques. *International Journal of Molecular Sciences* **15**, 22518-22538.

[350] Jelinek R (2011) *Lipids and Cellular Membranes in Amyloid Diseases*, Wiley.

[351] Kenoth R, Simanshu DK, Kamlekar RK, Pike HM, Molotkovsky JG, Benson LM, Bergen HR, Prendergast FG, Malinina L, Venyaminov SY, Patel DJ, Brown RE (2010) Structural Determination and Tryptophan Fluorescence of Heterokaryon Incompatibility C2 Protein (HET-C2), a Fungal Glycolipid Transfer Protein (GLTP), Provide Novel Insights into Glycolipid Specificity and Membrane Interaction by the GLTP Fold. *Journal of Biological Chemistry* **285**, 13066-13078.

[352] Krishnakumar SS, Brook SUoNYaS (2007) *Sequence to Topography Relationship in Membrane-inserted Hydrophobic Helices*, State University of New York at Stony Brook.

[353] Torchilin V, Weissig V (2003) *Liposomes: A Practical Approach*, OUP Oxford.

[354] Verza G, Bakás L (2000) Location of tryptophan residues in free and membrane bound Escherichia coli α-hemolysin and their role on the lytic membrane properties. *Biochimica et Biophysica Acta (BBA) - Biomembranes* **1464**, 27-34.

[355] Miao V, Coeffet-Legal MF, Brian P, Brost R, Penn J, Whiting A, Martin S, Ford R, Parr I, Bouchard M, Silva CJ, Wrigley SK, Baltz RH (2005) Daptomycin biosynthesis in Streptomyces roseosporus: cloning and analysis of the gene cluster and revision of peptide stereochemistry. *Microbiology* **151**, 1507-1523.

[356] Rubinchik E, Schneider T, Elliott M, Scott WR, Pan J, Anklin C, Yang H, Dugourd D, Muller A, Gries K, Straus SK, Sahl HG, Hancock RE (2011) Mechanism of action and limited cross-resistance of new lipopeptide MX-2401. *Antimicrob Agents Chemother* **55**, 2743-2754.

[357] Mengin-Lecreulx D, Allen NE, Hobbs JN, van Heijenoort J (1990) Inhibition of peptidoglycan biosynthesis in Bacillus megaterium by daptomycin. *FEMS Microbiol Lett* **57**, 245-248.

[358] Çapan R, Richardson TH, Lacey D (2001) The Langmuir properties of a mixed copolysiloxane monolayer. *Turkish Journal of Physics* **25**, 445-449.

[359] Matti V, Säily J, Ryhänen SJ, Holopainen JM, Borocci S, Mancini G, Kinnunen PKJ (2001) Characterization of Mixed Monolayers of Phosphatidylcholine and a Dicationic Gemini Surfactant SS-1 with a Langmuir Balance: Effects Of DNA. *Biophysical Journal* **81**, 2135-2143.

[360] Wang Z, Yang S (2009) Effects of fullerenes on phospholipid membranes: a langmuir monolayer study. *Chemphyschem* **10**, 2284-2289.

[361] Bonn M, Roke S, Berg O, Juurlink LB, Stamouli A, Müller M (2004) A molecular view of cholesterol-induced condensation in a lipid monolayer. *The Journal of Physical Chemistry B* **108**, 19083-19085.

[362] Choucair A, Chakrapani M, Chakravarthy B, Katsaras J, Johnston L (2007) Preferential accumulation of Aβ (1− 42) on gel phase domains of lipid bilayers: An AFM and fluorescence study. *Biochimica et Biophysica Acta (BBA)-Biomembranes* **1768**, 146-154.

[363] Ambroggio EE, Separovic F, Bowie J, Fidelio GD (2004) Surface behaviour and peptide–lipid interactions of the antibiotic peptides, Maculatin and Citropin. *Biochimica et Biophysica Acta (BBA)-Biomembranes* **1664**, 31-37.

[364] Neville F, Cahuzac M, Konovalov O, Ishitsuka Y, Lee KYC, Kuzmenko I, Kale GM, Gidalevitz D (2006) Lipid headgroup discrimination by antimicrobial peptide LL-37: insight into mechanism of action. *Biophysical journal* **90**, 1275-1287.

[365] Brockman H (1999) Lipid monolayers: why use half a membrane to characterize protein-membrane interactions? *Current opinion in structural biology* **9**, 438-443.

[366] Brogden KA (1991) Changes in pulmonary surfactant during bacterial pneumonia. *Antonie Van Leeuwenhoek* **59**, 215-223.

[367] Agassandian M, Mallampalli RK (2013) Surfactant phospholipid metabolism. *Biochimica et biophysica acta* **1831**, 612-625.

[368] Jounblat R, Clark H, Eggleton P, Hawgood S, Andrew P, Kadioglu A (2005) The role of surfactant protein D in the colonisation of the respiratory tract and onset of bacteraemia during pneumococcal pneumonia. *Respiratory Research* **6**, 126.

[369] Griese M (1999) Pulmonary surfactant in health and human lung diseases: state of the art. *Eur Respir J* **13**, 1455-1476.

[370] Gunther A, Siebert C, Schmidt R, Ziegler S, Grimminger F, Yabut M, Temmesfeld B, Walmrath D, Morr H, Seeger W (1996) Surfactant alterations in severe pneumonia,

acute respiratory distress syndrome, and cardiogenic lung edema. *Am J Respir Crit Care Med* **153**, 176-184.

[371] Evans EA, Waugh R, Melnik L (1976) Elastic area compressibility modulus of red cell membrane. *Biophysical Journal* **16**, 585-595.

[372] Polin RA, Fox WW, Abman SH (2011) *Fetal and Neonatal Physiology: Expert Consult - Online and Print*, Elsevier/Saunders.

[373] Rooney SA, Young SL, Mendelson CR (1994) Molecular and cellular processing of lung surfactant. *The FASEB Journal* **8**, 957-967.

[374] Bernhard W, Mottaghian J, Gebert A, Rau G, Hardt Hvd, Poets C (2000) Commercial versus Native Surfactants. *American Journal of Respiratory and Critical Care Medicine* **162**, 1524-1533.

[375] Ding J, Takamoto DY, von Nahmen A, Lipp MM, Lee KYC, Waring AJ, Zasadzinski JA (2001) Effects of Lung Surfactant Proteins, SP-B and SP-C, and Palmitic Acid on Monolayer Stability. *Biophysical Journal* **80**, 2262-2272.

[376] Keating E, Zuo YY, Tadayyon SM, Petersen NO, Possmayer F, Veldhuizen RAW (2012) A modified squeeze-out mechanism for generating high surface pressures with pulmonary surfactant. *Biochimica et Biophysica Acta (BBA) - Biomembranes* **1818**, 1225-1234.

[377] Ishitsuka Y, Pham DS, Waring AJ, Lehrer RI, Lee KY (2006) Insertion selectivity of antimicrobial peptide protegrin-1 into lipid monolayers: effect of head group electrostatics and tail group packing. *Biochim Biophys Acta* **1758**, 1450-1460.

[378] Zaknoon F, Sarig H, Rotem S, Livne L, Ivankin A, Gidalevitz D, Mor A (2009) Antibacterial Properties and Mode of Action of a Short Acyl-Lysyl Oligomer. *Antimicrobial Agents and Chemotherapy* **53**, 3422-3429.

[379] Gidalevitz D, Ishitsuka Y, Muresan AS, Konovalov O, Waring AJ, Lehrer RI, Lee KYC (2003) Interaction of antimicrobial peptide protegrin with biomembranes. *Proceedings of the National Academy of Sciences* **100**, 6302-6307.

[380] Drolle E, Gaikwad RM, Leonenko Z (2012) Nanoscale electrostatic domains in cholesterol-laden lipid membranes create a target for amyloid binding. *Biophys J* **103**, L27-29.

[381] Li J, Sun R, Hao C, He G, Zhang L, Wang J (2015) The behavior of the adsorption of cytochrome C on lipid monolayers: A study by the Langmuir-Blodgett technique and theoretical analysis. *Biophys Chem* **205**, 33-40.

[382] Weisenhorn AL, Egger M, Ohnesorge F, Gould SAC, Heyn SP, Hansma HG, Sinsheimer RL, Gaub HE, Hansma PK (1991) Molecular-resolution images of Langmuir-Blodgett films and DNA by atomic force microscopy. *Langmuir* **7**, 8-12.

[383] Chi L, Anders M, Fuchs H, Johnston R, Ringsdorf H (1993) Domain structures in Langmuir-Blodgett films investigated by atomic force microscopy. *SCIENCE-NEW YORK THEN WASHINGTON-* **259**, 213-213.

[384] Bhushan B, Kulkarni AV, Koinkar VN, Boehm M, Odoni L, Martelet C, Belin M (1995) Microtribological Characterization of Self-Assembled and Langmuir-Blodgett Monolayers by Atomic and Friction Force Microscopy. *Langmuir* **11**, 3189-3198.

[385] Kim K, Choi SQ, Zell ZA, Squires TM, Zasadzinski JA (2013) Effect of cholesterol nanodomains on monolayer morphology and dynamics. *Proc Natl Acad Sci U S A* **110**, E3054-3060.

[386] Nagashima T, Uematsu S (2015) Water-binding phospholipid nanodomains and phase-separated diacylglycerol nanodomains regulate enzyme reactions in lipid monolayers. *Langmuir* **31**, 1479-1488.

[387] Hagedorn S, Drolle E, Lorentz H, Srinivasan S, Leonenko Z, Jones L (2015) Atomic force microscopy and Langmuir-Blodgett monolayer technique to assess contact lens deposits and human meibum extracts. *J Optom* **8**, 187-199.

[388] Yuan C, Furlong J, Burgos P, Johnston LJ (2002) The Size of Lipid Rafts: An Atomic Force Microscopy Study of Ganglioside GM1 Domains in Sphingomyelin/DOPC/Cholesterol Membranes. *Biophysical Journal* **82**, 2526-2535.

[389] Yang XM, Xiao D, Xiao SJ, Wei Y (1994) Domain structures of phospholipid monolayer Langmuir-Blodgett films determined by atomic force microscopy. *Applied Physics A* **59**, 139-143.

[390] Tokumasu F, Jin AJ, Feigenson GW, Dvorak JA (2003) Nanoscopic Lipid Domain Dynamics Revealed by Atomic Force Microscopy. *Biophysical Journal* **84**, 2609-2618.

[391] Hagedorn S, Drolle E, Lorentz H, Srinivasan S, Leonenko Z, Jones L (2015) Atomic force microscopy and Langmuir–Blodgett monolayer technique to assess contact lens deposits and human meibum extracts(). *Journal of Optometry* **8**, 187-199.

[392] García-Sáez AJ, Schwille P (2010) Stability of lipid domains. *FEBS Letters* **584**, 1653-1658.

[393] Matsumoto K, Kusaka J, Nishibori A, Hara H (2006) Lipid domains in bacterial membranes. *Molecular Microbiology* **61**, 1110-1117.

[394] Buehler L (2015) *Cell Membranes*, Taylor & Francis Group.

[395] Eaton P, West P (2010) *Atomic Force Microscopy*, OUP Oxford.

[396] Kosaka PM, González S, Domínguez CM, Cebollada A, San Paulo A, Calleja M, Tamayo J (2013) Atomic force microscopy reveals two phases in single stranded DNA self-assembled monolayers. *Nanoscale* **5**, 7425-7432.

[397] Sheiko SS, Zhou J, Arnold J, Neugebauer D, Matyjaszewski K, Tsitsilianis C, Tsukruk VV, Carrillo J-MY, Dobrynin AV, Rubinstein M (2013) Perfect mixing of immiscible macromolecules at fluid interfaces. *Nature materials* **12**, 735-740.

[398] Drelich J, Mittal KL (2005) *Atomic Force Microscopy in Adhesion Studies*, Taylor & Francis.

[399] Magonov S, Elings V, Whangbo M-H (1997) Phase imaging and stiffness in tapping-mode atomic force microscopy. *Surface science* **375**, L385-L391.

[400] Drolle E, Bennett WF, Hammond K, Lyman E, Karttunen M, Leonenko Z (2016) Molecular dynamics simulations and Kelvin probe force microscopy to study of cholesterol-induced electrostatic nanodomains in complex lipid mixtures. *Soft Matter*.

[401] Liu G, Zhao S, Henderson RD, Leonenko Z, Abdel-Rahman E, Mi Z, Ban D (2016) Nanogenerators based on vertically aligned InN nanowires. *Nanoscale* **8**, 2097-2106.

[402] Yun JS, Seidel J, Kim J, Soufiani AM, Huang S, Lau J, Jeon NJ, Seok SI, Green MA, Ho-Baillie A (2016) Critical Role of Grain Boundaries for Ion Migration in Formamidinium and Methylammonium Lead Halide Perovskite Solar Cells. *Advanced Energy Materials*.

[403] Wagner T, Köhler D, Milde P, Eng LM (2013) Probing the local surface potential and quantum capacitance in single and multi-layer graphene. *Applied Physics Letters* **103**, 023102.

[404] Shirota K, Takeuchi D, Kato H, Makino T, Ogura M, Okushi H, Yamasaki S (2015) Potential profile evaluation of a diamond lateral p–n junction diode using Kelvin probe force microscopy. *physica status solidi (a)* **212**, 2589-2594.

[405] Rachana R, Banerjee R (2006) Effects of albumin and erythrocyte membranes on spread monolayers of lung surfactant lipids. *Colloids and Surfaces B: Biointerfaces* **50**, 9-17.

[406] Ackerman DG, Feigenson GW (2015) Lipid Bilayers: Clusters, Domains and Phases. *Essays in biochemistry* **57**, 33-42.

[407] Monteiro N, Martins A, Reis RL, Neves NM (2014) Liposomes in tissue engineering and regenerative medicine. *Journal of The Royal Society Interface* **11**.

[408] Messersmith PB, Vallabhaneni S, Nguyen V (1998) Preparation of calcium-loaded liposomes and their use in calcium phosphate formation. *Chemistry of materials* **10**, 109-116.

[409] Sullan RMA (2010) University of Toronto.

[410] Xie AF, Yamada R, Gewirth AA, Granick S (2002) Materials science of the gel to fluid phase transition in a supported phospholipid bilayer. *Physical review letters* **89**, 246103.

[411] Ahmed SN, Brown DA, London E (1997) On the origin of sphingolipid/cholesterol-rich detergent-insoluble cell membranes: physiological concentrations of cholesterol and sphingolipid induce formation of a detergent-insoluble, liquid-ordered lipid phase in model membranes. *Biochemistry* **36**, 10944-10953.

[412] Fidorra M, Duelund L, Leidy C, Simonsen AC, Bagatolli L (2006) Absence of fluid-ordered/fluid-disordered phase coexistence in ceramide/POPC mixtures containing cholesterol. *Biophysical journal* **90**, 4437-4451.

[413] McMullen TP, Lewis RN, McElhaney RN (2004) Cholesterol–phospholipid interactions, the liquid-ordered phase and lipid rafts in model and biological membranes. *Current opinion in colloid & interface science* **8**, 459-468.

[414] Drummond DC, Meyer O, Hong K, Kirpotin DB, Papahadjopoulos D (1999) Optimizing liposomes for delivery of chemotherapeutic agents to solid tumors. *Pharmacological reviews* **51**, 691-744.

[415] Maurer N, Fenske DB, Cullis PR (2001) Developments in liposomal drug delivery systems. *Expert opinion on biological therapy* **1**, 923-947.

[416] Papahadjopoulos D, Nir S, Ohki S (1972) Permeability properties of phospholipid membranes: effect of cholesterol and temperature. *Biochimica et Biophysica Acta (BBA)-Biomembranes* **266**, 561-583.

[417] Vemuri S, Rhodes C (1995) Preparation and characterization of liposomes as therapeutic delivery systems: a review. *Pharmaceutica Acta Helvetiae* **70**, 95-111.

[418] Coban O, Popov J, Burger M, Vobornik D, Johnston LJ (2007) Transition from nanodomains to microdomains induced by exposure of lipid monolayers to air. *Biophysical journal* **92**, 2842-2853.

[419] Simons K, Vaz WL (2004) Model systems, lipid rafts, and cell membranes 1. *Annu. Rev. Biophys. Biomol. Struct.* **33**, 269-295.

[420] Elder M, Hitchcock P, Mason R, Shipley GG (1977) A Refinement Analysis of the Crystallography of the Phospholipid, 1,2-Dilauroyl-DL-Phosphatidylethanolamine, and Some Remarks on Lipid-Lipid and Lipid-Protein Interactions. *Proceedings of the Royal Society of London. A. Mathematical and Physical Sciences* **354**, 157-170.

[421] Hauser H, Pascher I, Pearson R, Sundell S (1981) Preferred conformation and molecular packing of phosphatidylethanolamine and phosphatidylcholine. *Biochimica et Biophysica Acta (BBA)-Reviews on Biomembranes* **650**, 21-51.

[422] Boggs JM (1987) Lipid intermolecular hydrogen bonding: influence on structural organization and membrane function. *Biochimica et Biophysica Acta (BBA)-Reviews on Biomembranes* **906**, 353-404.

[423] Pascher I, Sundell S, Harlos K, Eibl H (1987) Conformation and packing properties of membrane lipids: the crystal structure of sodium dimyristoylphosphatidylglycerol. *Biochimica et Biophysica Acta (BBA)-Biomembranes* **896**, 77-88.

[424] Haines TH, Dencher NA (2002) Cardiolipin: a proton trap for oxidative phosphorylation. *FEBS letters* **528**, 35-39.

[425] Pollard TD, Earnshaw WC, Lippincott-Schwartz J (2007) *Cell Biology*, Elsevier Health Sciences.

[426] Attwood SJ, Choi Y, Leonenko Z (2013) Preparation of DOPC and DPPC Supported Planar Lipid Bilayers for Atomic Force Microscopy and Atomic Force Spectroscopy. *International Journal of Molecular Sciences* **14**, 3514-3539.

[427] Jena BP, Hörber JKH (2006) *Force Microscopy: Applications in Biology and Medicine*, Wiley.

[428] Schwarz JA, Contescu CI, Putyera K (2004) *Dekker Encyclopedia of Nanoscience and Nanotechnology*, M. Dekker.

[429] Richter R, Mukhopadhyay A, Brisson A (2003) Pathways of lipid vesicle deposition on solid surfaces: a combined QCM-D and AFM study. *Biophysical journal* **85**, 3035-3047.

[430] Melby ES, Mensch AC, Lohse SE, Hu D, Orr G, Murphy CJ, Hamers RJ, Pedersen JA (2016) Formation of supported lipid bilayers containing phase-segregated domains and their interaction with gold nanoparticles. *Environmental Science: Nano* **3**, 45-55.

[431] Lasic DD (1997) *Liposomes in Gene Delivery*, Taylor & Francis.

APPENDICES

APPENDIX A: PREPARATION OF SOLUTIONS

A.1 Buffer Solutions

A buffer solution is an aqueous solution that helps to maintain a consistent pH upon minute additions of acid or base. To make a buffer solution, one must combine a weak acid or weak base with a salt containing its conjugate base or acid, respectively.

In the work presented in this thesis, the buffer solutions that were used were made from HEPES (4-(2-hydroxyethyl)-1-piperazineethanesulfonic acid), a buffering agent that is commonly used to maintain physiological pH levels. Specifically, the HEPES buffer solution contained 20 mM HEPES and 150 mM NaCl at a pH of 7.4.

Procedures are given below to make 500 mL of a HEPES buffer, with HEPES and NaCl having molar masses of 238.3 g/mol and 58.44 g/mol respectively. Sample calculations are provided here to determine the amount of HEPES and NaCl to add to the solution.

Calculations:

Given: $M_{hepes} = 238.3$ g/mol $M_{NaCl} = 58.44$ g/mol $V = 500$ mL $= 0.50$ L

$C_{hepes} = 20$ mM $C_{NaCl} = 150$ mM

Equations: $n = m/M$ and $C = n/V$ so $m = CMV$

Find m_{hepes}: $m_{hepes} = (0.02 \text{ mol/L})(238.3 \text{ g/mol})(0.50 \text{ L}) = 2.383 \text{ g} =$ **2383 mg**

Find m_{NaCl}: $m_{NaCl} = (0.15 \text{ mol/L})(58.44 \text{ g/mol})(0.50 \text{ L}) = 4.384 \text{ g} =$ **4384 mg**

Procedure:

1. Make sure you clean a large beaker (greater than 500 mL), graduated cylinder (at least 500 mL), and bottle (at least 500 mL).
2. Add the following into the large beaker:
    a. 500 mL nanopure water with a graduated cylinder
    b. 2383 mg HEPES, weighed with weighing dish on analytical scale
    c. 4384 mg NaCl, weighed with weighing dish on scale
3. Mix the contents of the beaker using a magnetic stirrer on a stir plate.
4. Calibrate the pH meter and record the pH level.
    a. If the pH is lower than 7.4, prepare a basic NaOH solution. Add this solution drop by drop into the buffer until a pH of 7.4 is reached.
    b. If the pH is higher than 7.4, prepare an acidic HCl solution. Add this solution drop by drop into the buffer until a pH of 7.4 is reached.

5. Once a pH level of 7.4 has been reached, get a large, plastic and sterile syringe as well as a 25 mm diameter syringe filter (made with polypropylene with a pore size of 0.2 μm) for the syringe tip.
6. Transfer the buffer solution from the beaker to a clean bottle using the syringe and syringe filter. Here are some helpful tips:
    a. Every time you load up the syringe, the filter must be removed. Once the solution has been drawn up into the syringe, place the filter back on and push the solution past the filter and into the bottle.
    b. Do not push too hard when filtering the solution to prevent tearing of the filter membrane.

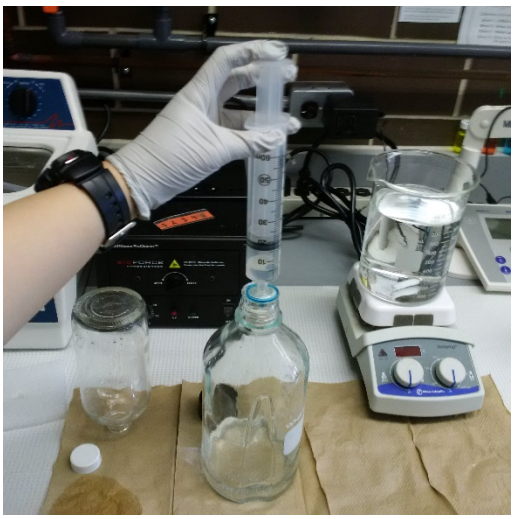

7. When done, label and store the buffer solution in the refrigerator at about 4°C.

A.2 Calcium Stock Solutions

The experiments in this thesis involved the use of calcium, which is required as part of daptomycin's and CB-182-462's mechanisms of action.

A 100 mM calcium stock solution was prepared using calcium chloride dihydrate ($CaCl_2 \cdot 2H_2O$, $M_{calcium}$ = 147.01 g/mol) for use in each experiment. Procedures and sample calculations are provided below for the preparation of 100 mL of 100 mM calcium stock solution.

Calculations:

Given: $M_{calcium}$ = 147.01 g/mol $C_{calcium}$ = 100 mM V = 100 mL = 0.10 L

Equations: $n = m/M$ and $C = n/V$ so $m = CMV$

Find $m_{calcium}$: $m_{calcium}$ = (0.10 mol/L)(147.01 g/mol)(0.10 L) = 1.4701 g = **1470.10 mg**

Procedure:

1. Add the following items into a beaker:
    a. 100 mL of HEPES buffer
    b. 1470.10 mg of calcium chloride dihydrate
2. Mix well using a magnetic stirrer on a stir plate.
3. Label and store the calcium stock solution in the refrigerator at 4°C until use.

A.3 Daptomycin and CB-182,462 Stock Solutions

Stocks solutions of daptomycin and CB-182,462 were required for the experiments in this thesis. Both stock solutions contained 1 mM of the respective antimicrobial peptide.

Calculations and procedures are provided below to make the 1 mM daptomycin stock solution, with daptomycin having a molar mass of 1620.67 g/mol.

Daptomycin Stock Calculations:

Given: M_{dap} = 1620.67 g/mol C_{dap} = 1 mM V = 10 mL = 0.01 L

Equations: $n = m/M$ and $C = n/V$ so $m = CMV$

Find m_{dap}: m_{dap} = (0.001 mol/L)(1620.67 g/mol)(0.01 L) = **16.21 mg**

Daptomycin Stock Procedure:

1. Add the following items into a beaker:
    a. 10 mL of HEPES buffer
    b. 16.21 mg of daptomycin
2. Mix well using a magnetic stirrer on a stir plate
3. Divide into 5 aliquots of 2 mL each to prevent repeated freeze-thaw cycles.
4. Label and store the daptomycin stock solution in the freezer at -20°C until use.

Calculations and procedures are provided below to make the 1 mM CB-182,462 stock solution, with CB-182,462 having a molar mass of 1687.82 g/mol.

CB-182,462 Stock Calculations:

Given: M_{462} = 1687.82 g/mol C_{462} = 1 mM V = 10 mL = 0.01 L

Equations: $n = m/M$ and $C = n/V$ so $m = CMV$

Find m_{462}: m_{462} = (0.001 mol/L)(1687.82 g/mol)(0.01 L) = **16.88 mg**

CB-182,462 Stock Procedure:

1. Add the following items into a beaker:
    a. 10 mL of HEPES buffer
    b. 16.88 mg of CB-182,462
2. Mix well using a magnetic stirrer on a stir plate
3. Divide into 5 aliquots of 2 mL each to prevent repeated freeze-thaw cycles.
4. Label and store the CB-182,462 stock solution in the freezer at -20°C until use.

APPENDIX B: FLUORESCENCE SPECTROSCOPY

B.1 Preparing Vesicle Solutions with an Extruder

For fluorescence spectroscopy experiments, unilamellar vesicles or liposomes were prepared using an extruder. The preparation of these vesicles involved multiple steps, including (1) measuring out the lipids for a specific membrane model and dissolving them in volatile solutions, (2) drying the solutions until a thin film forms, (3) rehydrating and resuspending the vesicles in a buffer solution, and (4) passing this solution through an extruder. Sample calculations and detailed procedures are provided below to make 3 mL of a 5 mM liposome solution with an extruder.

B.1.1 Measuring Out the Lipids for a Specific Membrane Model

There were four lipid systems used in this thesis: bacterial membrane model, human membrane model, lung surfactant model, and BLES®. The steps to preparing lipid models are identical, while BLES® required a different set of procedures to make the initial solution prior to drying.

B.1.1.1 Preparing the Lipid Mixture with Lipid Models: BM, HM, LS

Each lipid model contains a different ratio of lipids. The bacterial membrane model will be used for subsequent examples and sample calculations. The composition of the bacterial membrane model is a 20:20:60 molar ratio of DOPG:TOCL:POPE. Sample calculations and procedures

are provided below to create 3 mL of 5 mM BM liposomes starting with lipid stock in powder form.

Calculations:

Given: M_{CL} = 1501.98 g/mol M_{PE} = 718.01 g/mol M_{PG} = 797.04 g/mol

P_{CL} = 0.2 P_{PE} = 0.6 P_{PG} = 0.2 C_{BM} = 5 mM V = 3 mL = 0.003 L

Find n_{total}: $n_{total} = (C_{BM})(V) = (0.005 \text{ mol/L})(0.003 \text{ L}) =$ **1.5×10^{-5} mol**

Find m_{CL}: $m_{CL} = (P_{CL})(M_{CL})(n_{total}) = (0.2)(1501.98 \text{ g/mol})(1.5 \times 10^{-5} \text{ mol}) =$ **4.51 mg**

Find m_{PE}: $m_{PE} = (P_{PE})(M_{PE})(n_{total}) = (0.6)(718.01 \text{ g/mol})(1.5 \times 10^{-5} \text{ mol}) =$ **6.46 mg**

Find m_{PG}: $m_{PG} = (P_{PG})(M_{PG})(n_{total}) = (0.2)(797.04 \text{ g/mol})(1.5 \times 10^{-5} \text{ mol}) =$ **2.39 mg**

Procedure:

1. Thoroughly clean a round bottom flask by using an organic solvent to clean it (eg. methanol) and end with chloroform to help dissolve any remaining lipids from previous experiments.
2. Add the calculated amount of lipid powder for TOCL, POPE, and DOPG into the clean round bottom flask with the help of an analytical scale and some weighing paper.

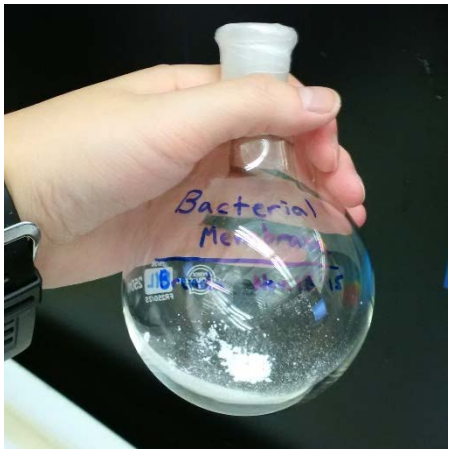

3. Add chloroform to the round bottom flask using a glass pipette. This helps to dissolve the lipids due to its weak polarity.
    a. Try to deposit the solvent at the mouth of the flask to catch any remaining lipid powder (from when you weighed it and added it into the flask).
    b. Add a sufficient amount of chloroform until you can see the lipids dissolving and the solution turning clear.
    c. If the lipid solution does not appear clear or has some undissolved specks of lipid powder still visible, don't worry – move onto the next step.
4. Add a small amount of methanol to the round bottom flask using a separate glass pipette.
    a. Adding a small amount of methanol should help dissolve additional lipids due to its increased polarity.
5. Swirl the round bottom flask until the lipids are fully dissolved. Make sure you keep the solution at the bottom half of the flask to make it easier for subsequent steps.

B.1.1.2 Preparing the Lipid Mixture with BLES®

BLES® is bovine lipid extract surfactant and comes in suspensions of 27 mg phospholipids per mL. The packaging for BLES® states that their manufacturing process selectively removes hydrophilic proteins while keeping hydrophobic phospholipids and surfactant-associated proteins SP-B and SP-C. Considering our lung surfactant model contains an 80:20 molar ratio of DPPC:DOPG, we will assume the same of these BLES® solutions to simplify our calculations and sample preparation.

The goal is to make an approximate 5 mM BLES® liposome solution to be used in conjunction with the other model liposome solutions for experimental purposes.

Lipid Extraction Procedure:

1. Add 2 mL of BLES® to a centrifuge tube.
2. Add a small amount of 4:1 chloroform:methanol solvent to the centrifuge tube.
3. Spin for 5 minutes at 2000 RPM.
4. There should be a separation of phases. Save the bottom phase by transferring it to another centrifuge tube. In the original tube, add more chloroform and methanol to the supernatant and centrifuge again.
5. Repeat Steps 3-4 a total of 18 times. With each transfer, transfer into the second tube where all the lipids are being stored.
6. You should now have a centrifuge tube (the second one) with a collection of "bottom phases" that you've transferred from the original tube. These are the lipids.

Making the BLES® Solution for Drying:

Let's assume that you end up with 3 mL of your extracted BLES® solution and you started out with 2 mL of original BLES® stock. Since the original stock had a concentration of 27 mg of phospholipids per mL, that means that a total of 54 mg of phospholipids were present in the solution. And since our lipid extraction procedure would have kept these lipids, this means that we can make an assumption and say that all the lipids, the 54 mg, were transferred to your new 3 mL of extracted BLES® solution.

We now have to make another assumption and say that these phospholipids are primarily composed of 80% DPPC and 20% DOPG. This means that from the original 54 mg of phospholipids, 43.2 mg of DPPC and 10.8 mg of DOPG are present in the extracted BLES® solution. Since we know that the molar masses of DPPC and DOPG are 734.05 g/mol and 797.04 g/mol respectively, we can calculate how many moles of phospholipids are present in total and use $C = n/V$ to determine the volume of HEPES buffer required to make an approximate 5 mM BLES® solution. This calculated volume will be required in the rehydration step in *Appendix B.1.3*.

The steps below are to make the BLES® solution prior to drying.

1. Thoroughly clean a round bottom flask by using an organic solvent to clean it (eg. methanol) and end with chloroform to help dissolve any remaining lipids from previous experiments.
2. Add all of the BLES® solution (no buffer) to the round bottom flask.
3. Swirl the round bottom flask and make sure the lipids are fully dissolved. Make sure you keep the solution at the bottom half of the flask to make it easier for subsequent steps.

B.1.2 Creating a Thin Film and Drying It

1. Using a narrow tube of nitrogen gas (from a compressed gas cylinder), insert the tube into the round bottom flask (without touching the inner walls of the flask or the solution) and gently dry/evaporate the mixture while simultaneously spinning the round bottom flask.
    a. These combined actions help the dissolved lipid mixture form a thin film around the bottom half of the round bottom flask once the entire solution is dry.
    b. Once you see a thin film form and everything is dry, you can stop.
2. Vacuum-dry the round bottom flask for at least 12 hours to ensure that the round bottom flask contents are completely dry.
3. Seal and store the round bottom flask in freezer (-20°C) until ready for liposome resuspension or rehydration.

B.1.3 Rehydration and Liposome Formation

When a thin lipid film, or cake, was created in the previous step, hydrating this dried layer of lipids promotes the formation of lipid vesicles, or liposomes. When water or a buffer is added, the dried lipid films will start to detach from one another as they get more and more hydrated,

and when agitated, these sheets will fully detach and self-close to form large multilamellar vesicles (LMV).

1. Whether you take the round bottom flask with the lipid thin film from the freezer or from the vacuum pump, the round bottom flask needs to be warmed up to at least room temperature so that it is above the majority of the lipids' transition temperatures.
2. Add 3 mL of HEPES buffer if you are using the BM, LS, or HM lipid models.
    a. If you are rehydrating a BLES® thin film, add the calculated amount of HEPES buffer from *Appendix B.1.1.1*
3. Swirl the flask around to agitate the mixture and promote vesicle formation.
4. As liposomes are resuspended, the solution will become cloudy.
    a. Make sure all (or most) of the liposomes are resuspended in the buffer by making sure the buffer is cloudy and that the thin film is no longer visible with the naked eye.
    b. If it is too difficult to resuspend, use a vortex to agitate the round bottom flask (around the remaining thin films) so as to promote its resuspension into the buffer.

5. Parafilm the mouth of the round bottom flask and set aside until ready for extrusion.

B.1.4 Extruding Liposomes to Reduce their Size

In the previous step, large multilamellar vesicles (LMV) were formed when the lipid films were hydrated. However, for experimental purposes, we want the size of these vesicles to be much smaller. To achieve smaller-sized vesicles, we can either sonicate or extrude the vesicles. For fluorescence spectroscopy, we wish to have smaller vesicles that are approximately the same size to maintain consistency across numerous trials and repeats. As a result, the extrusion technique will be used to enhance the consistency of our results.

There are many models of extruders that can be used. The one used in the experiments presented in this thesis is the 10 mL LIPEX™ Thermobarrel Extruder from Northern Lipids (now Transferra Nanosciences Inc.).

The procedures presented below relate to this particular model of extruder:

1. Clean and assemble the extruder according to the manufacturer's guidelines.
    a. Make sure 100 nm polycarbonate filters are used.
2. Since the temperature needs to be regulated to at least body temperature, circulate water through the thermobarrel jacket.

a. To heat the thermobarrel jacket, connect the outlet of a re-circulating water bath to the lower hose barb connection on the thermobarrel jacket and the inlet of the re-circulating bath to the upper hose barb.
b. You can use a heated water bath to set the appropriate extrusion temperature
c. Allow the unit some time (approximately 10-20 minutes) to equilibrate

3. There will be Tygon tubing coming out of the extruder, for the extruded vesicle solution to go.
    a. Make sure this tubing is secured to the mouth of a vial with parafilm.
    b. Also make sure that the parafilm doesn't cover the entire mouth of the vial as you need to extrude the same solution multiple times.
    c. You are now ready to start extruding.
4. Use a glass pipette to add all of the liposome solution (from the round bottom flask) to the extruder top's hole.
5. Close the extruder top with the Quick-Connect (QC) sleeve until you hear a "click" and close the pressure relief valve (black).
6. Turn on the pressure control valve (green) carefully and slowly until the solution flows out of the extruder into the vial through the Tygon tubing. Turn off the valve when done.
    a. Turn off or close the green valve as soon as the solution starts flowing out of the extruder to minimize bubbling of the solution in the vial, and possible overflow.
7. Open the black pressure relief valve to release the pressure in the extruder. Close this black pressure relief valve when finished (when the "hissing" has stopped).
8. Remove the QC sleeve.
9. Transfer the extruded solution from the vial to the extruder top's hole using a glass pipette.
10. Repeat the extrusion (Steps 5 to 9) at least 15 times until the solution is clear.

a. If the solution is not clear, you can centrifuge it to remove residual large particles that remain in suspension.

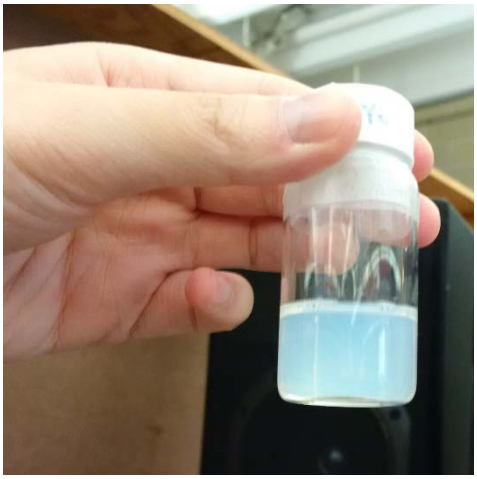

11. Store the vesicle preparation in the refrigerator (4°C) for a maximum of 3-4 days.

B.2 Using the PTI Spectrofluorimeter to take Fluorescence Readings

The fluorescence spectroscopy experiments required the use of a Photon Technology International (PTI) QuantaMaster Spectrofluorometer to take measurements of the samples in this work. The following steps detail the configurations and setup for the experiments.

1. Start the FeliX32 application on the computer.
2. Click on "Emission Scan"
3. Click on "Digital Configuration" and enter the following settings (for daptomycin readings specifically):
    a. Excitation 1: 365 nm for Kyn
    b. Emission 1 Emission Range: 400-600 nm
    c. Length: 200 nm
    d. Step Size: 3 nm
4. Click on "Acquire (Prep)" to prepare for the readings
    a. Make sure the instrument has micrometer settings at 2 mm for each slit, which allows for greater intensity
    b. Make sure the instrument is hooked up to a heated water bath at 37°C
5. Prepare your sample in a 1 mL cuvette and incubate at warm temperature for at least 3 minutes.
    a. Ensure that the amount of daptomycin, 462, vesicle solution and HEPES buffer you add into the 1 mL cuvette adheres to the correct concentrations.
6. Place your sample (in a 1 mL cuvette) in the holder, and click "Start"
    a. Fluorescence readings will be recorded and can be saved using the software.
7. Repeat steps 4-5 for each sample you want to take readings of.

APPENDIX C: LANGMUIR-BLODGETT TROUGH

C.1 Preparing Lipid Solutions

For the experiments involving the use of the Langmuir-Blodgett trough, lipid stock solutions were made for each of the models (BM, LS, HM) as well as for BLES®. The procedure for lipid models varies from the procedures for BLES® and both types are presented below.

C.1.1 Preparing Lipid Model Solutions

Each lipid model contains a different ratio of lipids. Similar to *Appendix B.1.1.1*, the amount of each lipid must be calculated and then weighed out in order to prepare the lipid mixture for a particular model. The composition of the bacterial membrane model is a 20:20:60 molar ratio of DOPG:TOCL:POPE and the following sample calculations and procedures will be relevant to making 10 mL of a 1 mM BM lipid stock.

Calculations:

Given: M_{CL} = 1501.98 g/mol M_{PE} = 718.01 g/mol M_{PG} = 797.04 g/mol

P_{CL} = 0.2 P_{PE} = 0.6 P_{PG} = 0.2 C_{BM} = 1 mM V = 10 mL = 0.01 L

Find n_{total}: $n_{total} = (C_{BM})(V) = (0.001 \text{ mol/L})(0.01 \text{ L}) =$ **1.0×10^{-5} mol**

Find m_{CL}: $m_{CL} = (P_{CL})(M_{CL})(n_{total}) = (0.2)(1501.98 \text{ g/mol})(1.0 \times 10^{-5} \text{ mol}) =$ **3.00 mg**

Find m_{PE}: $m_{PE} = (P_{PE})(M_{PE})(n_{total}) = (0.6)(718.01 \text{ g/mol})(1.0 \times 10^{-5} \text{ mol}) =$ **4.31 mg**

Find m_{PG}: $m_{PG} = (P_{PG})(M_{PG})(n_{total}) = (0.2)(797.04\ g/mol)(1.0 \times 10^{-5}\ mol) =$ **1.59 mg**

Procedure:

1. Take a sterile 20 mL scintillation vial and label it accordingly.
2. Add the calculated amount of lipid powder for TOCL, POPE, and DOPG into the vial with the help of an analytical scale and some weighing paper.
3. Add 10 mL of a 4:1 chloroform:methanol mixture to the vial
    a. You can add 8 mL of chloroform and 2 mL of methanol if you don't have a pre-mixed solution already.
4. Swirl the vial or use a magnetic stirrer on a stir plate to help agitate and dissolve the lipids throughout the solution.
5. Store the solution in the freezer (-20°C) when not in use.

C.1.2 Preparing BLES® Solutions

As mentioned in ***Appendix B.1.1.2***, BLES® is bovine lipid extract surfactant and comes in suspensions of 27 mg of phospholipids per mL. The first step is to extract the lipids from the BLES® stock using the "Lipid Extraction Procedure" presented in ***Appendix B.1.1.2***.

Our goal is to prepare a 1 mM stock solution of BLES® lipids. After the lipids have been extracted from 2 mL of BLES® (equivalent to 54 mg of phospholipids), it is assumed that all the phospholipids have been transferred over to the new vial and 54 mg of phospholipids still exists within the solution to allow for further calculations.

Since BLES® is highly comparable to model lung surfactant systems with 80% DPPC and 20% DOPG, we must also assume that our BLES® solution contains the same ratio of lipids. From the 54 mg, this would mean that 43.2 mg of DPPC and 10.8 mg of DOPG are present in the extracted BLES® solution. Since we know that the molar masses of DPPC and DOPG are 734.05

g/mol and 797.04 g/mol respectively, we can calculate how many moles of phospholipids are present in total and use $C = n/V$ to determine the volume of 4:1 chloroform:methanol mixture required to make an approximate 1 mM BLES® solution.

Once this value has been calculated, add the determined amount of chloroforom:methanol solution to the BLES® vial and mix well. Store in the freezer at -20°C until use.

C.2 Cleaning the Langmuir-Blodgett Trough

Prior to starting any experiments on the Langmuir-Blodgett trough, certain steps need to be taken to clean the surface of the trough as well as the barriers to prevent crossover contamination between samples. The following steps will allow you to clean the LB trough thoroughly.

1. Wet a Kimwipe (delicate task wipers made of virgin wood fibers) with HPLC methanol.
    a. Ensure that proper ventilation is in place, either by using a fume hood or opening windows.
2. Using the wet Kimwipe, wipe the PTFE (polytetrafluoroethylene) teflon surface of the trough.

3. Lift each PTFE Teflon barriers. Using the same Kimwipe, either fold or use a different area of the wiper and wipe the surface of these barriers as well.
4. Toss the Kimwipe after you are done.
5. Repeat the cleaning procedure from Steps 1-4 at least 5 times.
6. When finished with cleaning, let the LB trough dry for about 5-10 minutes prior to continuing on with subsequent steps and experiments.

C.3 Using the LB Trough to take Compression Isotherms

The Langmuir-Blodgett trough is capable of taking multiple types of measurements. One of these measurements is a compression isotherm, where the surface pressure of Langmuir monolayers can be measured as the area of the trough decreases. Depending on the composition of the monolayers being formed, the pressure-area isotherms allow us to characterize monolayer structure, phase transitions, monolayer compressibility, and more.

The compression isotherm experiments performed in this thesis involved the compression of a chosen monolayer toward the point of monolayer collapse on a small Langmuir-Blodgett trough from Nima.

The following procedures outline the setup, operation, and collection of such compression isotherms.

1. Make sure the LB trough is clean using the procedures outlined in *Appendix C.2*.
2. Attach a new or recycled Wilhelmy plate to the extension hook of the trough.
    a. The pre-cut paper Wilhelmy plate uses Whatman CHR1 chromatography paper that has a width of 10 mm.
    b. These Wilhelmy plates are capable of measuring the surface pressure of LB thin films at the air-liquid interface.

c. If you choose to recycle the paper Wilhelmy plates, you can submerge them overnight in a HPLC chloroform solution, then dry them on a Kimwipe or by nitrogen gas prior to use.

3. Fill the trough with 55 mL of nanopure water using a clean graduated cylinder.
    a. When the trough is filled with water, the Wilhelmy plate will begin to absorb the water and equilibrate with the water subphase.
    b. *Should an experiment require the addition of calcium into the subphase, add 1.1 mL of 100 mM calcium stock solution to the 55 mL of nanopure water in the graduated cylinder prior to adding it into the trough. This will give the trough a final calcium concentration of 2 mM.*
4. Allow approximately 10 minutes for the Wilhelmy plate to be fully equilibrated with the subphase.
    a. If you are uncertain as to whether the Wilhelmy plate is fully equilibrated, one way to check for this is to monitor the pressure reading. If the pressure reading stabilizes and does not fluctuate rapidly, then you are ready to proceed to the next step.
5. Zero the pressure sensor, open the barriers (by clicking on the 'O' button), and lift the pressure sensor (with the Wilhelmy plate) out of the water. Check to see whether a reading of about 70 mN/ is obtained for ideal room temperature conditions. If so, move on to the next step.
    a. If not, you will need to recalibrate the pressure sensor using the software's Calibrations Menu, which allows you to calibrate the pressure sensor by providing on-screen instructions. To calibrate, you will need a 100 mg calibration weight that is provided in the monolayer plate.
6. Once pressure equilibration has been achieved, you must check the trough's cleanliness before proceeding. Open the barriers to their farthest positions by clicking on the 'O' button and make sure that the lower edge of the Wilhelmy plate is just in contact with the surface of the subphase (in this case, water).

7. Close the barriers by clicking on the 'C' button and closely monitor the change in surface pressure as the barriers move closer and closer together.
    a. If the change in surface pressure is less than 0.1 mN/m, your subphase and trough are clean enough to proceed with the experiment and adding your lipid sample in.
    b. If the change in surface pressure exceeds 0.1 mN/m significantly, you will need to keep cleaning the trough by aspirating the surface of the subphase with the use of an aspirator pump.
        i. By aspirating the surface of the subphase with a small pipette tip, you are attempting to remove any surface contaminants and floating material that may be affecting surface pressure measurements, such as dust or amphiphilic contaminants.
        ii. The pipette tip should be held at an angle of approximately 30° to 45°. If positioned correctly slightly above the subphase, a loud suctioning noise will be heard as the tip is passed above the water.
        iii. The pipette tip should be moved around, across the surface of the water, to try and rid the entire surface of any contaminants.
        iv. Should too much water be sucked up, the trough can be refilled as necessary and the cleaning process continued. Just make sure that if additional water is required, add the water from behind the barriers (from the sides) so as not to disrupt or contaminate any of the cleaning that was performed in the center of the trough.
8. When you are ready to begin your experiment with a particular lipid model, open the Monolayer Menu within the software. A popup will appear where you can enter the ratio of lipids in your lipid sample, the molecular weight of each lipid, the concentration of your solution, the volume of your solution in μL, and other pertinent information regarding your sample. Make sure you save these monolayer settings so you can load them again for the same model during your next run.

9. Once the conditions have been set and the pressure has been zeroed, close the barriers so that they are approximately 75% open.
10. Draw up 30 μL of your lipid stock solution and deposit it drop by drop onto the surface of the water, without touching the surface but as close as possible to prevent unnecessary ripples.
    a. You will notice a significant increase in surface pressure readings, and they will be fluctuating regularly. This is normal as the solvents will be evaporating.
11. Let the solvent evaporate for at least 10 minutes until the surface pressure is around 10-20 mN/m.
12. Open the barriers fully, and you will see the surface pressure drop even further.
    a. This action further facilitates the evaporation of the solvent, and the pressure reading should now be close to 0 mN/m.
    b. When the reading is close to zero, continue to the next step.
13. Set the barrier speed of the trough to 20 cm^2/min by entering "20" in the Barrier Speed field.
14. Click on "Clear" or "Delete" to clear the memory of the software.
    a. The software can only hold data for up to three runs before it prevents you from taking further readings. As a result, when you start the software, you may not need to clear or delete the memory. But once you have taken a few isotherms, you will need to perform this step.
15. *If you are performing an experiment where daptomycin or CB-182,462 needs to be added into the trough, very slowly inject 220 μL of the desired 1 mM antimicrobial peptide stock solution.*
    a. *Make sure you use a bent or L-shaped syringe to inject the drug underneath one of the trough barriers, and therefore underneath the lipids on top of the subphase.*
    b. *By adding 220 μL of the drug solution, the final concentration of that particular antimicrobial peptide within the trough's boundaries would be 4 μM, above daptomycin's typical* MIC_{50}.
    c. *Once you have injected the solution, let it equilibrate for approximately 1-2 minutes before moving onto the next step. It is okay if the isotherm does not start at a pressure of 0 mN/m.*

16. Press the "Play" button as soon as you are ready to start the compression and the software has space to take another reading.
    a. As the compression is taking place, you can adjust the axes of the graph. For compression isotherms, typical axes were surface pressure vs. area.
17. Continue to monitor the compression isotherm and when the isotherm begins to collapse (steep, rapid drop in pressure readings), press the "Stop" button to stop the compression.
18. Remember to save the isotherm.
    a. You will be prompted to save both the data as a *.txt file and the operating conditions as a *.con file.
19. Suck up all the water and lipid from the trough after you have saved the isotherm, and properly clean the trough.
20. Take at least three compression isotherms for each scenario/sample you desire.

C.4 Using the LB Trough to Record Insertion Assays

Apart from compression isotherms, the Langmuir-Blodgett trough can also be used to record insertion assays. The goal of the insertion assay is to test the incorporation of a particular substance, like an antimicrobial peptide, into a preformed monolayer at a certain surface pressure.

The insertion assays involve compressing the lipids to a target pressure above which a monolayer is formed and is biologically relevant to the study. Once this target pressure is reached, an injection of antimicrobial peptides (or a blank) will take place and the resulting pressure changes recorded for a total of 5 minutes. It is expected that the greater the insertion of the molecules into the lipid monolayer, the larger the change in pressure readings from start to finish.

The following procedures outline the setup, operation, and collection of such insertion assays.

1. Make sure the LB trough is clean using the procedures outlined in *Appendix C.2*.
2. Set up the LB trough to prepare for a compression of lipids (to a set target pressure) by following Steps 1-12 of *Appendix C.3*.
    a. Make sure the surface pressure is close to or at zero prior to continuing on to further steps.
    b. At this stage, you will be ready to start your experiment.
3. Set the Barrier menu to "Pressure Control" and enter the following settings:
    a. Set the barrier speed of the trough to 20 cm^2/min
    b. Set the target pressure of the trough to 20 mN/m, which corresponds to the relevant biological membranes being studied
4. Click on "Clear" or "Delete" to clear the memory of the software.
    a. The software can only hold data for up to three runs before it prevents you from taking further readings. As a result, when you start the software, you may not need to clear or delete the memory. But once you have taken a few isotherms, you will need to perform this step.
5. Press the "Play" button as soon as you are ready to start the compression and the software has space to take another reading.
    a. As the compression is taking place, you can adjust the axes of the graph. For insertion assays, typical axes were surface pressure vs. time.
6. After 2 minutes, or 120 seconds (t = 120 s), change the settings to the following:
    a. Set the barrier speed of the trough to 0 cm^2/min, which will stop the movement of the barriers
    b. This action should result in a flat pressure reading as time passes by
7. Once you have frozen the barriers, let the readings continue on for 1 minute or 60 seconds (t = 180 s) to ensure that there is no leakage in the trough
    a. If there is leakage, you will need to start over and clean the trough, especially the two barriers.

b. If there is no leakage, that means that your lipid monolayer is still holding strong at 20 mN/m without the help of the barriers to constantly adapt by adjusting the area of the trough.

8. Once that minute has passed, at t = 180 s, inject 220 μL of the desired 1 mM antimicrobial peptide stock solution (or a blank for control and calcium-only scenarios).
    a. Make sure you use a bent or L-shaped Hamilton syringe to inject the drug underneath one of the trough barriers, and therefore underneath the lipid monolayer in the center.
    b. Make sure you try and use the same force and speed of injection for each run. It does not make a huge difference to inject slowly or quickly, but maintaining consistency is important.
    c. By adding 220 μL of the drug solution, the final concentration of that particular antimicrobial peptide within the trough's boundaries would be 4 μM
    d. For control runs, adding 220 μL of nanopure water acts as a blank and allows you to create a baseline for comparison amongst the other runs with daptomycin or CB-182,462.
9. Once you have completed the injection, let the insertion assay continue for another 5 minutes until $t \geq 500$ s.
10. When the insertion assay is done, press the "Stop" button to stop the current run.
11. Remember to save the insertion assay run.
    a. You will be prompted to save both the data as a *.txt file and the operating conditions as a *.con file.
12. Suck up all the water and lipid from the trough after you have saved the insertion assay, and properly clean the trough.
13. Record at least 3 insertion assays for each scenario/sample you have.

C.5 Using the LB Trough to Deposit Lipid Monolayers on Mica

The Langmuir-Blodgett trough is commonly used to prepare solid supported lipid monolayers on substrates. In this thesis, monolayers were deposited onto mica substrates to be imaged using various atomic force microscopy techniques.

To deposit a lipid monolayer onto a mica substrate, one must first submerge a freshly cleaved piece of mica into the well of the trough prior to forming a monolayer. Once the monolayer is formed via a targeted pressure compression, the mica can be very slowly withdrawn from the well while the monolayer deposits itself onto both sides of the mica as it is vertically removed from the subphase.

The following steps and procedures pertain to the creation of a solid supported lipid monolayer on a mica substrate using the LB trough.

1. Make sure the LB trough is clean using the procedures outlined in *Appendix C.2*.
2. Attach a new or recycled Wilhelmy plate to the extension hook of the trough.
    a. The pre-cut paper Wilhelmy plate uses Whatman CHR1 chromatography paper that has a width of 10 mm.
    b. These Wilhelmy plates are capable of measuring the surface pressure of LB thin films at the air-liquid interface.
    c. If you choose to recycle the paper Wilhelmy plates, you can submerge them overnight in a HPLC chloroform solution, then dry them on a Kimwipe or by nitrogen gas prior to use.
3. Fill the trough with 55 mL of nanopure water using a clean graduated cylinder.
    a. When the trough is filled with water, the Wilhelmy plate will begin to absorb the water and equilibrate with the water subphase.

b. *Should an experiment require the addition of calcium into the subphase, add 1.1 mL of 100 mM calcium stock solution to the 55 mL of nanopure water in the graduated cylinder prior to adding it into the trough. This will give the trough a final calcium concentration of 2 mM.*

4. Allow approximately 10 minutes for the Wilhelmy plate to be fully equilibrated with the subphase.
    a. If you are uncertain as to whether the Wilhelmy plate is fully equilibrated, one way to check for this is to monitor the pressure reading. If the pressure reading stabilizes and does not fluctuate rapidly, then you are ready to proceed to the next step.
5. While waiting for the Wilhelmy plate to equilibrate, cleave a square or rectangular piece of mica using Scotch® Magic™ tape.
    a. When cleaving mica, be sure to use gloves to prevent contamination of the mica surface.
    b. Press the tape firmly onto one side of the mica, and slowly peel off a layer of mica.
        i. If the cleave is successful, there will be no cracked appearance on the mica surface or discolouration of the peeled layer
        ii. If you see these abnormalities, re-cleave until you get a successful and clean cleave.
    c. Be sure to note which side is the cleaved surface – you only need to cleave one side.
6. Using tweezers, secure the mica onto the dipper arm by placing it in the substrate clamp at the bottom of the dipper rod.
    a. Make sure you know which side is the cleaved surface so you know how to store the sample once the monolayer has been deposited.
7. In the Dipper Menu, click on "Down" to ensure that the dipper arm is at its lowest position.

a. Adjust the dipper rod (held in place by a magnetic holder) and base so that the mica fits perfectly into the trough well.
b. The mica should be placed in such a position that it is parallel with the length of the trough barriers and the edge of the mica just above the subphase so that a curved meniscus is seen at the subphase/substrate boundary.

8. Set up the LB trough to prepare for a compression of lipids (to a set target pressure) by following Steps 5-12 of *Appendix C.3*.
    a. Make sure the surface pressure is close to or at zero prior to continuing on to further steps.
    b. At this stage, you will be ready to start your experiment.
9. Compress the monolayer to a target pressure of 20 mN/m by following Steps 3-5 of *Appendix C.4*.
10. Once the target pressure has been reached, wait 5 minutes (or 300 seconds) and make sure the pressure of the monolayer remains unchanged (to show its stability as a monolayer).
11. At t = 300 s, click on "Creep Up" on the Dipper Menu and you will see the dipper arm slowly raising itself and the mica substrate along with it.
    a. Since Pressure Control is still turned on, Creeping Up the dipper arm allows a consistent monolayer to be deposited onto the mica surface as it is removed from the subphase.
12. When the mica substrate is completely removed from the subphase, let it air-dry for approximately 5-10 minutes.
13. When done drying, place the mica substrate (cleaved side up) in a small petri dish and put it in a desiccator to store until ready for imaging.
    a. These samples can be kept at room temperature.
14. Thoroughly clean the trough and repeat all steps for each sample you prepare.

APPENDIX D: AFM, PHASE AND KPFM IMAGING IN AIR

Atomic force microscopy, phase imaging and Kelvin probe force microscopy experiments were performed in this thesis using the Advanced Integrated Scanning Tools for Nano-Technology (AIST-NT™) SmartSPM™ 1000 fully-automated scanning probe microscope.

The samples prepared for these experiments were monolayers deposited on solid mica substrates, and special care was taken into modifying the sample to allow for simultaneous AFM, phase and KPFM imaging using the AIST-NT™ instrumentation.

D.1 Preparing Samples for AFM, Phase and KPFM Imaging

The AIST-NT™ SmartSPM™ 1000 has the ability to record simultaneous AFM, phase and KPFM images. As a result, all the samples prepared were modified to be conductive (since mica is nonconductive) to allow for KPFM imaging. The following steps and procedures will explain this modification technique.

1. Deposit your monolayer onto a freshly cleaved mica substrate (about ½" square dimensions) as explained in *Appendix C.5*. Make sure the sample is completely dry (overnight in dessicator) prior to continuing onto Step 2.
2. Cut a piece of aluminum foil that is much larger than the dimensions of the mica substrate. Lay it down flat and make sure there are no creases in the foil.
3. Cut two equally-sized pieces of electrically-conductive, double-sided tape and place them side by side on the aluminum foil to form an approximate square.

a. The preferred tape is 3M™ XYZ Axis Tape Type 9712, which is available in 6.35 mm width. You can also use the 12.7 mm width (½" model) for this step, but you'll need the smaller-width tape for subsequent steps.
b. Assuming you are using the 6.35 mm width electrically conductive tape, you would cut out two pieces that are approximately ¼" inch (6.35 mm) in length so that when placed side by side, this would form a square that the mica substrate can fit on perfectly.
c. Make sure you don't cut out pieces that are greater than the dimensions of your mica substrate. In this case, ½".

4. When the two pieces of tape are stuck onto the aluminum foil side by side, remove the other sticky side of the conductive tape. You will expose the sticky, black, conductive fibres.
5. Using a tweezer, carefully position your mica sample onto this conductive tape and secure the substrate by pressing down on the edges.
    a. Do not touch or scrape the middle of the sample in any way to prevent contamination and sample damage.
6. Use scissors or a utility knife to cut away the excess aluminum foil so that approximately 3-5 mm of aluminum foil is sticking out of each end of the mica substrate.
7. When you have a 3-5 mm thick aluminum border around your sample, use a flat razor blade (or something with a thin, solid edge) to wrap the aluminum foil against the edge of the mica substrate and fold it over so that it covers the edge of the substrate.
    a. Once you have folded over the aluminum foil, use the flat edge to press down on the aluminum foil so that it is flush with the surface of the sample – you want to maximize contact throughout.
8. After all four aluminum foil edges have been properly folded, cut out four small pieces of double-sided electrically conductive tape.
    a. These small pieces of conductive tape need to be cut from the 6.35 mm width or smaller roll of double-sided conductive adhesives from 3M™.

b. The length of each piece should be about 2-3 mm (very thin and narrow).

9. Place one small piece of double-sided electrically conductive tape onto each corner of the mica sample's surface.
    a. This helps "tie" each edge of aluminum foil to the sample, acting as a bridge between the sample and the different sides of aluminum foil
10. When done placing all four small pieces of conductive tape onto each corner, pick one piece and remove the adhesive sticker on it (just one!).
11. Place the sample in the petri dish until ready for imaging.

D.2 Operating the AIST-NT™ SmartSPM™ for Air Imaging

The AIST-NT™ SmartSPM™ can be used to obtain simultaneous AFM, phase, and KPFM images in air through the conventional high-resolution Kelvin mode that is available on the instrumentation. But in order to get these high-resolution KPFM images, the SmartSPM™ must be properly set up before any imaging can be performed.

The KPFM mode used in the SmartSPM™ Kelvin Mode is AM-KPFM (amplitude modulation Kelvin probe force microscopy). Although FM-KPFM (frequency modulation KPFM) generally provides higher resolution due to the use of force gradients, AM-KPFM still provides high-resolution images when set up properly, and when the conductive tips being used are easily blunted or worn through multiple image scans.

The following procedures will go through the proper setup in SmartSPM's™ accompanying software, called AIST-NT SPM Control Software.

1. Make sure the power box to the SmartSPM™ is turned on and connected properly. Then turn on the computer and open the AIST-NT SPM Control Software program.

2. A pop-up window will appear asking whether you want to "Initialize SPM" or enter "View Only Mode". Click on "Initialize SPM".
3. When the program has loaded, you will see that the program tells you to choose an operating mode from the Tools menu. Click "Close".
4. Under the Tools menu at the top menu bar, click on "AC Mode".
5. The tip must be installed at this point. Inside the SmartSPM™, there is a tip holder with a clip. Remove the tip holder and place your desired cantilever inside the clip. Make sure that this cantilever is conductive to allow for KPFM imaging capabilities.
    a. Place the entire tip holder back into the SmartSPM™ as shown. Lock it in place with the silver lever.
    b. Push the end of the tip holder into the hole and make sure it is securely attached.
6. Once the tip has been installed, the sample must be installed as well.
    a. Before starting anything, make sure there is enough space between the tip and the sample stand so that you have some room to manipulate the sample with. You don't want to break the tip!
        i. Since the tip is fixed, it is the sample stage that can be moved up or down. If the sample stage is too far up, click on the "Z-motor" button in the AC Mode options. A ZMotor Ctrl pop-up control panel will appear. "Move" the sample stage a distance of -3.00 mm. Make sure the value is negative, which means the stage will move down.
    b. Select a KPFM sample holder (with the red pin) and place the KPFM sample holder onto a stand. Lock it in place by using the fixing clench rod (push the button at the bottom of the stand to raise the rod, place the sample inside, then release the clench to snap it in place).
    c. Once the sample holder is secure, make sure there is some conductive tape on the surface of the holder. If not, cut a small piece of double-sided conductive tape and place it in the centre of the holder.

d. Place your modified mica sample (wrapped in aluminum foil) on the KPFM sample holder and secure it in place with the holder's conductive tape.
e. The KPFM holder has a contact pin. Gently lift it up and place it onto the corner of the mica sample, where one of the conductive tape pieces are exposed. This acts to ground the sample or to apply a voltage to the sample for working in electrical modes of SPM.
f. When you have secured the sample onto the sample holder, remove it from the stand and place it into the AIST using a similar fixing clench procedure.
    i. There is a fixing clench handle at the bottom of the SmartSPM™. Turn this down 90° clockwise to lift the rod.
    ii. While the rod is lifted, slide the sample holder under the clench head and release the handle.
    iii. Wiggle the sample holder a bit to ensure the holder is fixed and centred for imaging.
g. Now that the sample is in place, the red pin from the sample holder needs to be placed in the tiny, golden hole located beside the stage. Make sure this red pin is inserted and secure in the hole.

7. With the sample in place, it is now necessary to find the tip.
    a. Go to the Laser Adjustment Window and click on the "Init position" button to set the cantilever holder to its initial position.
    b. Click on "Find Tip" to tell the software to begin its search for the tip. The cantilever holder will start moving from its current position, following an expanding trajectory until the laser beam hits the cantilever. Once the laser beam has found the cantilever, it will move up and down across the cantilever to determine its length and width. After that, the laser beam will settle on a specific location above the tip of the cantilever, marked by a red cross.

c. Once the tip has been found, click on "Adjust Diode" to adjust the position of the photodiode so that the laser beam reflected from the cantilever is located at its center.

8. At this point, it is possible for the SmartSPM™ to automatically set up the rest of the settings to allow for imaging by clicking the "Auto" button (with the magic wand) under the AC Mode control panel. However, we will go through each step manually, starting with finding the resonant frequency of the cantilever.
    a. Click on the "Init tuning" button on the AC Mode control panel. The software will search for the cantilever's resonant frequency. The highest peak within the selected range (which can be adjusted by setting low and high values) will automatically become the resonance peak, which defines the operating frequency.
    b. With the operating frequency set, the initial amplitude of the cantilever must be set as well.
        i. Enter the length of the cantilever in the "len" field in the AC Mode control panel.
        ii. Then enter the amplitude, in nm, in the "amp" field. This value is determined by the type of cantilever used. For non-contact modes, use values between 5 and 20 nm. The cantilevers used in the experimental work done in this thesis were set with an amplitude of 20 nm.
        iii. Click on "set amplitude" to set the amplitude.
9. Once the resonant frequency and amplitude of the cantilever have been set, it is necessary to approach the sample to the tip.
    a. If the sample stage is very far away from the tip, use the ZMotor Ctrl control panel to raise the sample stage (enter positive value) 1 mm at a time until it is very close to the tip.
    b. Click on "m_approach" in the AC Mode control panel to start the approach. In the Curves View window, a graph will show the dependence of the cantilever's

amplitude (Mag signal) on the scanner's vertical position. Near the sample's surface, the amplitude will drop.

c. Click on "fine tuning" to readjust the operating frequency since the approach procedure may have dampened the probe's oscillations.

d. Due to the same reason above, click on "set amplitude" to set the Mag signal to 25000 and automatically optimize the Phase signal.

e. Click on "landing" on the AC Mode control panel to start the landing procedure, where the scanner approaches the sample to the tip of the cantilever.

    i. A landing curve will appear in the Curves View window. You want to have a curve that has a steep drop. If this is not the case, then the sample may have too much static, therefore letting the sample sit in the SmartSPM™ chamber for a few hours may help, or try moving the tip to another area on the sample.

10. When the tip is now approached and landed on the sample surface, it is necessary to run spectroscopy on the curve and find a decent setpoint (either automated or manual).

    a. Once the tip has landed, click on the green arrow in the Curves View window to do a sweep of the landing curve and find a decent setpoint.

    b. The software will automatically choose a setpoint for you on the more vertical part of the curve. Look at the setpoint number at the top of the program window and make sure it doesn't correlate with any part of the curve that has more than one *x*-value for each colour (blue and red).

    c. If you want to change the setpoint, you can enter a number in the "Sp" field.

    d. Once you have the setpoint, go to the Scan Window.

11. Prior to working with Kelvin Mode, we need to be able to get a decent AFM image first.

    a. In the Scan Window, select "QScan Mode".

    b. Open the golden settings button and make sure "Adaptive" scanning is enabled.

    c. Click on "Signals" in the AC Mode control panel and make sure Height(Dac), Height(Sen), Mag and Phase are checked/selected.

d. Select a minimum number of points as 400 x 400, set the scanning speed to 1 Hz, and set the scan area to whichever size is required (for example, 1 μm square, 5 μm square or 10 μm square).
e. Click on the green arrow to start scanning.
f. You can continue to scan in QScan Mode to obtain high-speed AFM and phase images, or you can now move on to Kelvin mode to perform simultaneous AFM, phase and KPFM imaging.

12. If a clear Height(Dac) and Phase image can be obtained using QScan Mode, switch to Kelvin mode, which offers conventional amplitude modulation KPFM (AM-KPFM) imaging capabilities. This means that a tip is scanned across a surface and a feedback loop is used to keep the voltage equal between the tip and the surface. This two-pass technique measures topography on the first pass and surface contact potential difference on the second pass.
    a. Switch to Kelvin mode, and a Kelvin control panel will pop up.
    b. Click on "Auto Setup" to automatically adjust the instrument to switch on and work in KPFM mode.
    c. Click on 'Lift", and then "Show bird" to show a dependence curve between tip oscillation amplitude and the applied AC voltage. The goal is to see a nice "V" shape.
        i. If you cannot see a nice "V" shape, it is still possible to attempt KPFM imaging, but the image resolution will be low. Similar to other modes, you can try imaging different areas or let the sample sit for some time before attempting KPFM again to see if a better "V" shape can be obtained.
    d. Return to the Scan window and make sure the CPD[2] signal is checked. You can set the Signals so that in the first [1] pass, the Height(Dac), Height(Sen), Mag and Phase signals are recorded while on the second [2] pass, the CPD signal is recorded.

13. In the Scan window, after you have selected an area to scan, click on the green arrow to start scanning.
14. Continue scanning different areas of the sample until it is ready to switch to another location or another sample.
    a. When switching to another sample, make sure you lower the stage using the ZMotor control panel so that the sample is clear from the fragile tip.
    b. The tip may need to get switched out every few samples as it suffers increasingly from wear and tear (you will notice the resolution for both AFM and KPFM deteriorating with each additional scan).
15. When finished scanning, make sure the tip is away from the sample surface. Turn off the SPM control software, as well as the power box for the SmartSPM™.

APPENDIX E: AFM IMAGING IN LIQUID

Atomic force microscopy imaging in liquid was performed in this thesis using the JPK NanoWizard® II atomic force microscope.

The samples prepared for these experiments consisted of supported lipid bilayers on solid mica substrates, which were constantly hydrated in HEPES buffer solution. To prepare these samples, one must first create a unilamellar vesicle solution and then promote membrane formation via vesicle fusion onto the mica substrate. Once this sample has been made, it needs to be constantly hydrated before and during imaging, and is fairly time-sensitive.

E.1 Preparing Vesicle Solutions

Vesicle solutions can be prepared using an extruder to create large unilamellar vesicles (LUVs) or sonication to create small unilamellar vesicles (SUVs). For the purpose of these experiments, LUVs were used as they were prepared through an extruder with a 100 nm filter to promote consistency in vesicle size. If sonication is to be used, SUVs of sizes ranging from 5 nm to 50 nm could be created, and repeated periods of sonication and stirring would be required to promote the formation of uniform vesicles.

The instructions to prepare large unilamellar vesicles using an extruder are presented in *Appendix B1*.

E.2 Preparing Samples for AFM Liquid Imaging

To prepare a supported bilayer on a solid substrate, the choice of substrate is quite important. First of all, the substrate needs to be chemically inert and be hydrophilic, such as mica. Secondly, how you image your sample needs to be decided right from the beginning as imaging will occur in liquid. For atomic force microscopy, instruments such as the JPK NanoWizard® II have their own liquid cells that can be used to prevent leakage. If a liquid cell is to be used, the mica substrate must be placed and secured within the liquid cell holder prior to sample preparation. If a liquid cell is not to be used, an O-ring can be placed on top of the mica substrate and secured with glue or tape on the outside to hold it in place and prevent leakage. The experiments performed in this thesis used the liquid cell holder provided by the JPK NanoWizard® II.

Once the substrate and its holder are chosen, samples can be prepared. The goal is to add vesicles solutions to the substrate and incubate the sample for some time to allow the vesicles to adhere to the substrate and eventually reach a threshold concentration that ruptures the vesicles to form a bilayer.

The following steps and procedures will explain how to form a membrane using vesicle fusion.

1. Freshly cleave a piece of large, circular mica (make sure it fits perfectly inside the JPK liquid cell).
2. Assemble the JPK liquid cell by placing the mica substrate in the holder first, followed by the rubber piece and cover/clamp. Make sure the clamp is secure and tightened to prevent any leakage.
3. During this time, pick your vesicle solution depending on what you are studying.
4. Add approximately 200 μL of the vesicle solution to the surface of the mica substrate and let it incubate for 15 minutes to promote vesicle adhesion and fusion to the surface.
5. Once the sample has been incubated for some time, add in calcium and/or your antibiotic to the membrane and let this incubate for about 3 minutes.

a. Make sure that relevant amounts of daptomycin/CB-182,462 at 2 μM and calcium at 2 mM are added into the solution.

6. After incubation, use a pipette to gently rinse away the excess vesicle solution.
    a. To do this, remove 100 μL of the solution using one pipette, and add 100 μL of HEPES buffer using another pipette.
    b. Repeat approximately 10 to 15 times.
    c. Note that great care must be taken while rinsing the solution as any disturbances may create physical defects in the membrane.
7. After rinsing, the sample is ready to be imaged.
    a. The sample should be stable for at least 48 hours and must remain in constant hydration.

E.3 Operating the JPK NanoWizard® II for AFM in Liquid

The JPK NanoWizard® II can be used for both liquid and air atomic force microscopy imaging. But in order to get high-resolution AFM liquid images, the NanoWizard® II must be properly set up before any imaging can be performed. For liquid imaging, non-conductive cantilevers with low spring constants are recommended.

The following procedures will go through the proper setup and use of the JPK NanoWizard® II and its accompanying software.

1. Clean the JPK glass holder with ethanol, and then use KimWipes to dry it. Be very careful as it is fragile.
2. Get two tweezers. With the first one, pick up the cantilever chip and place it on the glass holder. The tip should be pointing towards the polished side and slightly sticking out. With the second tweezer, pick up the cantilever spring. Squeeze the bottom loops of the

spring firmly with this tweezer to open up the front part of the spring. Slide the spring into the groove so that it clamps the cantilever chip onto the glass block firmly.

3. The cantilever should now be secured on the glass block. Insert and lock this glass block onto the AFM head.
    a. This glass block is held in the AFM heading with a locking mechanism.
    b. The notches in the glass must be lined up with the metal tabs on the AFM head to insert the glass block inside the AFM head.
    c. Once inserted, turn the glass block clockwise or counterclockwise so that the tip is pointing towards the right (the spring is on the left side).
    d. Then lock it in position by turning the knob to the left.
4. If necessary, wash this area with ethanol. Use bibulous paper and compressed air spray to clean it and make sure it is dry before proceeding.
5. Place the AFM head back onto the AFM machine, making sure the farthest leg goes down first.
    a. Also make sure that there is nothing on the stand so that the glass block or tip will not hit something.
6. Use the eye viewer to look at the image. This should be the black nob located at the bottom of the AFM stand.
7. Focus the tip using the coarse and fine adjustment knobs on the side of the microscope. You may need to use the positioning screws to bring the tip into the field of view.
8. Start the JPK NanoWizard® II Control software. Once the tip is focused, use the camera view to see the image on the computer screen.
9. Open the Laser Alignment window.
    a. Use the laser adjustment screws to align the laser onto the cantilever tip.
    b. Use the detector adjustment screws to make sure that the vertical and lateral deflections are approximately 0 V and that the sum value is maximized.
10. Adjust the tip position (retract the piezo) by clicking the motor icon.

a. Bring the tip up a reasonable amount so that you can see a gap between the tip and the surface of the AFM stand. We do this so that when we install the sample, the tip and block are not in danger of crashing into the sample or the holder.

11. Remove the AFM head and place the JPK liquid cell onto the AFM stand.
12. Slowly put the AFM head back in position and ensure that the cantilever and glass block fit nicely inside the liquid cell.
    a. If you feel like the cantilever is too close to the mica surface, you can always raise the AFM head a bit more to create a larger gap between the tip and the surface.
13. Set up the JPK NanoWizard® Control.
    a. On startup, the screen should be fairly empty with many options running along the top and left of the viewport.
    b. Make sure the following settings and displays are on the screen throughout scanning: Image Viewer (Height Trace), Image Viewer (Lock-in Phase), Oscilloscope, Scan List, Laser Alignment.
14. Make sure the Intermittent Contact (Liquid) scanning mode is selected
15. Set up the system to save the scans automatically using the save and save settings icons.
16. Use the Stepper Motor to retract/extend the tip or piezo at an interval of your choice. Use the retract (up arrow) button to retract once and the approach (down arrow) button to approach the surface of the sample.
17. Set the scan size to your preferred dimensions and start with a resolution of 512 x 512 pixels with a line rate of 1 Hz.
18. Use the Outline Scanning Mode button to find an initial scan region. You can look through the microscope with your eyes to find this region, but keep in mind that movement within the liquid cell is limited.
19. Tune the cantilever using the Cantilever Tuning window. Here, you can find the cantilever resonance for intermittent contact mode. Make sure they are lined up like the images below. If there are too many peaks, clean the tip again and make sure it is still there.

20. Retract the tip again. Make sure the cantilever is tuned, and approach the surface by pressing the blue down arrow. Once it has approached, retract the tip again a few times.
    a. If the approach does not work, try adjusting the IGain/PGain values, and double-check the Cantilever Tuning settings to make sure your setpoint is still in the right place. You can also try increasing or lowering the setpoint.
21. Make sure the Z Range is adjusted to the maximum resolution at 1.5 μm.
22. Press the lock button on the oscilloscope (the button looks like a lock).
23. Recheck the settings, especially the tuning of the cantilever before you start scanning. Once ready, approach the surface by pressing the blue down arrow.
24. Once approached, press RUN to start scanning.
25. To take another image, you can always right-click the area and select "New Scan Region" to click and drag another area you want to scan.
26. The resolution can be adjusted at any point, and the files renamed to any preferred label you desire.
27. When finished with the scans, retract the tip.
28. Take the liquid cell out, drain it of its vesicle solution, clean it with ethanol at least 5 times and let it dry.
29. Take the tip out if you are not reusing it, or give it a good rinse with ethanol if you are reusing it for another sample.
30. When finished, make sure the AFM is clean, the light is off, and that the NanoWizard software is closed.

APPENDIX F: AFM IMAGES OF MONOLAYERS

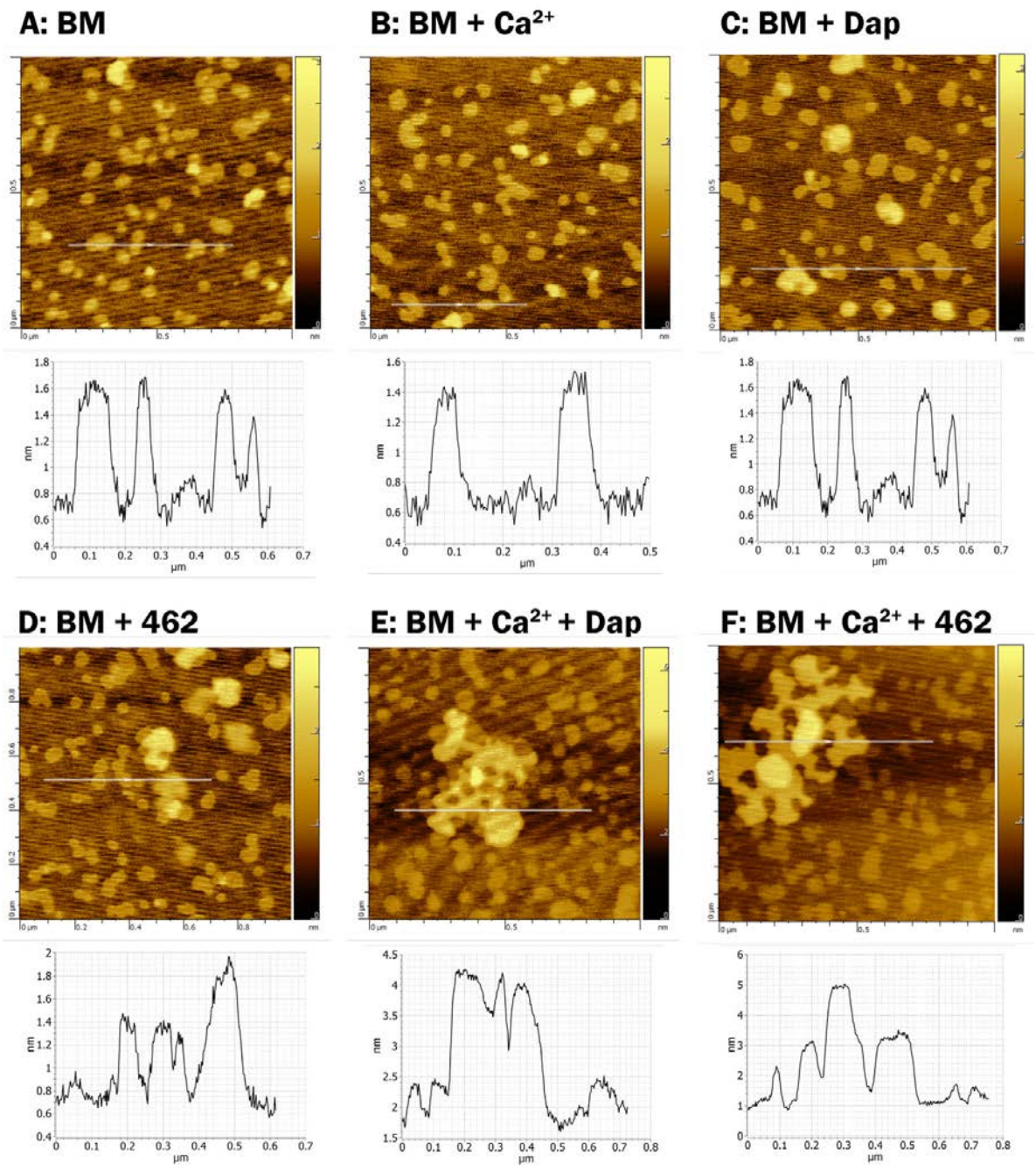

Figure F.1 AFM images of BM monolayer samples in different scenarios

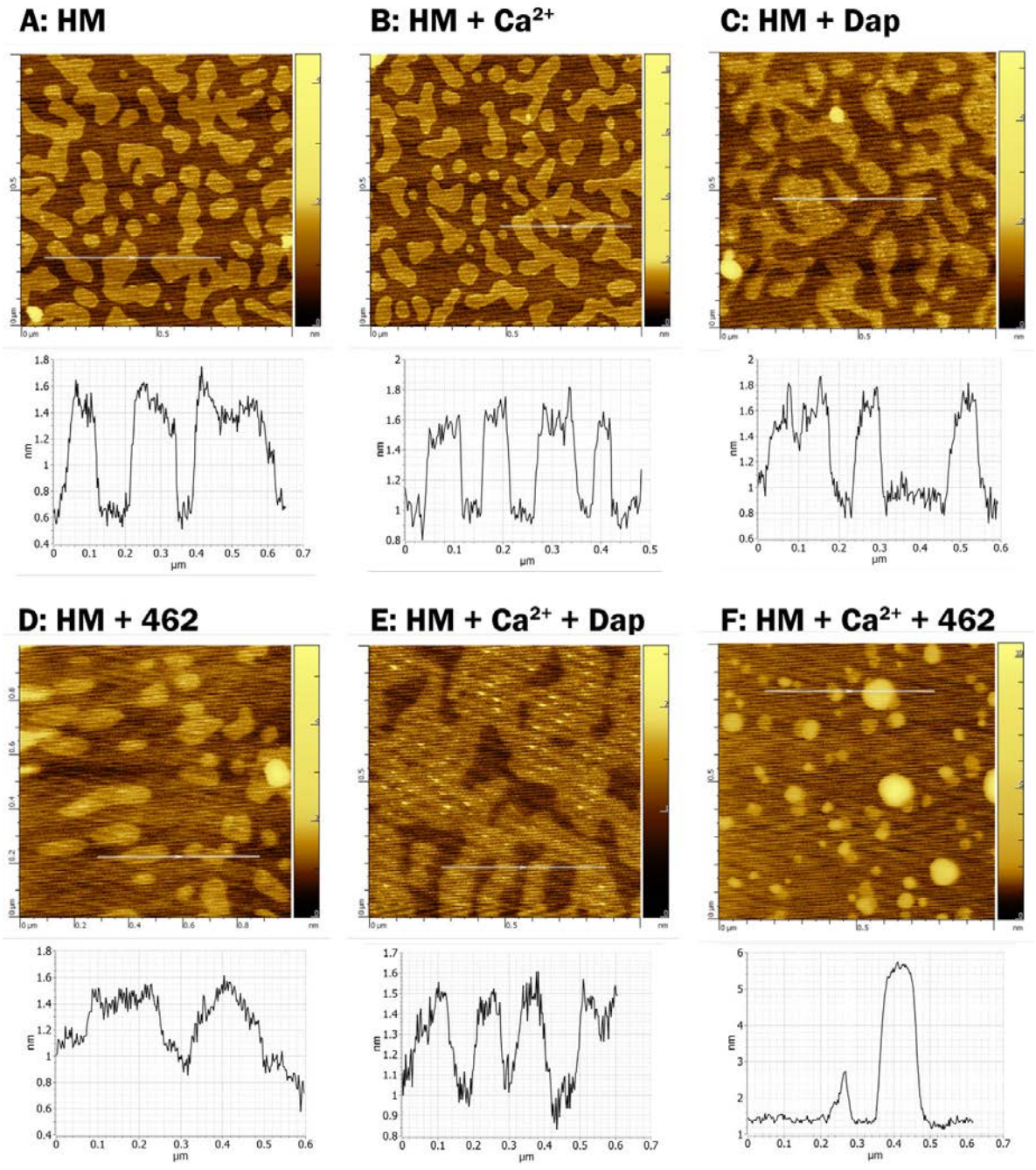

Figure F.2 AFM images of HM monolayer samples in different scenarios

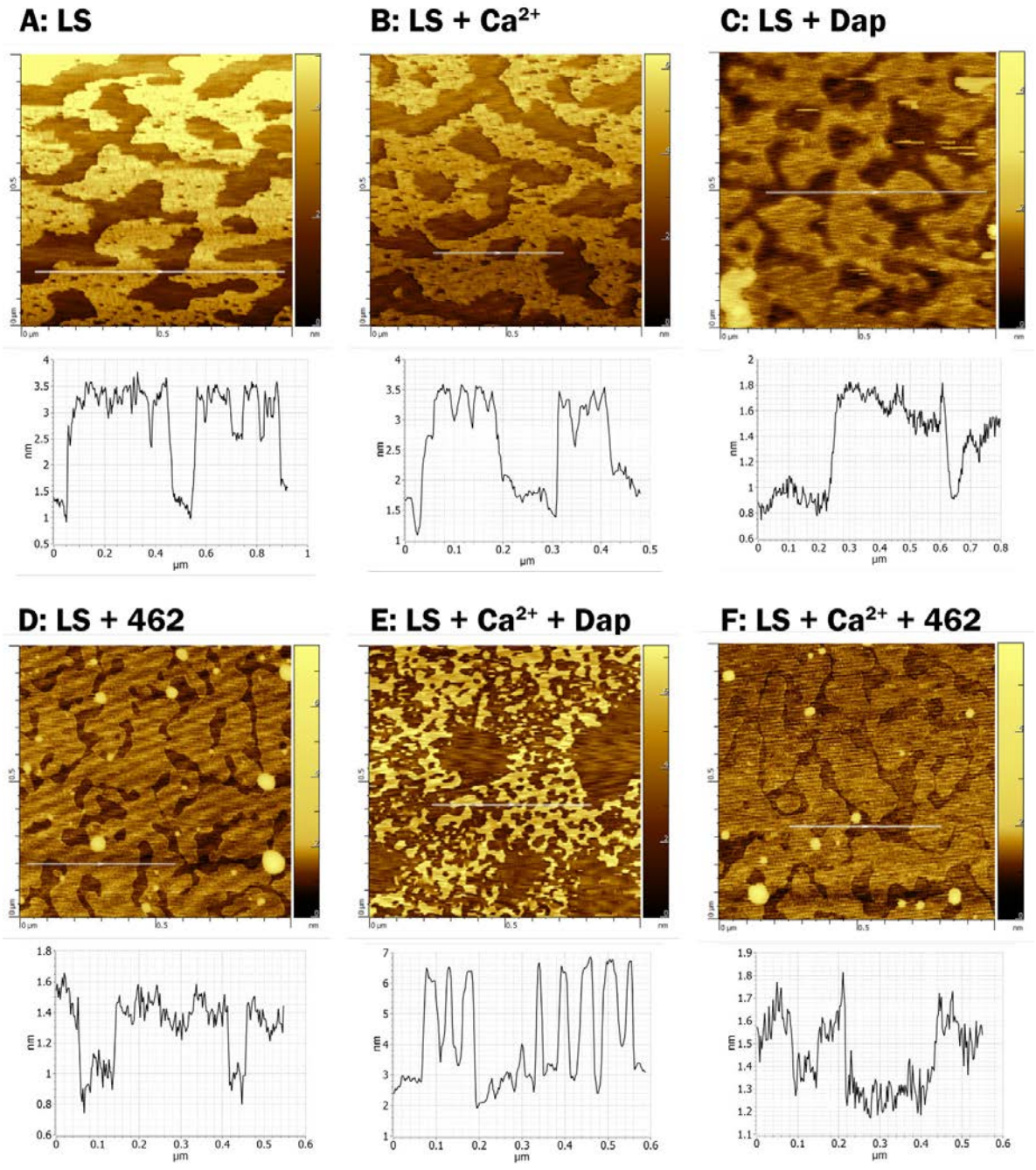

Figure F.3 AFM images of LS monolayer samples in different scenarios

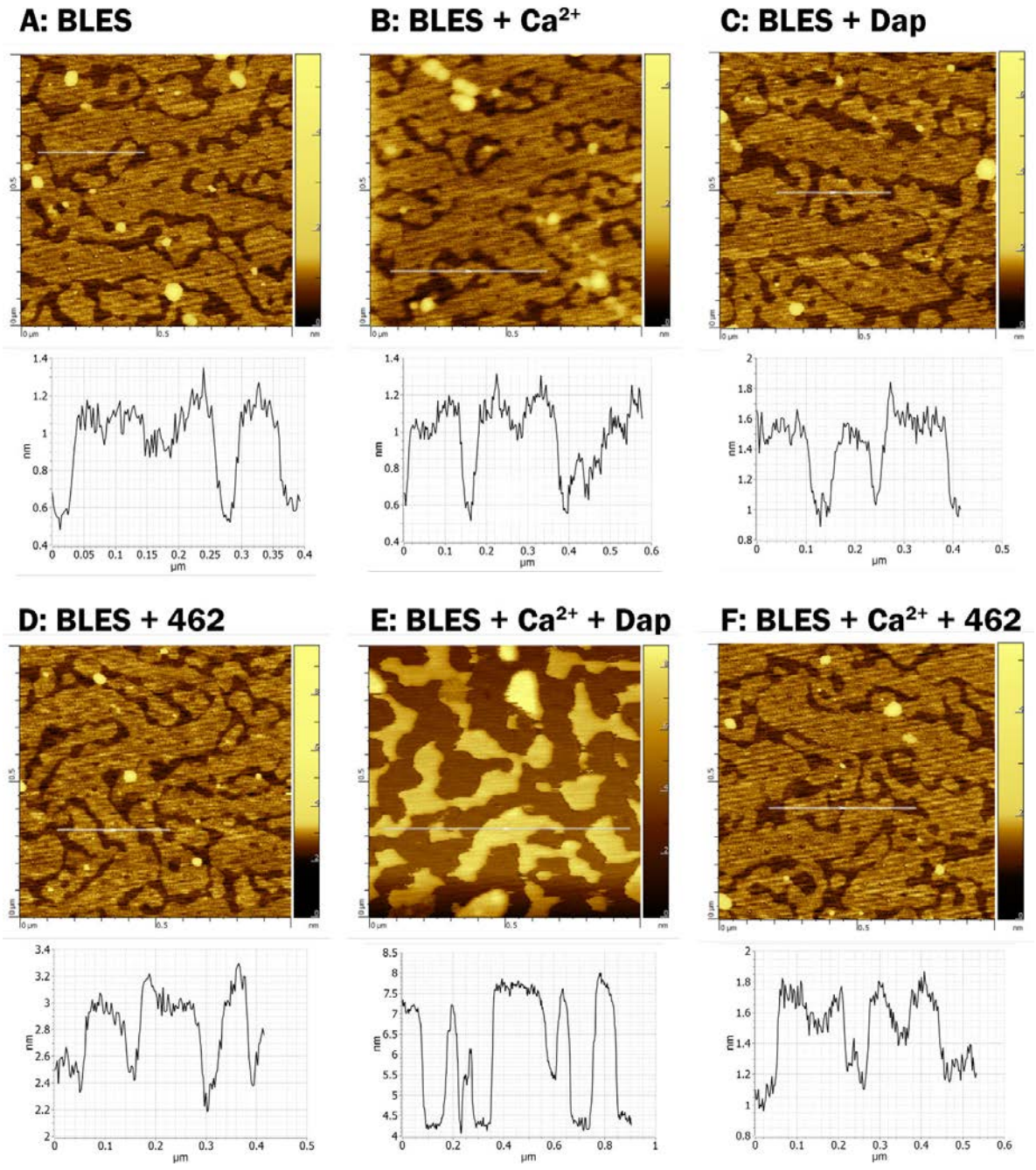

Figure F.4 AFM images of BLES® monolayers in different scenarios